THE THEORY OF PHONON-INDUCED INFRARED VIBRATIONAL LINE SHAPES AT SURFACES

By

Renfang Tu

A thesis submitted to
the School of Graduate Studies and Research
in partial fulfillment of the requirements
for the degree of Doctor of Philosophy

Department of Physics

University of Ottawa
Ottawa, Ontario
March 18, 1995

ISBN 0-612-15770-9

Canada

UNIVERSITÉ D'OTTAWA
UNIVERSITY OF OTTAWA

Abstract

Infrared radiation may be absorbed by a vibrational mode of an adsorption system at resonance. The homogeneous IR absorption line shape of a vibrational mode of an adsorbate is determined by its anharmonic interactions with other localized and delocalized modes of the adsorbate and substrate. These anharmonic interactions include both the adsorption potential between an adsorbed molecule or atom and the surface atoms, and the anharmonic couplings among the substrate atoms themselves at the adsorption site.

Temperature dependent effects of substrate phonons and local mode self interactions on the line broadening and frequency shift are studied in a finite temperature field theory for both the internal stretching mode and admolecule-substrate stretching mode of a diatomic admolecule at an ontop site, and adatom-substrate stretching mode of an adatom absorbed at a bridge site. Modified phonon emission and elastic phonon scattering processes are described in an unified formalism. For the adsorption of an admolecule or adatom at an ontop site, a reduction factor is found which reduces all substrate phonon contributions induced by the anharmonicity of the adsorption potential on the line shift and line width of the low frequency admolecule-substrate stretching or adatom-substrate stretching mode. For the adsorption of an admolecule or adatom at a bridge site, reduction factors are found which reduce only some of substrate phonon contributions induced by the same anharmonicity on the line shift and line width of the low frequency adatom-substrate stretching mode. A bulk Debye model and a semi-infinite elastic continuum model for the substrate are employed to describe the harmonic substrate behavior. The theory is applied to the extensively studied adsorption systems CO/Pt(111) and O/Cu(110). Qualitative agreement with experimental data is found in considering the partial contributions and simplicity of the model.

Acknowledgments

I would like to take this opportunity to express my gratitude to my supervisor Dr. Peter Piercy for introducing me to this subject, for giving me the encouragement and constant help. I am very grateful to him for his confidence and patience he showed throughout the years of the program.

I would like to express my sincere thanks to the members of advisory committee for their time they spent with me and for their valuable suggestions.

I would like to thank Dr. Zhen Ye for the discussions with him during his stay in Ottawa.

Many thanks are going to the professors in this department for all their help in the classes I attended. It has been a pleasure to stay with the staff and graduate students in this department.

Contents

List of Tables

List of Figures

Chapter 1. Introduction

1.1 Introduction

Photostimulated surface processes have been observed in a variety of situations such as adsorption, desorption etc.. These surface processes have received considerable attention in the last couple of decades. Now it is possible to explore an adsorption system with different experimental techniques such as electron energy loss spectroscopy (EELS), inelastic atom beam scattering (IABS), Raman spectroscopy and surface infrared spectroscopy (SIRS) etc.[1, 2]. Among them, infrared absorption spectroscopy is one of the most popular experimental techniques in studies of the vibrational lineshape of adsorbate[2]. The vibrational lineshape analysis will give an understanding of the surface and adsorbate vibrational modes which is of fundamental importance in many areas of the physics and chemistry of surfaces, mostly in the field of heterogeneous catalysis. It is influenced by both homogeneous coupling mechanism and surface heterogeneity[1, 3]. It contains valuable information about lifetimes, vibrational frequencies, gas-surface interaction, bonding structures[3] etc..

In this thesis, we will study adsorption systems in a simplified model and unified formalism. The homogeneous vibrational line shape is shifted and broadened due to damping and pure dephasing processes, arising from its anharmonic interactions with other localized and delocalized phonon modes, and/or low-lying electronic excitations at a metal surface[4, 5, 6, 7, 8, 9]. These interactions include the interactions between an admolecule or adatom and surface atoms, and the interactions among

the substrate atoms themselves. The interaction between an admolecule and surface atoms depends strongly on the geometry of the adsorption site, and affects the vibrational line shape of an admolecule differently at different adsorption sites on the same surface. The interactions among substrate atoms themselves depend on the vibrational properties of the substrate. A theoretical model for a molecule or an atom adsorbed at a solid surface is presented to predict the IR vibrational lineshape of an adsorbate local mode in a finite temperature field theory.

The rest of this chapter is organized to give a brief description of adsorption phenomena in Section 2, then review some previous experimental and theoretical works mostly on the infrared vibrational line shape of a molecule or atom absorbed at a solid surface in Section 3, and finally, introduce our work and give a brief outline for the chapters that follow.

1.2 Adsorption phenomena

When a gas molecule becomes localized at the solid surface in an energetically favorable configuration, the gas molecule is said to be absorbed at the surface. It is the result of the interaction of the gas molecule with the solid surface. This interaction is electromagnetic in nature[10]. The gas molecules adsorbed at a solid surface are called the *adsorbate*. The weakest form of adsorption at a solid surface is called physical adsorption, or *physisorption*. As a gas molecule approaches a solid surface, it first experiences an attraction due to long range van der Waals forces arising from the correlation of the fluctuating dipole moments in the gas molecule and solid. This interaction alone can lead to adsorption, termed *physisorption*. The typical physisorption systems include gases on metal or on alkali halide surfaces. CO/NaCl(100)[11] is one of the examples of this kind. The binding energy of a

physisorbed molecule is rather weak and generally less than a few tenths of an electron volt[12]. For CO/NaCl(100), the binding energy is about 0.2 eV[13]. Another distinctly different form of adsorption is chemical adsorption, or *chemisorption*[10]. A gas molecule or atom that strikes the surface of a solid may bind to one of surface sites through the formation of a surface chemical bond. The typical chemisorption systems are gases chemisorbed on metal surfaces. CO/Pt(111), CO/Ni(100) and dissociated oxygen atoms chemisorbed on a metal surface such as Cu(110) are examples of this kind. The binding force in a chemisorption system is a strong, short range chemical force between an admolecule or adatom and substrate[14]. The binding energy can be of the order of an electron volt. For CO/Pt(111), the binding energy is about 1.3 eV. At the same surface, the binding energy for O is even stronger, and about 2 eV[14]. Chemisorption is important in chemical processes.

For both physisorption and chemisorption, the adsorption potential depends on the details of the interaction between an adsorbed gas molecule or atom and the solid surface, which are often unknown. However, one can phenomenologicaly approximate it in terms of a few physical quantities such as the heat of adsorption, the distance of an admolecule or adatom from the surface and the width of the potential well. Some of these quantities can be determined from specific experiments[11, 15, 16]. Typically, people have used the adsorption potential forms of the Lennard Jones potential, Morse potential and minimum anharmonicity potential[17]. In the minimum anharmonicity model, the adsorption potential is a quadratic function of the adsorbate-surface bond length, with its minimum at the equilibrium adsorbate-surface bond length. Adsorption potential is important in understanding an adsorption system.

Diatomic molecules are interesting adsorbates since they have frustrated translational and internal degrees of freedom. CO is one of the adsorbates most thoroughly studied in the past. Consider the possible normal modes of a diatomic molecule oriented with its axis normal to a solid surface[18, 19]. If we neglect the surface structure, the discrete vibrational modes in the adsorption system is shown schematically in Fig. (1.1)

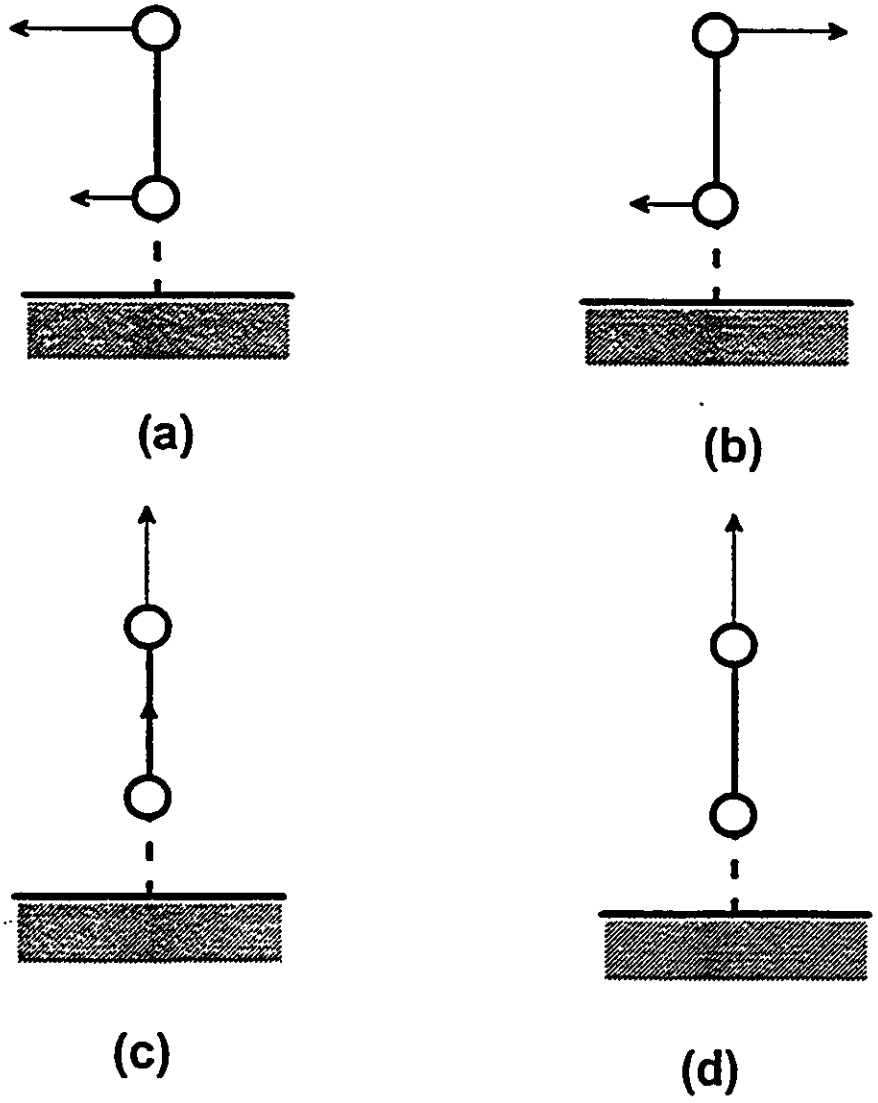

Figure 1.1: Schematic representation of the normal modes of an adsorbed diatomic molecule neglecting surface structure.

where

(a) represents a "frustrated translation" consisting mainly of translational but also some rotational motion,

(b) represents a "frustrated rotation" consisting mainly of rotational but also some translational motion,

(c) represents an adsorbate-surface stretching mode, and

(d) represents an internal stretching mode of the molecule.

When an atom is adsorbed at a solid surface, there are only lateral frustrated translational modes (a) and the perpendicular adsorbate-surface stretching mode (c) present. We will study the vibrational line shapes of adsorbate modes represented by (c) and (d) in this thesis. Note that, in (c), the internal vibration of an adınolecule will be ignored, and it will be treated simply as an adatom.

1.3 Review of early work by others

When a molecule is adsorbed on a solid surface, its vibrational frequency will be shifted and broadened, compared to the gas phase situation. The vibrational line shape has attracted many people's attention and has remained of current interest. Both experimentalists and theorists have made a lot of effort to explain them. Experimental studies of adsorption phenomena at solid surfaces usually require specific techniques, of which vibrational spectroscopy has been a main one for many years. Theoretical studies of the vibrational dynamics in an adsorption system have considered the interactions among the probing electric field, adsorbate and substrate

to explain the observed experiment results[10]. In IR spectroscopy, the basic principle is to apply an oscillating electric field at a solid surface and detect infrared absorption as one of the results of the interaction between the electric field at a solid surface and the local mode of adsorbate. The experimental situation consists of a monolayer of molecules or atoms adsorbed at a metal or alkali halide crystal surface illuminated by infrared radiation. It is not possible in an experiment to observe the line shapes of the vibrational modes of a single adsorbed molecule or atom. Instead, the sample is covered by a layer of adsorbate at a certain coverage. Coverage is usually defined as the ratio of the adsorbate particle density (atom/cm^2) to the substrate particle density so that one monolayer (coverage $\theta = 1$) corresponds to one adsorbed molecule or atom for each substrate surface atom. The spectrum observed in experiment is usually recorded as a function of surface coverage. In the case of infrared reflection absorption spectroscopy (IRAS), the optical theory is fully developed and predicts strong absorption only if there is a net active dipole moment change normal to the surface due to the adsorbate nuclear motion associated with the vibrational mode[20]. The incident infrared radiation can be absorbed by a diatomic admolecule in an adsorption system in several ways shown in Fig. (1.2)

1. Infrared radiation can be directly absorbed by the substrate, as in Fig. (1.2a). Generally this is a non-resonant process, which leads to localized heating of the surface region. This process is particularly important on a metal substrate.

2. Infrared radiation can also deposit its energy into the admolecule-surface bond, exciting the admolecule-substrate stretching mode at resonance, as in Fig. (1.2b). We will call the admolecule-substrate stretching mode the "T mode" later. The reflected infrared radiation will have less intensity than the incident

infrared radiation at the resonance frequency due to IR absorption by the "T mode".

3. Alternatively, infrared radiation may deposit its energy into the molecule's internal bond, exciting the internal molecular stretching mode at resonance, as in Fig. (1.2c) when the incident frequency is close to the internal vibrational frequency. We will call the internal vibration the "V mode" later.

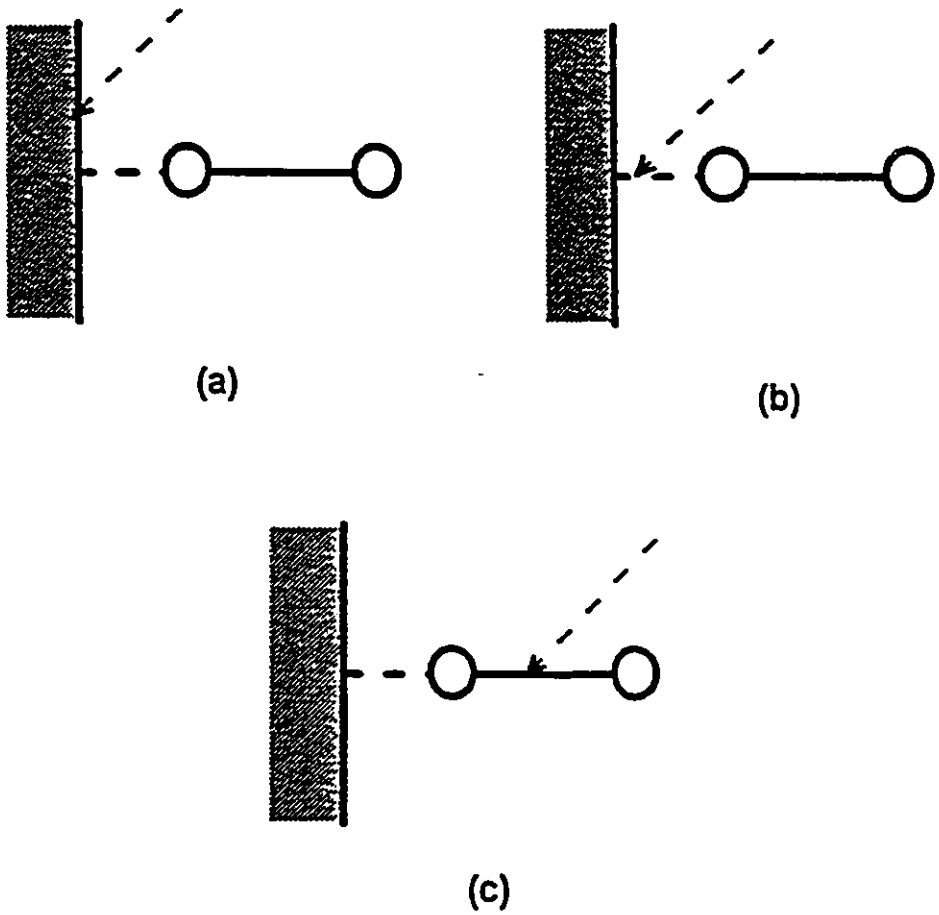

Figure 1.2: Possible channels for the absorption of infrared radiation by an adsorption system.

The infrared absorption processes shown in Fig. (1.2b) and Fig. (1.2c) have been detected experimentally to determine the vibrational line shapes of the adsorbate-surface stretching and internal stretching modes of diatomic admolecules by detecting the intensity changes between the incident and the reflected or transmitted infrared radiation. In experiment, the line shape of a vibrational mode is related to the relative infrared absorption intensity at frequency ω, which is given by

$$\frac{\Delta I(\omega)}{I_0(\omega)} = \frac{I_f(\omega) - I_0(\omega)}{I_0(\omega)}, \tag{1.1}$$

where $I_0(\omega)$ is the incident infrared radiation intensity, i.e., the incident energy flow per unit area and unit time at frequency ω, while $I_f(\omega)$ is the sum of the reflected and transmitted infrared radiation intensity at frequency ω. Without infrared absorption by the vibrational modes of the adsorbate or by the substrate, $I_f(\omega) = I_0(\omega)$. When the radiation frequency is near the vibrational frequency of an adsorbate mode, resonance occurs. As a result, $I_f(\omega) < I_0(\omega)$. IRAS has revealed that the vibrations of adsorbate modes considerably

- shift their frequencies from their gas phase value, and
- shift their frequencies with increasing surface coverage up to a saturation value, and
- shift and broaden depending on temperature for some systems.

It is now possible to detect submonolayers even for very weakly absorbing vibrational modes with energy under 500 cm^{-1}.

The observed spectrums in IRAS or EELS experiments have shown the temperature and coverage dependences of the vibrational line shift and width of adsorbates. Theoretically, it is believed that these dependences are due to dynamical processes

or inhomogeneity in an adsorption system. In order to calculate the frequency of a vibrational mode and its line width, one must take into account the coupling between IR-radiation and the vibrational mode, the coupling between adsorbate and substrate, and substrate dynamics. In general, using linear response theory or Fermi's Golden Rule, it has been shown that the relative infrared absorption intensity at frequency ω given in Eq. (1.1) is proportional to the imaginary part of the Fourier transform of the time ordered Green's function of the vibrational coordinate as follows: [3]

$$\frac{\Delta I(\omega)}{I_0(\omega)} = C\ ImD(\omega). \tag{1.2}$$

The time ordered Green's function $D(t)$ of the vibrational coordinate z is defined by

$$iD(t) = < Tz(t)z(0) >, \tag{1.3}$$

where the bracket "$< \ldots >$" represents a thermal average over the degrees of freedom of the adsorbate and substrate. The coefficient of proportionality in Eq. (1.2) is given by

$$C = \frac{\theta Q^2 \omega}{\hbar \epsilon_0 c} \left(\frac{E^{\perp}}{E_0}\right)^2 \tanh(\frac{1}{2}\frac{\hbar\omega}{kT}), \tag{1.4}$$

where θ is adsorbate coverage, E_0 and $E^{\perp}$ are the incident and full perpendicular components of the electric field at the solid surface, the effective charge $Q = (\partial\mu/\partial z)$, and μ is the dipole moment. The detail of the derivation will be given in Chapter 2.

Electron energy loss spectroscopy is another popular method used to study adsorption systems. Comparing to IRAS, EELS has contrasting strengths and weaknesses. It is more sensitive over a wider spectral range. However, its resolution

(> 20 cm^{-1}) has limited its use for line shape studies. In an EELS experiment, a vibrational mode of the adsorbate is excited by an electron beam, instead of the infrared radiation in IRAS. Near the specular direction, the intensity distribution shows a sharp peak due to dipole scattering which is a long range effect. The interaction hamiltonian for dipole scattering has the same form $H = -\hat{\vec{\mu}} \cdot \vec{E}$ as the interaction between IR radiation and vibrations of the admolecule which will be given in Eq. (2.8). Therefore, at metal surfaces, they both have the "normal dipole selection rule". The energy absorption rate due to dipole scattering is also proportional to the imaginary part of the Fourier transform of the time ordered Green's function of the vibrational coordinate as given in Eq. (1.3). However, the coefficient of proportionality is different from that given in Eq. (1.4). In off-specular directions where impact scattering is important, these comments do not apply and the "normal dipole selection rule" breaks down.

Eq. (1.2) relates the observed spectrum to the Fourier transformed Green's function of the relevant vibrational coordinate. The line width and frequency shift thus are contained in the vibrational self energy of the localized molecular or atomic vibrational mode, influenced by the interactions in the adsorbate-substrate system. There are different interactions in the adsorption system such as gas-substrate interaction, admolecule-admolecule interaction and the interaction of vibrational mode in question with other lower frequency molecular or atomic modes. In principle, all these kinds of interactions will affect the vibrational spectrum. Theoretical attempts to predict the infrared absorption line shape of a vibrational mode of an adsorbed molecule or atom have mainly concentrated on simplified models of the actual adsorption situations encountered experimentally.

The vibrational line width is partly caused by vibrational energy relaxation. Vibrational energy can be dissipated via multiphonon excitation within surface and substrate, or via electron-hole pair excitation. Theoretically, the vibrational energy relaxation of a single diatomic molecule such as CO adsorbed upright on a metal surface, due either to phonon or electron-hole pair creation in the substrate has been calculated in lowest order perturbation theory[4, 5, 21]. A vibrational mode can also decay by emitting a substrate phonon and exciting other lower frequency local mode[21]. Experimentally, a lack of temperature dependence was taken as a signature of the electron-hole pair excitation mechanism in Ryberg's experiment for CO/Cu(100)[22, 1].

Vibrational line broadening is also caused by vibrational phase relaxation or dephasing due to the decay of temporal correlation of the mode in question[3]. Vibrational state remains the same. There is no transfer of vibrational energy but the vibrational mode in question, after a certain time due to its anharmonic coupling with other localized and delocalized modes, will be out of phase compared with unperturbed harmonic oscillator[2]. Fig. (1.3) shows the pictorial description of energy and phase decay from Gadzuk and Luntz[3]. Characteristic for this kind of interaction would be a strong temperature dependence. The so-called exchange model describes dephasing due to the thermal excitation of another vibrational mode localized at the adsorbed molecule or atom[23, 24, 25, 26]. In addition, the elastic scattering of delocalized phonons of the substrate, at the admolecule or adatom, leads to further dephasing, as has been derived in the past[27]. These two processes are in fact related and can be treated together formally[28, 29], and a cross-term between these two mechanisms has been independently derived in the context of photodesorption kinetics in a master equation formalism[30].

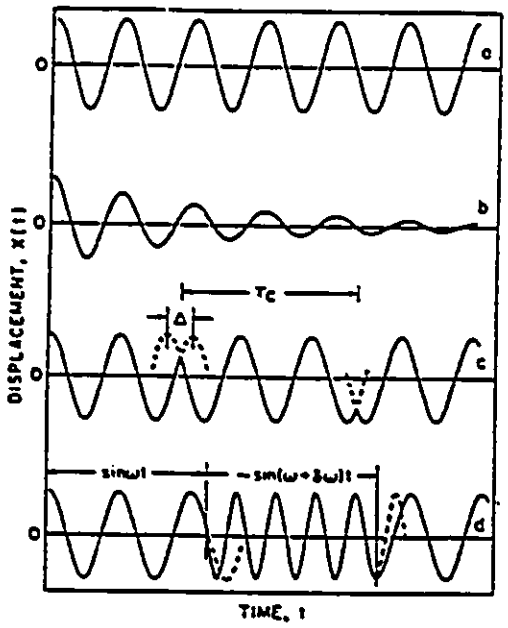

Figure 1.3: Schematic representation of the displacement of an oscillation as a function of time from Ref. [3].

Beyond the temperature dependence of the vibrational line shift and line width, the infrared spectrum for different isotopic mixtures showed that as the admolecule coverage is increased to the monolayer maximum, the vibrational frequency observed for the internal mode of an admolecule shifts to higher frequency by an amount 25-130 cm^{-1} [31, 32, 33] depending on the adsorption system. For the adsorption system CO/Cu(100), the shift of the internal vibrational mode of the admolecule is about 50 cm^{-1}. The coverage dependence of vibrational frequency is mainly due to dipole-dipole interaction between the vibrating admolecules. This was proposed first by Hammaker[34].

In experiment, the measured vibrational line shape of a vibrational mode in a particular system is the total effect of the different interactions. It is important to sort out the effect of each mechanisms so that we will be able to explain the

experimental results and predict vibrational line shapes. Now, the previous experimental and theoretical works for a diatomic admolecule and an adatom are briefly summarized.

1.3.1 Diatomic adsorbate

High frequency intramolecular mode

The vibrational frequency of the internal stretching mode of adsorbed CO on a metal surface generally decreases from its gas phase value of 2143 cm^{-1}, depending on the adsorption site. For example, in one of the first systems studied by IRAS, CO/Pt(111)[31], a single C-O stretching band is observed around 2100 cm^{-1} corresponding to ontop bonded CO, for all coverages up to $\theta = 0.33ML$ at which a $(\sqrt{3} \times \sqrt{3})R30°$-like LEED pattern is observed[35]. When the coverage is increased to $\theta = 0.5ML$, a second C-O stretching band appears at 1850 cm^{-1}, corresponding to bridge bonded CO, as a (4×2) LEED pattern is established. A strongly temperature dependent line shape is found in the experiment. Fig. (1.4) shows the temperature dependence of the peak position and full width at half maximum (FWHM) when CO is adsorbed at a Pt(111) surface at ontop sites. A similar temperature dependence is found in the CO/Ni(111) adsorption system[24]. In this case, the CO adsorbate forms an ordered $c(4 \times 2)$ structure at saturation coverage $\theta = 0.5ML$ with all molecules adsorbed at bridge sites. The peak position and the line width of the C-O stretching mode as a function of temperature were measured by Ryberg[36, 23]. Since the frequency of the internal vibrational mode of the adsorbed diatomic molecule is much higher than the maximum frequency of delocalized phonon in the substrate, the damping of this mode via the creation of delocalized phonons is a process with small probability, because from pure energy

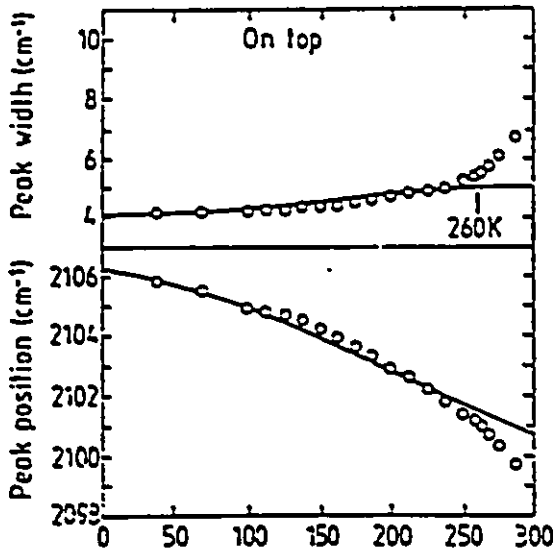

Figure 1.4: The temperature dependence of the peak width and peak position of the "V mode" for CO/Pt(111) at ontop sites from Ref. [37].

conservation, it requires about 6-8 phonons to be created almost simultaneously. It is believed that the line shift and line broadening are mostly due to phase relaxation processes. As seen in the Fig. (1.4), the peak width increases strongly with increasing temperature and there is a small downward shift of the peak position for CO/Pt(111). It has been observed that both the peak width and the peak position reach a constant value for very low temperatures.

The exchange coupling mechanism of vibrational phase relaxation has been used to analyse the line shape of CO/Pt(111) system in addition to CO/Ni(111) and CO/Ru(001)[25]. In the exchange model, the high frequency vibrational mode with vibrational coordinate u is assumed to couple anharmonically to a low frequency vibrational mode with vibrational coordinate v via a quartic term with form u^2v^2. This term is the lowest order interaction which gives rise to pure dephasing in second order perturbation theory. Because of the anharmonic coupling between the

high frequency and low frequency modes, the frequency of the high frequency mode depends on the state of the low frequency mode. The excitation and de-excitation of the low frequency mode by either resonant energy transfer from neighboring molecules or by interaction with the thermal phonon modes can cause dephasing. In order to contribute to the line width of the high frequency vibrational mode via exchange mechanism, the vibration of the low frequency mode has to be anharmonic. Persson *et al.*[23, 25] and Harris[26] groups independently developed their theories to explain the temperature dependent line shape using the exchange model. Persson started by considering Brownian motion in a semiclassical theory, while Harris used a density matrix technique within the constrains of a Markoff approximation. In the weak coupling and low temperature limit, both theories agree with each other. The frequency shift and line width of the high frequency mode are given by

$$\begin{aligned} \Delta\Omega &= e^{\beta\omega_0}\delta\omega, \\ \Gamma &= e^{\beta\omega_0}\frac{2(\delta\omega)^2}{\eta}, \end{aligned} \tag{1.5}$$

where $\beta = \hbar/k_B T$. Basically, both theories contain three parameters, which describe the dephasing mechanism in the exchange model:

- the frequency ω_0 of the low frequency mode;
- the coupling strength $\delta\omega$;
- the damping rate η of the low frequency mode.

The solid lines in Fig. (1.4) are the best fit to the experimental data, giving the following values for the parameters above:[37, 38]

$$\omega_0 = 60\ \text{cm}^{-1}, \quad \delta\omega = -2\ \text{cm}^{-1}, \quad \eta = 10\ \text{cm}^{-1}.$$

This is a good fit to the experimental data assuming an anharmonic coupling to one specific low frequency mode. The frequency ω_0 agrees with that for the parallel frustrated translation obtained by Lahee *et al.*[39]. More experimental data for low frequency mode[39, 40] is needed in order to give a definite explanation.

Richardson, Heidberg etc. reported their experimental results on the system of CO adsorbed on the NaCl(100) surface[11, 41]. They studied experimentally the line shape of the C-O stretching mode over the temperature range from 4 to 55 K with the coverage remaining unchanged. This mode exhibits temperature dependence in the peak center position and FWHM. Unlike CO adsorbed on metals, the vibrational frequency of the C-O stretching mode in CO/NaCl(100) increases from its gas phase value of 2143 cm^{-1} to about 2154 cm^{-1} and undergoes a blue shift of about $\Delta\Omega = 0.2$ cm^{-1} as temperature increases from 4 to 55 K. The absorption band width is in the order of 10^{-1} cm^{-1} over the same temperature range. In this adsorption system, the vibrational frequency of the adsorbate-surface stretching mode is degenerate with the substrate phonon band. Theoretically, we studied this adsorption system in a finite temperature field theory. Both the frequency shift and the FWHM have the same trend as, but are an order of magnitude smaller than, the experimental result[42].

Since Hammaker first proposed dipole-dipole coupling, now the theory to explain the coverage dependence of the vibrational frequency shift has been developed[43, 44, 45, 46, 47] to include also a) the interaction between a dipole and its own image, and the images of other dipoles; and b) the screening of dipole images and the external field by the electronic polarisability of the adsorbate at a surface. Although Lucas and Mahan[43] initially concluded that dipole coupling could only yield a frequency shift of ~ 10 cm^{-1} when they did not treat the interaction of a dipole

with its own image properly, Scheffler[44] and Persson[45] have later concluded that the experimentally observed shifts are compatible with theory for CO adsorbed on metal surfaces such as Cu(100), Pt(111) and Ru(001) surfaces after they took into account of the screening of dipole images and the external field by the electronic polarizability of the adsorbate. The theory showed that when the admolecules in an ordered monolayer have large dynamic dipole moments, dipole-dipole coupling has to be considered. Dipole-dipole coupling may also affect the vibrational line width and cause an asymmetric line shape[48, 49, 50]. Since we only concentrate on the vibrational line shape of a single adsorbed molecule or atom in this thesis, we will not discuss this further here.

Low frequency adsorbate-substrate mode

Studies of the admolecule-surface stretching modes are very important for the understanding of adsorption systems as they give rise to the vibrational levels in the adsorption potential. The vibrational frequencies of these modes are much lower compared to the internal stretching modes and usually under 500 cm^{-1}. Experimentalists have for a long time tried to extend the infrared measurements to this region. The infrared measurements on the admolecule-surface stretching modes on single crystalline surfaces have been carried out by Tobin and Richards[51, 52, 6]. Systems such as CO chemisorbed on Ni(100), Pt(111) and Cu(100) have so far been investigated. The initial study[52] of the c(2 × 2)CO/Ni(100) system was made at room temperature, and showed a weak absorption peak at 475 cm^{-1} with a width of about 15 cm^{-1}. The vibrational energy lies in the two-phonon band of the Ni substrate, so the relatively large width could be caused by the strong vibrational damping caused by two-phonon excitation. Such a mechanism should exhibit a

strong temperature dependence. However, the weak infrared signal did not permit a more detailed study of the temperature dependence of this system. Instead, Tobin and Richards applied the technique to the CO/Pt(111) system[6]. They found, for the c(4 × 2) structure, at 200 K a peak at 460 cm^{-1} with a width of about 7 cm^{-1}. Furthermore, for the CO/Pt(111) system they were able to study the temperature dependence above 200 K, which was found to be rather weak. Together with a large spread in the values of the widths, this indicated that the peak width was determined by inhomogeneous broadening. So far, there is no experimental data reported on the temperature dependent line width and shift for an admolecule at a bridge site.

In the theoretical studies of this mode, Persson *et al.*[53] considered, in a classical fashion, the surface adiabatic effects on the vibrational modes for the adsorbate at ontop sites. Taking into account the bilinear coupling between the local vibration of an admolecule and the continuum phonon modes, they found an important "reduction factor" which was missed in the previous literature. This dramatically reduces the effects of some dynamical processes which were previously believed to make significant contributions to the line shape[54, 55, 56, 57, 58]. For example, the contribution to the line width from multiple phonon emission due to the anharmonicity of the adsorption potential was made negligible by this "reduction factor" at ontop sites. Following a Green's function approach, Langreth et al[17]reconsidered this "reduction factor" by perturbatively solving a set of Bethe-Salpeter equations, again for an adsorbate at ontop sites. They commented that all phonon modes polarized perpendicular to the surface can be neglected when the effect of the anharmonicity of the adsorption potential on the vibrational line shape of the adsorbate at ontop

sites is discussed. However, in their study, the renormalization of the wave function is ignored. They didn't explicitly consider the relation between the localized adsorbate field and delocalized substrate phonon field.

Z. Ye and P. Piercy extended their studies for both the delocalized phonon modes and the localized mode of an admolecule rigorously where the bilinear term is treated exactly in the sense that the fundamental physical relations such as the Heisenberg equations and commutation relations are satisfied by the Heisenberg fields[59]. They studied this in a simple one dimensional model also for an admolecule at an ontop site and found that the vibrational coordinate of an admolecule has a contribution from the delocalized substrate phonon modes. In turn, the displacement of the surface atom underneath the admolecule is affected by the localized mode of the admolecule. This gives rise to an additional delocalized phonon contribution to the vibrational line shape of the admolecule due to the anharmonicity of substrate. They didn't consider this effect for an admolecule at a bridge site. In fact, when an admolecule is adsorbed at a bridge site, the "reduction factor" will not be present for out of phase motion of two bridge atoms at a surface. We will study this in Chapter 4 and 6.

For the adsorbate-substrate stretching vibration, the dynamical dipole-dipole coupling is extremely weak and can be neglected[53].

1.3.2 Atomic adsorbate

A class of systems of particular interest is atomic adsorbates, as dissociated molecules play an important role in most chemical reactions. The experimental problems for infrared spectroscopy of such atomic adsorbates are severe. First of all, by necessity they only exhibit adsorbate-substrate vibrational modes with frequencies usually

lower than the internal vibrational mode of a diatomic admolecule. For a light adsorbed atom such as hydrogen, the frequency of the symmetric stretching mode is around 1000 cm^{-1}, while in other cases, for example, oxygen adsorbed on a metal surface, this frequency is usually under 500 cm^{-1}. Secondly, they may be sitting very deep into the surface, making the electronic screening by the conduction electrons strong and hence weakening the infrared absorption. Y. Chabel and coworkers studied atomic adsorption of H/W(100)[60]. They found a broad infrared absorption peak at 1070 cm^{-1} which is assigned to the symmetric adatom-surface stretching mode. Its line shape is described within the theory of Langreth for an electron-hole pair damped mechanism[5]. Tobin and Richards[6] detected the Pt-O stretching mode of atomic oxygen chemisorbed on a Pt(111) surface. Even though the vibrational frequency lies in the same region (460 cm^{-1}) as that of the Pt-CO mode, they found that the peak width is about 5 times larger.

Obviously, the development of infrared spectrometers that can study adsorbate modes in the low energy region will not only give interesting information about the low frequency modes of adsorbed molecules but will also make it possible to probe the equally important field of atomic adsorbates. For a vibrational mode with frequency lower than 500 cm^{-1}, EELS is sensitive, but its resolution is quite low. H. Dürr and A. P. Baddorf studied the vibrational line shape of the adatom-surface stretching mode in the O/Cu(110) adsorption system in EELS over the temperature range from 100 to 600 K[61]. The energy peak found at 48.2 meV is assigned to the oxygen-surface vibration. The observed peak position and full width at half maximum (FWHM) are displayed in Fig. (1.5) over the measured temperature range. Theoretically, for a quantitative evaluation, they assumed that the vibration of O-Cu stretching is an anharmonic oscillator described by Morse

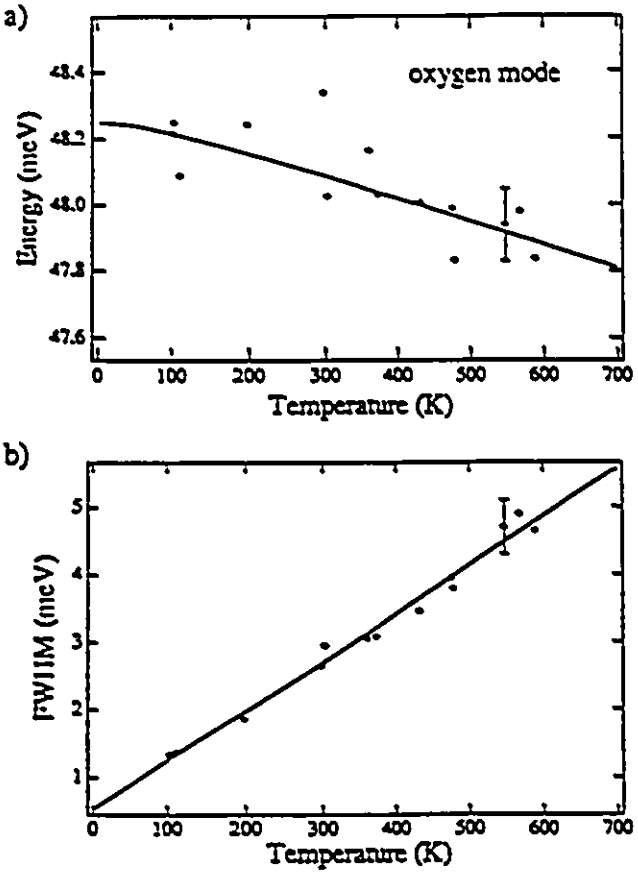

Figure 1.5: The temperature dependence of the peak position a) and peak width b) of the "T mode" for O/Cu(110) at bridge sites from Ref. [61].

potential whose energy eigenvalues can be obtained analytically[61]. The measured peak position in EELS is the thermal averaged energy level spacing when this Morse oscillator is in equilibrium with the thermal bath of the substrate phonons. Within their theory, they have shown that at high temperature, the energy shift increases linearly with temperature, which agrees with the experimental data. However, they have not been able to correctly explain the linear relation between the line width and temperature. We will study this temperature dependent line width in Chapter 6.

1.4 Scope of our work

The temperature dependence of the vibrational line shape of an adsorbed molecule is often attributed to the exchange model, phonon-induced dephasing and decay mechanisms, due to the anharmonic couplings between the admolecule and substrate and among the substrate atoms themselves. Since Langreth studied the exchange model in great detail[17], we will devote ourselves mostly to the phonon-induced vibrational line shape. We are also interested in the vibrational line shape for both the admolecule-substrate stretching mode and the high frequency intramolecular vibrational mode shown in Figs. (1.2b) and (1.2c). However, in some cases, the vibrational line shape of the internal stretching mode is very much dependent of the information for low frequency modes such as the admolecule-substrate stretching mode. Hence, we will pay more attention to the line shape of the latter mode. Since the line shape induced by the electron-hole pair damping process is nearly temperature independent, we exclude this effect in our entire work.

In Chapter 2, a theoretical model of the vibrational lineshape at a surface will be presented. Using linear response theory, the IR vibrational lineshape can be predicted in terms of the imaginary part of the Fourier transform of the time ordered Green's function of a vibrational coordinate. The time ordered Green's function is calculated in a finite temperature field theory – Thermo Field Dynamics(TFD). As the first step, in Chapter 3, we consider a diatomic molecule adsorbed at an ontop site in a one dimension model. The bilinear coupling between the local adsorbate mode and substrate phonons is treated both perturbatively and nonperturbatively. In a simple one dimensional model, some specific energy and phase relaxation processes will be explored in a unified formalism. These processes were considered

by Persson, Langreth, and others in different methods for each mechanism. For simplicity, we approximate the substrate in a bulk Debye model. The results are discussed in terms of two treatments of the bilinear coupling. For this adsorption situation, a "reduction factor" will be induced by the nonperturbative treatment of the bilinear term. This "reduction factor" will reduce the anharmonic coupling to the substrate phonons, by the adsorption potential[59]. The anharmonic couplings among the substrate atoms themselves at the adsorption site will play a significant role. However, for an admolecule at a bridge site, both the adsorption potential and the anharmonicity of substrate are effective. In Chapter 4, we will show this in a simple one dimensional model.

To improve the description of the substrate and to include the effects of surface phonon modes on the vibrational line shape, we will review the phonon dynamics of a solid and introduce generalized density of states in a semi-infinite elastic continuum model in Chapter 5. This approach to describe the substrate phonon behavior is compared with the bulk Debye model and lattice dynamics calculations.

Finally, in Chapter 6, we will generalize the theory in the one dimensional model to a three dimensional model to include the effect of the lateral motions of both the adsorbate and substrate phonons. A central force approximation is employed to describe the pair interactions between atoms. For simplicity, the model is constructed for an adatom adsorbed at a bridge site. However, the theory can be easily extended to other adsorption situations such as an admolecule or adatom adsorbed at a three fold hollow site. As an example, the theory is applied to calculate the vibrational line width due to two phonon emission processes in the weak coupling limit. As a model study, we will discuss the influences of the different aspects of an adsorption system on the temperature dependent line width. The line shift due to

local mode self interaction is also considered. Numerically, we will apply our theory to the O/Cu(110) adsorption system. Our theory does not include the contributions from other processes. Nevertheless, our calculation still provides us some important information about the line shift and line width of a local mode in a real system.

Chapter 2. IR vibrational line shape model theory

2.1 Introduction

Infrared absorption is the result of the interaction between the IR radiation and the sample. In our case, the sample is an adsorption system. The adsorbate could be an atom or a molecule. There are different vibrations possible for an adatom and an admolecule which have been shown in Fig. (1.1). Among them, only those associated with a dipole moment variation (infrared-active) can give rise to infrared absorption. More specifically, IR absorption is the result of the interaction between the IR radiation and the vibrational dipole moment of adsorbate. The infrared radiation intensity absorbed $\Delta I(\omega)$ due to this interaction is usually small compared to the incident intensity, so that we can treat this interaction as a perturbation to the adsorption system. The IR absorption occurs only at resonance where the incident frequency is close to that of the vibrational mode of the adsorbate.

In Section 2, classical electromagnetic theory is used to estimate the infrared radiation intensity and its change due to IR absorption. The basic formalism of the vibrational lineshape is presented. We will model the interaction between a dipole moment and a classical IR radiation field, and develop the absorption fraction $\Delta I(\omega)/I_0(\omega)$ in linear response theory to describe the line shape. The quantum approach will arrive at the same result. The temperature dependent vibrational line shape depends on the hamiltonian of the adsorption system itself. Theoretically, in order to describe this absorption phenomena, we need to consider a specific model

for an adsorption system. We initially consider a low coverage, homogeneous adsorbate of localized adatoms exhibiting only the low frequency mode and diatomic admolecules with both the low frequency adsorbate-surface stretching mode and the high frequency internal vibrational mode. The wavelength of the infrared radiation is long compared with the interatomic distance so that the excitation will be almost completely in phase for neighboring dipoles. We ignore the coupling between dipoles so that each adatom or admolecule can be assumed to be identical. Therefore, in our model, we only consider a single admolecule or adatom at a solid surface.

We will calculate the vibrational line shape based on the hamiltonian of an adsorption system. In Section 3, we limit ourselves to a single admolecule or adatom at an ontop site as an example and construct the hamiltonian of the adsorption system, including appropriate interaction terms.

For a localized vibrational mode of the adsorbate, interactions with substrate phonons and with other local modes lead to line shift and broadening. This line shift and broadening can be calculated in a quantum field theory at finite temperature. In Section 4, thermo field dynamics (TFD) in the finite temperature field theory is introduced to calculate the time ordered Green's function and line shape.

2.2 Line shape formalism

2.2.1 Adsorption system, Infrared radiation field and their interaction

For a molecule or an atom adsorbed at an infinite crystal surface, Langreth[17] has shown that the harmonic hamiltonian may be divided into the two parts for the perpendicular and parallel motions, respectively. By symmetry, these two parts are independent in the harmonic approximation. Furthermore, when the adsorbate is at

a metal surface, infrared absorption obeys a "metal-surface selection rule" which demands that only those vibrational modes with a component of their dynamic dipole moments perpendicular to the surface can be observed since there is no parallel component of the electric field at a metal surface. To stress the main theory and to simplify the calculations we assume that the axis of the vibrational coordinate of an adsorbed molecule or atom is oriented perpendicular to the surface. We will furthermore restrict atom 1 and 2 of a diatomic molecule to motion along this axis. See Fig. (2.1). In Fig. (2.1a), the vibrational coordinate of the internal mode of

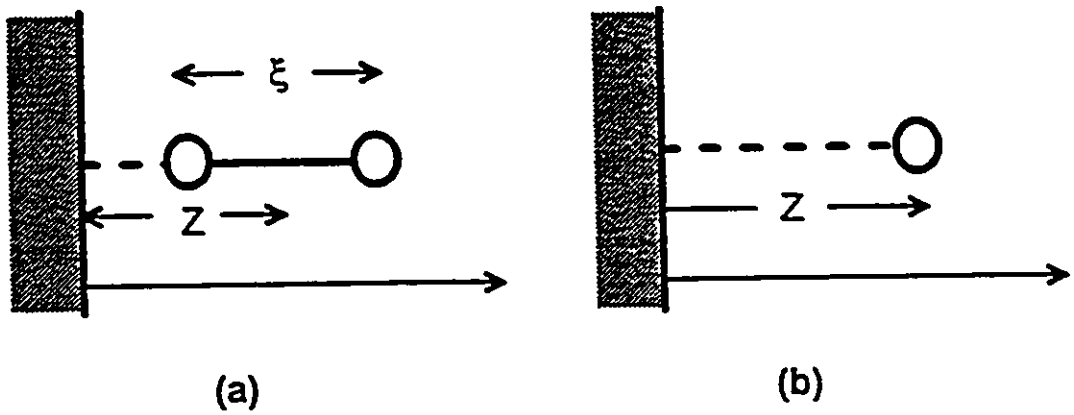

Figure 2.1: Adsorbed molecule and atom configurations.

a diatomic admolecule is denoted by $\xi(t)$. We will specifically study CO molecule adsorbed on solid surfaces since it is one of the adsorbates most thoroughly studied by IRAS. In these cases, CO stands normal to solid surfaces with C inward. The internal mode of the adsorbate is absent when we consider an atomic adsorbate. In Fig. (2.1), the vibrational coordinate of the admolecule-surface stretching mode or adatom-surface stretching mode is denoted by $Z(t)$ which describes the position of the center of mass of an admolecule or the position of an adatom. In adsorption

systems such as CO/Pt(111) and CO/Ni(100), the frequency of this mode is above the maximum phonon frequency of the substrate.

We intend to describe IR absorption by a single adsorbate-surface stretching mode ("T mode") or the internal vibrational mode ("V mode") and calculate its IR vibrational lineshape as it is excited by an oscillating electric field normal to the solid surface. The lateral motions of the adsorbate and substrate atoms are excluded for now. We will consider a three dimensional model including these lateral motions in Chapter 6. Since the "T mode" and the "V mode" are perpendicular to the surface, it is found that a one dimensional model gives results that are qualitatively similar to our full, three dimensional theory. We will show this in Chapter 6.

The dipole moment of an adsorbate vibration

The infrared radiation from a source can interact with an infrared active vibration. The dipole moment of a vibration is a function of its vibrational coordinate. As an example, let us consider the "T mode". We can expand its dipole moment in a Taylor expansion

$$\hat{\mu}_T = \hat{\mu}_{0T} + \left(\frac{\partial \hat{\mu}}{\partial Z}\right)_{Z=Z_0} (\hat{Z} - \hat{Z}_0) + \cdots, \tag{2.1}$$

where $\hat{\mu}_{0T}$ is the dipole moment at equilibrium, and Z_0 is the equilibrium position of the vibrational coordinate $Z(t)$. Define $Q_T = \left(\frac{\partial \hat{\mu}}{\partial Z}\right)_{Z=Z_0}$ as the effective charge. Taking $\hat{\mu}_{0T} = 0$ and ignoring higher order terms gives

$$\begin{aligned} \hat{\mu}_T &= Q_T(\hat{Z} - \hat{Z}_0) \\ &= Q_T \hat{z}, \end{aligned} \tag{2.2}$$

where $\hat{z} = \hat{Z} - \hat{Z}_0$ is the vibrational displacement of the admolecule or adatom away from its equilibrium position.

Similarly, for the "V mode", we only need to change the vibrational coordinate $\hat{Z}(t)$ into $\hat{\xi}(t)$. Assuming $\hat{\xi}_0$ is the equilibrium position of the vibrational coordinate $\hat{\xi}$ and defining $\hat{\zeta} = \hat{\xi} - \hat{\xi}_0$, then the "V mode" dipole moment can be written as,

$$\hat{\mu}_V = Q_V \hat{\zeta}. \tag{2.3}$$

The incident infrared radiation intensity

In our calculation, we classically treat the infrared radiation field as a plane wave so that the electric field at the surface can be written as[62]

$$\vec{E}_{ext} = \vec{E}_0 \cos(\omega t - \vec{k} \cdot \vec{R}), \tag{2.4}$$

where $\vec{k}$ is the wave vector of IR radiation. Its direction is the direction of wave propagation. For infrared radiation, the electric field changes very slowly over atomic distance, $\vec{k} \cdot \vec{R} \ll 1$, and can be treated as

$$\vec{E}_{ext} = \vec{E}_0 \cos(\omega t). \tag{2.5}$$

The energy flux is described by Poynting vector so that the incident radiation intensity is given by

$$\begin{aligned} I_0(\omega) &= |\vec{S}| \\ &= |\frac{1}{\mu_0} \vec{E}_{ext} \times \vec{B}_{ext}| \\ &= \sqrt{\frac{\varepsilon_0}{\mu_0}} E_0{}^2 \cos^2(\omega t), \end{aligned} \tag{2.6}$$

where the magnetic field $\vec{B}_{ext}$ has magnitude $1/c$ times of that of the electric field $\vec{E}_{ext}$. They are perpendicular to each other and to the direction of propagation. For practical purposes, we are often not interested in the instantaneous energy flux but

only their time average value. Taking an average over one period of the wave, we obtain

$$I_0(\omega) = \frac{1}{2}\sqrt{\frac{\epsilon_0}{\mu_0}}E_0{}^2. \tag{2.7}$$

The interaction between IR and dipole moment

When a dipole moment is placed in an electric field, the interaction between the dipole moment and the electric field can be written as

$$\hat{H}_{ext} = -\hat{\vec{\mu}} \cdot \vec{E}, \tag{2.8}$$

where $\hat{\vec{\mu}}$ is the dipole moment in question and $\vec{E}$ is the sum of the external field $\vec{E}_{ext}$ and the effective field $\vec{E}_{eff}$ due to the polarization of electrons in the admolecule and the polarization of other atoms in the substrate. For simplicity, we assume the presence of the admolecule does not substantially modify the local electric field. Hence we ignore this dielectric screening due to the molecule in the later calculation. Taking the "T mode" as an example, and limiting ourselves to one dimension, we can simplify this interaction by substituting Eq. (2.2) into Eq. (2.8) to give

$$\hat{H}_{ext} = -Q_T \hat{z} E^{\perp} \cos(\omega t). \tag{2.9}$$

For the "V mode", we obtain a similar interaction by replacing the dipole moment μ_T with μ_V and $\hat{z}$ with $\hat{\zeta}$ in the above equation.

2.2.2 Energy absorption rate and line shape

Infrared radiation acts as a probe to detect the vibrational line shape. This weak field perturbs the adsorption system. The interaction between the infrared radiation and the vibrational dipole moment causes the excitation of certain vibrational states

in the adsorption system. The line shape receives contributions from all energy and phase relaxation mechanisms and is related to the absorption fraction $\Delta I(\omega)/I_0(\omega)$ given in Eqs. (1.1) and (1.2). Now we show that the absorption fraction is given by Eq. (1.2), i.e.

$$\Delta I(\omega)/I_0(\omega) = \frac{\theta\omega Q^2}{c\varepsilon_0\hbar}\left(\frac{E^{\perp}}{E_0}\right)^2 \tanh(\frac{1}{2}\frac{\hbar\omega}{kT})ImD(\omega). \tag{2.10}$$

The energy absorption rate $\Delta I(\omega)$ can be calculated by using linear response theory since we can treat the IR radiation-dipole interaction as a weak external perturbation.

In order to calculate the energy absorption rate, let us first look at the linear response of a vibrational dipole moment to an external field $\vec{E}_{ext}$.

Without the interaction hamiltonian $\hat{H}_{ext}$ given in Eq. (2.9), the adsorption system is in thermal equilibrium. Assume $|j\rangle$ is an exact eigenstate of full unperturbed hamiltonian $\hat{H}$ and number operator $\hat{N}$ with eigenvalues $E_j(N)$ and N. If the adsorption system is perturbed from equilibrium at $t = t_0$ by an interaction hamiltonian $\hat{H}_{ext}$ which can be treated as perturbation, the wave function in the presence of the perturbation in the interaction picture is given by[63]

$$|j\rangle_{ext} = U(t,t_0)|j\rangle \qquad (t > t_0), \tag{2.11}$$

where $U(t,t_0)$ is the evolution operator that determines the wave function at time t $(t > t_0)$ in terms of the wave function at time t_0 and given by

$$\begin{aligned} U(t,t_0) &= T\left\{exp\left[-i\hbar^{-1}\int_{t_0}^{t}\hat{H}_{ext}(t')dt'\right]\right\} \\ &= 1 - i\hbar^{-1}\int_{t_0}^{t}\hat{H}_{ext}(t')dt' + \cdots \quad (t > t_0). \end{aligned} \tag{2.12}$$

Therefore, the diagonal matrix element of a dipole moment $\hat{\mu}$ in response to an

external perturbation can be written in terms of the unperturbed wave function as follows

$$\begin{aligned}\langle j|\hat{\mu}|j\rangle_{ext} &= \langle j|\hat{\mu}|j\rangle + \\ &\langle j|i\hbar^{-1}\int_{t_0}^{t}\left[\hat{H}_{ext}(t'),\hat{\mu}\right]dt'|j\rangle + \cdots \ (t > t_0),\end{aligned} \tag{2.13}$$

where the square bracket '[ ]' denotes the commutator

$$[A,B] = AB - BA. \tag{2.14}$$

Ignoring the higher order terms in $\hat{H}_{ext}$, the first order change of the diagonal matrix element of the dipole moment reduces to

$$\begin{aligned}\langle j|\hat{\mu}|j\rangle_{ext} - \langle j|\hat{\mu}|j\rangle = \\ \langle j|i\hbar^{-1}\int_{t_0}^{t}\left[\hat{H}_{ext}(t'),\hat{\mu}\right]dt'|j\rangle.\end{aligned} \tag{2.15}$$

The occupation of the different states $|j\rangle$ is determined by the density operator of the system

$$\hat{\rho_H} = \frac{e^{\beta(\hat{H}-\mu_c\hat{N})}}{Tre^{\beta(\hat{H}-\mu_c\hat{N})}}, \tag{2.16}$$

where μ_c is chemical potential. The first order change in the ensemble average of the dipole moment can be evaluated by adding the contribution of each state $|j\rangle$, weighted according to the unperturbed ensemble as

$$\langle\hat{\mu}\rangle_{ext} - \langle\hat{\mu}\rangle_0 = i\hbar^{-1}\int_{t_0}^{t}dt'Tr\left\{\hat{\rho}_H[\hat{H}_{ext}(t'),\hat{\mu}_(t)]\right\}. \tag{2.17}$$

At equilibrium, $\langle\hat{\mu}\rangle_0 = 0$. Substituting Eq. (2.2) and Eq. (2.9) into Eq. (2.17) gives the ensemble average of the "T mode" dipole moment

$$\begin{aligned}\langle\hat{\mu}\rangle_{ext} &= Q^2i\hbar^{-1}\int_{t_0}^{t}dt'Tr\left\{\hat{\rho}_H[\hat{z}(t),\hat{z}(t')]\right\}\hat{E}^{\perp}_{ext}(t') \\ &= -\frac{Q^2}{\hbar}\int_{t_0}^{t}dt'D^R(t,t')E^{\perp}_{ext}(t'),\end{aligned} \tag{2.18}$$

where for generality, subscript "T" has been ignored. The retarded Green's function $D^R(t,t')$ evaluated in the equilibrium grand canonical ensemble is defined by

$$\begin{aligned} iD^R(t,t') &= Tr\left\{\hat{\rho}_H[z(t),z(t')]\right\}\theta(t-t') \\ &= \langle[z(t),z(t')]\rangle\theta(t-t'), \end{aligned} \tag{2.19}$$

where the bracket "⟨...⟩" represents a thermal average over the degrees of freedom of the admolecule or adatom and substrate. Since the unperturbed hamiltonian of the adsorption system is time-independent, this retarded Green's function has form $D^R(t-t')$. The analysis of the linear response is then reduced to the calculation of a retarded Green's function. After a variable transformation, we have

$$\langle\hat{\mu}\rangle_{ext} = -\frac{Q^2}{\hbar}\int_{-\infty}^{\infty} dt' D^R(t')E^{\perp}_{ext}(t-t'). \tag{2.20}$$

We assume that the external field is a plane wave given by Eq. (2.5) or

$$E^{\perp}_{ext} = E^{\perp}\frac{1}{2}(e^{i\omega t} + e^{-i\omega t}). \tag{2.21}$$

In an experiment, the energy absorption is recorded over a certain observation period T. The time average of the energy absorption rate over this period can be calculated as

$$\begin{aligned} \Delta I(\omega) &= \theta\frac{1}{T}\int_0^T dt\frac{\partial\langle\hat{H}_{ext}\rangle}{\partial t} \\ &= -\theta\frac{1}{T}\int_0^T dt\frac{\partial E^{\perp}{}_{ext}}{\partial t}\langle\hat{\mu}_T\rangle_{ext} \\ &= -\frac{1}{2\hbar}\theta\omega Q^2 E^{\perp 2} Im D^R(\omega), \end{aligned} \tag{2.22}$$

where θ is the coverage of adsorbate, $D^R(\omega)$ is the Fourier transform of the retarded Green's function $D^R(t)$ defined as

$$D^R(\omega) = \int_{-\infty}^{\infty} dt e^{i\omega t} D^R(t). \tag{2.23}$$

Its imaginary part is related to the imaginary part of the Fourier transform of the time-ordered Green's function $D(t)$ defined in Eq. (1.3) by a thermal factor, $\tanh(\frac{1}{2}\frac{\hbar\omega}{kT})$, as follows:

$$ImD^R(\omega) = \tanh(\frac{1}{2}\frac{\hbar\omega}{kT})ImD(\omega). \tag{2.24}$$

At low temperature, i.e., $k_BT \ll \hbar\omega$, the thermal factor is typically near unity. In most cases, $k_BT \gg \Gamma$ (half width at half maximum of the vibrational mode) at typically room temperature, so the thermal factor varies slowly with frequency ω. It will not have an important effect on the vibrational lineshape. In our later calculation, we ignore this factor and calculate $ImD(\omega)$ directly to predict the vibrational line shape. In a quantum treatment, $(E^\perp)^2$ is the matrix element between the initial and final photon states.

Combining Eq. (2.22) and Eq. (2.7) gives energy absorption rate. The line shape is seen in the energy absorption rate

$$\Delta I(\omega)/I_0(\omega) = \frac{\theta\omega Q^2}{c\varepsilon_0\hbar}\left(\frac{E^\perp}{E_0}\right)^2 \tanh(\frac{1}{2}\frac{\hbar\omega}{kT})ImD(\omega). \tag{2.25}$$

In this equation, the line shape depends on a few factors such as the external field, coverage, frequency, and the imaginary part of the Fourier transform of a time-ordered Green's function. However, our interest is not in the absolute intensity of the infrared absorption peak. We are more interested in the line width and line shift which contain the important information on the vibrational mode and depend on the imaginary part of the Fourier transform of the time-ordered Green's function. We can also derive the same formula by using Fermi's Golden Rule. The time ordered Green's function will be determined by the hamiltonian of the adsorption system which will be considered in the next section.

For the "V mode" line shape, we only need to replace the "T mode" vibrational coordinate z with the "V mode" vibrational coordinate ζ above.

2.3 The hamiltonian of an adsorption system

In this section, we consider the hamiltonian of a single adsorbate at an ontop site in a one dimensional model. This hamiltonian will be constructed in second quantized form. We start with a simple case where an atom or a diatomic molecule is adsorbed at a static solid surface. Then, we will consider the substrate phonon vibrations and include them in the full hamiltonian.

2.3.1 The static hamiltonian of adsorbate

Fig. (2.1b) showed an atom adsorbed at a semi-infinite, static, solid surface. We will ignore the thermal vibration of the solid surface for now and begin with the adatom-solid interaction named the static surface potential. This is the interaction that the adatom experiences when it approaches the surface of a solid at zero temperature without the transition of the electronic states or substrate phonons in the so-called adiabatic approximation. It is a function of the distance z that the atom is away from its equilibrium position at the surface, and is denoted by $V(z)$.

Fig. (2.2) shows all the bound states due to the potential $V(z)$ labeled by the quantum index j. Near the bottom of the well, the bound states of the potential $V(z)$ are nearly the same as the eigenstates of a single harmonic oscillator. At low temperature, the adatom occupies the low energy level most of the time. Since the physics of a single harmonic oscillator is well-known, we intend to treat the surface potential $V(z)$ as a perturbed harmonic oscillator in our calculation. Now, if we

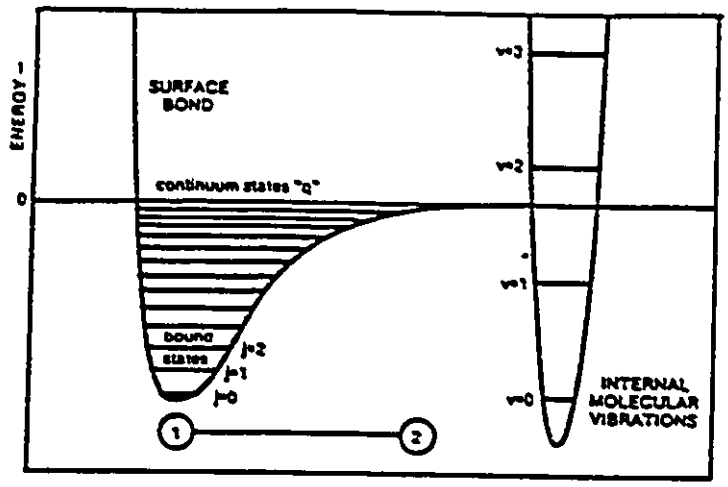

Figure 2.2: Bound states of an adsorption potential from Ref. [12].

describe an adatom in quantum mechanics, the static hamiltonian of the adatom can be written as

$$H_{st}(z) = -\frac{\hbar^2}{2m}\frac{\partial^2}{\partial z^2} + V(z), \tag{2.26}$$

where m is the mass of the adatom.

Similarly, for a diatomic admolecule, the hamiltonian can be expressed in terms of the center of mass variables (see Appendix A). The surface potential is assumed to depend on the vertical distance from the inward end of the diatomic molecule to the surface, which is related to the center of mass displacement z from its equilibrium position and the internal vibrational displacement ζ from its thermal equilibrium position. The potential of the outward atom of the diatomic molecule has been ignored since it is farther away from the surface. The internal vibrational potential $U(\zeta)$ depending on the displacement of the internal bond length from its equilibrium value can be approximated as a harmonic oscillator so that $U_{anh}(\zeta) = 0$. This was used in the calculation of photodesorption kinetics. Therefore, the static hamiltonian

for a diatomic admolecule is

$$H_{st}(z,\zeta) = -\frac{\hbar^2}{2\mu}\frac{\partial^2}{\partial\zeta^2} + U(\zeta) - \frac{\hbar^2}{2m}\frac{\partial^2}{\partial z^2} + V(z - \frac{\mu}{m_1}\zeta), \tag{2.27}$$

where m_1 is the mass of the inward atom of the diatomic admolecule. The energy levels of potential $U(\zeta)$ is also shown in Fig. (2.2).

2.3.2 The thermal vibrations of the substrate atoms

In reality, the solid surface in the experiment can not be kept at zero temperature. To treat the solid adequately requires the consideration of the thermal phonons in the solid. The simplest way to approximate the surface displacement due to the thermal phonons is to use a bulk Debye model where the solid is treated as an infinite elastic continuum. In this model, the displacement of a mass element at $\vec{r}$ can be expanded as a superposition of all possible plane waves with frequency $\omega_{\vec{k}\sigma}$, i.e., $e^{i(\vec{k}\cdot\vec{r}-\omega_{\vec{k}\sigma}t)}$. Here $\vec{k}$ is the wave vector, and σ denotes the polarization of a wave. For a given wave vector $\vec{k}$, there are two transverse waves with wave velocity c_t labeled by T_1, T_2 and one longitudinal wave with wave velocity c_l labeled by L. If we introduce $b_{\vec{k}\sigma}$ and $b^\dagger_{\vec{k}\sigma}$ as phonon annihilation and creation operators, respectively, then the displacement field in second quantized form is

$$\begin{aligned}\vec{a}(\vec{r},t) &= \sum_{\vec{k}\sigma}\hat{e}_{\vec{k}\sigma}\sqrt{\frac{\hbar}{2\rho_0\omega_{\vec{k}\sigma}V}}\left[b_{\vec{k}\sigma}e^{i(\vec{k}\cdot\vec{r}-\omega_{\vec{k}\sigma}t)} + b^\dagger_{\vec{k}\sigma}e^{-i(\vec{k}\cdot\vec{r}-\omega_{\vec{k}\sigma}t)}\right] \\ &= \sum_{\vec{k}\sigma}\hat{e}_{\vec{k}\sigma}d^0_{\vec{k}\sigma}(t),\end{aligned} \tag{2.28}$$

with

$$d^0_{\vec{k}\sigma}(t) = \sqrt{\frac{\hbar}{2\rho_0\omega_{\vec{k}\sigma}V}}\left[b_{\vec{k}\sigma}e^{i(\vec{k}\cdot\vec{r}-\omega_{\vec{k}\sigma}t)} + b_{\vec{k}\sigma}{}^\dagger e^{-i(\vec{k}\cdot\vec{r}-\omega_{\vec{k}\sigma}t)}\right]. \tag{2.29}$$

Here $\hat{e}_{\vec{k}\sigma}$ is a unit polarization vector that for the longitudinal wave ($\sigma = L$) is in the direction of propagation $\vec{k}$, and for the two transverse ones ($\sigma = T_1, T_2$) is orthogonal to $\vec{k}$ and mutually orthogonal, V is the volume of the solid, $\omega_{\vec{k}\sigma}$ represents the phonon vibrational frequency, and operators $b_{\vec{k}\sigma}$ and $b^{\dagger}_{\vec{k}\sigma}$ obey the bose commutation relation

$$[b_{\vec{k}\sigma}, b^{\dagger}_{\vec{k}'\sigma'}] = \delta_{\vec{k},\vec{k}'}\delta_{\sigma,\sigma'}. \tag{2.30}$$

The summation in Eq. (2.28) involves the phonon spectra of bulk acoustic modes. The bulk Debye model is a crude approximation to the normal mode dispersion relations in a solid. It replaces all branches of a phonon vibrational spectrum with the same linear dispersion relation

$$\omega = ck. \tag{2.31}$$

In addition, the volume of the first Brillouin zone is chosen to equal the volume of a sphere with radius k_D, so that the cutoff wave vector can be determined by the relation

$$\frac{4\pi}{3}k_D^3 = \frac{(2\pi)^3}{v_c}, \tag{2.32}$$

where v_c is the volume of the unit cell, and k_D is magnitude of the cutoff wave vector for all branches. In practice, it is convenient to define a Debye frequency by

$$\omega_D = ck_D. \tag{2.33}$$

Evidently k_D is a measure of the inverse interparticle spacing, and ω_D is a measure of the maximum phonon frequency. All branches have an average sound velocity c, which is given by equation

$$\frac{1}{c^3} = \frac{1}{3}(\frac{1}{c_l^3} + \frac{2}{c_t^3}) \tag{2.34}$$

Hence

$$\frac{1}{\omega_D{}^3} = \frac{1}{3}(\frac{2}{\omega_t^3} + \frac{1}{\omega_l^3}), \tag{2.35}$$

with

$$\begin{aligned} \omega_t &= c_t k_D, \\ \omega_l &= c_l k_D. \end{aligned} \tag{2.36}$$

The bulk Debye model is appropriate at low temperatures for which long wavelength phonon displacements dominate in $\vec{a}(\vec{r},t)$. By employing bulk phonon modes to describe the surface displacement, we have neglected the softening of certain surface vibrational modes (Rayleigh waves) due to the reduced coordination of the surface atoms. As a consequence, the mean squared thermal surface displacement derived from $\vec{a}(\vec{r},t)$ is somewhat small, and its effect on an adsorbed molecule is correspondingly diminished. Therefore, since the adsorption occurs at a solid surface, the bulk Debye model can not give us a accurate description about surface behavior. We will improve this model in Chapter 5.

If we include the effect of the thermal phonon vibrations of the substrate into the full hamiltonian of an adsorption system, the distance of the admolecule or adatom to the surface now becomes $Z - a_z$. Correspondingly, we can obtain the surface potential by replacing z in the static surface potential with $z - a_z(\vec{r},t)$, i.e.

$$V(z) \rightarrow V(z - a_z(\vec{r},t)) \tag{2.37}$$

for an adatom, and

$$V(z,\zeta) \rightarrow V(z - a_z(\vec{r},t),\zeta) \tag{2.38}$$

for a diatomic admolecule.

Note that with the surface displacement given by Eq. (2.28), the hamiltonian of a solid, in the harmonic approximation, is

$$H_s = \sum_{\vec{k}\sigma} \hbar\omega_{\vec{k}\sigma}(b_{\vec{k}\sigma}{}^{\dagger} b_{\vec{k}\sigma} + \frac{1}{2}). \tag{2.39}$$

We ignore the anharmonicity of the solid for now and will consider it in Chapter 4.

2.3.3 The complete hamiltonian

We can now construct the complete hamiltonian for an adsorption system. Since we are dealing with vibrations, naturally, we separate the complete hamiltonian H into the harmonic part H_0 which describes harmonic oscillators and anharmonic part H_{anh}. Generally,

$$H_0 = \sum_i \hbar\omega_i(b_i^{\dagger} b_i + \frac{1}{2}), \tag{2.40}$$

where i denotes the harmonic oscillators in an adsorption system.

$$H_{anh} = sum\ of\ all\ anharmonic\ coupling \tag{2.41}$$

For the adatom case, there are both the adatom-surface stretching mode ("T mode") and substrate phonon modes, hence $i = (T, \{\vec{k}\sigma\})$ so that $H_0 = H_T + H_s$. As we mentioned above, we ignore the anharmonicity of the substrate here; therefore $H_{anh} = V_{anh}(z - a_z)$. This includes the anharmonic terms in the Taylor series expansion of the surface potential $V(z - a_z)$ about the equilibrium positions of both the adatom and the surface.

For a diatomic admolecule, there is an additional internal vibrational mode ("V mode"), compared to an a atomic adsorption system, and hence $i = (T, V, \{\vec{k}\sigma\})$ so that $H_0 = H_T + H_V + H_s$. We treat the internal molecular vibration as a harmonic

oscillator. Therefore, $U_{anh} = 0$ and $H_{anh} = V_{anh}(z - a_z - \frac{\mu}{m_1}\zeta)$. V_{anh} represents the anharmonic terms in the Taylor's expansion of the surface potential $V(z - a_z - \frac{\mu}{m_1}\zeta)$.

More precisely, in the above discussion

$$H_T = -\frac{\hbar^2}{2m}\frac{\partial^2}{\partial z^2} + V_0 + \frac{1}{2!}V_2 z^2, \tag{2.42}$$

$$H_V = -\frac{\hbar^2}{2\mu}\frac{\partial^2}{\partial \zeta^2} + U_0 + \frac{1}{2!}U_2 \zeta^2. \tag{2.43}$$

For an adatom,

$$\begin{aligned} H_{anh} &= V_{anh}(z - a_z), \\ &= {\sum_{l,m}}' \frac{1}{l!m!} V_{l+m}(-a_z)^l z^m. \end{aligned} \tag{2.44}$$

For a diatomic admolecule,

$$\begin{aligned} H_{anh} &= V_{anh}(z - a_z - \frac{\mu}{m_1}\zeta) \\ &= {\sum_{l,m,n}}' \frac{1}{l!m!n!} V_{l+m+n}(-a_z)^l (-\frac{\mu}{m_1}\zeta)^m z^n. \end{aligned} \tag{2.45}$$

Note that the local mode frequencies for the "T mode" and "V mode" are determined by $V_2 = m\omega_0^2$ and $U_2 = \mu\Omega^2$, respectively. Here ω_0 denotes the vibrational frequency of the "T mode", Ω denotes the internal vibrational frequency of the "V mode". The sum in Eqs. (2.44) and (2.45) excludes the harmonic terms $\frac{1}{2}V_2 z^2, \frac{1}{2}U_2\zeta^2$. The bilinear coupling between the adsorbate and the substrate phonons $-V_2 a_z z$ will be discussed in a nonperturbative treatment in Chapter 3. In this chapter, we include the bilinear coupling into the anharmonic hamiltonian and treat it as a perturbation.

2.4 Thermo field dynamics

In general, with the complete hamiltonian, we are able to calculate the time-ordered Green's function for a specific vibrational coordinate by using the well-known Matsubara method[63, 64]. In this method, all thermodynamics properties of a system can be directly expressed in terms of a time-ordered Green's function at a finite temperature. However, at finite temperature, it is inconvenient to calculate a time-ordered Green's function $D(t)$ directly, and it is necessary to introduce a corresponding temperature Green's function $\mathcal{D}(\tau)$ which depends on an imaginary-time variable $\tau = it$. Its perturbation expansion is very similar to that for the zero temperature Green's function. Wick's theorem then can be generalized to produce Feynmam diagrams to calculate the temperature Green's function in a diagrammatic analysis. The Lehman representation provides a direct connection between a time-ordered Green's function and its temperature Green's function in a finite temperature formalism. However, the complicated frequency summation makes the Feynman diagram calculation tedious and extremely difficult.

In our study, to avoid the complicated frequency summation, we use thermo field dynamics (TFD) instead of the Matsubara method to formulate the time-ordered Green's function for an adsorption system[65]. The TFD method was originally developed in the study of conventional bulk superconductivity. It has been used extensively in various fields such as magnetic and layered superconductivity[66]. Recently, TFD has been applied in the surface spectroscopy problems such as desorption[12]. Since TFD starts with the real-time formalism, zero-temperature field theory can be easily extended to finite temperatures. It has been shown that some of the techniques employed in zero temperature field theory such as Feynman diagrams

can be utilized in TFD. In our question, we study the vibrational states of an adsorption system which can be quantized as bosons. Therefore, we only discuss the time-ordered Green's function for bosons here in thermo field dynamics.

Boson fields at finite temperature can be obtained through a simple thermal Bogoliubov transformation from their zero temperature counterparts. The Fourier transform of the time-ordered Green's function at a finite temperature can be obtained in terms of this transformation of boson fields. All the temperature dependent calculations related to the time-ordered Green's function at a finite temperature then become transparent and systematically easy. We will show the details as follows.

2.4.1 Thermo-ground state and "tilde" field

Some basic elements of TFD theory are now introduced. Details are found in the text on this subject by Umezawa, Matsumoto, and Tachiki, and in earlier papers referenced there[65, 66].

In the harmonic approximation, the vibrational states of an adsorption system are the eigenstates of the harmonic oscillators in the system denoted by $|N_s) = \prod_i |N_i)$. Here i describes the normal modes of an adsorption system. The boson annihilation and creation operators $b_i, b_i^\dagger$ satisfy the boson commutation relation

$$[b_{i'}, b_i^\dagger] = \delta_{i,i'}. \tag{2.46}$$

When a quantum of energy $\hbar\omega_i$ is annihilated in the system, this process can be regarded as the action of an annihilation operator b_i.

We now associate with the boson field $b_i, b_i^\dagger$ a duplicate field or "tilde" field built

up from a duplicate set of boson operators $\tilde{b}_i$ and $\tilde{b}_i^\dagger$. Let's use the doublet notation

$$b_i^\alpha = \begin{pmatrix} b_i^1 \\ \\ b_i^2 \end{pmatrix} = \begin{pmatrix} b_i \\ \\ \tilde{b}_i^\dagger \end{pmatrix}, \tag{2.47}$$

where $\alpha = 1, 2$ denotes the original field and "tilde" field, respectively. The "tilde" field is introduced from the mathematical reasons which will be discussed later. At a finite temperature, the local vibrational mode of an adsorbate is not isolated but immersed in a thermal reservoir. The presence of the thermal reservoir maintains a certain number of excited particles. The absorption of energy by the vibrational mode i occurs in two ways: it is absorbed either by the excitation of an additional quanta $b_i^\dagger(\beta)$ or by the annihilation of a thermal hole described by $\tilde{b}_i(\beta)$. Hence, $b_i^\dagger$ is a linear combination of two thermal operations $b_i^\dagger(\beta)$ and $\tilde{b}_i(\beta)$ which are called thermal operators. Here $\beta = \hbar/k_B T$ is used to specify the temperature. Boson operators $b_i, b_i^\dagger$ and their thermal counterparts $\tilde{b}_i(\beta), \tilde{b}_i^\dagger(\beta)$ satisfy the same commutation relation. Therefore, the thermal field operators $b_i(\beta)$ and $\tilde{b}_i^\dagger(\beta)$ are related to the original boson field b_i and its duplicate field $\tilde{b}_i^\dagger$ by the Bogoliubov transformation, i.e.

$$\begin{pmatrix} b_i \\ \\ \tilde{b}_i^\dagger \end{pmatrix} = \begin{pmatrix} \cosh\theta_i & \sinh\theta_i \\ \\ \sinh\theta_i & \cosh\theta_i \end{pmatrix} \begin{pmatrix} b_i(\beta) \\ \\ \tilde{b}_i^\dagger(\beta) \end{pmatrix} = U_B(\omega) \begin{pmatrix} b_i(\beta) \\ \\ \tilde{b}_i^\dagger(\beta) \end{pmatrix}, \tag{2.48}$$

where $U_B(\omega)$ is called the Bogoliubov matrix, and θ_i is determined by the thermal average of the number operator n_i of the quanta in the system in terms of

$$\sinh\theta_i = n_i^{1/2} = \frac{1}{e^{\frac{\hbar\omega_i}{kT}} - 1}. \tag{2.49}$$

Therefore, the Bogoliubov matrix is $U_B(\omega) = \begin{pmatrix} c_B & d_B \\ \\ d_B & c_B \end{pmatrix}$ with $c_B = \cosh\theta_i =$

$(n_i + 1)^{1/2}$ and $d_B = \sinh\theta_i = n_i^{1/2}$. $U_B(\omega)$ depends on the vibrational frequency through the thermal average of the number operator n_i.

The inverse of the above transformation is

$$\begin{pmatrix} b_i(\beta) \\ \tilde{b}_i^{\dagger}(\beta) \end{pmatrix} = \begin{pmatrix} \cosh\theta_i & -\sinh\theta_i \\ -\sinh\theta_i & \cosh\theta_i \end{pmatrix} \begin{pmatrix} b_i \\ \tilde{b}_i^{\dagger} \end{pmatrix}. \tag{2.50}$$

Similar to the "tilde" field, we associate with the boson state $|N_s\rangle$ a "tilde" state $|\tilde{N}_s\rangle$ in a one to one correspondence. Define the thermal ground state (a ground state at a finite temperature)

$$|0(\beta)\rangle = \rho_s^{1/2} \sum_{N_s} |N_s\rangle|\tilde{N}_s\rangle, \tag{2.51}$$

where the thermal density matrix is $\rho_s = \frac{e^{-\beta H_0}}{Tr_s[e^{-\beta H_0}]}$, with H_0 being the harmonic hamiltonian of the adsorption system. The inclusion of the "tilde" states is crucial to the evaluation of the thermal expectation value

$$\begin{aligned} \langle 0(\beta)|\hat{A}(t)|0(\beta)\rangle &= \sum_{N_s}\sum_{N_s'} \langle N_s|\rho_s^{1/2}\hat{A}(t)\rho_s^{1/2}|N_s'\rangle\langle\tilde{N}_s|\tilde{N}_s'\rangle \\ &= \sum_{N_s} \langle N_s|\rho_s\hat{A}(t)|N_s\rangle \\ &= Tr[\rho_s\hat{A}(t)], \end{aligned} \tag{2.52}$$

where the term $\langle\tilde{N}_s|\tilde{N}_s'\rangle = \delta_{N_s,N_s'}$ reduces the double sum above to a single one, so that the trace formula for the thermal average of an operator can be expanded as an expectation value in the thermal ground state.

The thermal ground state satisfies

$$b_i(\beta)|0(\beta)\rangle = 0 = \tilde{b}_i(\beta)|0(\beta)\rangle. \tag{2.53}$$

This can be verified by combining the Bogoliubov transformation with the definition

of $|0(\beta)\rangle$ and ρ_s. The hamiltonian of the "tilde" field is $-\tilde{H}$. The negative sign reflects the fact that the thermal hole carries negative energy. $\tilde{H}$ can be obtained by the "tilde" operation (changing all real fields to their corresponding "tilde" fields and all complex coefficients to their complex conjugates) on the real fields in H. Then the total hamiltonian of an adsorption system is given by

$$\hat{H} = H - \tilde{H}. \tag{2.54}$$

The first part in above equation determines the equations of motion of real fields, while the second part determines the equations of motion of "tilde" fields.

The inverse Bogoliubov transformation gives

$$b_i|0(\beta)\rangle = \tanh\theta_i \tilde{b}_i^\dagger|0(\beta)\rangle, \tag{2.55}$$

which shows that the addition of the $\tilde{b}_i$-quantum to the ground state $|0(\beta)\rangle$ is equivalent to the elimination of the b_i-quantum. In this sense, the $\tilde{b}_i$-quantum behaves as a hole of the b_i-quantum. The Bogoliubov transformation also shows that the thermal field operators, $b_i(\beta)$ and $\tilde{b}_i(\beta)$, have independent physical roles. Consider for a moment the original phonon operators, b_i and $\tilde{b}_i$ acting on the thermal ground state. Since $|0(\beta)\rangle$ is the thermal equilibrium state of the system. It contains excited states, of course, so $b_i|0(\beta)\rangle \neq 0$ and $b_i^\dagger|0(\beta)\rangle \neq 0$. This means simply that it is possible to both annihilate an excitation of the phonon mode "i" contained in $|0(\beta)\rangle$, and to create an additional excitation of the phonon mode "i" in $|0(\beta)\rangle$. Actually, using the Bogoliubov transformation, we have

$$b_i|0(\beta)\rangle = \sinh\theta_i \tilde{b}_i^\dagger(\beta)|0(\beta)\rangle, \tag{2.56}$$

$$b_i^\dagger|0(\beta)\rangle = \sinh\theta_i b_i^\dagger(\beta)|0(\beta)\rangle. \tag{2.57}$$

This clearly tells us $b_i^\dagger(\beta)$ creates an additional phonon excitation when it operates

on $|0(\beta)\rangle$, while the "tilde" thermal operator $\tilde{b}_i^\dagger(\beta)$ annihilates phonon modes in $|0(\beta)\rangle$ by creating "thermal holes".

The equations of motion of the "tilde" fields are similar to those for the original fields. For example, the original boson annihilation operator b_i obeys the Heisenberg equation

$$i\hbar\frac{d}{dt}b_i t = [b_i(t), H_0], \tag{2.58}$$

which gives

$$b_i(t) = b_i e^{-i\omega_i t}, \tag{2.59}$$

by using $H_0 = \sum_i \hbar\omega_i(b_i^\dagger b_i + 1)$ and the boson commutation relation $[b_i(t), b_{i'}^\dagger(t)] = \delta_{i,i'}$. Similarly, the Heisenberg equation for $\tilde{b}_i$ has a negative sign in front of the time derivative which leads to

$$\tilde{b}_i(t) = \tilde{b}_i e^{i\omega_i t}. \tag{2.60}$$

The positive frequency associated with the "tilde" operator above is consistent with the earlier identification of $\tilde{b}_i^\dagger(\beta)$ with the creation of "thermal holes".

The discussion above has dealt specifically with the bosons in an adsorption system. The normal modes of this system in the harmonic approximation depends on the type of adsorbate and substrate. For an adatom, no "V mode" is present in the system. Hence $i = (T, \{\vec{k}\sigma\})$. For a diatomic admolecule, $i = (V, T, \{\vec{k}\sigma\})$. Correspondingly, the thermal ground state for an atomic adsorption system can be written as

$$|0(\beta)\rangle = |0(\beta_T)\rangle \prod_{\{\vec{k}\sigma\}} |0(\beta_{\vec{k}\sigma})\rangle, \tag{2.61}$$

while for an diatomic admolecule, the thermal ground state is given by

$$|0(\beta)\rangle = |0(\beta_V)\rangle|0(\beta_T)\rangle \prod_{\{\vec{k}\sigma\}} |0(\beta_{\vec{k}\sigma})\rangle, \tag{2.62}$$

Note the harmonic hamiltonian H_0 excludes the bilinear coupling between the "T mode" and the substrate phonons.

The theory described above is now applied to the time-ordered Green's function calculation.

2.4.2 Green's function

In thermo field dynamics, to simplify the notation, we introduced the thermal doublet symbol for the boson field in Eq. (2.47). Hence the propagators of vibrational coordinates are 2×2 matrixes. The time-ordered Green's function of the vibrational coordinate z (for the "V-mode", this coordinate becomes ζ) in an adsorption system in Heisenberg picture can be written as

$$iD^{\alpha\beta}(t) = \langle 0(\beta)|Tz^{\alpha}(t)z^{\beta}(0)|0(\beta)\rangle, \tag{2.63}$$

where T is the time-ordering operator, z^{α} is the Heisenberg operator. Green's function is an expectation value in the thermal ground state. The (1,1) component of the time-ordered Green's function in thermo field dynamics corresponds to the time-ordered Green's function defined in Eq. (1.3). The thermal ground state $|0(\beta)\rangle$ of an adsorption system is constructed by the thermal ground states of all vibrational states in the adsorption system. The total hamiltonian of an adsorption system is

$$\begin{aligned} \hat{H} &= H - \tilde{H} \\ &= H_0 + H' - \tilde{H}_0 - \tilde{H}' \\ &= \hat{H}_0 + \hat{H}', \end{aligned} \tag{2.64}$$

where $\hat{H}_0$ is the harmonic hamiltonian. We require that $\hat{H}$ is weakly equal to the $\hat{H}_0$ so that the anharmonic hamiltonian $\hat{H}'$ can be treated as a perturbation.

Corresponding to the $\hat{H}_0$ hamiltonian, the bare propagator of the vibrational coordinate z in TFD is defined as

$$iD_0^{\alpha\beta}(t) = \langle 0(\beta)|Tz_0^{\alpha}(t)z_0^{\beta}(0)|0(\beta)\rangle. \tag{2.65}$$

It is the propagator for the non-interacting boson field $z(t)$. The Heisenberg operator $z_0^{\alpha}(t)$ is related to the thermal operator $z_0^{\alpha}(t,\beta)$ via the Bogoliubov transformation given by Eq. (2.48). Therefore, after some simplification (see Appendix B for details), the bare propagator in ω-space in TFD can be written as

$$D_0(\omega) = U_B d_0(\omega,\beta)U_B^{\dagger}, \tag{2.66}$$

where we have ignored the indices α,β. The thermal Green's function in ω-space $d_0(\omega,\beta)$ is defined as the Fourier transform of the propagator

$$id_0^{\alpha\beta}(t) = \langle 0(\beta)|Tz^{\alpha}(t,\beta)z^{\beta}(0,\beta)|0(\beta)\rangle, \tag{2.67}$$

and is given by

$$d_0(\omega,\beta) = \frac{\hbar\tau}{2m\omega_0}\left(\frac{1}{\omega-\omega_0+i\eta\tau} - \frac{1}{\omega+\omega_0-i\eta\tau}\right), \tag{2.68}$$

where ω_0 is the vibrational frequency of the local mode with vibrational coordinate $z(t)$, η is real, positive and infinitesimal, and $\tau = \begin{pmatrix} 1 & 0 \\ 0 & -1 \end{pmatrix}$. Note that the Bogoliubov matrix U_B is not unitary, but it satisfies the relation $U_B\tau U_B = \tau$. Now, we can write

$$D_0(\omega) = \frac{\hbar}{m}\frac{\tau}{\omega^2-\omega_0^2} - i\pi\sigma_c^0(\omega)U_B(\omega)U_B(\omega), \tag{2.69}$$

with $\sigma_c^0(\omega) = \frac{\hbar}{2m\omega_0}[\delta(\omega-\omega_0)+\delta(\omega+\omega_0)]$ which is the spectral function of the bare propagator $D_0(t)$. This free Green's function has a resonance at $\omega \sim \omega_0$. The δ function in the imaginary part of the bare Green's function represents a sharp peak at $\omega = \omega_0$ for the single harmonic oscillator with the frequency ω_0.

The spectral representation of the full Green's function requires that the full Green's function has the same form as the bare Green's function, i.e.[67]

$$D(\omega) = ReD(\omega)\tau - i\pi\sigma_c(\omega)U_B(\omega)U_B(\omega), \tag{2.70}$$

where $\sigma_c(\omega)$ is the spectral function of the full Green's function in ω-space $D(\omega)$ which will be given in Appendix C.

The relation given in Eq. (2.66) for the bare propagator is also true for the full Green's function.

2.4.3 Dyson's equation

In the interaction picture, the full Green's function defined in Eq. (2.63) becomes

$$iD^{\alpha\beta}(t) = \langle 0(\beta)|TSz_0^\alpha(t)z_0^\beta(0)|0(\beta)\rangle, \tag{2.71}$$

where the S matrix can be expanded in the powers of the interaction hamiltonian $\hat{H}' = H' - \tilde{H}'$ in TFD as follows

$$\begin{aligned} S &= T\left\{exp\left[\frac{1}{i\hbar}\int_{-\infty}^{\infty} dt\hat{H}'(t)\right]\right\} \\ &= \sum_{n=0}^{\infty}\frac{1}{n!}(\frac{1}{i\hbar})^n\int_{-\infty}^{\infty} d\tau_1 d\tau_2 ... d\tau_n T\left[\hat{H}'(\tau_1)\hat{H}'(\tau_2)...\hat{H}'(\tau_n)\right]. \end{aligned} \tag{2.72}$$

Note that H' and $\tilde{H}'$ in $\hat{H}'$ are given by the vibrational fields and their "tilde" counterparts, respectively. Furthermore, the vibrational fields and their "tilde" counterparts are linear combinations of the annihilation and creation thermal operators

and their thermal "tilde" operators as defined by the Bogoliubov transformation. Wick's theorem is therefore applicable in terms of the vibrational fields. This leads to a standard Feynman diagram expansion which can be formally summed to yield an integral equation called Dyson's equation shown in Fig. (2.3). Double (single)

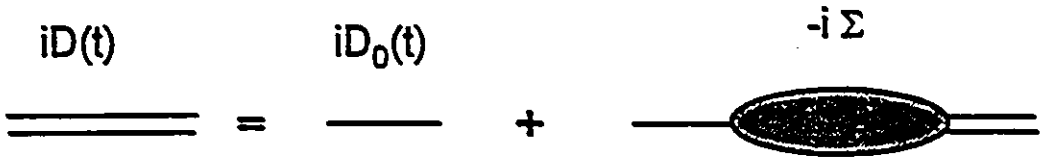

Figure 2.3: Dyson's equation.

lines in Fig. (2.3) are the full (bare) Green's function and the shaded oval is the proper self energy insertion which is the summation of various dynamic processes. The Feynman diagram rules will be given in Appendix D. In ω-space, the Dyson's equation given in Fig. (2.3) reads

$$D^{\alpha\beta}(\omega) = D_0^{\alpha\beta}(\omega) + D_0^{\alpha a}(\omega)\Sigma^{ab}(\omega)D^{b\beta}(\omega). \tag{2.73}$$

In principle, the calculation of the full Green's function now amounts to

1. evaluating the self energy corrections to the desired accuracy;

2. solving the Dyson's equations for the vibrational propagators.

In practice, we only keep the first few terms in the Taylor's expansion of H_{anh} and calculate their lowest corrections to the self energy. Since the anharmonic hamiltonian H_{anh} is a power expansion of all vibrational coordinates in an adsorption system and they are small quantities, the higher order terms of these coordinates are expected to provide small, quantitative corrections to the vertex functions, but

will not cause qualitative differences. In perturbation theory, the full hamiltonian is close to the harmonic hamiltonian H_0, hence the higher order corrections to self energy are small. Usually we only take the lowest order into account.

2.4.4 Solution of Dyson's equation

The solution of Dyson's equation given by Eq. (2.73) will give us the time-ordered Green's function in ω-space. The imaginary part of its (1,1) component will give the line shape. In the limits $kT \ll \hbar\omega_0$, and $|\omega - \omega_0| \ll \omega_0$, the vibrational line shape has the form

$$\frac{\Delta I(\omega)}{I_0} \propto ImD^{11}(\omega) \sim \frac{\hbar}{2m\omega_0} \frac{\Gamma}{(\omega - \omega_0 - \Delta\omega)^2 + \Gamma^2} \tag{2.74}$$

where the real frequency shift $\Delta\omega$ and the line width Γ (half width at half maximum) are given in terms of the real and imaginary parts of the self energy of an adsorption system.

Combining Dyson's equation given by Eq. (2.73) and the spectral representation of the Green's functions given by Eqs. (2.69) and (2.70) requires that the self energy $\Sigma^{\alpha\beta}(\omega)$ has the form (see Appendix E)[67]

$$\Sigma^{\alpha\beta}(\omega) = Re\Sigma(\omega)\tau^{\alpha\beta} - i\sigma(\omega)[U_B^{-1}(\omega)U_B^{-1}(\omega)]^{\alpha\beta}, \tag{2.75}$$

where

$$\begin{aligned} \Sigma(\omega) &= \Sigma^{11}(\omega), \\ \sigma(\omega) &= -U_B(\omega)Im\Sigma(\omega)U_B(\omega). \end{aligned} \tag{2.76}$$

Taking this form of the self energy into account and solving the 2×2 Dyson's equation

matrix gives (as shown by Ye[67])

$$\begin{aligned} D(\omega) &= \frac{\left[\frac{m}{\hbar}(\omega^2-\omega_0^2)-Re\Sigma\right]\tau+i\sigma U_B^2}{\left[\frac{m}{\hbar}(\omega^2-\omega_0^2)-Re\Sigma\right]^2+\sigma^2} \\ &= U_B d(\omega,\beta)U_B, \end{aligned} \tag{2.77}$$

where the thermal Green's function has form

$$d(\omega,\beta)=\frac{\tau}{\frac{m}{\hbar}(\omega^2-\omega_0^2)-Re\Sigma-i\sigma\tau}. \tag{2.78}$$

At resonance,

$$\begin{aligned} \omega &\approx \omega_0+\frac{\hbar}{2m\omega_0}Re\Sigma(\omega)+i\frac{\hbar}{2m\omega_0}\sigma\tau \\ &= \omega_R+i\Gamma\tau, \end{aligned} \tag{2.79}$$

where the real part represents the line position or shifted frequency, and gives us the line shift $\Delta\omega=\omega_R-\omega_0$ which is given by the real part of the self energy, while the imaginary part represents the inverse of the lifetime of the vibrational mode or the line width which is given by the imaginary part of the self energy, i.e.

$$\begin{aligned} \Delta\omega &= \omega_R-\omega_0 \\ &= \frac{\hbar}{2m\omega_0}Re\Sigma(\omega_R) \end{aligned} \tag{2.80}$$

$$\begin{aligned} \Gamma &= \frac{\hbar}{2m\omega_0}\sigma(\omega_R) \\ &= -\frac{\hbar}{2m\omega_0}U_B(\omega_R)Im\Sigma(\omega_R)U_B(\omega_R). \end{aligned} \tag{2.81}$$

In summary, we have shown that the self energy is an important part in the line shape calculation. Both the line shift and the line width are related to the self energy. For a vibrational mode, its self energy depends on its interactions with the other modes in the system. The Feynman diagram rules provide a tool to calculate the self energy. In the next chapter, we will apply the theory above to some sample systems.

Chapter 3. The treatments of bilinear coupling

3.1 Introduction

Now we apply the theory introduced in the last chapter to a specific local mode of the adsorbate at ontop sites. In this study, the bilinear coupling between the molecular or atomic vibration of the adsorbate and the surface phonon vibrations plays an important role. Treating this coupling differently can lead to contrasting results for the same system. In this chapter, we will show two treatments of this bilinear coupling and discuss the results from both treatments.

Firstly, for simplicity without losing the main components of the line shape theory, we include the bilinear coupling between the local mode and the substrate phonons into the anharmonic hamiltonian, treat it as a perturbation in Section 3.2. The perturbative treatment of the bilinear term makes the harmonic hamiltonian simple, obvious and exactly solvable. In this way, we can easily demonstrate our theory and summarize the Feymman diagram rules in the self energy calculation. The same treatment has been considered by other people[54, 27, 55, 57] using Fermi's Golden Rule or a master equation to calculate the line shape. In the last chapter, we did not actually calculate the self energy which determines the vibrational line shape. Here we will concentrate on the self energy expansion and consider the line shape contributions of some specific dynamic processes. However, this approximation is limited due to the strength of the bilinear term and has to be improved. Since the line shape of the internal vibrational mode ("V mode") of a diatomic admolecule due

to the exchange mechanism is very much dependent on the line shape of adsorbate-surface stretching mode ("T mode"), we will study the "T mode" line shape first and then the "V mode" in a similar way.

Secondly, we will show the improvement in the line shape calculation by including the bilinear term into the harmonic hamiltonian and treating it nonperturbatively, as described in Section 3.3. The so-called "reduction factor" induced by this improvement will reduce phonon effects on the vibrational line shape due to the anharmonicity of the adsorption potential in this adsorption situation. On the other hand, the anharmonicity of the substrate will result in an additional phonon contribution to the line shape. The nonperturbative treatment of the bilinear term was previously introduced by Piercy and Ye[59] using TFD. We extend their work to include the combined effects of both the adsorption potential and the anharmonicity of substrate on the vibrational line shape. Since the bilinear term will mostly affect the "T mode", we thus concentrate on the "T mode" line shape in the revised line shape formalism.

In this chapter, the substrate phonons are described by the simplest model for the substrate – a bulk Debye model introduced in Section 2.3.2. At this stage, we would rather emphasize the basic features of the relaxation mechanisms in an adsorption system than go into the details of the substrate.

Finally, we will apply the line shape theory to a model system in Section 3.4.

3.2 The perturbative treatment of the bilinear term and its limitations

In this section, we study the vibrational line shape of an admolecule at an ontop site in a one dimensional model using the perturbative treatment of the bilinear term. In this treatment, at the harmonic level, the vibrations of an admolecule and the substrate phonons are independent simple harmonic oscillators. Their hamiltonians are given by Eqs. (2.39), (2.42) and (2.43) in Chapter 2, respectively. The solutions of these harmonic hamiltonians will give the normal modes with the vibrational coordinates a^0, z^0 and ζ^0, respectively. The time-ordered Green's functions of these coordinates at a given temperature are easy to calculate as bare propagators given in Appendix B. The general form of the anharmonic hamiltonian has been given in Eq. (2.44) or Eq. (2.45) in Chapter 2 depending on the adsorption system. All dynamic processes due to the anharmonic interactions among the localized and delocalized modes can be expanded in terms of the different combinations of the bare propagators. However, this treatment assumes that the bilinear term is much smaller than the harmonic term which is not true in this case. We will take this fact into account in the next section. The results of this section will be modified by including the bilinear term into the harmonic hamiltonian there. Nevertheless, it is still worth while to study the perturbation treatment in TFD based on this simple model, to calculate the vibrational line shape due to different relaxation mechanisms such as elastic phonon scattering, exchange mechanism and "cross term" between them which have been considered in different methods by other people[54, 17, 4].

3.2.1 The "T mode" vibrational line shape

We start with the line shape of the adsorbate-surface stretching mode ("T mode"). The anharmonic hamiltonian for a diatomic admolecule case in the one dimensional model are given by Eq. (2.45) in Chapter 2. There we have limited the molecule to motion perpendicular to surface and ignored all the lateral motion and rotations of the adsorbate and substrate atoms. Since the frequency of the internal vibrational mode ("V mode") Ω is much higher than the frequency of the admolecule-surface stretching mode ("T mode") ω_0, we therefore can ignore the effect of the "V mode" on the "T mode" line shape, i.e., all terms with the internal vibrational coordinate ζ can be ignored when we consider the "T mode" line shape. The "T mode" is then broadened and shifted by its interactions with the phonon bath, and the self interaction terms with form $\frac{1}{n!}V_n z^n$. Hence the anharmonic terms contributing to the "T mode" line shape for a diatomic admolecule are same as those for an adatom given by Eq. (2.44) in Chapter 2 in this model. Therefore, from now on, when we study the "T mode" line shape, we treat an admolecule as an adatom by ignoring the internal motion of the admolecule. Its displacement (as a whole) is described by the displacement of its center of mass.

We only consider the anharmonic terms up to the 4^{th} derivative of the adsorption potential, i.e.

$$H_{anh} \approx -V_2 a_z z + \frac{1}{3!}V_3(z-a_z)^3 + \frac{1}{4!}V_4(z-a_z)^4. \tag{3.1}$$

In this treatment, we have one localized vibrational coordinate z for the "T mode" and the delocalized phonon vibrational coordinate a_z for the perpendicular displacement of the surface atom at the on top site underneath the adatom. At very low

temperature, the substrate surface is nearly static, i.e., The displacements of the surface atoms $a_z \approx 0$. The adsorption potential is a function of the localized vibrational coordinate z and can be expanded in powers of z.

Define the free Green's function or bare propagators for z and a_z as

$$iD_T^{0,\alpha\beta}(t) = \langle Tz^{0,\alpha}(t)z^{0,\beta}(0)\rangle, \tag{3.2}$$

$$iB^{0,\alpha\beta}(t) = \langle Ta_z^{0,\alpha}(t)a_z^{0,\beta}(0)\rangle, \tag{3.3}$$

represented by the dashed lines and the wavy lines in the Feyman diagram expansion, respectively. $(\alpha,\beta) = (1,2)$ are the doublet notation for a boson operator defined by in Eq. (2.47) in Chapter 2. With the anharmonic hamiltonian given by Eq. (3.1) above, the lowest order contributions to the "T mode" self energy Σ_T can be expanded by using Feymman diagram techniques in terms of the bare propagators $D_T^{0,\alpha\beta}(t)$ and $B^{0,\alpha\beta}(t)$. According to the diagram expansion rules, the proper self energy insertion is given by diagrams in Fig. (3.1), where we only include the

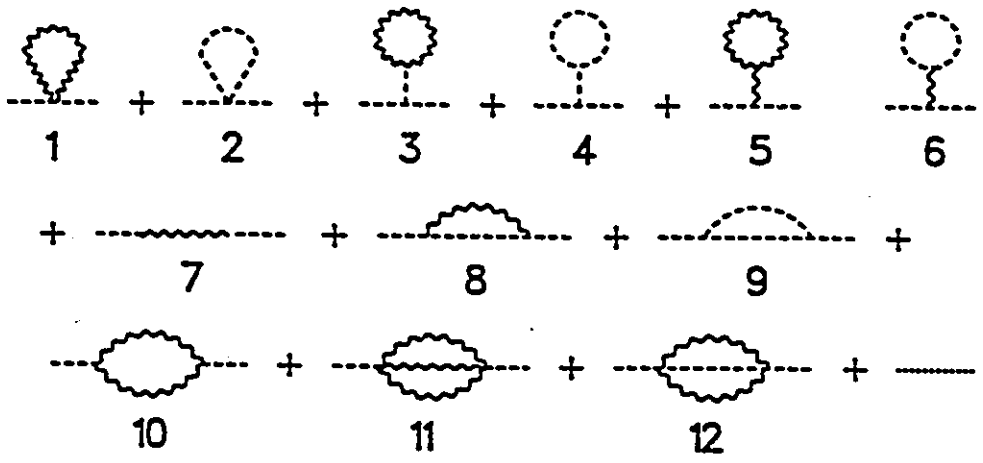

Figure 3.1: "T mode" self energy expansion for an adatom at an ontop site.

diagrams with one and two vertices.

The "T mode" line shift and line width in TFD

We start our discussion with the line shift. In principal, all the self energy diagrams with non zero real part will contribute to the line shift. However, the lower order terms shown in the diagrams 1 to 6 in Fig. (3.1) are expected to dominate the contribution.

The first two diagrams contain only a single vertex due to the anharmonic interactions $\frac{1}{4}V_4 a_z^2 z^2$ and $\frac{1}{4!}V_4 z^4$. Note $V_4 > 0$. They both give blue shifts. The first diagram can be interpreted as follows. The displacements of the substrate phonon modes change very slowly with time compared to that of the "T mode" since in most cases substrate phonon frequencies $\{\omega_k\} < \omega_0$. In a very short time duration, we can approximately take a_z as a constant, then the anharmonic interaction $\frac{1}{4}V_4 a_z^2 z^2$ will just add an extra factor to the harmonic coupling constant $m\omega_0^2$ and enlarge the "T mode" vibrational frequency ω_0 so that we say this diagram gives a blue shift. The explicit calculation gives,

$$\Delta\omega_1 = \frac{3V_4\hbar}{8mM_s\omega_0\omega_D{}^3}\int_0^{\omega_D} d\omega\omega(2n_\omega + 1), \tag{3.4}$$

where we have used the replacement

$$\sum_{\vec{k}\sigma} |e^z_{\vec{k}\sigma}|^2 \to \frac{3N_s}{\omega_D{}^3}\int_0^{\omega_D} d\omega\omega^2, \tag{3.5}$$

by assuming a bulk Debye model for the substrate phonons and assuming $\omega_{\vec{k}\sigma}$ is independent of the phonon polarization σ. The same replacement will be used in the following calculation. The second diagram gives a similar line shift

$$\Delta\omega_2 = \frac{V_4\hbar}{8m^2\omega_0{}^2}(2n_{\omega_0} + 1), \tag{3.6}$$

The diagrams 3 to 6 have two vertices due to the different combinations of

the anharmonic interactions $-\frac{1}{2}V_3 a_z z^2$, $\frac{1}{2}V_3 z a_z^2$, $\frac{1}{6}V_3 z^3$ and $-\frac{1}{6}V_3 a_z^3$. The propagator connecting the two vertices in these diagrams is evaluated at zero frequency which is required by energy conservation at each vertex. The self energies contributed by these diagrams have only real parts and give red shifts to the vibrational frequency. The actual shifts due to the diagrams 3 to 6 depend on the propagators connecting two vertices and the propagator loops and are given by

$$\Delta\omega_3 = -\frac{3\hbar V_3^2}{8m^2 M_s \omega_0{}^3 \omega_D{}^3}\int_0^{\omega_D} d\omega\omega(2n_\omega+1), \tag{3.7}$$

$$\Delta\omega_4 = -\frac{\hbar V_3^2}{8m^3\omega_0{}^4}(2n_{\omega_0}+1), \tag{3.8}$$

$$\Delta\omega_5 = -\frac{9\hbar V_3^2}{8mM_s^2\omega_0\omega_D{}^5}\int_0^{\omega_D} d\omega\omega(2n_\omega+1), \tag{3.9}$$

$$\Delta\omega_6 = -\frac{3\hbar V_3^2}{8m^2 M_s \omega_0{}^2\omega_D{}^2}(2n_{\omega_0}+1). \tag{3.10}$$

Diagrams 8, 9 and 10 in Fig. (3.1) also have two vertices but due to the anharmonic interactions $\frac{1}{2}V_3 a_z z^2$, $\frac{1}{6}V_3 z^3$ and $\frac{1}{2}V_3 a_z^2 z$, respectively. The two vertices are the same in each self energy diagram of diagrams 8, 9 and 10. The shifts contributed by diagrams 8 and 9 are always negative, while the shift contributed by diagram 10 is always positive for $\omega_0 > 2\omega_D$. The actual shifts due to these diagrams are

$$\Delta\omega_8 = -\frac{3\hbar V_3^2}{8m^2 M_s \omega_0{}^2\omega_D{}^3}\int_0^{\omega_D} d\omega\omega n_\omega\left(\frac{1}{2\omega_0-\omega}+\frac{1}{2\omega_0+\omega}\right), \tag{3.11}$$

$$\Delta\omega_9 = -\frac{\hbar V_3^2}{12m^3\omega_0{}^4}(2n_{\omega_0}+1), \tag{3.12}$$

$$\Delta\omega_{10} = \frac{9\hbar V_3^2}{8mM_s^2\omega_0\omega_D{}^6}\int_0^{\omega_D} d\omega_1 d\omega_2\omega_1\omega_2(2n_{\omega_1}+1) \left[\frac{\omega_2-\omega_1}{\omega_0{}^2-(\omega_2-\omega_1)^2}+\frac{\omega_2+\omega_1}{\omega_0{}^2-(\omega_2+\omega_1)^2}\right]. \tag{3.13}$$

These are principal value integrals. It is easy to see that the temperature dependence of each frequency shift contribution is contained either in the delocalized phonon

mode or the localized phonon mode occupation number at equilibrium. This dependence becomes linear at the high temperature region.

The shift contributed by diagram 7 is temperature independent and therefore ignored here since we are considering the temperature dependent line shifts.

The shifts contributed by the two-vertex diagrams 11 and 12 due to the interaction $\frac{1}{6}V_4 a_z^3 z$ and $\frac{1}{4}V_4 a_z^2 z^2$ are expected to be small and therefore neglected. Note that the line shifts contributed by the self energy diagrams 2, 4 and 9 are purely due to the self interactions of the local mode of the form $\frac{1}{n!}V_n z^n$ with $n \geq 3$.

In this treatment, the low order contributions to the line width of the "T mode" are given by the imaginary parts of the two-vertex diagrams 7, 8, 10, 11 and 12 in Fig. (3.1). Diagrams 7, 10 and 11 describe the excitation of the local mode by absorbing one, two or three phonons from the thermal phonon bath and de-excitation of the local mode by emitting one, two or three phonons to the thermal phonon bath, due to the couplings $-V_2 a_z z, \frac{1}{2}V_3 a_z^2 z$ and $-\frac{1}{6}V_4 a_z^3 z$, respectively. One phonon emission process will contribute to the line width only if the vibrational frequency ω_0 of the adsorbate-surface stretching mode is less than the maximum phonon frequency ω_D of the substrate. The physisorption system CO/NaCl(100) is an example of this case[68, 69, 70]. The two phonon emission processes are important in the adsorption system for which the local mode vibrational frequency ω_0 lies between the maximum phonon frequency ω_D and $2\omega_D$ in this purely perturbative treatment. One example is the chemisorption system CO/Ni(100) at an ontop site with $\omega_0 \approx 1.7\omega_D$[52]. Similarly, three phonon emission processes are nonnegligible when the local mode vibrational frequency ω_0 lies between $2\omega_D$ and $3\omega_D$. The chemisorption system CO/Pt(111) at an ontop site with $\omega_0 \approx 2.3\omega_D$ is one example of this kind[71].

According to the Feymman diagram rules given in Appendix D, the "T mode"

line widths (half width at half maximum) contributed by these phonon emission processes are given by

$$\Gamma_{T7} = \frac{3\pi V_2^2}{4m_s M_s \omega_D{}^3}\theta(\omega_D - \omega_0), \tag{3.14}$$

$$\Gamma_{T10} = \frac{9\pi\hbar V_3^2}{16mM_s^2\omega_0\omega_D{}^6}\int_0^{\omega_D} d\omega\omega(\omega_0-\omega)(n_\omega + n_{\omega_0-\omega}+1) \times\theta(\omega_D-\omega_0+\omega)\theta(\omega_0-\omega), \tag{3.15}$$

$$\Gamma_{T11} = \frac{9\pi\hbar^2 V_4^2}{32mM_s^3\omega_0\omega_D{}^9}\int_0^{\omega_D} d\omega_1 d\omega_2\omega_1\omega_2(\omega_0-\omega_1-\omega_2) \times[(n_{\omega_1}+1)(n_{\omega_2}+1)(n_{\omega_0-\omega_1-\omega_2}+1) - n_{\omega_1}n_{\omega_2}n_{\omega_0-\omega_1-\omega_2}] \times\theta(\omega_D-\omega_0+\omega_1+\omega_2)\theta(\omega_0-\omega_1-\omega_2). \tag{3.16}$$

They are the thermal averages of the transition rates for emitting one, two or three phonons to the phonon bath from all local mode excited states minus the thermal averages of the transition rates for absorbing one, two or three phonons from the phonon bath. Γ_{T10} and Γ_{T11} involve a single and double integral, respectively, over the substrate phonon frequencies which are in the range $0 < \omega < \omega_D$. The step function $\theta(\omega)$ insures that the phonon frequencies are in this range.

Diagram 12 in Fig. (3.1) represents a dephasing process which may be interpreted as elastic phonon scattering by the "T mode" of an adsorbate due to the anharmonic interaction $\frac{1}{4}V_4 a_z^2 z^2$. The phonon wave vector will not change its magnitude but only its direction during this process, as is required by energy conservation. The line width contributed by this diagram is given by

$$\Gamma_{T12} = \frac{9\pi\hbar^2 V_4^2}{16m^2M_s^2\omega_0^2\omega_D{}^6}\int_0^{\omega_D} d\omega\omega^2 n_\omega(n_\omega+1). \tag{3.17}$$

Diagram 8 in Fig. (3.1) represents the absorption or emission of a soft phonon ($\omega_k \approx 0$) by the "T mode" of the adsorbate due to the anharmonic interaction $-\frac{1}{2}V_3 a_z z^2$. Applying the Feymann diagram rules gives the line width contributed

by this process as

$$\Gamma_{T8} = \frac{3\pi\hbar V_3^2}{8m^2 M_s \omega_0^2 \omega_D{}^2} \frac{T}{T_D}, \tag{3.18}$$

where T_D is the Debye temperature of the substrate solid. This width is a linear function of temperature. As the temperature increases, the width gets unreasonably large due to the mistreatment of the bilinear coupling. This gives us an indication that we need to include the bilinear coupling into the harmonic hamiltonian.

The total line width of the "T mode" will be the sum of the contributions from all the self energy diagrams considered above. Each diagram represents a dynamical process and plays a different role for a particular adsorption system. We will discuss this in terms of the numerical calculation for a sample system in Section 4. The "T mode" line width will enter the "V mode" line width calculation only when the exchange mechanism is considered.

A simple treatment of the line shift by time-independent, quantum mechanical perturbation theory

In order to give a more intuitive picture about the "T mode" line shift, we now show an alternative derivation of some line shift contributions using the time independent perturbation theory in quantum mechanics. In quantum mechanics, up to the second order, the energy correction of an energy level E_i due to a time independent perturbation H' is given by

$$\Delta E_i = \langle i|H'|i\rangle + \sum_j{}' \frac{\langle i|H'|j\rangle\langle j|H'|i\rangle}{E_i^0 - E_j^0}, \tag{3.19}$$

where $\langle i|H'|j\rangle$ is a matrix element, $|i\rangle$ and E_i^0 are the eigenstate and eigen energy of the harmonic potential. The sum Σ' excludes the terms $j = i$. In the presence of

a thermal phonon bath, this energy correction needs to be evaluated as a thermal average over all the thermal phonon states $|\{\vec{k}\sigma\})$ of the substrate, i.e.

$$\Delta E_i = \sum_{\{\vec{k}\sigma\}} \rho(\{\vec{k}\sigma\}) \left[\langle i|\langle\{\vec{k}\sigma\}|H'|\{\vec{k}\sigma\}\rangle|i\rangle + \sum_j{}' \frac{\langle i|\langle\{\vec{k}\sigma\}|H'|\{\vec{k}\sigma\}\rangle|j\rangle\langle j|\langle\{\vec{k}\sigma\}|H'|\{\vec{k}\sigma\}\rangle|i\rangle}{E_i^0 - E_j^0} \right] \tag{3.20}$$

Now let us look at some examples in this simple picture. First, we take one term $H' = \frac{1}{4}V_4 a_z^2 z^2$ in the anharmonic hamiltonian given in Eq. (3.1) and calculate the energy correction it gives to the energy level E_i. The lowest order energy correction to the energy level E_i is

$$\begin{aligned} \Delta E_i &= \sum_{\{\vec{k}\sigma\}} \rho(\{\vec{k}\sigma\}) \langle i|\langle\{\vec{k}\sigma\}|\frac{1}{4}V_4 a_z^2 z^2|\{\vec{k}\sigma\}\rangle|i\rangle \\ &= \sum_{\{\vec{k}\sigma\}} \rho(\{\vec{k}\sigma\}) \frac{1}{4}V_4 \langle\{\vec{k}\sigma\}|a_z^2|\{\vec{k}\sigma\}\rangle\langle i|z^2|i\rangle \\ &= \frac{3V_4\hbar^2}{16mM_s\omega_0{\omega_D}^3}(2i+1)\int_0^{\omega_D} d\omega\omega(2n_\omega+1). \end{aligned} \tag{3.21}$$

Therefore, the spacing between the energy levels E_i and E_{i+1} in considering the perturbation of $H' = \frac{1}{4}V_4 a_z^2 z^2$ is

$$\begin{aligned} E_{i+1} - E_i &= E_{i+1}^0 + \Delta E_{i+1} - E_i^0 - \Delta E_i \\ &= \hbar\omega_0 + \frac{3V_4\hbar^2}{8mM_s\omega_0{\omega_D}^3}\int_0^{\omega_D} d\omega\omega(2n_\omega+1), \end{aligned} \tag{3.22}$$

which gives a blue shift from the harmonic energy level spacing $\hbar\omega_0$ of the local mode. The corresponding frequency shift is same as that given by Eq. (3.4) and corresponds to the shift contribution of the self energy diagram 1 in Fig. (3.1).

Secondly, we take two terms $H' = \frac{1}{2}V_3 a_z^2 z + \frac{1}{6}V_3 z^3$ in the anharmonic hamiltonian given in Eq. (3.1) and calculate the energy correction due to the cross term of these

two terms to the energy level E_i. In quantum mechanics, this corresponds to the second order energy correction given by the second term in Eq. (3.20) and can be calculated as follows:

$$\begin{aligned}
\Delta E_i &= \sum_{\{\vec{k}\sigma\}} \rho(\{\vec{k}\sigma\}) \frac{1}{12} V_3^2 \\
&\quad \left[\sum_j{}' \frac{\langle i|(\{\vec{k}\sigma\}|a_z^2 z|\{\vec{k}\sigma\})|j\rangle\langle j|(\{\vec{k}\sigma\}|z^3|\{\vec{k}\sigma\})|i\rangle}{E_i^0 - E_j^0} \right. \\
&\quad \left. + \frac{\langle i|(\{\vec{k}\sigma\}|z^3|\{\vec{k}\sigma\})|j\rangle\langle j|(\{\vec{k}\sigma\}|a_z^2 z|\{\vec{k}\sigma\})|i\rangle}{E_i^0 - E_j^0} \right] \\
&= \sum_{\{\vec{k}\sigma\}} \rho(\{\vec{k}\sigma\}) \frac{1}{12} V_3^2 \left[\sum_j{}' \frac{\langle\{\vec{k}\sigma\}|a_z^2|\{\vec{k}\sigma\}\rangle\langle i|z|j\rangle\langle j|z^3|i\rangle}{E_i^0 - E_j^0} \right. \\
&\quad \left. + \frac{\langle\{\vec{k}\sigma\}|a_z^2|\{\vec{k}\sigma\}\rangle\langle i|z^3|j\rangle\langle j|z|i\rangle}{E_i^0 - E_j^0} \right] \\
&= -\frac{3\hbar^2 V_3^2}{16 m^2 M_s \omega_0{}^3 \omega_D{}^3} (2i+1) \int_0^{\omega_D} d\omega \omega (2n_\omega + 1). \qquad (3.23)
\end{aligned}$$

Therefore, the energy spacing between levels E_i and E_{i+1} is

$$\begin{aligned}
E_{i+1} - E_i &= E_{i+1}^0 + \Delta E_{i+1} - E_i^0 - \Delta E_i \\
&= \hbar\omega_0 - \frac{3\hbar^2 V_3^2}{8 m^2 M_s \omega_0{}^3 \omega_D{}^3} \int_0^{\omega_D} d\omega \omega (2n_\omega + 1), \qquad (3.24)
\end{aligned}$$

which gives a red shift from the harmonic energy level spacing $\hbar\omega_0$ of the local mode, indicated by the negative sign. The corresponding frequency shift is the same as that given by Eq. (3.7) and corresponds to the shift contribution of the self energy diagram 3 in Fig. (3.1).

In analogy to the above discussion, we find that all the self energy diagrams with the same shape as diagram 1 in Fig. (3.1) give blue shifts, while all self energy diagrams with same shape as diagram 3 in Fig. (3.1) give red shifts.

Some of the anharmonic terms in Eq. (3.1) are purely due to the local mode self interactions in form $\frac{1}{n!}V_n z^n$ without the presence of the thermal phonon coordinate. Thermal average over the local mode states will be involved in the line shift calculation. We will now extend the present intuitive picture about the line shift calculation in terms of a one mode Green's function to show the thermal average over the local mode states in the following.

The one-mode Green's function of the local vibration

The line shifts we have calculated in Eqs. (3.6), (3.8) and (3.12) are due to the anharmonic self interaction terms of the local mode: $\frac{1}{3!}V_3 z^3$ and $\frac{1}{4!}V_4 z^4$. Their sum represents the thermal average of the frequency shift from the harmonic frequency of the harmonic oscillator. However, without the presence of the thermal phonon bath, all the self interaction terms together with the harmonic term $\frac{1}{2}V_2 z^2$ give a series of non equally spaced discrete energy levels as shown in terms of the bound states labeled by the index j in Fig. (2.2). In other words, instead of one peak broadened and shifted by the local mode self interactions, there are a series of discrete peaks. The positions of the energy levels are found by solving the Schrödinger equation for the adsorption potential $V(z)$. If we define $|i\rangle$ as the eigenstate of the potential $V(z)$, $\{E_i\}$ as discrete energy levels, then $\omega_{ij} = (E_i - E_j)/\hbar$ describes the peak position due to a transition between the energy level E_i and E_j. Note that only the local mode is now present in the system without the presence of the thermal phonon bath.

As we know, the vibrational line shape is given by the imaginary part of the Fourier transform of the retarded Green's function of the local mode vibrational

coordinate z. The retarded Green's function is defined by

$$iD^R(t) = \theta(t)\langle[z(t), z(0)]\rangle, \tag{3.25}$$

where "$\langle\cdots\rangle$" represents the thermal average over all discrete local mode states. Its Fourier transform is given by

$$D^R(\omega) = \int d\omega e^{i\omega t} D^R(t). \tag{3.26}$$

Therefore

$$\begin{aligned}
\Delta I &\propto Im\ D^R(\omega) \\
&= -\pi \sum_{i,j} \rho_i |z_{ij}|^2 [\delta(\omega + \omega_{ij}) - \delta(\omega - \omega_{ij})] \\
&= -\pi \left[\sum_{i<j} \rho_i |z_{ij}|^2 \delta(\omega + \omega_{ij}) - \sum_{i>j} \rho_i |z_{ij}|^2 \delta(\omega - \omega_{ij}) \right] \\
&= -\pi \sum_{i<j} (\rho_i - \rho_j) |z_{ij}|^2 \delta(\omega - \omega_{ji}),
\end{aligned} \tag{3.27}$$

where z_{ij} is the matrix element $\langle j|z|i\rangle$, and $|z_{ij}|^2 = |z_{ji}|^2$, ρ_i is the matrix element $\langle i|\rho|i\rangle$. This represents all discrete lines at frequencies $\{\omega_{ij}\}$. The first term represents local mode excitation from the energy level E_i to E_j by absorbing a photon with frequency ω_{ji}, while the second term represents local mode de-excitation from the energy level E_j to E_i by emitting a photon with frequency ω_{ji}. The peak at ω_{ji} is weighted by the net absorption rate $(\rho_i - \rho_j)|z_{ij}|^2$. The envelope of these peaks at $\{\omega_{ji}\}$ is a large asymmetric broad peak or distribution of discrete peaks. Only the envelope of these peaks is seen in experiments when each discrete peak is broadened enough by other sources.

In the harmonic approximation, the possible transition from the energy level i to a higher energy level j occurs only for $j = i + 1$, for which, $|z_{i,i+1}|^2 \propto (i + 1)$.

The anharmonic terms $\frac{1}{3!}V_3 z^3$ and $\frac{1}{4!}V_4 z^4$ shift the harmonic energy levels. Taking the $\frac{1}{4!}V_4 z^4$ term in first order perturbation theory and $\frac{1}{3!}V_3 z^3$ in second order gives the lowest order contributions to the line shift, i.e.

$$\begin{aligned}\Delta\omega_{i+1,i} &= (\Delta E_{i+1} - \Delta E_i)/\hbar \\ &= \left[\frac{V_4\hbar}{8m^2{\omega_0}^2} - \frac{5V_3^2\hbar}{24m^3{\omega_0}^4}\right](i+1). \end{aligned} \tag{3.28}$$

At zero temperature, the adsorbate only occupies the ground state, i.e., $i = 0$. There is no excited vibrational state occupied. The local vibrational mode can be excited from its ground state by absorbing a photon. In this case, the frequency shift $\Delta\omega_{i+1,i}$ for $i = 0$ agrees with the sum of $\Delta\omega_2, \Delta\omega_4, \Delta\omega_9$ calculated in TFD in the zero temperature limit with $n_{\omega_0} \to 0$ as $T \to 0$.

However, at non zero temperature, the higher energy levels other than the ground state are thermally occupied so that both local mode excitation and de-excitation can occur for all energy levels $i = 0, 1, \cdots, \infty$. From the one-mode Green's function formula, the peak at $\omega_{i+1,i}$ is weighted by $(\rho_i - \rho_{i+1})|z_{i,i+1}|^2$. Therefore, the thermal average of the line shift $\Delta\omega_{i+1,i}$ over all the local mode states can be calculated as

$$\begin{aligned}\langle\Delta\omega\rangle &= \sum_{i=0}^{\infty} \Delta\omega_{i+1,i}(\rho_i - \rho_{i+1})|z_{i+1,i}|^2 \\ &= \left[\frac{V_4\hbar}{8m^2{\omega_0}^2} - \frac{5V_3^2\hbar}{24m^3{\omega_0}^4}\right](2n_{\omega_0}+1), \end{aligned} \tag{3.29}$$

where normalization $\sum_i\{\rho_i|z_{i,i+1}|^2 - \rho_{i+1}|z_{i+1,i}|^2\} = 1$ has been used. This thermal average of the line shift gives the weighted average position of the asymmetric envelop of all the discrete peaks of the one mode Green's function, and also corresponds to the sum of $\Delta\omega_2, \Delta\omega_4$ and $\Delta\omega_9$ calculated in TFD.

3.2.2 The "V mode" vibrational line shape

Now we study the vibrational line shape of the internal mode of a diatomic admolecule with vibrational coordinate ζ. Compared to the "T mode" line shape calculation, there is an additional coordinate ζ here. The interaction between the "T mode" and the "V mode" also contribute to the line shape in addition to the phonon-"V mode" interaction. The anharmonic interaction between the fields $\zeta(t), z(t)$ and $a_z(t)$ can be assumed to take the form given in Eq. (2.45) as

$$\sum_{l,m,n}{}' V_{l+m+n}\frac{1}{l!m!n!}(-\frac{\mu}{m_1}\zeta)^l z^m(-a_z)^n, \tag{3.30}$$

with $V_{l+m+n} = \frac{\partial^{(l+m+n)}}{\partial y^{(l+m+n)}}V(y)|_{equilibrium}$ being coupling constant. This sum $\sum'$ excludes the terms $l+m+n \leq 2$. Since $V_2 \ll \mu\Omega^2$ with μ being the reduced mass of the diatomic molecule, the bilinear terms $V_2 a_z\zeta$ and $-V_2 z\zeta$ will not affect the "V mode" shift and width significantly in the perturbation theory. We therefore ignore them in the calculation. Note that this anharmonic hamiltonian is based on the one dimensional model introduced in Chapter 2. Expanding the sum, we have

$$\begin{aligned} H_{anh} &= V_3\left[a\zeta' z+\frac{1}{2!}(-a^2\zeta'+a^2 z-\zeta'^2 a+\zeta'^2 z-z^2 a-z^2\zeta')\right. \\ &\quad \left.+\frac{1}{3!}(-a^3-\zeta'^3+z^3)\right] \\ &\quad +V_4\left[\frac{1}{4!}(a^4+\zeta'^4+z^4)+\frac{1}{3!}(a^3\zeta'-a^3 z+\zeta'^3 a-\zeta'^3 z-z^3 a-z^3\zeta')+\right. \\ &\quad \left.+\frac{1}{2!2!}(a^2 z^2+\zeta'^2 a^2+\zeta'^2 z^2)+\frac{1}{2!}(-a^2 z\zeta'-\zeta'^2 az+a\zeta' z^2)\right]+\cdots, \end{aligned} \tag{3.31}$$

where $\zeta' = (\frac{\mu}{m_1})\zeta$. The lowest order diagram expansion of the "V mode" self energy is presented in Fig. (3.2), where the solid lines denote the free Green's function $D_V^{0,\alpha\beta}(t)$ for the "V mode" vibrational coordinate ζ defined by

$$iD_V^{0,\alpha\beta}(t) = \langle T\zeta^\alpha(t)\zeta^\beta(0)\rangle. \tag{3.32}$$

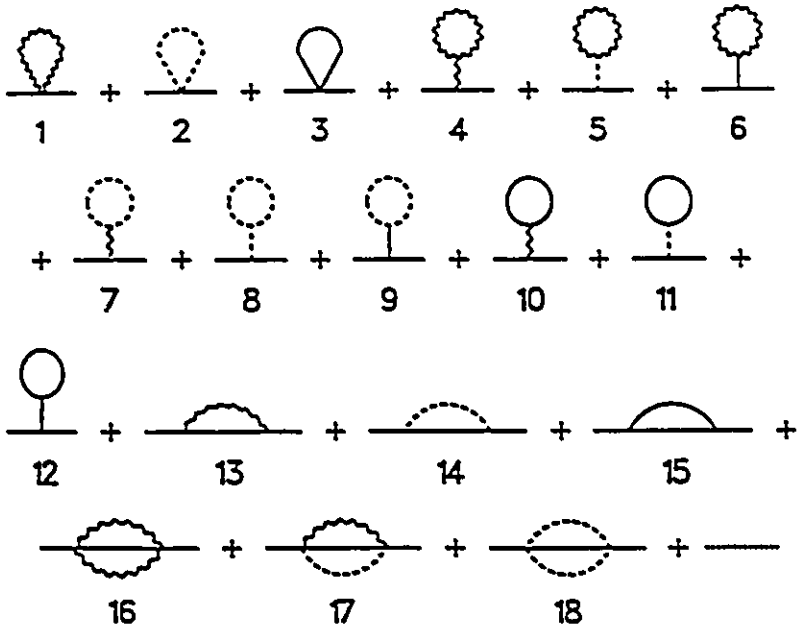

Figure 3.2: The "V mode" self energy expansion for an admolecule at an ontop site.

The dashed lines and wavy lines have the same meaning as that in Fig. (3.1). Similar to the "T mode", the first three diagrams contain only a single vertex due to the anharmonic interaction $\frac{1}{4}V_4 a_z^2\zeta^2$, $\frac{1}{4}V_4 z^2\zeta^2$ and $\frac{1}{4!}V_4\zeta^4$. They all enlarge the vibrational frequency Ω and give blue shifts as follows:

$$\Delta\Omega_1 = \frac{3V_4\hbar\mu}{8M_s m_1^2\Omega{\omega_D}^3}\int_0^{\omega_D} d\omega\omega(2n_\omega+1), \tag{3.33}$$

$$\Delta\Omega_2 = \frac{V_4\hbar\mu}{8mm_1^2\Omega\omega_0}(2n_{\omega_0}+1), \tag{3.34}$$

$$\Delta\Omega_3 = \frac{\mu^2 V_4\hbar}{8m_1^4\Omega^2}(2n_\Omega+1). \tag{3.35}$$

Here m_1 is the mass of the inward atom of the diatomic molecule, and $\Delta\Omega_3$ can be ignored since the frequency of the internal vibration Ω is so high that $\Delta\Omega_3$ is nearly temperature independent.

The diagrams 4 to 12 in Fig. (3.2) all have two vertices due to the different combinations of the interaction terms $\frac{1}{2}V_3 z\zeta^2$, $\frac{1}{2}V_3 a_z\zeta^2$, $\frac{1}{6}V_3\zeta^3$, $\frac{1}{2}V_3 z a_z^2$, $\frac{1}{2}V_3 z^2\zeta$, $\frac{1}{2}V_3 a_z^2\zeta$, $\frac{1}{6}V_3 z^3$, $\frac{1}{2}V_3 z^2 a_z$ and $\frac{1}{6}V_3 a_z^3$. The self energies contributed by these diagrams have only real parts and give red shifts to the frequency Ω. After a detailed calculation, we find

$$\frac{\Delta\Omega_4 + \Delta\Omega_5 + \cdots + \Delta\Omega_{12}}{\Delta\Omega_1 + \Delta\Omega_2 + \Delta\Omega_3} = -\frac{V_3^2}{V_4}\left[\left(\frac{\mu}{m_1}\right)^2 \frac{1}{\mu\Omega^2} + \frac{1}{m\omega_0^2} + \frac{3}{M_s{\omega_D}^2}\right]. \quad (3.36)$$

The diagrams 13 to 18 also contribute to the line shift, but their contributions are very small compared to the contributions of the diagrams 1 to 12 and therefore ignored.

The lowest order line width of the "V mode" is possibly contributed by the two vertex diagrams 13 to 18 in Fig. (3.2). Similarly to the "T mode", diagram 13 now represents the absorption or emission of one soft phonon by the "V mode". It has non-zero imaginary part due to the lack of adiabaticity in this treatment. The diagram 14 and 15 have no imaginary parts. The decay of the "V mode" via the creation of the substrate phonons is a process with only small probability, because the "V mode" frequency Ω is much higher than the maximum substrate phonon frequency ω_D. From pure energy conservation, it requires about 6-8 substrate phonons to be created almost simultaneously. The diagrams 16 to 18 all describe the vibrational dephasing processes. The line width contributions due to these diagrams are given by the imaginary parts of the self energies corresponding to each diagram. The diagram 16 due to the interaction $\frac{1}{4}V_4\zeta^2 a_z^2$ describes the elastic phonon scattering by the "V mode" of a diatomic admolecule. The diagram 17 due to the interaction $\frac{1}{2}V_4\zeta^2 a_z z$ is called "cross term" contribution which describes the absorption of a substrate phonon and excitation of the "T mode" vibration by the "V mode", or vise versa. Diagram 18 due to the interaction $\frac{1}{4}V_4\zeta^2 z^2$ describes the exchange

mechanism of dephasing of the "V mode" due to the anharmonic coupling with the "T mode". The "T mode" propagator in this diagram now represents a full Green's function with line width Γ_T. How well we determine the "T mode" line width will affect the "V mode" line width due to this exchange mechanism.

The "V mode" line width based on the above considerations is now

$$\Gamma_V = \Gamma_{V13} + \Gamma_{V16} + \Gamma_{V17} + \Gamma_{V18}, \tag{3.37}$$

with

$$\Gamma_{V13} = \frac{3\pi\hbar\mu V_3^2}{8m_1^4 M_s \Omega^2 {\omega_D}^2} \frac{T}{T_D}, \tag{3.38}$$

$$\Gamma_{V16} = \pi \left[\frac{3\mu\hbar V_4}{4m_1^2 M_s \Omega {\omega_D}^3}\right]^2 \int_0^{\omega_D} d\omega \omega^2 n_\omega (n_\omega + 1), \tag{3.39}$$

$$\Gamma_{V17} = \frac{3\pi\mu^2\hbar^2 V_4^2}{8mm_1^4 M_s \Omega^2 {\omega_D}^3} n_{\omega_0}(n_{\omega_0}+1)\theta(\omega_D - \omega_0), \tag{3.40}$$

$$\Gamma_{V18} = \left[\frac{\mu\hbar V_4}{4m_1^2 m\Omega\omega_0}\right]^2 \frac{n_{\omega_0}(n_{\omega_0}+1)}{2\Gamma_T}. \tag{3.41}$$

The $\theta(\omega)$ function in Γ_{V17} reflects the fact that the "cross term" contributes to the "V mode" line width only in the situation where the local mode frequency ω_0 is within the substrate phonon band. The dephasing processes represented by the diagrams 16 to 18 were also considered by other people by using different methods. Persson[54] calculated the transition rate due to the elastic phonon scattering by using Fermi's Golden rule. Similar exchange terms were studied by Langreth, Persson and Harris etc.[17, 53, 72]. The "cross term" has been previously derived in the context of photodesorption kinetics[4].

3.2.3 Discussion and limitation

We have calculated the line shift and line width of the localized adsorbate-surface stretching mode and the internal vibration of a diatomic adsorbate, respectively, in

a purely perturbative approach. In this treatment, these two modes are equivalent since both modes play equivalent roles at the harmonic level. For simplicity, we have calculated the line width in a one dimensional model and excluded the effects of other modes such as the lateral translational modes and some frustrated rotational modes of the adsorbate and substrate atoms. For each additional mode, we will have an additional propagator. This propagator will result in some additional self energy diagrams in the Feymann diagram expansion. The results obtained above can easily be reformulated by adding a propagator for each additional mode and including its interaction with other modes[19]. We will extend our picture to a three dimensional model and include lateral motion in the line shape theory in Chapter 5.

All higher order diagrams[73] in the self energy expansion are neglected here, such as the terms with derivatives of the potential higher than the fourth order and the terms with the number of vertices greater than 2. Langreth[55] showed in 1987 that the fourth order perturbation of a cubic term would give a contribution which is comparable to the second order perturbation of a quadratic term. Since the "reduction factor" will reduce the substrate phonon contributions due to the anharmonicity of the adsorption potential and our aim in this section is to show the method in a simple and obvious way, we do not consider the cubic term to higher order perturbation of the perturbation here.

The above calculation has shown that the relaxation processes involving the substrate phonons can be important processes in the "T mode" line shape calculation. On the other hand, some unphysical result is revealed such as the one phonon dephasing term, which represents the absorption and emission of a soft phonon by the "T mode" or the "V mode" with phonon frequency $\omega_k \approx 0$. This is due to a lack of adiabaticity in the purely perturbative approach. At low frequency, $\omega_k \sim 0$, the

substrate phonons will not affect the motion of the adsorbate. But in the purely perturbative approach the one phonon dephasing term could incorrectly give a large line width contribution which we will show in Section 4.

We noticed that the bilinear coupling of the localized lower frequency mode to the substrate phonons $-V_2 a_z z$ has the same coupling constant as the harmonic coupling constant of the adsorbate-surface stretching mode, and the phonon displacement a_z has the same order of magnitude as that of the adatom or admolecule when the "T mode" frequency is not much greater than the maximum substrate phonon frequency. Therefore, $|-V_2 a_z z| \not\ll |\frac{1}{2} V_2 z^2|$, and the bilinear term $-V_2 a_z z$ should be treated at the same level as the harmonic term $\frac{1}{2} V_2 z^2$. As the result of pure perturbative treatment of the bilinear term, the "T mode" and the "V mode" vibrational line shift and line width contributed by the dynamical processes involving the delocalized phonons of the substrate are incorrectly overestimated.

In the recent study of the IR absorption by the "T mode", the interaction term $-V_2 z a_z$ was treated in a nonperturbative method, for the case in which this localized mode has a frequency greater than the maximum phonon frequency of the substrate[53]. In that case, a modified interaction hamiltonian was derived. As a result, the amplitude of the k^{th} phonon displacement d_k^0 of the substrate atom was reduced by the "reduction factor" $\omega_k{}^2/\omega_0{}^2 - \omega_k{}^2$, leading in turn to a dramatic reduction of the effect of the anharmonic coupling to the substrate phonon modes in that case. This would be reflected in above calculations involving the substrate phonon motions. We will show how the "reduction factor" reduces the phonon effect in the next section. Ye and Piercy studied the bilinear term exactly for the case in which the "T mode" is degenerate with the phonon continuum, and compared with the purely perturbative approach introduced in this section. CO/NaCl(100) was

considered there as an example. See Ref.(42) for details. In both cases, whether $\omega_0 > \omega_D$ or $\omega_0 < \omega_D$, the unphysical line width in the purely perturbative approach from the one-phonon dephasing term vanishes, when the bilinear coupling of the "T mode" to the substrate phonons is treated nonperturbatively, for an admolecule at an ontop site. We will show more details in the next section.

3.3 Nonperturbative treatment of the bilinear term

As we noticed in the last section, the bilinear coupling between the "T mode" and substrate phonon modes $-V_2 z a_z$ is comparable in magnitude to the "T mode" bare harmonic potential $\frac{1}{2}V_2 z^2$. The purely perturbation treatment is not good enough to describe this situation. Now, we include the bilinear term into the harmonic hamiltonian for the same adsorption situation and solve the problem in a nonperturbative manner. Our previous results on the vibrational line shape will undergo a dramatic change by treating the bilinear term in this way. The effect of phonons on the "T mode" vibrational line shape induced by the adsorption potential is almost negligible for the case where the "T mode" frequency ω_0 is outside of the substrate phonon band. However, the new solution to the harmonic hamiltonian makes it possible to look into an additional phonon effect on the "T mode" vibrational line shape due to the anharmonicity of the substrate. Ye and Piercy have considered the lowest order contributions of the substrate phonons on the vibrational line shape purely due to the anharmonicity of the substrate in a one dimensional model. However, they have not included the contribution due to the "cross-interaction" between the anharmonicities of the adsorption potential and the substrate which might be important in some cases such as adsorption at a bridge site. We will include all line shape contributions due to the anharmonicities of the adsorption potential and

substrate individually, as well as their "cross-interactions", in this section as well as in Chapter 6.

The temperature dependence of vibrational lineshape is often attributed to phonon-induced dephasing and decay mechanisms. Decay mechanisms are more efficient on the "T mode" because its vibrational frequency is closer to substrate phonon frequency so that fewer phonons are excited in the process. Since the "V mode" line width due to the exchange mechanism is very dependent on the "T mode" line width, we are more interested in the dynamics of the "T mode". From now on, we will concentrate on the phonon-induced vibrational lineshape of an adatom vibrating against the surface.

In this section, we will show a nonperturbative treatment of the bilinear coupling between the adsorbate and substrate, which was introduced by Ye and Piercy using TFD[59]. In this treatment, the anharmonic coupling by the adsorption potential, of long wavelength acoustic phonons to the localized vibration of an adatom against the surface, is relatively inefficient at an ontop site, because the adsorbate follows the motion of the surface approximately adiabatically. The vibrational coordinate of the admolecule is expanded as a superposition of the normal modes of the local vibration of the adsorbate and delocalized phonons of the substrate after the bilinear coupling is included in the harmonic hamiltonian. The surface atom displacement, in turn, is also affected by the local mode vibration, which give rise to an additional phonon effect on the "T mode" vibrational line shape due to the anharmonicity of the solid. This expansion can be found by solving the equation of motion for the harmonic hamiltonian including the bilinear term in the present one dimensional model. We start with the same simple one dimensional model as that in Section 2, and introduce a solution to the equation of motion for the harmonic hamiltonian

with the bilinear term for an admolecule at an ontop site.

The perturbation expansion will involve a weighted vibrational coordinate of the local mode. As a result, the vertex and propagator in the Feynman diagram rules given in Appendix D will be modified.

3.3.1 The harmonic hamiltonian including the bilinear term

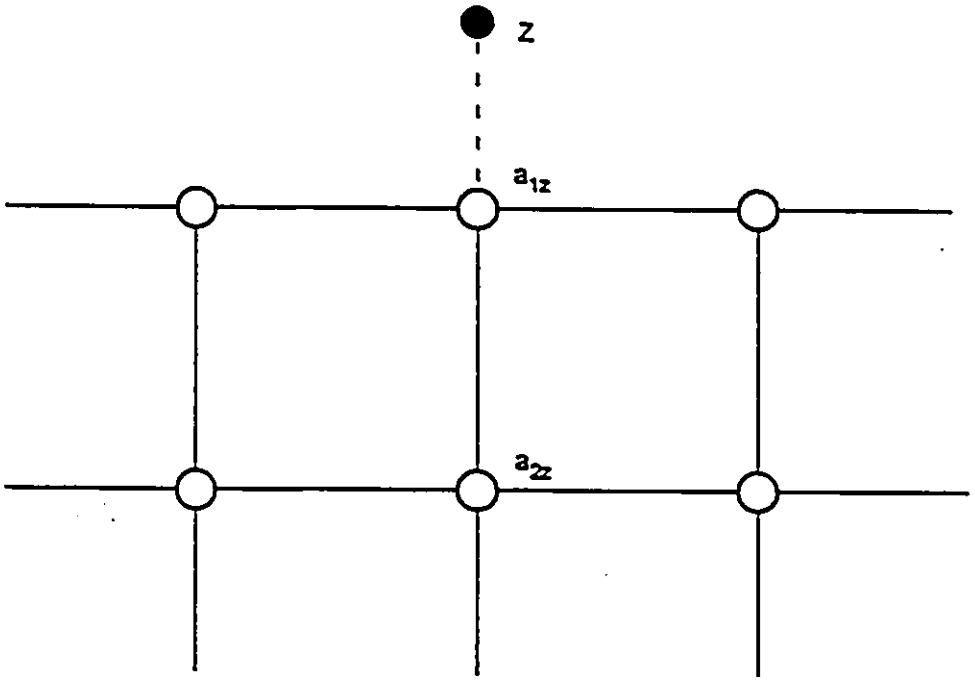

Figure 3.3: A model adsorption system, shown for the (100) surface of a simple cubic substrate.

Fig. (3.3) shows a model adsorption system of an admolecule at an ontop site at a simple cubic solid (100) surface. The perpendicular displacements from the equilibrium of the adsorbed molecule, the surface atom at an ontop site and the atom in the second layer beneath the surface atom have components z, a_{1z} and a_{2z}, respectively.

Adsorption is modeled by a single pair-wise central force potential to the surface atom under the admolecule. The Taylor series expansion of the adsorption potential $V(z-a_{1z})$ gives three second derivative terms $V_2(\frac{1}{2}a_{1z}^2+\frac{1}{2}z^2-a_{1z}z)$. The term $\frac{1}{2}V_2a_{1z}^2$ acts as a point mass defect in a harmonic solid due to the adsorbate since we consider the substrate as an infinite medium here. If we ignore this term, then the harmonic problem here reduces to a single harmonic oscillator coupled bilinearly to a harmonic phonon continuum with the hamiltonian

$$H_{harm} = H_T + H_s - m{\omega_0}^2 a_{1z}z, \tag{3.42}$$

where, H_T describes the motion of an admolecule at a static surface, and H_s describes a harmonic solid without the adsorbate, approximated here by a bulk Debye model with the maximum phonon frequency ω_D. In the final term, the bilinear coupling constant is that of the bare local mode of the perpendicular vibration of the admolecule defined by $V_2 = m{\omega_0}^2$. The bilinear term $-V_2a_{1z}z$ couples the motion of the admolecule to that of the surface atom beneath it in the harmonic approximation.

It is worthwhile to recall the normal modes of the single harmonic oscillator denoted by $z^0(t)$ and the harmonic substrate phonons denoted by $\{d_k^0(t)\}$. From Chapter 2, we know

$$z^0(t) = \sqrt{\frac{\hbar}{2m\omega_0}}[b_T(t)+b_T^\dagger(t)], \tag{3.43}$$

is the normal mode of the single harmonic oscillator with the hamiltonian $H_T = \frac{1}{2}m\dot{z^0}^2(t)+\frac{1}{2}m{\omega_0}^2{z^0}^2(t)$.

$$d_k^0(t) = \sqrt{\frac{\hbar}{2M_SN\omega_k}}[b_k(t)+b_{-k}^\dagger(t)], \tag{3.44}$$

is the phonon displacement of the delocalized phonon mode with the wave vector k which is the solution of the harmonic hamiltonian $H_s = \sum_k [\frac{1}{2} M_s N \dot{d}_k^{0\dagger} \dot{d}_k^0 + \frac{1}{2} M_s N \omega_k{}^2 d_k^{0\dagger} d_k^0]$. The free vibrational displacement of a substrate atom at the lattice position $\vec{R}_i$, in the direction perpendicular to the surface, is thus given by

$$a_{iz}^0(t) = \sum_k e_k^z e^{i\vec{k}\cdot\vec{R}_i} d_k^0(t), \tag{3.45}$$

where e_k^z is the perpendicular component of unit polarization vector $\hat{e}_k$, and the index $k = (\vec{k}, \sigma)$ includes both the phonon wave vector and the polarization. In other words, $z^0(t)$ and $a_{iz}^0(t)$ are the solution of the harmonic hamiltonian without the bilinear interaction. If lattice positions are defined with respect to the on-top site, then we can set $\vec{R}_1 = 0$. Since it is hard to solve harmonic hamiltonian with bilinear term given in Eq. (3.42), we will try to approximate the displacements of the admolecule $z(t)$ and the surface atom $a_{iz}(t)$ in terms of $z^0(t)$ and $a_{iz}^0(t)$.

3.3.2 The equations of motion for H_{harm} and their solutions

We are specifically interested in the relationship between the displacement fields $z(t)$ and $d_k(t)$ since they are the quantities which enter the anharmonic hamiltonian given by Eq. (2.44). Following Ye and Piercy's consideration[59], the time dependence of these fields are governed by the harmonic hamiltonian H_{harm}, and the free fields $z^0(t)$ and $d_k^0(t)$, which independently follow the hamiltonians H_T and H_s, respectively. The displacement of the surface atom at the ontop site can be written in terms of the delocalized phonon amplitude $d_k(t)$

$$a_{1z}(t) = \sum_k e_k^z d_k(t). \tag{3.46}$$

Based on the H_{harm} in Eq. (3.42), from the Heisenberg equation

$$i\hbar\dot{z} = [\dot{z}, H_{harm}], \tag{3.47}$$

we find the equation of motion for the adatom

$$(-\frac{\partial^2}{\partial t^2} - {\omega_0}^2)z(t) = -{\omega_0}^2 a_{1z}(t). \tag{3.48}$$

Similarly, for the phonon amplitude,

$$(-\frac{\partial^2}{\partial t^2} - {\omega_k}^2)d_k(t) = -\frac{m{\omega_0}^2}{M_s N}z(t), \tag{3.49}$$

where we have used the boson commutation relation at equal time and assumed that z and a_{1z} obey the same commutation relation as z^0 and a^0_{1z}, respectively. The equations of motion given by Eq. (3.48) and Eq. (3.49) are hard to be solved exactly. Here, we will introduce Green's function solutions to these equations of motion for the case in which the perpendicular molecule-surface vibrational frequency is outside of the substrate phonon band, i.e. $\omega_0 > \omega_D$. The solutions for $\omega_0 < \omega_D$ can be found in Ref. [64, 42].

Define the retarded Green's functions for z^0, d^0_k as

$$\Delta^z_R(t-t') = i\theta(t-t')\left[z^0(t), z^0(t')\right], \tag{3.50}$$

$$\Delta^k_R(t-t') = i\theta(t-t')\left[d^0_k(t), d^0_k(t')\right], \tag{3.51}$$

in terms of the boson commutator. The Green's function solutions of their equations of motion therefore can be obtained as

$$z(t) = z^0(t) + \int dt' \Delta^z_R(t-t')(-{\omega_0}^2)a_{1z}(t'), \tag{3.52}$$

$$d_k(t) = d^0_k(t) + \int dt' \Delta^d_R(t-t')(-\frac{m{\omega_0}^2}{M_s N})z(t'). \tag{3.53}$$

They are the integral equations for the Green's function. The detailed calculation can be found in Ref. [74].

Substituting the Green's functions given by Eq. (3.50) and Eq. (3.51) into Eqs. (3.52) and (3.53), and simplifying them gives

$$z(t) = z^0(t) + \sum_k e_k^z \frac{{\omega_0}^2}{{\omega_0}^2 - {\omega_k}^2} d_k^0(t), \tag{3.54}$$

$$d_k(t) = d_k^0(t) + e_k^z \frac{m}{M_s N} \frac{{\omega_0}^2}{{\omega_k}^2 - {\omega_0}^2} z^0(t). \tag{3.55}$$

Hence

$$a_{1z} = a_{1z}^0(t) + \sum_k |e_k^z|^2 \frac{m}{M_s N} \frac{{\omega_0}^2}{{\omega_k}^2 - {\omega_0}^2} z^0(t), \tag{3.56}$$

where we have taken the prefactors in front of z^0 and d_k^0 as 1. This is only valid in the weak coupling limit, i.e., $m/M_s \ll 1$ and ω_0 is not too close to ω_D. For other situation, these prefactors can be determined so that the displacements z and a_{1z} are normalized to satisfy the boson commutation relations.

Note that in the above equations, $z^0(t)$ is the displacement of the harmonic oscillator with frequency ω_0' shifted slightly from ω_0[64]. On the other hand, the frequency ω_k of the delocalized phonon modes are assumed to be negligibly affected by the single adsorbed molecule or atom.

Eq. (3.54) and Eq. (3.56) may be regarded as the approximate normal mode expansions in terms of the free field z^0 and d_k^0. They show that at the harmonic level, the vibrational motion of the adatom includes not only a localized component $z^0(t)$, but also a delocalized phonon component $d_k^0(t)$, while the surface atom displacement takes on a local mode component $z^0(t)$, due to the bilinear coupling $-V_2 a_{1z} z$. As a result, the difference of the vibrational amplitudes between the adatom and the surface atom beneath it becomes

$$z - a_{1z} = \left[1 - \sum_k e_k^z \frac{m}{MN} \frac{{\omega_0}^2}{{\omega_k}^2 - {\omega_0'}^2}\right] z^0(t) + \sum_k e_k^z \frac{{\omega_k}^2}{{\omega_0}^2 - {\omega_k}^2} d_k^0(t)$$

$$= R_T^V z^0 + \sum_k e_k^z R_k^V d_k^0, \tag{3.57}$$

where we have defined

$$R_T^V = \left[1 - \sum_k e_k^z \frac{m}{MN} \frac{{\omega_0}^2}{{\omega_k}^2 - {\omega_0}'^2}\right] \sim 1, \tag{3.58}$$

$$R_k^V = \frac{{\omega_k}^2}{{\omega_0}^2 - {\omega_k}^2}. \tag{3.59}$$

The coefficient R_T^V is nearly unity in the weak coupling limit, i.e., $m/M \ll 1$, while the coefficient in front of the phonon amplitude d_k^0 above is given by the so-called "reduction factor" $R_k^V = \frac{{\omega_k}^2}{{\omega_0}^2 - {\omega_k}^2}$, which is the result originally derived by Persson and Ryberg[53]. This also describes nearly adiabatic motion of an adatom in response to long wavelength phonon ($\omega_k \sim 0$) motion of solid surface. This "reduction factor" significantly reduces the adsorbate coupling to acoustic-phonon field d_k^0. Therefore, the phonon effects, due to the anharmonicity of the adsorption potential, on the "T mode" lineshape can be ignored for an adatom at an on top site.

On the other hand, we noticed the fact that the surface atom displacement takes on a local mode component $z^0(t)$, due to the bilinear coupling $-V_2 a_{1z} z$. The anharmonic interactions between the surface atom underneath the admolecule and its nearest neighbors in the substrate couple the delocalized phonon modes to the localized vibrational mode. These couplings lead us to consider the additional phonon effects, from the anharmonicity of the interatomic interactions of the substrate, on the vibrational lineshape of the local mode of the admolecule. The difference in displacements between the surface atom at the ontop site and its nearest neighbor j in the second layer of the substrate becomes

$$a_{1z} - a_{jz} = a_{1z}^0(t) + \left[\sum_k e_k^z \frac{m}{MN} \frac{{\omega_0}^2}{{\omega_k}^2 - {\omega_0}^2}\right] z^0(t) - a_j^0(t)$$

$$= R_T^{\phi} z^0 + \sum_k e_k^{\bar{z}} R_k^{\phi} d_k^0, \tag{3.60}$$

where we have defined,

$$R_T^{\phi} = \sum_k e_k^{\bar{z}} \frac{m}{MN} \frac{{\omega_0}^2}{{\omega_k}^2 - {\omega_0}^2} \sim (\frac{m}{M_s}), \tag{3.61}$$

$$R_k^{\phi} = e^{i\bar{k}\cdot\bar{R}_1} - e^{i\bar{k}\cdot\bar{R}_j}. \tag{3.62}$$

In Eq. (3.61) , we have included the spread of the localized vibrational mode as far as the first layer surface atom $i = 1$ only. The local component of the vibrational field decays rapidly with distance from the adsorbed molecule or atom, and is estimated to be about $0(10^{-2})$ times smaller for the second layer atoms in the substrate, although the exact amplitude depends on the details of the phonon-band structure and on ω_0. We have therefore let the substrate atoms in the second layer have displacement $a_{jz} = a_{jz}^0$. The differences in atomic displacements given by Eq. (3.60) allow the free vibrational coordinate of the localized mode z^0 to be coupled by the anharmonicity of the substrate to a modified phonon amplitude $\sum_k e_k^{\bar{z}} R_k^{\phi} d_k^0$.

3.3.3 Anharmonic hamiltonian and self energy

Anharmonic hamiltonian

The total anharmonic hamiltonian of the adsorption potential and solid in our one dimensional model that we study here is

$$H_{anh} = V_{anh}(z - a_{1z}) + \sum_{(i,j)pair} \phi_{anh}(r_{ij}). \tag{3.63}$$

The anharmonic expansion of the adsorption potential depends on the difference in the vibrational displacements of the admolecule and the surface atom beneath it, as given by Eq. (3.57). The "reduction factor" given by Eq. (3.59) significantly

reduces the coupling of the local mode to the acoustic phonon field $a_k^0(t)$. In $\sum_{(i,j)pair}\phi_{anh}(r_{ij})$, it is the anharmonic interactions $\phi_{anh}(r_{1j})$ (j=nearest neighbors of the surface atom 1) of the surface atom $i=1$ (at the ontop site), with its nearest neighbors in the substrate, that explicitly couple to the localized vibrational mode. The other anharmonic interactions between the substrate atoms will not affect the local mode and therefore are ignored[75, 76, 77]. As an example, here we consider a special case of adsorption at an ontop site on a (100) surface of a simple cubic solid which has also been considered by Ye and Piercy and showed in Fig. (3.3)[59]. The surface atom $i=1$ only has one nearest neighbor beneath it denoted by $j=2$. The anharmonic hamiltonian due to the substrate depends on the difference in atomic displacements $a_{1z}-a_{2z}$, which is given by Eq. (3.60). In our perturbation theory, we only consider the anharmonic terms up to the 4^{th} derivatives. Hence

$$\begin{aligned} H_{anh} &= \frac{V_3}{3!}(z-a_{1z})^3+\frac{V_4}{4!}(z-a_{1z})^4+\cdots \\ &\quad +\frac{\phi_3}{3!}(a_{1z}-a_{2z})^3+\frac{\phi_4}{4!}(a_{1z}-a_{2z})^4+\cdots \end{aligned} \tag{3.64}$$

Self energy

Based on the anharmonic hamiltonian given by Eq. (3.64), the lower order diagrams of the self energy are same as those in Fig. (3.1) except diagram 7 due to the bilinear term is absent since we include it in the harmonic hamiltonian. Furthermore, the vertices and propagators in the Feymann diagram rules given in Appendix D have to be modified due to the nonperturbative treatment of the bilinear term. Each diagram in the self energy expansion now represents the total contribution from both the anharmonicities of the adsorption potential and the substrate. The phonon propagator denoted by the wavy lines comes with a corresponding prefactor $(R_k^V)^2$, $(R_k^\phi)^2$ or $R_k^V R_k^\phi$, while the local mode propagator denoted by the dash lines comes

with a corresponding prefactor $(R_T^V)^2$, $(R_T^\phi)^2$ or $R_T^V R_T^\phi$ depending on the interactions. The superscripts V and ϕ in all prefactors denote the contributions of the adsorption potential and the substrate, respectively. The vertex function can be produced by the derivatives of the adsorption potential $V(z - a_{1z})$ or the interatomic potential of the solid $\phi(a_{1z} - a_{jz})$.

Line shift and line width

According to the new rules, we now take the self energy diagram 1 and 12 in Fig. (3.1) as examples and write out their contributions to the vibrational line shift and line width in the nonperturbative treatment of bilinear term. Diagram 1 only gives a contribution to the line shift due to the anharmonic couplings of the adsorption potential and the substrate

$$\Delta\omega_1 = \frac{3\hbar}{8mM_s\omega_0{\omega_D}^3}\int_0^{\omega_D} d\omega\omega(2n_\omega+1) \left[(R_T^V)^2 V_4\left(\frac{\omega^2}{{\omega_0}^2-\omega^2}\right)^2 + (R_T^\phi)^2\phi_4 2\left(1-\frac{sin\frac{\omega}{\omega_D}k_D r_0}{\frac{\omega}{\omega_D}k_D r_0}\right)\right], \quad (3.65)$$

where k_D is the Debye wave vector and r_0 is the distance between the nearest neighbors of the substrate atoms. The first term due to the anharmonicity of the adsorption potential can be ignored since the "reduction factor" reduces its effect at least by $\left(\frac{{\omega_D}^2}{{\omega_0}^2-{\omega_D}^2}\right)^2$, which is very small for $\omega_0 \gg \omega_D$ case. This term was considered by Zhang[78]. He also considered the line shift contributions of self energy diagrams 3, 8 and 10. In his calculation, he simply enlarged the coupling constant to fit observed shift. The second term due to the anharmonicity of the solid ϕ_{anh} dominates the line shift contribution which was considered by Ye and Piercy[59]. They also considered the line shift contribution of the self energy diagram 5 and the line width contribution of the self energy diagram 10.

Diagram 12 gives contributions to both the line shift and the line width due to the anharmonic couplings of the adsorption potential and the substrate. Its contribution to the line shift is small compared to the contribution of diagram 1. Its contribution to the line width is given by

$$\Gamma_{T12} = \frac{9\pi\hbar^2}{16m^2M_s^2\omega_0^2\omega_D{}^6}\int d\omega\omega^2 n_\omega(n_\omega+1) \left[(R_T^V)^4V_4^2\left(\frac{\omega^2}{\omega_0{}^2-\omega^2}\right)^4+(R_T^\phi)^4\phi_4^2 4\left(1-\frac{sin\frac{\omega}{\omega_D}k_Dr_0}{\frac{\omega}{\omega_D}k_Dr_0}\right)^2+ (R_T^V)^2V_4\left(\frac{\omega^2}{\omega_0{}^2-\omega^2}\right)^2(R_T^\phi)^2\phi_4 2\left(1-\frac{sin\frac{\omega}{\omega_D}k_Dr_0}{\frac{\omega}{\omega_D}k_Dr_0}\right)\right]. \quad (3.66)$$

Similarly to the line shift contribution, the first term due to the anharmonicity of the adsorption potential can be ignored since the "reduction factor" reduces its effect at least by $\left(\frac{\omega_D{}^2}{\omega_0{}^2-\omega_D{}^2}\right)^4$, which is very small for $\omega_0 \gg \omega_D$ case. The second term due to the anharmonicity of solid ϕ_{anh} is significant compared to the first term. The third term due to the "cross interaction" between the two anharmonicities for the two vertex diagram may also be significant in some cases.

The imaginary part due to the one phonon dephasing term given by diagram 7 in Fig. (3.1) vanishes since both the prefactors R_k^V and $R_k^\phi \to 0$ when $\omega_k \to 0$. The effects of phonon on the "T mode" line shape due to the anharmonicity of the adsorption potential V is reduced by the "reduction factor" dramatically. However, the anharmonicity of the substrate will give an additional delocalized phonon contribution to the "T mode" line shape. In the next section, we will show this numerically in terms of a sample system.

In principle, above results can be applied to any adsorption systems with an adatom at an on top site. However, the theory is not limited to this site. One can generalize the calculation to any other adsorption situations such as at a bridge

site etc. with only some modification in the hamiltonian. The kinds of relaxation processes permitted are governed by the interaction hamiltonian or anharmonic hamiltonian. Using the Feymann diagram rules, we can also calculate the line shape due to the different processes for other adsorption systems.

3.4 Model system results with numerical calculation

In this section, the line shift and line width of the adsorbate-surface stretching mode ("T mode") and the internal mode ("V mode") of a diatomic adsorption system are explicitly calculated for the adsorption system CO/Pt(111) with the CO sitting at an ontop site and the C atom inward to the surface. A detailed experimental study of this system has been carried out in Ref. [37].

We assume the shape of the adsorption potential to be a Morse potential which has the form

$$V(z) = V_0(e^{-2\alpha z} - 2e^{-\alpha z}), \tag{3.67}$$

where the depth and the range of the potential are given by V_0 and α^{-1}, respectively. For the temperature range in which the IR experiment was performed, $kT \ll V_0$. In thermal equilibrium, the system occupies the ground state and the excited states near it so that we can treat the anharmonic terms of the Morse potential as a perturbation. The n^{th} derivative of the Morse potential is given by

$$V_n = V_0\left[(-2\alpha)^n - 2(-\alpha)^n\right]. \tag{3.68}$$

Only the anharmonic terms up to the 4^{th} derivative of the adsorption potential are considered in our calculation. The coupling constants are specifically given by

$$V_2 = 2V_0\alpha^2, \tag{3.69}$$

Table 3.1: Input and derived parameters for CO/Pt(111) at an ontop site

substrate atom mass M_s (amu)	195.1
adsorbate mass m (amu)	28.0
reduced mass for adsorbate (amu)	6.9
mass of atom C (amu)	12.0
well depth V_0 (eV)	1.3
potential well width α^{-1} (Å)	0.34
local mode frequency ω_0 (cm^{-1})	470
Debye frequency of substrate ω_D (cm^{-1})	167
internal vibrational frequency Ω (cm^{-1})	2090.0

$$V_3 = -6V_0\alpha^3, \tag{3.70}$$

$$V_4 = 14V_0\alpha^4. \tag{3.71}$$

The input and derived parameters for CO adsorbed at an ontop site of the Pt(111) surface are listed in Table (3.1).

The local mode frequency ω_0 is taken from IR absorption experiments at one monolayer coverage for this system[71]. The experiment shows the "T mode" absorption peak at about 462 cm^{-1} at the temperature T= 100 K. As the temperature is increased from 100 K to 250 K, the peak position shifts downwards by about 1.6 cm^{-1}. The vibrational line width [full width at half maximum (FWHM)=$2\Gamma_T$] increases by about 2 cm^{-1} over the same temperature range. See Fig. (3.4) for the experimental results. The internal vibrational frequency Ω is studied in other IR experiments[37, 79]. As temperature is increased from 50 K to 300 K, the peak position shifts from 2106 cm^{-1} to 2100 cm^{-1} and the line width increases from 4 cm^{-1} to 7 cm^{-1}. See Fig. (1.4). The depth of the potential well is taken from the experimental result of Ertl etc.[15], and its width is fixed via the relation $V_2 = m\omega_0^2$. We do not expect to fully explain this data in our simple model, but at least show some partial contributions due to the substrate phonons.

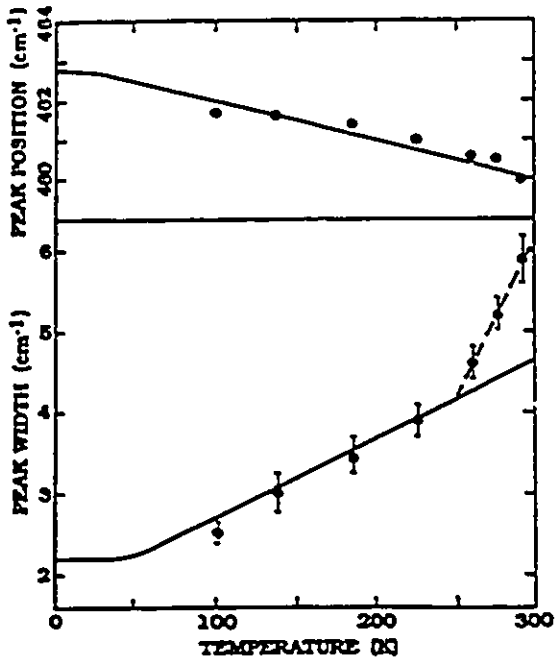

Figure 3.4: IR experiment results for the "T mode" of CO/Pt(111) system from Ref. [71].

3.4.1 Perturbative treatment of the bilinear term

"T mode"

Using the input parameters in Table 3.1, the line shift of the "T mode" for CO adsorbed at an ontop site of the Pt(111) surface is computed from the results given in Eqs. (3.4–3.13). The temperature dependence of the "T mode" shift is plotted in Fig. (3.5a). Fig. (3.5a) shows red shifts due to both the phonon-"T mode" interactions and the local mode self interactions. The dash line represents the temperature dependence of the line shift contributions due to the thermal phonon excitation. At high temperature, this shift is extremely large compared to the experimental result due to the perturbative treatment of the bilinear term. We will see this corrected in the next subsection. The dotted line represents the temperature dependence of

the line shift contributions related to the thermal occupation of the local mode.

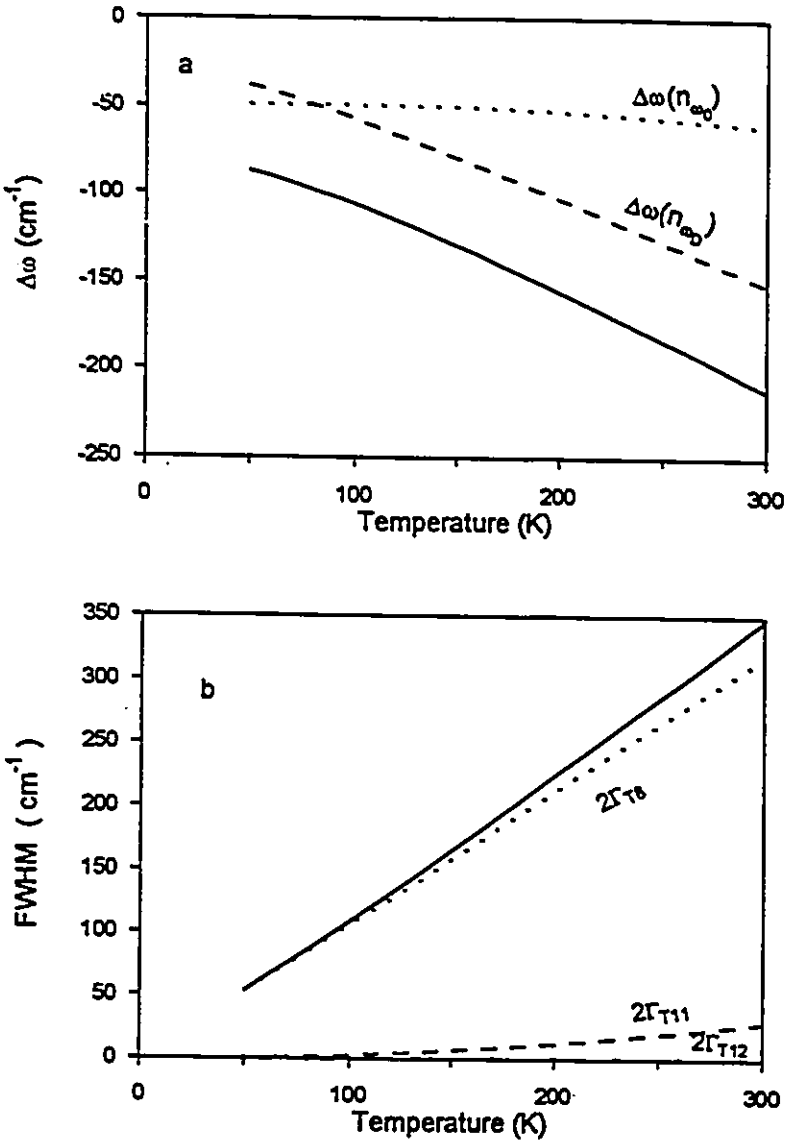

Figure 3.5: The "T mode" line shift (a) and the line width (b) for the CO/Pt(111) system in purely perturbative approach (see text).

Since the "T mode" frequency is in the range $2\omega_D < \omega_0 < 3\omega_D$, energy conservation requires at least three phonon emission processes contributing to the "T mode" line width. The line width due to the one phonon dephasing process, the three phonon emission processes and the elastic phonon scattering processes are shown in Fig. (3.5b). The line width contributed by the one phonon dephasing process is proportional to temperature and gives an unreasonably large result over the temperature range from 50 to 300 K. This contribution will disappear after we treat the bilinear term properly. The dephasing processes of the elastic phonon scattering processes give the smallest contribution.

As we mentioned in Section 3.1, this treatment is not quite right due to the coupling strength of the bilinear term. It enlarges the contributions of the substrate phonons due to the anharmonicity of the adsorption potential. The total line width is unreasonably larger than the experimental results. All the line width contributions calculated here need to be modified by the nonperturbative treatment of the bilinear term.

"V mode"

The line shifts due to the phonon-V-T mode interaction, the T-V mode interaction and the " V mode" self interaction V-V are shown in Fig. (3.6a). Similarly to the "T mode", the phonon effects on the "V mode" line shape are also over-estimated due to the purely perturbative treatment of the bilinear term. The overall shift is about 5 times larger than the experimental result. The "V mode" line width is mainly due to the one phonon dephasing term. The line width contribution of the exchange mechanism is very small due to the large "T mode" line width in this treatment. See Fig. (3.6b). People usually believe that the "V mode" line width is due to the

interaction with lower frequency local modes. If we reduce the "T mode" line width to the experimental result, the contribution of the exchange term will increase to 2.6 cm^{-1} which is in the range of the experimental result.

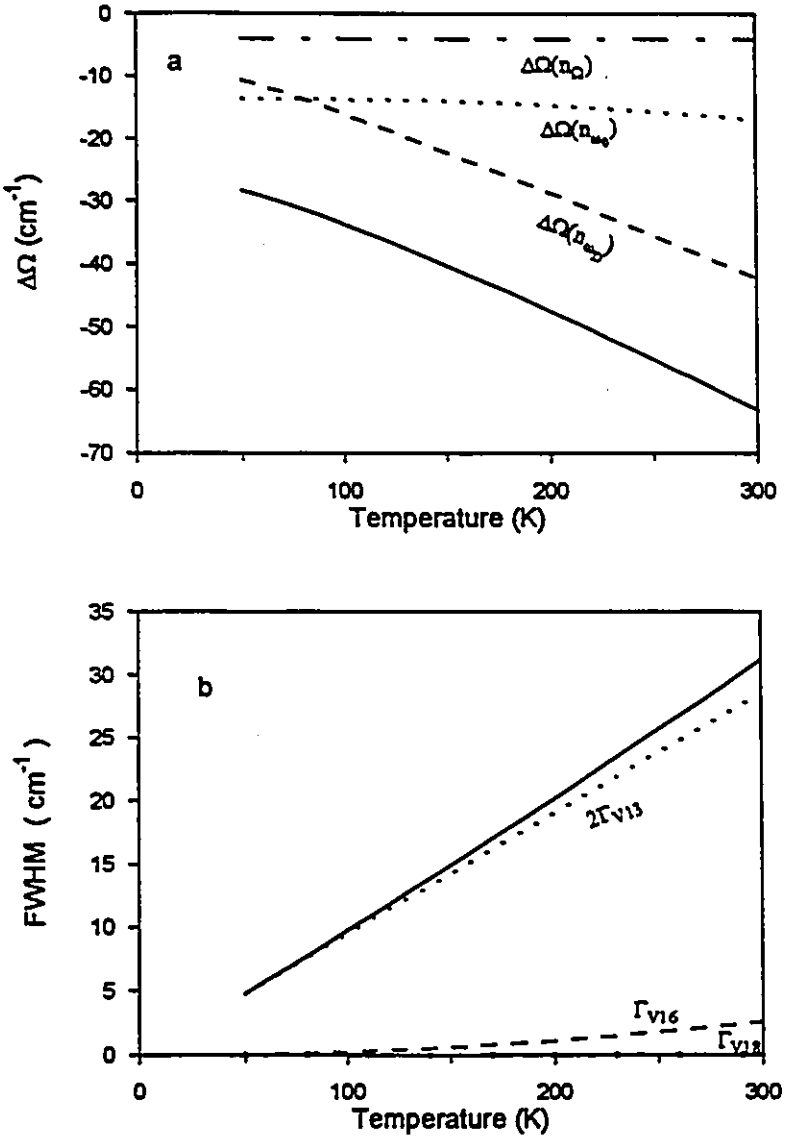

Figure 3.6: The "V mode" line shift (a) and line width (b) of the CO/Pt(111) system in the purely perturbative approach.

3.4.2 Nonperturbative treatment of the bilinear term

In this treatment, the difference in displacement $z - a_{1z}$ between an admolecule and the surface atom from their equilibrium positions, which will enter V_{anh}, can be expanded as a combination of the normal modes z^0 and d_k^0. The prefactors are R_T^V and R_k^V, respectively. The phonon propagators due to the anharmonic interaction V_{anh} come with a factor $(R_k^V)^2$. Considering the three phonon emission processes of the CO/Pt(111) as an example, the "reduction factor" reduces the line width by $(R_{k_1}^V)^2(R_{k_2}^V)^2(R_{k_3}^V)^2$, which is

$$\left(\frac{\omega_{k_1}^2}{\omega_{k_1}^2-\omega_0{}^2}\right)^2\left(\frac{\omega_{k_2}^2}{\omega_{k_2}^2-\omega_0{}^2}\right)^2\left(\frac{\omega_{k_3}^2}{\omega_{k_3}^2-\omega_0{}^2}\right)^2 < \left[\frac{1}{1-\frac{\omega_0{}^2}{\omega_D{}^2}}\right]^6. \qquad (3.72)$$

This factor is less than 10^{-6} for the CO/Pt(111) which makes the line width contribution of the three phonon emission processes due to the anharmonicity of the adsorption potential very small. Similarly, elastic phonon scattering due to the same anharmonicity will come with a factor less than 10^{-4} which makes its contribution negligible. The line width contribution of the one phonon dephasing process disappears due to the fact that the "reduction factor" R_k^V goes to zero for the soft phonon. Therefore, all phonon effects on the "T mode" line width due to the anharmonicity of adsorption potential alone are negligible. Numerical calculation shows that at room temperature, the phonon-induced "T mode" line shift and line width due to the anharmonicity of the adsorption potential are -0.15 $cm^{-1}$and 1.26×10^{-3} cm^{-1}, respectively.

Ye and Piercy did some numerical calculation for the contribution from the anharmonicity of the substrate ϕ_{anh}[59]. The "T mode" line shift due to this anharmonicity is calculated for the CO/Pt(111) and the result due to diagrams 1 and 5 in Fig. (3.1) is plotted in Fig. (3.7).

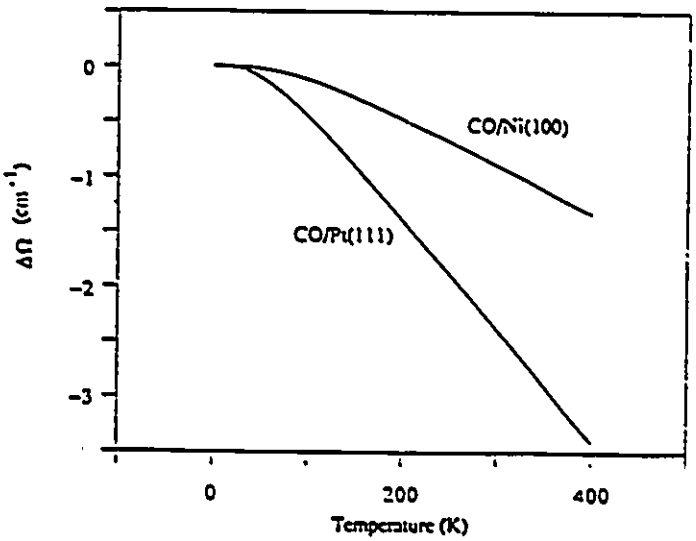

Figure 3.7: The "T mode" line shift contributed by the ϕ_{anh} for CO/Pt(111) from Ref. [59].

This is the total contribution of the self energy diagrams 1 and 5. The contribution of diagram 1 is the second term in Eq. (3.65). The calculated frequency shift over the temperature range from 100 to 300 K is -1.8 cm^{-1} which is in the same order of magnitude as the experimental results of -2 cm^{-1} observed by Ryberg[71] and by Malik and Trenary[80] at the coverage of 0.5 and 0.19 ML, respectively. This result shows that the anharmonicity in the substrate plays an important role in determining the frequency shift in this system. Also, the theoretical prediction compares remarkably well with the experimental result, considering the simplicity of the model used. They completely ignored the line shift contribution due to anharmonicity of adsorption potential.

The line width of the "T mode" is also contributed by the anharmonic coupling with other lower frequency modes, such as the parallel frustrated translation, via phase relaxation. Many people have interpreted the temperature dependent line shift and line width of the "T mode" in terms of exchange mechanisms with a few fitting

parameters[17, 53]. Since Langreth *et al.*[17] have summarized this contribution in great detail, we do not discuss this dephasing contribution further here.

Chapter 4. A simple model for adsorption at a bridge site

4.1 Introduction

Up to now, we have considered adsorption at an ontop site. We have shown that the coupling of the local mode to the substrate phonons, mediated by the anharmonicity of the adsorption potential, is negligible for an adsorbate at ontop sites. An adsorbate may sit at different sites even at the same surface[37]. The IR absorption line position and line width will be affected by the adsorption geometry. In order to understand the influence of the adsorption geometry on the local mode vibrational line shift and line width, we study the phonon-induced vibrational line shape of an adatom at a bridge site mediated by the anharmonicity of the adsorption potential in a simple one dimensional model in this chapter. The method used in the last two chapters also can be applied to this adsorption situation with some modifications of the hamiltonian of the adsorption system, for an adatom at a bridge site. The theory is applicable to an admolecule at a bridge site if we ignore the internal motion of the molecule.

When an atom is adsorbed at a bridge site, it is bound symmetrically to two neighboring surface atoms nearest to it. The thermal phonon motion of these neighboring surface atoms are generally not in phase, in accordance with the spatial dependence of the substrate phonon field. Our study will show that the out of phase phonon motion of the two bridge atoms is coupled to the local mode, mediated by the anharmonicity of the adsorption potential, and gives an additional contribution

to the vibrational dynamics that is absent in the previous ontop site model. We will concentrate on this enhancement contributed by the adsorption potential in this chapter. Although the anharmonicity of the solid as well as the cross interactions between both the anharmonicities are also expected to contribute significantly at a bridge site, we will not put much effort on them here and will study a full three dimensional picture including both the anharmonicities and cross interaction between them in Chapter 6. From now on, we purely concentrate on the dynamics of the "T mode", corresponding to the symmetric stretch of the adatom bonding to the two bridge atoms at the surface since it contains both decay and dephasing mechanisms. The decay of the local vibrational mode may occur efficiently via the interactions with acoustic phonons.

In Section 2, the hamiltonian of the adsorption system of an adatom at a bridge site is constructed. In Section 3, the normal mode expansions of vibrational coordinates are obtained by solving the harmonic hamiltonian in the weak coupling limit. In Section 4, the self energy expansion is given in terms of Feynman diagrams based on the anharmonic hamiltonian for this adsorption situation. Finally, the line shift and line width are calculated and the results is applied to the CO/Pt(111) and O/Cu(110) adsorption systems.

4.2 The hamiltonian

We consider an adatom of mass m, adsorbed at a bridge site on the (100) surface of a simple cubic lattice as in Fig. (4.1). As an initial study, in this simple model here we only include the components of the atomic displacements perpendicular to the surface. Adsorption at a bridge site is assumed here to be governed by the pairwise interactions with the two bridge atoms which have equilibrium positions at $\vec{R}_1$ and

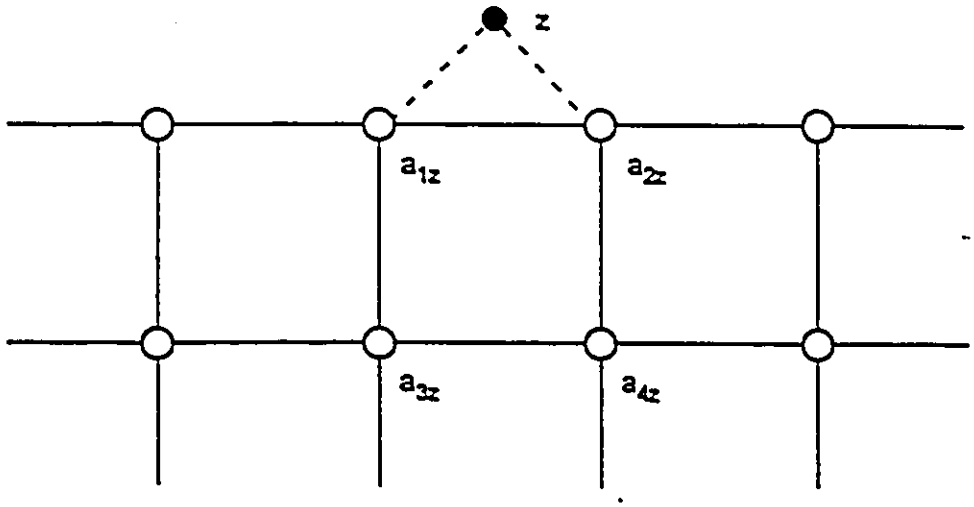

Figure 4.1: Adsorption configuration for an adatom at a bridge site on the (100) surface of a simple cubic lattice.

$\vec{R}_2$ with respect to the adatom. The adsorption potential

$$V_{total}(z, a_{1z}, a_{2z}) = V(z - a_{1z}) + V(z - a_{2z}) \tag{4.1}$$

is composed of identical pair potentials $V(z - a_{iz})$ which are assumed to depend on the vertical distances between the adatom and the two bridge atoms and can be expanded in terms of their equilibrium. z, a_{1z} and a_{2z} denote the perpendicular components of the vibrational displacements of the adatom and the two bridge atoms at the surface, respectively. The pair potential $V(z - a_{iz})$ can be expanded in powers of the perpendicular displacements z and a_{iz} with $i = 1, 2$. The harmonic part of the adsorption potential couples the local vibrational coordinate z to the displacements a_{iz} of the two bridge atoms (i=1,2) it is bound to. Similarly to the nonperturbative treatment of the bilinear coupling for an adatom at an ontop site cases, we ignore the terms $\frac{1}{2}V_2 a_{1z}^2$ and $\frac{1}{2}V_2 a_{2z}^2$. Therefore the harmonic hamiltonian

reads

$$H_{harm} = H_T + H_s - V_2 z(a_{1z} + a_{2z}), \tag{4.2}$$

where $V_2 = \frac{1}{2}m\omega_0^2$ is the second derivative of the potential $V(z - a_{iz})$ since the adatom is bound to two bridge atoms at the surface now. H_T describes the hamiltonian of the free oscillator of the adatom vibrating with frequency ω_0 at a static surface, while H_s describes the harmonic hamiltonian of the substrate which we again approximate in a bulk Debye model for an infinite solid. H_s, H_T and their solutions are given by Eqs. (2.39), (2.42), (3.44) and (3.43), respectively. The bilinear terms $V_2 z a_{1z}$ and $V_2 z a_{2z}$ couple the motion of the adatom to that of the two bridge atoms it is bound to. This harmonic hamiltonian describes a localized mode interacting with all delocalized phonon modes in the substrate via the two bilinear terms.

The anharmonic hamiltonian is made up of the anharmonicities of the adsorption potential and the substrate. In this chapter, we intend to see the role of the anharmonicity of the adsorption potential for an adatom at a bridge site; we therefore will pay more attention to it. For completeness, we also include the anharmonicity of the substrate in our calculation. The pair potentials are assumed to depend on the perpendicular components of the vibrational displacements of the pair atoms so that the differences $z - a_{1z}$ and $z - a_{2z}$ will enter the anharmonic terms of the adsorption potential, while $a_{1z} - a_{j_1 z}$ and $a_{2z} - a_{j_2 z}$ (j_1, j_2 are the nearest neighbors of bridge atoms 1 and 2, respectively) will enter the anharmonic terms of the substrate pair potentials, i.e.

$$H_{anh} = V_{anh}(z - a_{1z}) + V_{anh}(z - a_{2z}) + \sum_{j_1} \phi_{anh}(a_{1z} - a_{j_1 z})$$

$$+\sum_{j_2}\phi_{anh}(a_{2z}-a_{j_2z}), \tag{4.3}$$

where we have assumed that all the pair interactions in the solid are described by the same potential ϕ. This anharmonic hamiltonian can be expanded in powers of the differences $z-a_{1z}$, $z-a_{2z}$, $a_{1z}-a_{j_1z}$ and $a_{2z}-a_{j_2z}$. Once we have found the differences by solving the harmonic hamiltonian, we can draw the Feynman diagrams based on the anharmonic hamiltonian expansion.

4.3 Equation of motion and its solution in the harmonic approximation

Similar to the case of an adatom at an ontop site case, the perpendicular displacement of a surface atom can be expanded in form

$$a_{iz}(t)=\sum_k e_k^z e^{i\vec{k}\cdot\vec{R}_i}d_k(t), \tag{4.4}$$

where $\vec{R}_i$ is the equilibrium position of bridge atom i=1 or 2, $\vec{k}$ is the wave vector, e_k^z is the perpendicular component of the unit polarization vector $\vec{e}_k$, and d_k is the k^{th} phonon amplitude. Based on the H_{harm} given in Eq. (4.2), the Heisenberg equations of motion lead to

$$(-\frac{\partial^2}{\partial t^2}-{\omega_0}^2)z(t) = -\frac{1}{2}{\omega_0}^2[a_{1z}(t)+a_{2z}(t)], \tag{4.5}$$

$$(-\frac{\partial^2}{\partial t^2}-{\omega_k}^2)d_k(t) = -e_k^z\frac{m}{2MN}{\omega_0}^2 z(e^{-i\vec{k}\cdot\vec{R}_1}+e^{-i\vec{k}\cdot\vec{R}_2}). \tag{4.6}$$

These are the equations of motion for an adatom and the substrate delocalized phonon displacements, respectively. The right hand sites of them are due to the bilinear coupling between an adatom and the two bridge atoms at surface $-V_2z(a_{1z}+a_{2z})$. They act as forces on the free vibrations of the localized and delocalized phonon

modes. We only consider the case in which the local mode frequency ω_0 is outside of the continuum phonon band.

In the weak coupling limit, the Green's function solution of the equations of motion gives the approximate normal mode expansion of the vibrational coordinates in analogy with the ontop site case as follows:

$$z(t) = z^0(t) + \sum_k e_k^z \frac{\frac{1}{2}{\omega_0}^2}{{\omega_0}^2 - {\omega_k}^2}(e^{i\vec{k}\cdot\vec{R}_1} + e^{i\vec{k}\cdot\vec{R}_2})d_k^0(t), \tag{4.7}$$

$$d_k(t) = d_k^0(t) - e_k^z \frac{m}{MN}\frac{\frac{1}{2}{\omega_0}^2}{{\omega_0}^2 - {\omega_k}^2}(e^{-i\vec{k}\cdot\vec{R}_1} + e^{-i\vec{k}\cdot\vec{R}_2})z^0(t), \tag{4.8}$$

where $z^0(t)$ describes the local mode amplitude of the atomic motion at a static surface with $a_{iz} = 0$; $d_k^0(t)$ is the displacement of the k^{th} phonon mode of the harmonic substrate, and ω_k is the delocalized phonon frequency. Combining Eq. (4.4) and Eq. (4.8) gives the displacements of the two bridge atoms

$$a_{1z}(t) = a_{1z}^0(t) - \sum_k |e_k^z|^2 \frac{m}{MN}\frac{\frac{1}{2}{\omega_0}^2}{{\omega_0}^2 - {\omega_k}^2}(e^{i\vec{k}\cdot(\vec{R}_1 - \vec{R}_2)} + 1)z^0(t), \tag{4.9}$$

$$a_{2z}(t) = a_{2z}^0(t) - \sum_k |e_k^z|^2 \frac{m}{MN}\frac{\frac{1}{2}{\omega_0}^2}{{\omega_0}^2 - {\omega_k}^2}(e^{i\vec{k}\cdot(\vec{R}_2 - \vec{R}_1)} + 1)z^0(t). \tag{4.10}$$

Define

$$\begin{aligned} g &= \sum_k |e_k^z|^2 \frac{m}{MN}\frac{\frac{1}{2}{\omega_0}^2}{{\omega_0}^2 - {\omega_k}^2}\left[e^{-i\vec{k}(\vec{R}_2 - \vec{R}_1)} + 1\right] \\ &= \sum_k |e_k^z|^2 \frac{m}{MN}\frac{\frac{1}{2}{\omega_0}^2}{{\omega_0}^2 - {\omega_k}^2}\left[e^{i\vec{k}(\vec{R}_2 - \vec{R}_1)} + 1\right]. \end{aligned} \tag{4.11}$$

In the second line above we have replaced $\vec{k}$ with $-\vec{k}$ which does not change the value of the sum since Σ_k includes all wave vectors in all directions. The constant g gives the vibrational amplitude of the local mode at the surface atom i. It is small but not negligible in the weak coupling limit. With this definition, we can rewrite

Eq. (4.9) and (4.10) as

$$a_{1z}(t) = a^0_{1z}(t) - gz^0(t), \tag{4.12}$$

$$a_{2z}(t) = a^0_{2z}(t) - gz^0(t). \tag{4.13}$$

The displacements $a_{1z}(t)$ and $a_{2z}(t)$ of the surface atoms gain a localized contribution proportional to $z^0(t)$ as given in Eqs. (4.9) and (4.10). Similarly, the vibrational displacement $z(t)$ of an adsorbed atom also includes both the localized and delocalized phonon components in Eq. (4.7). Eqs. (4.9) and (4.10) are analogies to Eq. (3.56). If $\vec{R}_1 = \vec{R}_2 = 0$, i.e., the two bridge atoms at the surface overlap and are positioned at zero, Eqs. (4.9) and (4.10) reduce to Eq. (3.56) given for an adatom at an ontop site.

The vertical distance between the adatom and either bridge atom (i=1,2) may be written as

$$z(t) - a_{iz}(t) = (1+g)z^0(t) + (-1)^i A(t) + B(t), \tag{4.14}$$

where we have defined,

$$A(t) = \frac{1}{2}\sum_k e^z_k (e^{i\vec{k}\cdot\vec{R}_2} - e^{i\vec{k}\cdot\vec{R}_1}) d^0_k(t). \tag{4.15}$$

$$B(t) = \frac{1}{2}\sum_k e^z_k \frac{{\omega_k}^2}{{\omega_0}^2 - {\omega_k}^2} (e^{i\vec{k}\cdot\vec{R}_1} + e^{i\vec{k}\cdot\vec{R}_2}) d^0_k(t). \tag{4.16}$$

The effects of the phonon motions of the two bridge atoms are included in $A(t)$ and $B(t)$ given in Eq. (4.15) and Eq. (4.16). $B(t)$ describes the phonon displacements of the in-phase motion of the two bridge atoms, modified by a "reduction factor" $\frac{{\omega_k}^2}{{\omega_0}^2 - {\omega_k}^2}$. This term gives relatively weak coupling effects as we showed in the case of an adatom at an ontop site and is therefore ignored here. $A(t)$ describes the out of phase components of the motions of the two bridge atoms. The atomic vibration

coupling to the delocalized phonons can occur much more efficiently via $A(t)$, which is due to the difference in the phonon displacements of the two bridge atoms. We will specifically calculate the line shape contributed by this effect later.

The anharmonicity of the substrate is also expected to contribute to the "T mode" vibrational lineshape. Following a discussion similar to the ontop site case, we assume the second layer atoms will not be affected by the adsorbate, i.e., the second layer substrate atoms have a displacement $a_j = a_j^0$. Hence the difference of the displacements between the surface atom i and its nearest neighbor j beneath it becomes

$$\begin{aligned} a_{iz} - a_{jz} &= a_{iz}^0 - a_{jz}^0 - gz^0 \\ &= A_{ij} - gz^0, \end{aligned} \tag{4.17}$$

where

$$\begin{aligned} A_{ij}(t) &= a_{iz}^0(t) - a_{jz}^0(t) \\ &= \sum_k e_k^z (e^{i\vec{k}\cdot\vec{R}_i} - e^{i\vec{k}\cdot\vec{R}_j}) d_k^0(t), \end{aligned} \tag{4.18}$$

is the vertical difference in the displacements of the surface atom i and its nearest neighbor j. In this expression, we have included the spread of the localized vibrational mode as far as the first layer surface atom $i = 1, 2$ only. This difference $a_{iz} - a_{jz}$ in the atomic displacements will enter the anharmonic terms of the substrate pair potential ϕ and show that the free vibrational coordinate of the localized mode z^0 is coupled by the anharmonicity of the substrate to the difference of the phonon amplitude $A_{ij}(t)$.

4.4 Feynman diagrams and self energy

We still consider the anharmonic terms with the coupling constant up to the 4^{th} derivative of the pair potentials. The in phase motion contribution of the two bridge atoms to the line shape is ignored due to the "reduction factor" as we discussed above. The out of phase motion of the two bridge atoms $A(t)$ has opposite sign in the two vertical distances between the adatom and either bridge atom, in Eq. (4.14), due to the symmetry of the bridge site. Therefore, the anharmonic terms of the two adsorption bonds with the odd powers of $A(t)$ always cancel each other and only the anharmonic terms with the even powers of $A(t)$ in the total adsorption potential make contributions to the vibrational relaxation and line shape of the molecular or atomic vibration, i.e.

$$\begin{aligned} V_{anh}^{total} &= V_3(R_T z^0)A^2 + \frac{1}{2!}V_4(R_T z^0)^2 A^2 + \cdots \\ &\quad + \frac{1}{3}V_3(R_T z^0)^3 + \frac{1}{12}V_4(R_T z^0)^4 + \cdots, \end{aligned} \tag{4.19}$$

where $R_T = 1 + g$ is the prefactor of the local mode. $A(t)$ is composed of the free phonon displacement $d_k^0(t)$ whose Green's function can be easily calculated. Eq. (4.19) excludes, for example, the three phonon emission channel for vibrational energy relaxation. For a (100) surface of a simple cubic lattice, each bridge atom has one nearest neighbor beneath it as in Fig. (4.1). In this adsorption situation, there are only two anharmonic bonds in the substrate which affect the "T mode" line shape since we have ignored the parallel motions of the substrate atoms. The total anharmonic hamiltonian of the solid which affects the "T mode" line shape is composed of these two anharmonic bonds due to the anharmonic pair potentials in the substrate between surface atom 1 and the substrate atom 3, and between the surface atom 2 and the substrate 4. The other anharmonic pair potentials for the

atoms in the substrate are independent of the local mode coordinate $z^0(t)$; and thus will not affect the local mode vibration. Therefore, the anharmonic potential of the substrate we need to include here is

$$\begin{aligned} \phi_{anh} &= \frac{\phi_3}{3!}[A_{13} - gz^0]^3 + \frac{\phi_4}{4!}[A_{13} - gz^0]^4 + \cdots \\ &+ \frac{\phi_3}{3!}[A_{24} - gz^0]^3 + \frac{\phi_4}{4!}[A_{24} - gz^0]^4 + \cdots, \end{aligned} \tag{4.20}$$

where the prefactor of the local mode now is $-g$, and A_{13} and A_{24} are also composed of a sum of the free phonon displacements d_k^0 with different prefactors which are determined by the equilibrium positions of the substrate atoms 1, 2, 3, and 4. See Fig. (4.1).

Based on the anharmonic hamiltonian given by Eqs. (4.19) and (4.20), the lowest-order diagram expansion of the self energy is given by Fig. (4.2). The vertex

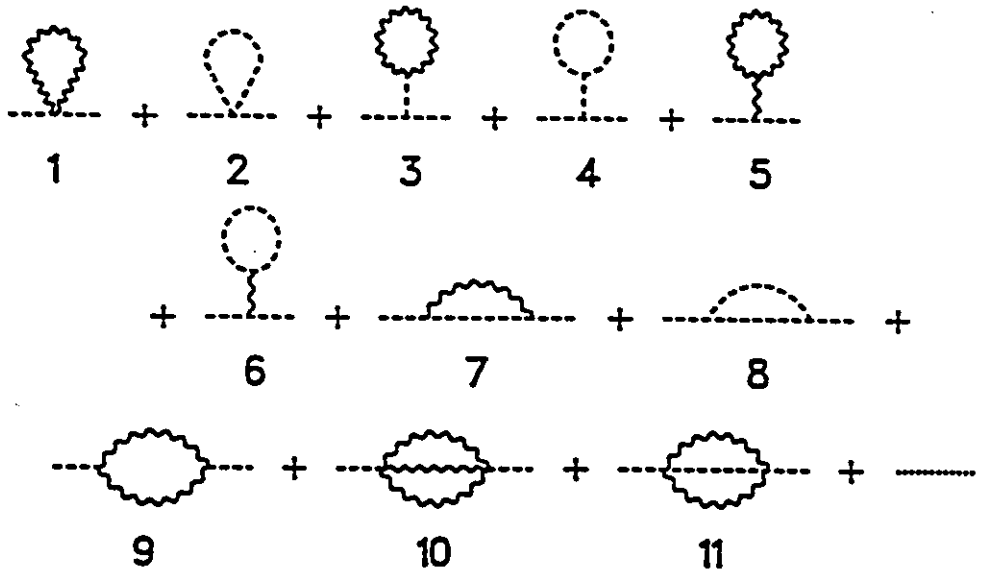

Figure 4.2: The "T mode" self energy expansion for an adatom at a bridge site on the (100) surface of a simple cubic lattice.

and wavy lines now have different meanings from those in the last chapter. The

Feynman diagram rules in Appendix D change slightly due to the nonperturbative treatment of the bilinear terms. Each diagram in the self energy expansion now represents the total contribution from both anharmonicities of the adsorption potential and the substrate. Compared to the displacement differences of the interaction bonds included for an adatom at an ontop site, prefactors R_T^V, R_T^ϕ, R_k^V and R_k^ϕ given in Eq. (3.58), (3.61), (3.59) and (3.62) are now replaced by $1+g, -g, \frac{1}{2}\left[e^{i\vec{k}\cdot\vec{R}_2} - e^{i\vec{k}\cdot\vec{R}_1}\right]$, and $\left[e^{i\vec{k}\cdot\vec{R}_i} - e^{i\vec{k}\cdot\vec{R}_j}\right]$, respectively. The wave lines in the self energy expansion represent the delocalized phonon propagators $\langle TA(t)A(0)\rangle$, $\langle TA_{ij}(t)A_{i'j'}(0)\rangle$, $\langle TA_{ij}(t)A(0)\rangle$, and $\langle TA(t)A_{ij}(0)\rangle$ depending on the anharmonic interaction represented by the vertices in the self energy diagram. Similarly, the dash lines in the self energy expansion represent the localized phonon propagators $\langle T(1+g)z^0(t)(1+g)z^0(0)\rangle$, $\langle T(-g)z^0(t)(-g)z^0(0)\rangle$, $\langle T(1+g)z^0(t)(-g)z^0(0)\rangle$, and $\langle T(-g)z^0(t)(1+g)z^0(0)\rangle$, respectively.

The three phonon emission term is purely contributed by the anharmonicity of the substrate. The "cross interactions" between the two anharmonicities for the two vertex diagrams are also expected to contribute to the "T mode" lineshape. The self energy diagrams given in Fig. (4.2) together give the dominate contributions to the "T mode" vibrational line shift and line width. Since we approximate the pair potentials between the atoms in terms of the vertical displacement differences between the atoms, the self energy diagrams due to the self interactions are similar to that for an adatom at an ontop site which we have discussed in details in last chapter. Here, we only consider the phonon-induced vibrational line shape.

The line shift is mainly given by the diagrams 1 and 3 in Fig. (4.2). Following

the Feynman diagram rules, we can write out the shift contributed by diagram 1 as

$$\Delta\omega_1 = \Delta\omega_{1v} + \Delta\omega_{1\phi} = \frac{3\hbar}{8mM_s\omega_0{\omega_D}^3}\int_0^{\omega_D} d\omega\omega(2n_\omega+1)$$
$$\left\{V_4(1+g)^2\left[1-\frac{sin(ka_{12})}{ka_{12}}\right]+\phi_4(-g)^2 4\left[1-\frac{sin(ka_{13})}{ka_{13}}\right]\right\}, \quad (4.21)$$

where the first term is contributed by the anharmonicity of the adsorption potential, while the second is from the substrate anharmonicity, $k=\omega(k_D/\omega_D)$ with k_D being the maximum wavevector, and a_{12} and a_{13} are the distances between the atoms 1 and 2, and between the atoms 1 and 3, respectively.

Similarly, the line width is contributed by the diagrams 9, 10 and 11 in Fig. (4.2) and reads

$$\Gamma = \Gamma_{9V} + \Gamma_{9\phi} + \Gamma_{10\phi} + \Gamma_{11V} + \Gamma_{11\phi}. \quad (4.22)$$

The two phonon emission process denoted by diagram 9 and the phonon elastic scattering process denoted by diagram 11 are possibly initiated by both anharmonicities of the adsorption potential and the substrate. Their line width contributions are given by

$$\begin{aligned}
\Gamma_9 &= \Gamma_{9V}+\Gamma_{9\phi} \\
&= \frac{9\pi\hbar}{16mM_s^2\omega_0{\omega_D}^6}\int d\omega\omega(\omega_0-\omega)(n_\omega+n_{\omega_0-\omega}+1)\theta(\omega_D-\omega_0+\omega)\theta(\omega_0-\omega) \\
&\quad \left\{V_3^2(1+g)^2\left[1-\frac{sin(ka_{12})}{ka_{12}}\right]\left[1-\frac{sin((k_0-k)a_{12})}{(k_0-k)a_{12}}\right]+\right. \\
&\quad \phi_3^2(-g)^2 16\left[1-\frac{sin(ka_{13})}{ka_{13}}\right]\left[1-\frac{sin((k_0-k)a_{12})}{(k_0-k)a_{12}}\right]+ \\
&\quad 4V_3(1+g)\phi_3(-g)\left[1-\frac{sin(ka_{12})}{ka_{12}}\right]\left[1-\frac{sin((k_0-k)a_{13})}{(k_0-k)a_{13}}\right]+ \\
&\quad \left.4V_3(1+g)\phi_3(-g)\left[1-\frac{sin((k_0-k)a_{12})}{(k_0-k)a_{12}}\right]\left[1-\frac{sin(ka_{13})}{ka_{13}}\right]\right\}, \quad (4.23) \\
\Gamma_{11} &= \Gamma_{11V}+\Gamma_{11\phi}
\end{aligned}$$

$$= \frac{9\pi\hbar^2}{16m^2M_s^2\omega_0^2\omega_D{}^6}\int d\omega\omega^2 n_\omega(n_\omega+1)$$
$$\left\{V_4^2(1+g)^4\left[1-\frac{sin(ka_{12})}{ka_{12}}\right]^2+\phi_4^2(-g)^4 16\left[1-\frac{sin(ka_{13})}{ka_{13}}\right]^2+\right.$$
$$\left.8V_4(1+g)^2\phi_4(-g)^2\left[1-\frac{sin(ka_{12})}{ka_{12}}\right]\left[1-\frac{sin(ka_{13})}{ka_{13}}\right]\right\}. \quad (4.24)$$

The three phonon emission process denoted by diagram 10 is purely due to the substrate anharmonicity since the odd powers of $A(t)$ are absent in the anharmonic expansion of the adsorption potential. The line width contributed by the three phonon emission process is given by

$$\Gamma_{10\phi} = \frac{9\pi\hbar^2\phi_4^2g^2}{4mM_s^3\omega_0\omega_D{}^9}\int d\omega_1 d\omega_2\omega_1\omega_2(\omega_0-\omega_1-\omega_2)$$
$$[(n_{\omega_1}+1)(n_{\omega_2}+1)(n_{\omega_0-\omega_1-\omega_2}+1)-n_{\omega_1}n_{\omega_2}n_{\omega_0-\omega_1-\omega_2}]$$
$$\left[1-\frac{sin(k_1a_{13})}{k_1a_{13}}\right]\left[1-\frac{sin(k_2a_{13})}{k_2a_{13}}\right]\left[1-\frac{sin(k_3a_{13})}{k_3a_{13}}\right]$$
$$\theta(\omega_D-\omega_0+\omega_1+\omega_2)\theta(\omega_0-\omega_1-\omega_2), \quad (4.25)$$

where $k_3 = k_0 - k_1 - k_2$. For a specific adsorption system, the $\theta(\omega)$ functions above ensure the energy conservation in the local mode vibrational decay processes by emitting delocalized phonons. The line shifts and line widths contributed by the anharmonicity of the substrate above are similar to those in Ye and Piercy's calculation[59]. The differences in our model are

- there are two anharmonic bonds in the substrate which affect the local mode line shape.
- the prefactor g depends on both bridge atom positions.
- the local mode vibrational frequency for the admolecule CO at a bridge site is smaller than that at an ontop site at the Pt(111) surface.

Table 4.1: The input and derived parameters for the CO/Pt(111) and O/Cu(110) with the admolecule or adatom at a bridge site

	CO/Pt(111)	O/Cu(110)
substrate atom mass M_s (amu)	195.1	63.6
adsorbate mass m (amu)	28.0	16.0
well depth $2V_0$ (eV)	1.3	10.0
potential well width α^{-1} (Å)	0.42	1.5
local mode frequency ω_0 (cm^{-1})	380	389
Debye frequency of substrate ω_D (cm^{-1})	167,195	219

4.5 Numerical results for CO/Pt(111) and O/Cu(110)

To demonstrate the dynamic effects of these anharmonic interactions proposed above, the model is now applied to study the adsorption of CO/Pt(111) and O/Cu(110) for the adatom at a bridge site. The input and derived parameters are listed in Table (4.1). For simplicity, the dependence of the pair potential on the perpendicular motion is approximated by a Morse potential, with depth and width parameters fixed by the heat of adsorption and the local mode frequency ω_0. When the potential well depth V_0 and the vibrational frequency ω_0 are fixed, the width of the potential well is determined by the relation $4V_0\alpha^2 = m\omega_0^2$. As we mentioned, we would like to understand the influence of the adsorption site, more specifically, to study the phonon effects on the vibrational line shape due to the adsorption potential for different sites. In Chapter 3, we have shown the anharmonicity of the adsorption potential is negligible in the calculation of the vibrational line shift and line width when an adatom is adsorbed at an ontop site. Now we numerically study the same anharmonicity in the calculation of vibrational line shift and line width for an adatom at a bridge site. Since the anharmonic terms with the odd powers of the delocalized phonon coordinate $A(t)$ are canceled out due to the symmetry of

the two bridge atoms at the surface in this model, as a result, only the self energy diagrams 1 and 3 in Fig. (4.2) will contribute to the phonon-induced vibrational line shift. Diagrams 2, 5 and 8 in Fig. (4.2) will contribute to the "T mode" line shift via the local mode self interaction, due to V_{anh}.

4.5.1 CO/Pt(111)

For the CO/Pt(111) adsorption system, as the coverage increases, CO will occupy both ontop and bridge sites. When CO is adsorbed at a bridge site, the CO-Pt symmetric stretching mode has the vibrational frequency measured by EELS to be $\omega_0 = 380$ cm^{-1}[35]. The heat of adsorption of CO/Pt(111) for the admolecule at a bridge site is very close to that at an ontop site[37]. We thus approximate it with the same value as that at an ontop site, i.e., $2V_0 = 1.3$ eV. The cut-off frequency ω_D used to model the substrate phonon spectrum is estimated in two ways here. The low temperature specific heat data for Pt gives the Debye frequency $\omega_D \approx$ 167 cm^{-1}[81]. However, lattice dynamics calculations[82, 83] suggest the maximum phonon frequency of about 195 cm^{-1}. Choosing the latter cut-off frequency allows us to consider the two phonon emission processes which are expected to be important in this adsorption situation.

The line shift contributions for this adsorption system are plotted in Fig. (4.3) with these two choices of cut-off frequency. Figs. (4.3a) and (4.3b) show the line shifts due to the diagrams 1 and 3 over the temperature range from 50 to 300 K for the two cut off frequencies 167 cm^{-1} and 195 cm^{-1}, respectively. The self energy diagram 1 in Fig. (4.2) gives a blue shift, while diagram 3 gives a red shift for both cut-off frequencies. The red shift is almost canceled by the blue shift, and the net shift is negative. At T= 300 K, it is -2.76 cm^{-1} for $\omega_D = 167$ cm^{-1}. The net shift

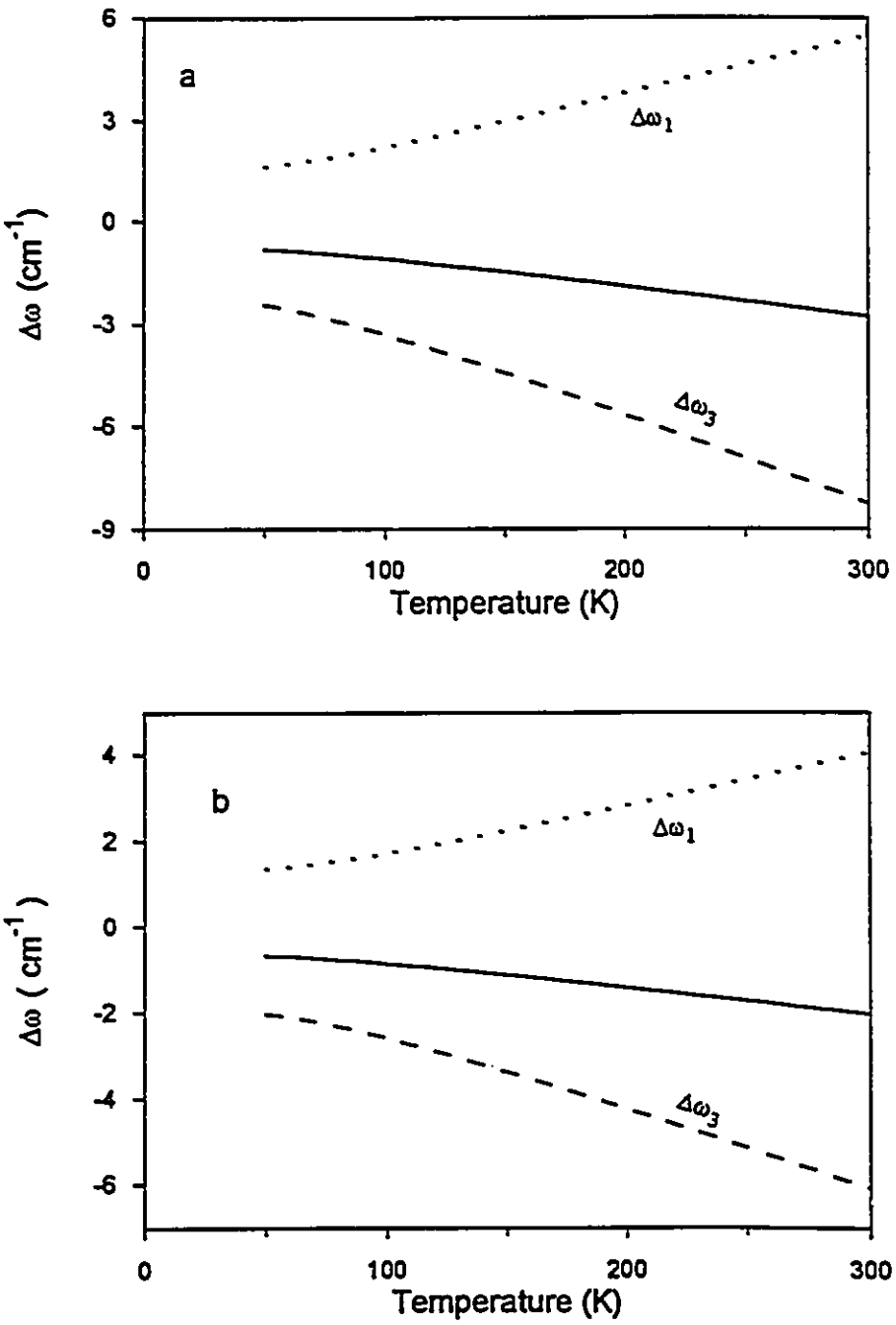

Figure 4.3: The "T mode" shifts due to the phonon effects of the adsorption potential for $\omega_D = 167$ cm^{-1} (a) and $\omega_D = 195$ cm^{-1} (b).

contributed by the substrate phonons due to the anharmonicity of the adsorption potential depends slightly on the cut-off frequency. We have discussed in detail the line shifts contributed by the local mode self interaction terms in the last chapter. The spectrum for a Morse oscillator gives a series of discrete peaks. The shift due to the local mode self interactions in our calculation corresponds to a weighted average of the discrete peak positions. For this system, the frequency spacing between the two nearest discrete peaks is much larger than the line widths in our calculation and in the experiment so that the discrete peaks will not overlap with each other. In the temperature range in which the experiment was performed, only the transition from the ground state can be observed if the resolution in the experiment is sharp. Therefore we ignore the line shift due to the local mode self interactions here.

Contributions to the vibrational line width for the CO/Pt(111) system are also calculated for the two different choices of the phonon cut-off frequencies discussed above. For $\omega_D = 167$ cm^{-1}, the two phonon emission term (diagram 9) is cut off since $\omega_0 \approx 2.3\omega_D$, and elastic phonon scattering (diagram 11) alone gives a line width (FWHM) increasing with temperature to 1.6 cm^{-1} at 300 K. The contribution of the three phonon emission processes is zero due to the symmetry of two bridge atoms in this case. When we increase the cut-off frequency to 195 cm^{-1}, the two phonon emission processes (diagram 9) as well as the elastic phonon scattering (diagram 11) contribute to the "T mode" line width. The elastic phonon scattering processes give a smaller contribution compared to the lower cut-off frequency case. The total line width increases from 0.7 to 2.3 cm^{-1} over the temperature range 50 to 300 K, and is dominated by the two phonon emission processes, as expected. The results are plotted in Fig. (4.4).

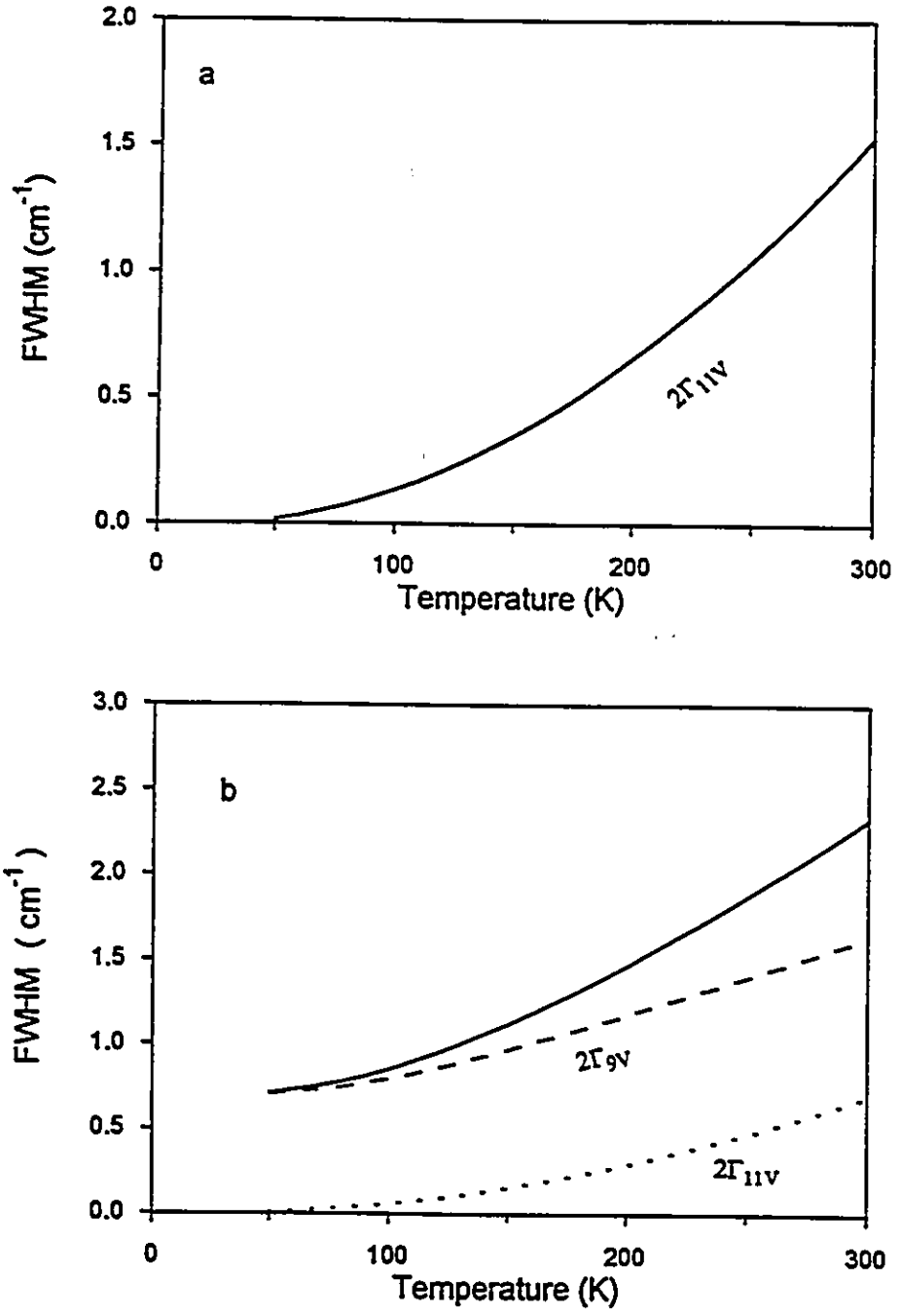

Figure 4.4: Phonon-induced "T mode" line width due to the anharmonicity of the adsorption potential for $\omega_D = 167$ cm^{-1} (a) and $\omega_D = 195$ cm^{-1} (b).

Although we are not aware of an experimental infrared absorption line shape study of this vibrational mode for CO absorbed at a bridge site at present, it is nevertheless interesting to note that these theoretical data are of the same order of magnitude as the experimental line width data for CO adsorbed at ontop sites on Pt(111) surface[71], as well as the estimated phonon-induced line shift due to the substrate anharmonicity at an ontop site, discussed by Ye and Piercy[59].

4.5.2 O/Cu(110)

The adsorption of oxygen on the Cu(110) surface is more complicated than CO on the Pt(111) surface. H. Dürr and A. P. Baddorf also studied the temperature dependent lineshape of the perpendicular oxygen vibrational mode in high resolution electron energy loss spectroscopy (HREELS). They found that this "oxygen mode" at 48.2meV (389 cm^{-1}) is the symmetric oxygen-copper bond stretching vibration which is localized at the surface. The negative energy shift over the temperature range $100 - 700$ K is about 3.2 cm^{-1} and the FWHM increases over the same temperature range by about 33 cm^{-1}. See Fig. (1.5). For this adsorption system, a surface reconstruction has been observed in the experiment. In the simple one dimension model, we will not go into the details of the substrate structure, but simply assume that the oxygen is attached to the two bridge atoms and consider the line shift and line width contribution of the anharmonicity of the adsorption potential only. We will reconsider this adsorption system with a more detailed calculation in Chapter 6. In Table (4.1), we choose the depth of the adsorption potential well for this system as 10 eV[84]. The Debye frequency ω_D is taken as 219 cm^{-1}[81]. Therefore, the local mode frequency ω_0 is within the range $\omega_D < \omega_0 < 2\omega_D$.

For this system, the line shift is contributed by the interaction of the local mode with the substrate phonons, and the local mode self interaction since the discrete peaks due to the self interaction are broadened enough by the interaction with other modes and instrument resolution so that a single large peak is observed in the experiment. The line shift due to the interaction with the substrate phonons shifts from -0.29 to -1.46 cm^{-1}, while the line shift due to the local mode self interactions decreases from -0.02 to -4.5 cm^{-1}, over the temperature range 100 to 700 K. The total shift in this simplified model is in the same order of magnitude of the observed experimental result.

Similar to CO/Pt(111), the line width is contributed by two phonon emission processes and elastic phonon scattering. The total line width (FWHM) increases from 0.9 to 4.3 cm^{-1} over the temperature range 100 to 700 K, and is dominated by the two phonon emission processes. This line width is a partial contribution since the one dimensional model has eliminated the contributions due to dephasing via other lower frequency modes and the contributions of the lateral phonon motion. We will discuss more about this adsorption system in Chapter 6.

4.6 Summary

In this chapter, a simple model has been used to calculate and compare the anharmonic coupling effects of the adsorption potential and the substrate anharmonicity on the line shape of the localized perpendicular vibration of an adatom at a bridge site. The nonperturbative treatment of the bilinear term, in the adsorption systems with the adatom sitting at a bridge site and for which the local mode is outside of the substrate phonon band, leads to a dramatic reduction of the phonon effects due to in-phase motion of two bridge atoms on the vibrational line shape. On the other

hand, the anharmonicity of the adsorption potential couples effectively to the out of phase motion of the two bridge atoms, as demonstrated via the cubic and quadratic terms in the adsorption potential. This gives increased contributions of the anharmonicity of the adsorption potential to phonon-induced vibrational relaxation, dephasing and line shift compared to the adsorption system at an ontop site. The anharmonicity of the substrate also contributes to the vibrational lineshape. We expect that the "cross interaction" between the adsorption potential and the substrate anharmonicities will be important for an adatom at a bridge site. For completeness, we will consider, in Chapter 6, the phonon effects of both the anharmonicities of the adsorption potential and the substrate, on the vibrational line shape in a unified and complete form in a three dimensional model. In this way, the lateral motion of both adsorbate and the substrate atoms will be included. Meanwhile, a better description of the substrate is necessary. Before we get into a full three dimensional picture, we will improve the bulk Debye model, which we have been using, with a semi-infinite elastic continuum model in the next chapter.

Chapter 5. Phonon dynamics of a solid

5.1 Introduction

Up to now, for simplicity, we have been working with an idealized model of an infinitely extended solid – the bulk Debye model to describe the phonon motion in the substrate. In doing this, we have neglected an important effect of the surface. However, a better description of the substrate is necessary. We are now going to improve the bulk Debye model of the substrate and include surface phonon modes in the line shape theory.

Since the microscopic structure of the surface of most specimens tends to be irregular such as with surface steps, defects etc. inhomogeneity, the actual physics at a surface is quite complex. We have no intention to look into the detail of surface physics, but consider phonon behavior of a semi-infinite medium with no defects. The surface is approximated as a stress free plane boundary of a semi-infinite medium. As we have seen in the previous calculation, the dynamical interaction of a gas particle with a solid surface is largely controlled by the vibrational degrees of freedom of the solid. The densities of states play a crucial role in our theory since we are mostly considering the phonon induced vibrational line shape which is dependent on the specific model of solid. In this chapter, we will just review the phonon dynamics of the substrate with an infinite clean surface which will be used in Chapter 6.

Basically, as we know, there are two kinds of major approaches to a harmonic

solid, namely the elastic continuum approach and lattice dynamics. In continuum mechanics, the substrate can be treated as a semi-infinite, isotropic, elastic medium, bounded by a single stress free planar surface. Although the results from the use of continuum mechanics are valid only in the limit of long wavelength and low frequency, they provide useful insights about surface phonon modes in a simple way. On the other hand, lattice dynamics provides the true description of surface vibrations at all wavelength, but it requires the knowledge of the interaction potential between atoms which is hard to determine accurately. For simplicity, we will concentrate on elastic continuum approach and discuss some results of lattice dynamics by others[85, 86, 87].

We will introduce the elastic continuum approach for a solid in Section 2, where the standard elastic continuum theory can be found in any text book on elasticity[81]. The solid with surface can be approximated in the semi-infinite elastic continuum model. The orthogonal and complete set of eigenfunctions of the wave equations in the semi-infinite elastic continuum model was originally developed by Ezawa[88]. Section 2 is an outline of his derivation.

The wave functions derived by Ezawa will be used, in Section 3, to calculate the generalized phonon density of states in the semi-infinite elastic continuum model, based on the definition of Gortel and Kreuzer[10, 89]. A similar definition of density of states can be found in other works[85]. In contrast to the bulk Debye model, Gortel and Kreuzer introduced a surface Debye model in which each phonon branch has a cutoff frequency. In calculating the diagonal density of states, they average these cutoff frequencies so that the diagonal density of states is normalized. Our calculation differs in that we will not average the cutoff frequencies. Instead, we will normalize generalized density of states in a different way in the next chapter.

In addition, we will also include off-diagonal densities of states in our calculation.

In order to understand the roles of different phonon branches – especially surface phonon modes – we define a partial density of states for each phonon branch, which will be used in the line shape calculation in the next chapter. Finally, we will compare the generalized density of states in the semi-infinite elastic continuum model with that in the bulk Debye model and in the lattice dynamics calculation.

5.2 Phonons in elastic continuum model

The classical theory of elasticity ignores the microscopic atomic structure of a solid, and treats it as a continuum in which the atomic displacements vary slowly from atom to atom. A general deformation of a solid is described in terms of a continuous displacement field $\vec{a}(\vec{r})$, specifying the vector displacement of the part of the solid that in equilibrium occupies position $\vec{r}$. The fundamental assumption of elasticity theory is that the contribution to the energy density of the solid at point $\vec{r}$ depends only on the value of $\vec{a}(\vec{r})$ in the immediate vicinity of $\vec{r}$, or, more precisely, only on the first derivatives of $\vec{a}(\vec{r})$ at point $\vec{r}$. One can derive the continuum theory of elasticity from the theory of lattice vibrations, by considering only lattice deformations that vary slowly on a scale determined by the range of the interatomic forces. One must also assume that one can specify the deformation of the basis ions within each primitive cell entirely in terms of the vector field $\vec{a}(\vec{r})$, specifying the displacement of the entire cell.

The continuum approximation is usually valid in the long wavelength or low frequency limit. The propagation of sound waves is described by the macroscopic equation of motion of the elastic medium. The basic idea is to use Hooke's law and Newton's second law to find the equations of motion for the deformation $\vec{a}(\vec{r})$ of a

mass element at $\vec{r}$. The solution of the equation of motion will give the displacements of the substrate atoms.

5.2.1 Equation of motion in elastic continuum approach

Letting $\vec{a}(\vec{r},t)$ be the displacement at time t of a mass element at point $\vec{r} = (x_1, x_2, x_3)$ in the elastic continuum, the strain tensor is defined as

$$\epsilon_{ij} = \frac{1}{2}\left[\frac{\partial a_i}{\partial x_j} + \frac{\partial a_j}{\partial x_i}\right]. \tag{5.1}$$

Hooke's law states that for a sufficiently small deformation the strain is directly proportional to the stress, so that the strain components are linear functions of the stress components; conversely, the stress components are linear functions of strain components. Let σ_{ij} denote the j^{th} component of the forces per unit surface area perpendicular to the i^{th} direction, on a volume element at point $\vec{r}$, then

$$\sigma_{ij} = C_{ijkl}\epsilon_{kl}, \tag{5.2}$$

where Einstein's summation convention over double indices is implied. $\{C_{ijkl}\}$ are called elastic constants. The symmetries $\sigma_{ij} = \sigma_{ji}$, $\epsilon_{kl} = \epsilon_{lk}$, and $C_{ijkl} = C_{klij}$ imply that there are at most 21 independent elastic constants in an anisotropic elastic medium. Newton's equations of motion are closed and read

$$\rho_0 \frac{\partial^2}{\partial t^2} a_i = \sum_j \frac{\partial \sigma_{ij}}{\partial x_j} = C_{ijkl}\frac{\partial^2 a_k}{\partial x_l \partial x_j}, \tag{5.3}$$

where ρ_0 is mass density of the solid. For an isotropic continuum, there are only two independent constants which one conventionally chooses as the Lame constants

$$\mu = C_{1122} = C_{1133} = C_{2233}, \tag{5.4}$$

$$\lambda = C_{2323} = C_{1313} = C_{1212}, \tag{5.5}$$

$$\lambda + 2\mu = C_{1111} = C_{2222} = C_{3333}, \tag{5.6}$$

so that the equations of motion can be written as

$$\rho_0 \frac{\partial^2}{\partial t^2} a_i = \mu \nabla^2 a_i + (\mu + \lambda) \frac{\partial^2 a_k}{\partial x_i \partial x_k}, \tag{5.7}$$

where the Laplacian is defined as

$$\nabla^2 = \frac{\partial^2}{\partial x_1^2} + \frac{\partial^2}{\partial x_2^2} + \frac{\partial^2}{\partial x_3^2}. \tag{5.8}$$

For a cubic crystal, the constant μ, combined with $\lambda + 2\mu$ gives the bulk modulus, while λ is the shear modulus in (100) direction on (100) plane.

It is easy to show that the velocities of longitudinal and transverse waves are given by the Lame constants λ, μ and the mass density of the solid ρ_0 as follows[88]

$$c_l^2 = \frac{\lambda + 2\mu}{\rho_0}, \; c_t^2 = \frac{\mu}{\rho_0}. \tag{5.9}$$

Eq. (5.7) can be rewritten as a vector equation in terms of c_l and c_t

$$\frac{\partial^2}{\partial t^2} \vec{a} = c_l^2 \; grad \; div \; \vec{a} - c_t^2 \; curl \; curl \; \vec{a}. \tag{5.10}$$

This is the well-known elastic wave equation. Obviously, the longitudinal sound velocity c_l is greater than the transverse sound velocity c_t.

5.2.2 Semi-infinite elastic continuum model

If we approximate the substrate as a semi-infinite elastic continuum, in order to solve the wave equation given by Eq. (5.10), we have to specify boundary conditions. Following Ezawa's derivation[88], for a free surface, the boundary conditions reflect the fact that there are no net forces acting on it. With n_j being the j^{th} component of a unit vector normal to the surface, they read

$$\sigma_{ij} n_j = 0, \tag{5.11}$$

implying for an isotropic medium

$$\left[(c_l^2 - 2c_t^2)\frac{\partial a_k}{\partial x_k}\delta_{ij} + c_t^2\left(\frac{\partial a_i}{\partial x_j} + \frac{\partial a_j}{\partial x_i}\right)\right] n_j = 0. \tag{5.12}$$

We consider an elastic continuum filling the half space ($z < 0$) with a stress-free plane boundary at $z = 0$. The (x, y)-plane is parallel to the surface.

With the boundary condition given by Eq. (5.12) and the lateral symmetry of the solid surface, the displacement vector $\vec{a}(\vec{r}, t)$ can be expanded in a set of vibrational normal mode eigenvectors $\vec{a}^{(J)}(\vec{R}, z)$ as

$$\vec{a}(\vec{r}, t) = \sum_J \sqrt{\frac{\hbar}{2\rho_0\omega_J}}\left[b_J\vec{a}^{(J)}(\vec{R}, z)e^{-i\omega_J t} + b_J^\dagger\vec{a}^{(J)*}(\vec{R}, z)e^{i\omega_J t}\right], \tag{5.13}$$

where $\vec{R}$ and z are the lateral and perpendicular positions of the substrate atoms, respectively, b_J and $b_J^\dagger$ are the annihilation and creation operators for the J^{th} phonon in the substrate. In Eq. (5.13), the index J labels different eigenmodes which Ezawa has identified as consisting of $(\vec{\kappa}, c, \sigma)$ with eigenvalue ω_J and eigenvector

$$\begin{aligned}\vec{a}^{(J)}(\vec{R}, z) &= \frac{1}{\sqrt{A}}e^{i\vec{\kappa}\cdot\vec{R}}\vec{g}(\kappa, c, \sigma; z) \\ &= \frac{1}{\sqrt{A}}e^{i\vec{\kappa}\cdot\vec{R}}\hat{O}(\frac{\vec{\kappa}}{\kappa})\cdot\vec{f}(\kappa, c, \sigma; z),\end{aligned} \tag{5.14}$$

where $\kappa = |\vec{\kappa}|$ is the magnitude of a two-dimensional wave vector $\vec{\kappa}$ parallel to the exposed surface area A of the solid, $c = \omega_J/\kappa$ is the apparent sound velocity with which the elastic wave propagates along the surface, and the discrete index σ labels five different acoustic branches in the semi-infinite continuum model. The rotation operator $\hat{O}(\frac{\vec{\kappa}}{\kappa})$ is in the (x, y) plane around the z-axis and is defined by the equation

$$\hat{O}(\frac{\vec{\kappa}}{\kappa})\cdot\begin{pmatrix}\kappa\\0\\0\end{pmatrix} = \begin{pmatrix}k_1\\k_2\\0\end{pmatrix}, \tag{5.15}$$

where $\vec{\kappa} = (k_1, k_2)$ so that the wave function $\vec{f}$ in Eq. (5.14) can be calculated for a wave propagating in the direction of $\vec{\kappa}$ as follows.

If the $\vec{f}$-function is calculated for a wave propagating in direction x, as given below, $\hat{O} \cdot \vec{f}$ gives wave traveling in other directions of $\vec{\kappa}$. All the eigenvectors $\vec{a}^{(J)}(\vec{R}, z)$ form a complete and orthogonal set of the eigenmodes which is ensured by the index $J = (\vec{\kappa}, c, \sigma)$ as follows

$$\begin{aligned} \sum_J a_i^{(J)}(\vec{R}, z) a_j^{(J)*}(\vec{R}', z') &= \delta_{ij}\delta(\vec{R} - \vec{R}')\delta(z - z') \\ \int_V \vec{a}^{(J)*}(\vec{R}, z) \cdot \vec{a}^{(J')}(\vec{R}, z) &= \delta_{J,J'}. \end{aligned} \tag{5.16}$$

We now list the $\vec{f}$-functions for a wave propagating in the x-direction[10, 88].

SH-mode

This wave is polarized perpendicular to both the directions of the propagation $\vec{\kappa}$ and z-axis; the mode with such a polarization is called the shear horizontal mode or $\sigma = \text{SH}$ mode. The wave function is given by

$$f(\kappa, c, \sigma = SH; z) = \theta(c - c_t)\sqrt{\frac{2c\kappa}{\pi c_t^2 \beta}} \begin{pmatrix} 0 \\ cos(\kappa\beta z) \\ 0 \end{pmatrix}, \tag{5.17}$$

with

$$\beta = \sqrt{(c/c_t)^2 - 1}. \tag{5.18}$$

Its apparent velocity along the surface $c = \omega_J/\kappa$ is restricted to $c_t < c < \infty$. This is a bulk-like mode. The horizontal component of the incident shear wave is completely reflected at the surface. As a result, the amplitude of the wave oscillates into the solid with the wave vector $\kappa\beta$.

Mixed P-SV Modes

There are two mixed P-SV modes ($\sigma = \pm$). The component polarized perpendicular to both the directions of propagation $\vec{\kappa}$ and the z-axis are zero. The other components are the combinations of the pressure wave (P-wave) or longitudinal wave and the shear wave with vertical polarization (SV-wave). After the normalization, the wave function is given by

$$f(\kappa, c, \sigma = \pm; z) = \theta(c - c_l)\sqrt{\frac{\kappa}{4\pi c}} \times \begin{pmatrix} \mp\frac{1}{\sqrt{\alpha}}(e^{i\kappa\alpha z} - \xi_\pm e^{-i\kappa\alpha z}) + i\sqrt{\beta}(e^{i\kappa\beta z} + \xi_\pm e^{-i\kappa\beta z}) \\ 0 \\ \pm\sqrt{\alpha}(e^{i\kappa\alpha z} + \xi_\pm e^{-i\kappa\alpha z}) + \frac{i}{\sqrt{\beta}}(e^{i\kappa\beta z} - \xi_\pm e^{-i\kappa\beta z}) \end{pmatrix} \tag{5.19}$$

with

$$\alpha = \sqrt{(c/c_l)^2 - 1}, \tag{5.20}$$

$$\xi_\pm = \frac{(\beta^2 - 1 \pm 2i\sqrt{\alpha\beta})^2}{(\beta^2 - 1)^2 + 4\alpha\beta}, \tag{5.21}$$

and

$$|\xi_\pm| = 1. \tag{5.22}$$

The apparent velocity along the surface is restricted to $c_l < c < \infty$. $|\xi_\pm| = 1$ carries the physical meaning that the energy flux is conserved upon reflection at the surface. These two modes are also bulk-like modes. In the case of P-wave incidence, the reflected waves are P-wave and SV-wave. On the other hand, in the case of SV-wave incidence, reflected waves are also P-wave and SV-wave. The mixing upon reflection at the surface is controlled by $\xi_\pm$. The P-wave propagates into the solid

with wave vector $\alpha\kappa$, while the SV-wave propagates into the solid with wave vector $\beta\kappa$.

Rayleigh mode

If the apparent velocity c gets smaller than c_t, then α and β defined in Eqs. (5.20) and (5.18) become imaginary, so that the terms in the mixed P-SV modes can no longer coexist. Choosing the positive imaginary root of β^2 and α^2 as η and γ, the terms with $e^{i\kappa\alpha z}$ and $e^{i\kappa\beta z}$ in Eq. (5.19) will disappear inside the solid. With the normalization condition, the Rayleigh mode ($\sigma = R$) wave function is given by

$$f(\kappa, c, \sigma = R; z) = i\delta(c - c_R)\sqrt{\frac{\kappa 2\gamma_R\eta_R^2}{(\gamma_R - \eta_R)(\gamma_R - \eta_R + 2\gamma_R\eta_R^2)}} \times \begin{pmatrix} e^{\kappa\gamma_R z} - \frac{2\gamma_R\eta_R}{1+\eta_R^2}e^{\kappa\eta_R z} \\ 0 \\ i\gamma_R e^{\kappa\gamma_R z} - \frac{2i\gamma_R}{1+\eta_R^2}e^{\kappa\eta_R z} \end{pmatrix}, \tag{5.23}$$

with

$$\gamma_R = \sqrt{1 - (\frac{c_R}{c_l})^2}, \tag{5.24}$$

$$\eta_R = \sqrt{1 - (\frac{c_R}{c_t})^2}, \tag{5.25}$$

where γ_R and η_R are decay constants and both are real; c_R is the velocity of the Rayleigh wave along the surface, which is a root of the equation

$$4\gamma_R\eta_R - (1 + \eta_R^2)^2 = 0. \tag{5.26}$$

This equation, called the Rayleigh condition, is known to have, apart from the trivial root $c_R = 0$, a single, positive root c_R which is smaller than c_t. The Rayleigh mode is completely confined to the surface region. It decays into the solid exponentially.

The generalized Rayleigh mode

Similar to Rayleigh mode, if the apparent velocity c is in the range $c_t < c < c_l$, α defined in Eq. (5.20) becomes imaginary, but β is still real. In the mixed P-SV waves, the terms from P-wave with $e^{i\kappa\alpha z}$ disappear. It means the total reflection of the P-wave at the surface. The SV-wave will have the same form. This mode is called the generalized Rayleigh mode ($\sigma = GR$) since part of it decays exponentially into the solid. Defining $\gamma = \sqrt{1-(c/c_l)^2}$, the normalized wave function is given by

$$\begin{aligned} f(\kappa, c, \sigma = GR; z) &= \theta(c_l - c)\theta(c - c_t) i \sqrt{\frac{\kappa}{2\pi c\beta}} \\ &\times \begin{pmatrix} Be^{\kappa\gamma z} + \beta(e^{i\kappa\beta z} + Ae^{-i\kappa\beta z}) \\ 0 \\ i\gamma Be^{\kappa\gamma z} + (e^{i\kappa\beta z} - Ae^{-i\kappa\beta z}) \end{pmatrix}, \end{aligned} \tag{5.27}$$

with

$$A = \frac{(\beta^2-1)^2 - 4i\gamma\beta}{(\beta^2-1)^2 + 4i\gamma\beta}, \tag{5.28}$$

$$B = \frac{4\beta(\beta^2-1)}{(\beta^2-1)^2 + 4i\gamma\beta}, \tag{5.29}$$

and

$$|A| = 1. \tag{5.30}$$

It differs from the mixed P-SV modes ($\sigma = \pm$) in that part of its amplitude decays exponentially into the solid. The identity $|A| = 1$ is again an expression of the energy flux conservation.

Substituting the above $\vec{f}$-functions into Eq. (5.14) gives the eigenvectors $\vec{a}^{(J)}(\vec{R}, z)$ of a semi-infinite elastic medium. We have noticed that these eigenvectors satisfy the following relation

$$\vec{a}^{(-J)*}(\vec{R}, z) = c_\sigma \vec{a}^{(J)}(\vec{R}, z), \tag{5.31}$$

with

$$c_\sigma = \begin{cases} -1, & \sigma = SH; \\ \xi_\sigma^*, & \sigma = \pm; \\ A^*, & \sigma = GR; \\ 1, & \sigma = R, \end{cases} \tag{5.32}$$

where $|c_\sigma| = 1$. If we define

$$d_J^0(t) = \sqrt{\frac{\hbar}{2\rho_0\omega_J}}\left[\frac{1}{\sqrt{c_\sigma}}b_J(t) + \sqrt{c_\sigma}\, b_{-J}^\dagger(t)\right], \tag{5.33}$$

the displacement field can be simplified as

$$\vec{a}(\vec{r},t) = \sum_J \vec{a}^{(J)}(\vec{R},z)\sqrt{c_\sigma}d_J^0(t). \tag{5.34}$$

5.3 Phonon propagator, the generalized density of states and surface Debye model

Using the substrate atom displacement given by Eq. (5.34), we can calculate the phonon propagator in the semi-infinite elastic continuum model. Unlike isotropic bulk solids, where all parts in the substrate are equivalent in directions x, y and z, in the semi-infinite elastic continuum model, the behaviors of surface atoms are much different from that of the atoms deep inside the substrate. Phonon motions in the directions perpendicular and parallel to the surface also will be much different due to the existence of the surface. Generally, the phonon propagator depends on the atomic positions and the components of their displacements in x, y and z directions, and can be defined by

$$iB_{ij}^{\alpha\beta}(t) = \langle T a_{i\alpha}(t) a_{j\beta}(0)\rangle$$

$$= \sum_J a_{i\alpha}^{(J)} a_{j\beta}^{(J)*} \langle T d_J^0(t) d_{-J}^0(0) \rangle, \tag{5.35}$$

where $a_{i\alpha}(t)$ is the αth component of the displacement of an atom at site i, and $\langle T d_J^0(t) d_{-J}^0(0) \rangle$ is the time-ordered Green's function of the J^{th} phonon. We can calculate it in the same way as that in the bulk model given in Eqs. (2.28) and (3.3) by replacing ω_k with ω_J. In order to evaluate this time-ordered Green's function and explore the related phonon processes such as two phonon emission in the line shape calculation, in this section, we will introduce the generalized density of states and a surface Debye model. This is a extension of the model introduced by Gortel and Kreuzer[10], in which we also included the off-diagonal terms $i \neq j$ or $\alpha \neq \beta$ in Eq. (5.35).

5.3.1 Definition of the generalized density of states

The generalized density of states is defined as[85]

$$\rho_{ij}^{\alpha\beta}(\omega) = \sum_J a_{i\alpha}^{(J)} a_{j\beta}^{(J)*} \delta(\omega - \omega_J), \tag{5.36}$$

where J denotes mode, ω_J is the frequency of the J^{th} normal mode of the system, and $a_{i\alpha}^{(J)}$ is the α^{th} component of the normalized eigenvector of the equation of motion evaluated at site i. This generalized density of states enables us to write the phonon propagator given in Eq. (5.35) as

$$\langle T a_{i\alpha}(t) a_{j\beta}(0) \rangle = \int_0^\infty d\omega \rho_{ij}^{\alpha\beta}(\omega) \langle T d_J(t) d_{-J}(0) \rangle \tag{5.37}$$

The generalized density of states $\rho_{ij}^{\alpha\beta}(\omega)$ provides some information on the characteristic frequencies which contributes to the phonon correlations between the displacements $a_{i\alpha}$ and $a_{j\beta}$. The phonon propagator in the special case where $i = j$ and $\alpha = \beta$ is equal to, for $t \to 0^+$, the mean square displacement of the atom at

site i in the direction α. The diagonal density of states $\rho_{ii}^{\alpha\alpha}(\omega)$ describes the frequency spectrum of the motion of atom i in the direction α. This diagonal term was evaluated by Gortel and Kreuzer[10] Deep inside the substrate, i.e., $z \to -\infty$, the $\rho_{ii}^{\alpha\alpha}(\omega)$ are necessarily equal and independent of i for $\alpha = x, y, z$. As we move from deep inside the solid into the near surface region, the three directions are no longer equivalent by symmetry in the semi-infinite elastic continuum model, i.e., functions $\rho_{ii}^{zz}(\omega) = \rho_{ii}^{yy}(\omega) \neq \rho_{ii}^{zz}(\omega)$. For $i \neq j$, $\rho_{ij}^{\alpha\beta}(\omega)$ may differ dramatically near the surface from the form appropriate to the bulk of the solid.

There is a sum rule obeyed by $\rho_{ij}^{\alpha\beta}(\omega)$ due to the completeness of the set of normal modes. Integrating Eq. (5.36) over ω, we find that the total number of the vibrational states per unit volume which is normalized to a δ function in this model, i.e.,

$$\int_0^\infty d\omega \rho_{ij}^{\alpha\beta}(\omega) = \delta_{\alpha\beta}\delta(\vec{R}_i - \vec{R}_j)\frac{1}{v_c}, \tag{5.38}$$

where v_c is the volume of a unit cell. This can be used as a check on our numerical calculation of $\rho_{ij}^{\alpha\beta}(\omega)$ in the semi-infinite elastic continuum model.

Since the quantum number J is composed of $(\vec{\kappa}, \sigma, c)$, and σ denotes a branch of the phonon spectrum in the semi-infinite elastic continuum model, we then introduce a partial density of states $\rho_{ij}^{\alpha\beta(\sigma)}(\omega)$ for branch σ so that we can study the properties of each branch separately. The generalized density of states $\rho_{ij}^{\alpha\beta}(\omega)$ then is the sum of the partial densities of states for all branches, i.e.[10]

$$\rho_{ij}^{\alpha\beta}(\omega) = \sum_\sigma \rho_{ij}^{\alpha\beta(\sigma)}(\omega). \tag{5.39}$$

In the semi-infinite elastic continuum model, there are five branches labeled by $\sigma = SH, \pm, GR, R$ in the last section. It is found that the partial density of states

of branch σ, for a given polarization and atom sites, has form

$$\rho_{ij}^{\alpha\beta(\sigma)}(\omega) = S_{ij}^{\alpha\beta(\sigma)}(\omega, \vec{R}_i, \vec{R}_j, z_i, z_j)\frac{\omega^2}{2\pi^2 c_t^3}\theta(\omega_D{}^{(\sigma)} - \omega), \tag{5.40}$$

where $S_{ij}^{\alpha\beta(\sigma)}(\omega, \vec{R}_i, \vec{R}_j, z_i, z_j)$ is defined as a weight function and $\omega_D{}^{(\sigma)}$ is the maximum frequency of the phonons in branch σ. Only at $z_i = z_j = 0$ are all partial densities of states proportional to ω^2, which is similar to the behavior of the density of states of an infinite solid in the bulk Debye model. For $z_i \neq 0$, the weight function depends on the frequency and gives a deviation from the ω^2-dependence.

5.3.2 Weight function

Now the question comes to calculate weight function $S_{ij}^{\alpha\beta(\sigma)}(\omega)$ in the semi-infinite continuum model in order to find the generalized density of states. After some simplification, the weight function becomes a single integral over the apparent velocity c parallel to the surface, and is given by

$$S_{ij}^{\alpha\beta(\sigma)}(\omega, \vec{R}_i, \vec{R}_j, z_i, z_j) = \int_{x_{min}^{\sigma}}^{x_{max}^{\sigma}} dx \left[M_1 \cdot N_1^{(\sigma)} + M_2 \cdot N_2^{(\sigma)}\right], \tag{5.41}$$

with

$$x = \frac{c_t}{c};$$

$$M_1 = \begin{pmatrix} \frac{1}{2}[J_0(r_{ij}) - cos2\alpha_{ij}J_2(r_{ij})] & -\frac{1}{2}sin2\alpha_{ij}J_2(r_{ij}) & cos\alpha_{ij}J_1(r_{ij}) \\ -\frac{1}{2}sin2\alpha_{ij}J_2(r_{ij}) & \frac{1}{2}[J_0(r_{ij}) + cos2\alpha_{ij}J_2(r_{ij})] & sin\alpha_{ij}J_1(r_{ij}) \\ cos\alpha_{ij}J_1(r_{ij}) & sin\alpha_{ij}J_1(r_{ij})] & J_0(r_{ij}) \end{pmatrix};$$

$$M_2 = \begin{pmatrix} \frac{1}{2}[J_0(r_{ij}) + cos2\alpha_{ij}J_2(r_{ij})] & \frac{1}{2}sin2\alpha_{ij}J_2(r_{ij}) & 0 \\ \frac{1}{2}sin2\alpha_{ij}J_2(r_{ij}) & \frac{1}{2}[J_0(r_{ij}) - cos2\alpha_{ij}J_2(r_{ij})] & 0 \\ 0 & 0 & 0 \end{pmatrix};$$

$$N_1^{(\sigma)} = \frac{\pi c_t^2}{\omega} \begin{pmatrix} f_{ix}^{(\sigma)} f_{jx}^{(\sigma)*} & f_{ix}^{(\sigma)} f_{jx}^{(\sigma)*} & i f_{ix}^{(\sigma)} f_{jz}^{(\sigma)*} \\ f_{ix}^{(\sigma)} f_{jx}^{(\sigma)*} & f_{ix}^{(\sigma)} f_{jx}^{(\sigma)*} & i f_{ix}^{(\sigma)} f_{jz}^{(\sigma)*} \\ i f_{iz}^{(\sigma)} f_{jx}^{(\sigma)*} & i f_{iz}^{(\sigma)} f_{jx}^{(\sigma)*} & f_{iz}^{(\sigma)} f_{jz}^{(\sigma)*} \end{pmatrix};$$

$$N_2^{(\sigma)} = \frac{\pi c_t^2}{\omega} \begin{pmatrix} f_{iy}^{(\sigma)} f_{jy}^{(\sigma)*} & f_{iy}^{(\sigma)} f_{jy}^{(\sigma)*} & 0 \\ f_{iy}^{(\sigma)} f_{jy}^{(\sigma)*} & f_{iy}^{(\sigma)} f_{jy}^{(\sigma)*} & 0 \\ 0 & 0 & 0 \end{pmatrix}; \text{ and}$$

$$r_{ij} = \kappa|\vec{R}_i - \vec{R}_j|;$$

$$\alpha_{ij} = sin^{-1}\left[\frac{R_{iy} - R_{jy}}{|\vec{R}_i - \vec{R}_j|}\right], \tag{5.42}$$

where J_n is the n^{th} order of Bessel function, the '$\cdot$' product of matrixes means element-by-element operation, i.e., if $A \cdot B = C$, then $C_{ij} = A_{ij}B_{ij}$, and A, B, C have the same number of rows and columns. The integral limits for modes $\sigma = SH, \pm, R, GR$ are $(x_{min}^{\sigma}, x_{max}^{\sigma}) = (0,1), (0, l_s), (l_R, l_R), (l_s, 1)$, respectively, with $l_s = c_t/c_l$ and $l_R = c_t/c_R$. The weight function is dimensionless .

We begin the discussion of the weight function $S_{ij}^{\alpha\beta(\sigma)}$ defined in the partial densities of states in Eq. (5.40) with a special case $i = j$ and $\alpha = \beta$. For this case, since $\vec{R}_i = \vec{R}_j$ and $z_i = z_j$, i.e., $r_{ij} = 0$, we have the symmetry relation

$S_{ii}^{xx(\sigma)} = S_{ii}^{yy(\sigma)}$ for all branches.

1. $\sigma =$ SH

   For a wave propagating in x direction along the surface, the wave function for this mode is non-zero only for the $\alpha = y$ component. Therefore the weight functions are non-zero only for the lateral polarizations and independent of $l_s = \frac{c_t}{c_l}$. The oscillations represent, for fixed ω, standing waves that decay into

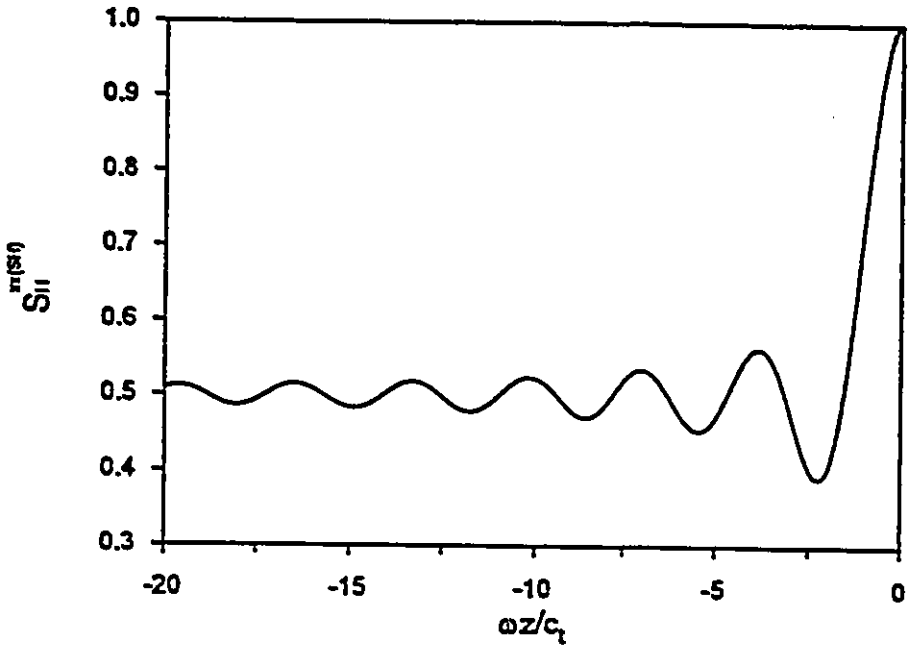

Figure 5.1: The weight function $S_{ii}^{xx(SH)}$ defined in the partial densities of states.

   the solid towards the bulk value of 0.5. For a fixed substrate atom position z, the oscillation will be cut off at $\omega_D{}^{(SH)} z/c_t$. $S_{ii}^{xx(SH)}$ is plotted in Fig. (5.1).

2. $\sigma = \pm$

   For these modes, the weight functions are non-zero for all polarizations and depend on the ratio of sound velocities l_s. $S_{ii}^{xx(\pm)}$ and $S_{ii}^{xx(\pm)}$ are plotted in Fig.

(5.2) and Fig. (5.3) for $l_s = 0.5$, respectively. These two modes exhibit two oscillation periods due to the mixing of the P-wave and SV-wave, and oscillate far into the solid. Near the surface region, the parallel components are larger than the perpendicular components.

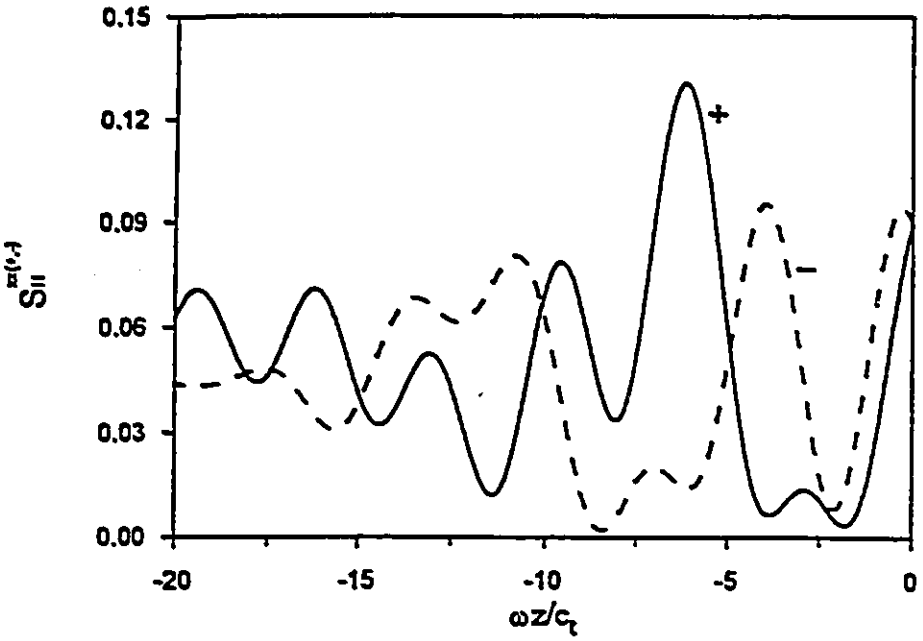

Figure 5.2: The weight function $S_{ii}^{xx(\pm)}$ defined in the partial densities of states.

3. σ =GR and R

The weight functions for these two modes depend on ratio $l_s = c_t/c_l$ and $l_R = c_t/c_R$, respectively. l_R is determined by l_s through Rayleigh condition given in Eq. (5.26). The weight functions are plotted in Fig. (5.4) and Fig. (5.5) for the lateral and perpendicular polarizations for $l_s = 0.5$.

The localization of the Rayleigh wave in the surface region is clearly displayed. Note that the decay in the z direction is proportional to ω^{-1} so that the long-wavelength Rayleigh mode can penetrate deeply into the solid, but it still

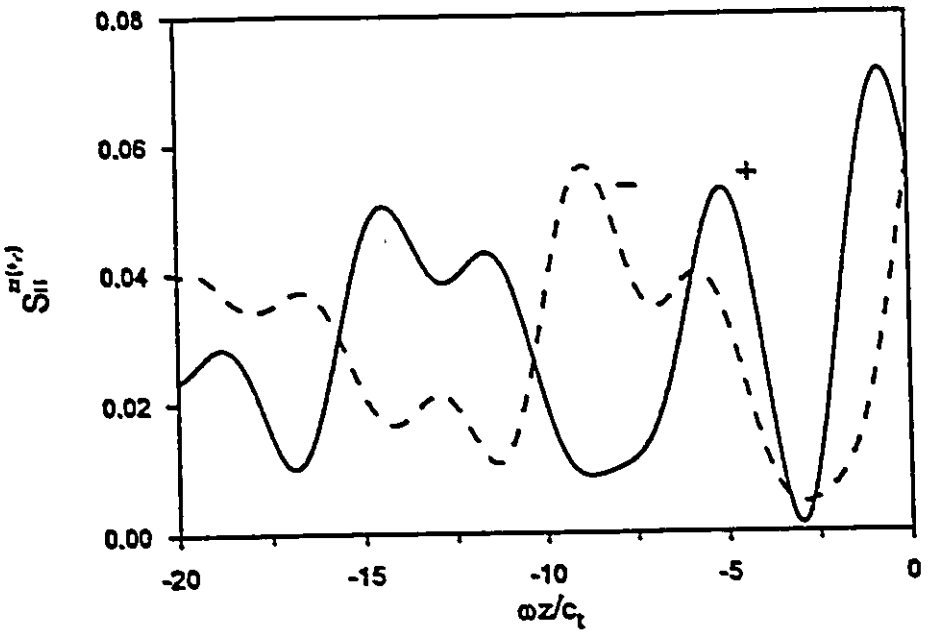

Figure 5.3: The weight function $S_{ii}^{zz(\pm)}$ defined in the partial densities of states.

decays. The perpendicular polarization in the surface region is significantly larger than the lateral polarization. The generalized Rayleigh mode decays to its asymptotic value over the same depth. Note that its z-polarization is depleted in the surface region.

4. Total

In Fig. (5.6), we finally give the total contributions for x-, y- and z-polarizations and their sum. Some of features displayed by the individual modes actually are canceled in their sum. Near the surface region, the Rayleigh mode $\sigma = R$ dominates the contributions to the perpendicular polarization, while the shear horizontal mode $\sigma = SH$ dominates the contributions to the lateral polarization for $l_s = 0.5$. As l_s increases, both x and z polarizations are dominated by the Rayleigh mode. Our study is mostly limited in the first few layers near the

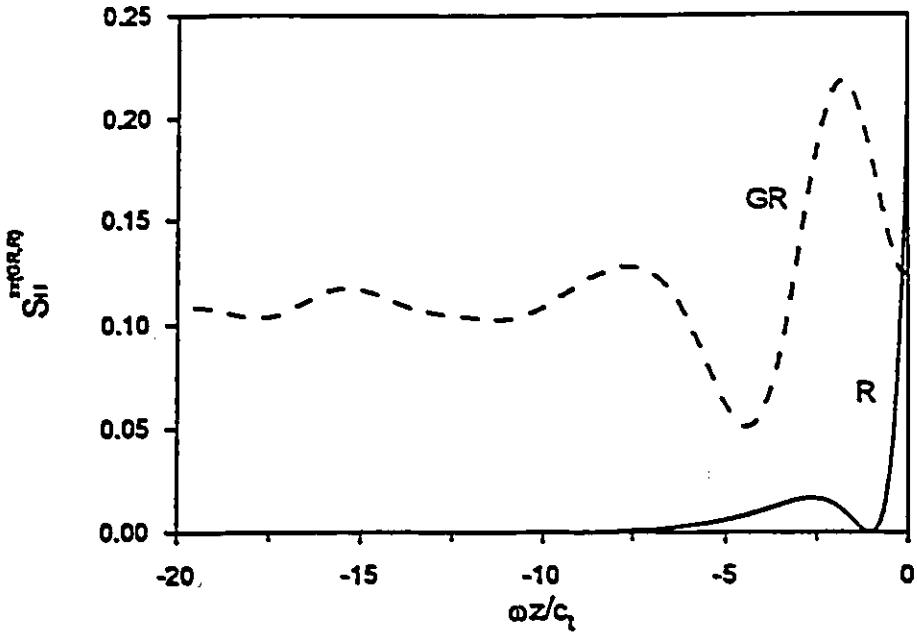

Figure 5.4: The weight function $S_{ii}^{xx(GR,R)}$ defined in the partial densities of states.

surface. We thus leave out the detailed discussion for the atoms deep inside the solid here.

When a weight function represents the correlation between different substrate atoms in the same layer or different layers, i.e., $i \neq j$, we no longer have symmetry in x and y polarizations. For $\alpha = \beta$, all components of the weight function will be non-zero and different. As an example, let's consider the Rayleigh mode and the correlation of the two nearest atoms $i = 1$ and $j = 2$ sitting on the x axis. The weight functions for x, y and z polarizations are plotted in Fig. (5.7) for $l_s = 0.5$, where $S_{12}^{xx(R)}$ and $S_{12}^{yy(R)}$ are no longer the same. Since $\vec{R}_{12}$ is in the x-direction, the correlation in the x-direction is stronger than that in the y-direction. The correlation in z-direction is independent of the orientation of vector $\vec{R}_{12}$.

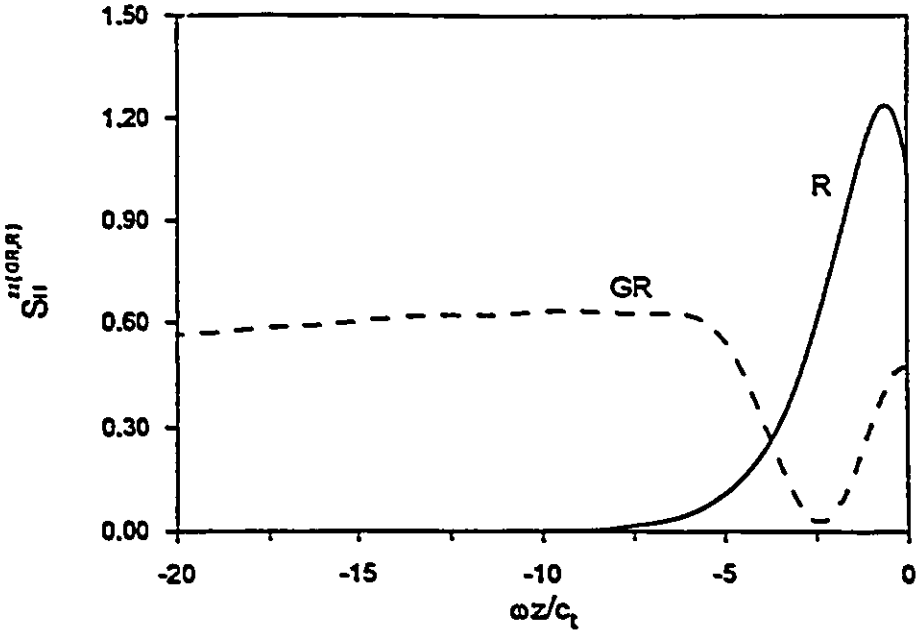

Figure 5.5: The weight function $S_{ii}^{zz(GR,R)}$ defined in the partial densities of states.

5.3.3 Surface Debye model

In principal, with the corresponding weight function, one can find the generalized density of states defined by Eq. (5.36). However, the actual solid is a discrete lattice. The wave vector is limited to a finite maximum because of the boundary of Brillion zone. Correspondingly, in order to satisfy the sum rule obeyed by the generalized density of states, one needs to limit the upper frequency of each branch. In analogy to the bulk Debye model for an infinite solid, Gortel and Kreuzer constructed a surface Debye model for the semi-infinite elastic continuum model of the substrate and determine the maximum phonon frequencies of each branch $\omega_D{}^{(\sigma)}$. Firstly, they imposed two dimensional Born-Von Karman boundary conditions on a finite surface A. As a result, the two dimensional wave vector $\vec{\kappa}$ can assume only discrete values. Introducing the two dimensional lattice periodicity explicitly with $\vec{R}_l$ being Bravais

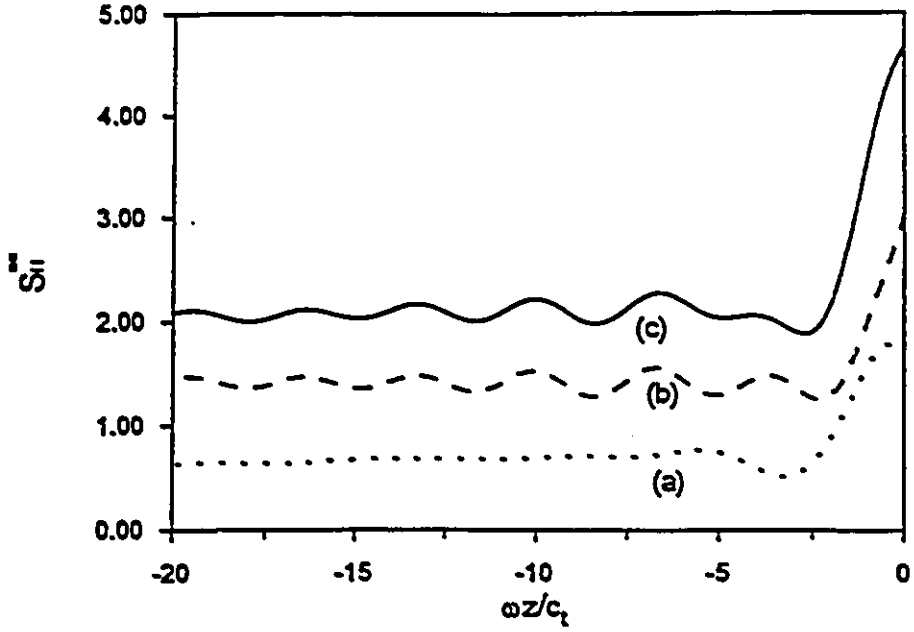

Figure 5.6: The weight function $S_{ii}^{\alpha\alpha}$ in the vertical (a), parallel (b) polarization and their sum (c).

lattice translational vector, one must restrict $\vec{\kappa}$ to the two-dimensional first Brillouin zone. Secondly, to construct a Debye model for surface waves, they recalled that in the bulk Debye model, one equates the volume of the three-dimensional Brillouin zone to that of a sphere of radius k_D such that

$$\frac{4\pi}{3}k_D^3 = \frac{(2\pi)^3}{v_c}, \tag{5.43}$$

where $v_c = \frac{M_s}{\rho_0}$ is the volume of a crystal unit cell. This relation determines the maximum wave vector in the bulk Debye model. In analogy, in the surface Debye model, they equated the area of the two dimensional Brillouin zone to that of a disc of radius κ_D so that

$$\pi\kappa_D^2 = \frac{(2\pi)^2}{a_s}, \tag{5.44}$$

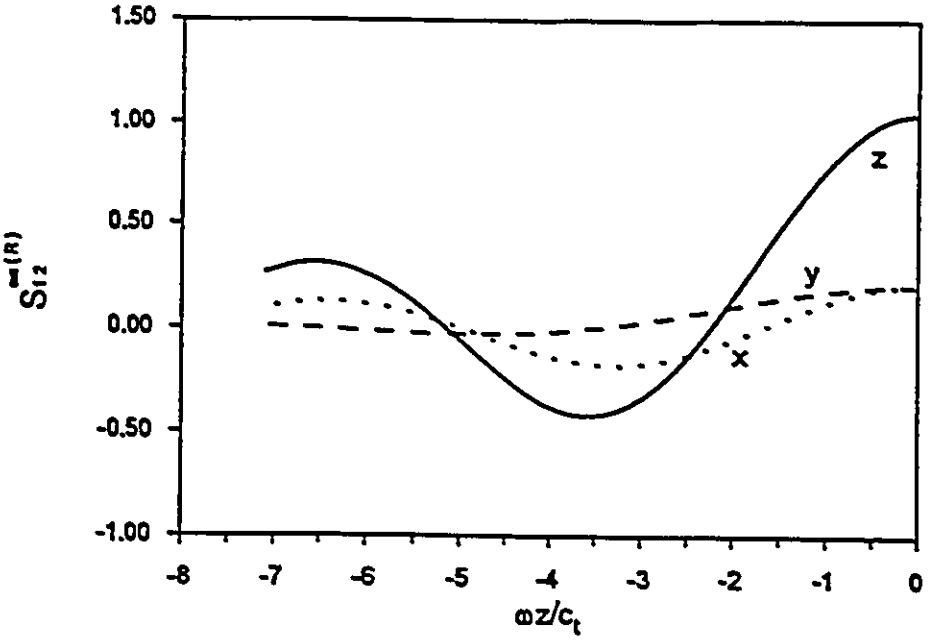

Figure 5.7: The weight function $S_{12}^{\alpha\alpha(R)}$ defined in the partial densities of states.

where a_s is the area of a surface unit cell. For the (100) surface of a simple cubic lattice with lattice constant a, $a_s = a^2$. Consequently, in the surface Debye model, one must restrict the two-dimensional wave vector to disc

$$\kappa < \kappa_D = \sqrt{4\pi/a_s}. \tag{5.45}$$

The two dimensional wave vectors of all the phonons have the same cutoff at κ_D. In the bulk Debye model, the cutoff frequency or Debye frequency is defined by the dispersion relation of the acoustic phonons $\omega_D = c|\vec{k}_D|$, where c is the average velocity of the sound wave. However, in the surface Debye model, since the apparent velocities of sound waves are limited in different ranges for different branches, the cutoff frequencies will be different. Using the relation

$$\omega_J = \omega_\sigma(c, \kappa) = c\kappa, \tag{5.46}$$

one can get

$$\kappa = \frac{\omega_J}{c} \leq \frac{\omega_J}{c_{min}^{(\sigma)}} \leq \kappa_D = \frac{\omega_D{}^{(\sigma)}}{c_{min}^{(\sigma)}}, \tag{5.47}$$

where $c_{min}^{(\sigma)}$ is the minimum apparent velocity of branch σ along the surface, i.e., $c_{min}^{(SH)} = c_{min}^{(GR)} = c_t$, $c_{min}^{(\pm)} = c_l$ and $c_{min}^{(R)} = c_R$. The surface Debye cutoff frequencies $\omega_D{}^{(\sigma)}$ thus depend on the minimum apparent sound velocities along the surface $c_{min}^{(\sigma)}$ and maximum wavevector κ_D which is determined by the surface structure. How well one can determine the sound velocity will affect the cutoff frequencies. Let $l_s = c_t/c_l$ and $l_R = c_t/c_R$, then, the cutoff frequencies for a simple cubic lattice are given by

$$\omega_D{}^{(SH)} = \omega_D{}^{(GR)} = (\frac{2+l_s^3}{3})^{1/3}\frac{(4\pi)^{1/2}}{(6\pi^2)^{1/3}}\omega_D, \tag{5.48}$$

$$\omega_D{}^{(\pm)} = \frac{1}{l_s}\omega_D{}^{(SH)}, \tag{5.49}$$

$$\omega_D{}^{(R)} = \frac{1}{l_R}\omega_D{}^{(SH)}, \tag{5.50}$$

where ω_D is the bulk Debye frequency and given by

$$\omega_D = c_t\left[\frac{\rho_0 18\pi^2}{M_s(2+l_s^3)}\right]^{1/3}, \tag{5.51}$$

in terms of Eq. (5.43) and the definition of the average Debye frequency given by Eq. (2.36). For branch σ, phonon frequency will be cutoff at $\omega_D{}^{(\sigma)}$.

5.4 The generalized density of states at surface – comparison of different methods

With the cutoff frequencies, we now can plot the generalized density of states in the semi-infinite elastic model which we will use in the next chapter. In this section,

we will show the generalized density of states in the semi-infinite elastic continuum model for some special cases considering both vertical and parallel polarizations and compare them with that in the bulk Debye model and qualitatively with the results from lattice dynamics calculation[90].

In the semi-infinite elastic continuum model, we have noticed the cutoff frequencies and most weight function depend on the ratio $l_s = c_t/c_l$ which is related to the details of the lattice interactions in the solid. As an example, in this section, we will show the generalized density of states for a simple cubic lattice for $l_s = 0.5$.

5.4.1 Vertical polarization

Fig. (5.8) shows the diagonal density of states of a simple cubic lattice for $l_s = 0.5$ in vertical polarization in the bulk Debye model (dashed line) and the surface Debye model (solid line) for the atoms at the surface, the second layer and the 10^{th} layer, respectively. The cutoff frequencies for bulk-like modes in the surface Debye model are similar to those of the corresponding modes in the bulk Debye model. In surface Debye model, the generalized density of states projected onto a surface atom exhibits a huge peak mainly contributed by Rayleigh mode. When we move to the second layer, the Rayleigh mode rapidly decays into the solid and gives a smaller contribution. The generalized Rayleigh mode is depleted near the surface. The peak near the Rayleigh cutoff frequency becomes much smaller than that in the previous case. Also an oscillation occurs in this case due to the mixed modes. When we get deeper into the solid to the 10^{th} layer, the wavelength of the oscillation decreases, the Rayleigh mode has no contribution but the generalized Rayleigh mode now contributes with its asymptotic value. The peaks look very similar to the bulk Debye model, but the peak positions and peak heights are a little different. As l_s

increases, the generalized Rayleigh mode becomes less important than other modes and the two major peaks in the semi-infinite elastic continuum model becomes closer and the difference of the peak heights is larger.

J. E. Black[86] studied the diagonal density of states for Ni(111) using lattice dynamics. He found that the diagonal density of states for the vertical motion of a surface atom has one huge peak which is contributed by the surface modes such as Rayleigh wave. This peak is positioned at about half of the maximum phonon frequency similarly to the result from the surface Debye model for $l_s = 0.5$. However, unlike the surface Debye model, near the maximum phonon frequency, there is no peak in his calculation. For the atoms in the second layer, the diagonal density of states oscillates and there are two major peaks looking similar to the bulk case. When he moved to deeper inside the solid, the two peaks look more and more like the diagonal density of states of an atom in the bulk. Our calculation has shown the same conclusion as his results for the substrate atoms in the second and deeper layers. In our results, the peak height near the maximum phonon frequency is always lower than that of the lower frequency peak contributed by surface modes and the shear horizontal mode. The lattice dynamics calculation shows similar results for the atoms in the second and third layers below the surface. Deeper than the third layer in the substrate, ρ_{ii}^{zz} has settled down to its bulk behavior.[86]

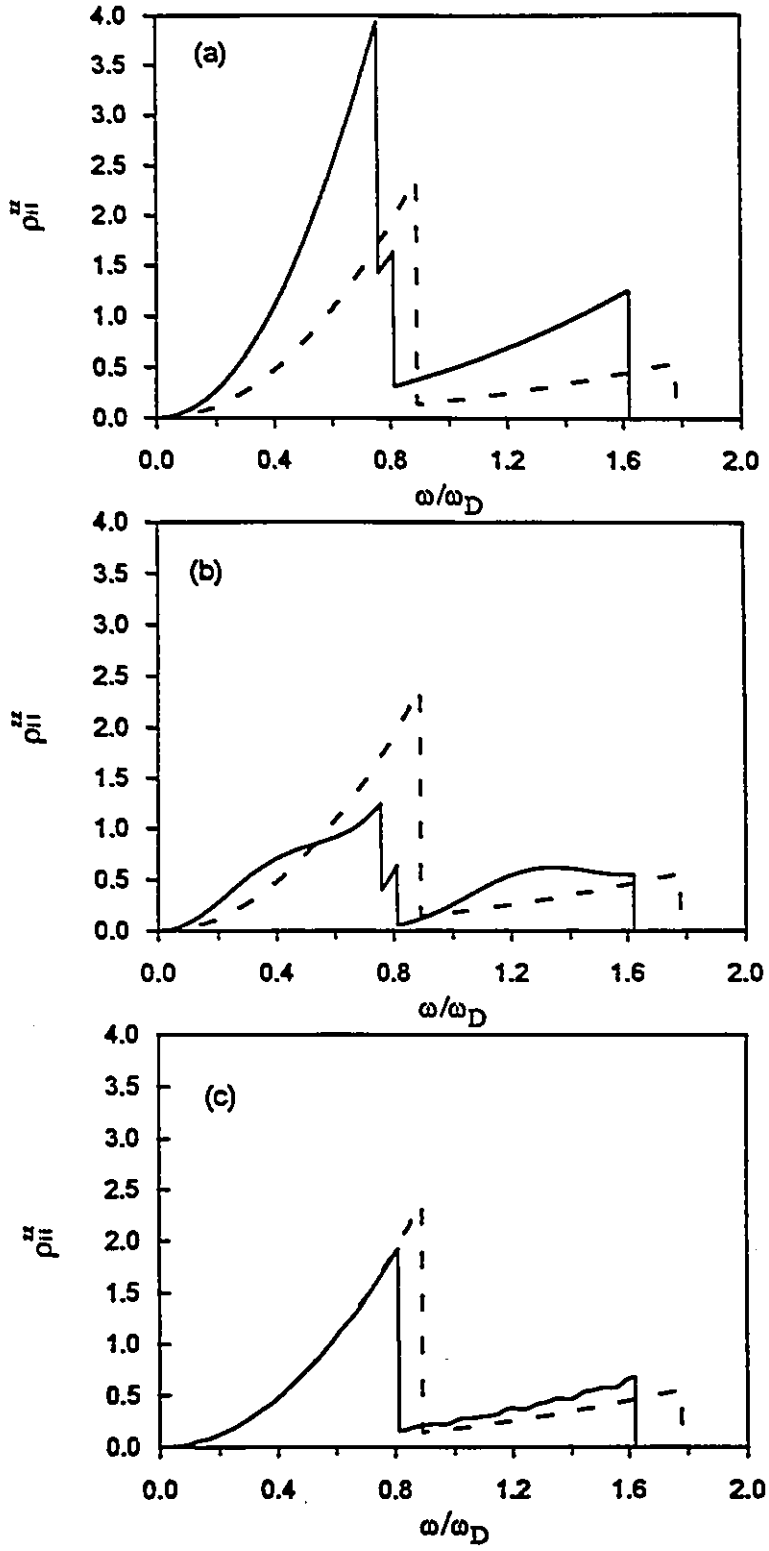

Figure 5.8: The diagonal density of states ρ_{ii}^{zz} of a simple cubic lattice for $l_s = 0.5$ for atoms at the surface (a), the second layer (b) and the 10^{th} layer (c), respectively.

5.4.2 Lateral polarization

In the semi-infinite elastic continuum model, the diagonal density of states corresponding to the lateral motion is independent of the lateral directions due to the symmetry of the surface, i.e., x and y directions are equivalent for the lateral polarization of the diagonal density of states. Fig. (5.9) shows the lateral polarization of the diagonal density of states of a simple cubic lattice for $l_s = 0.5$ in the bulk Debye model (dashed line) and the surface Debye model (solid line) for the atoms at the surface, the second layer and at the 10^{th} layer, respectively. For the atoms at the surface, the diagonal density of states exhibits three peaks. The one near Rayleigh cutoff frequency and the one near the SH cutoff frequency have almost the same height which shows that the SH mode dominates the contribution and the Rayleigh mode is not important for the lateral motion. The height of peaks are not as different as the vertical case. When we move to the atoms at the second layer, the Rayleigh mode rapidly decays into the solid and gives very small contribution. The peak at Rayleigh cutoff frequency almost disappears. Differently from the vertical motion, the lateral component of the generalized Rayleigh mode decays slower than its vertical component. The heights of peaks are closer to each other and look like the diagonal density of states of a bulk atom. The oscillation also appears due to the mixed modes $\sigma = \pm$. When we get to deeper inside the solid to the 10^{th} layer, similarly to the vertical motion, the wavelength of the oscillation decreases. The Rayleigh mode gives no contribution but the generalized Rayleigh mode now contributes with its asymptotic value, SH mode still dominates the contribution. The peaks now look more like that in the bulk Debye model. Similar to the vertical motion, as l_s increases, the generalized Rayleigh becomes less important than other modes and the two major peaks in the semi-infinite elastic continuum model

becomes closer and the difference in the peak heights is larger.

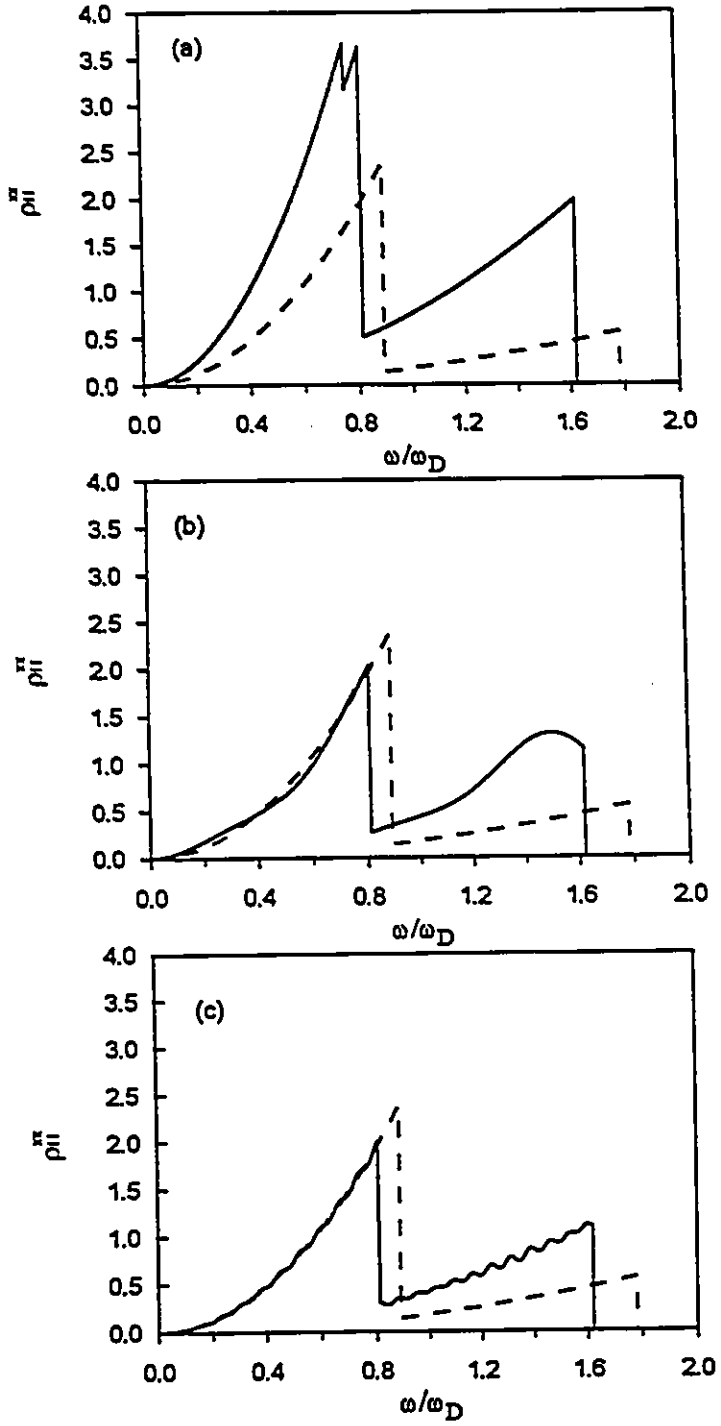

Figure 5.9: The diagonal density of states $\rho_{ii}^{\sigma\sigma}$ of a simple cubic lattice for $l_s = 0.5$ for the atoms at the surface (a), the second layer (b) and the 10^{th} layer (c), respectively.

In J. E. Black's calculation, the diagonal density of states for the lateral motion of the surface atoms differs only slightly from the result for atoms in the bulk. Even in the first layer below the surface, $\rho_{\parallel}^{zz}$ is very similar to the bulk behavior. Our calculations have shown the same trends. These two models have also shown that the motion of substrate atoms parallel to the surface is less strongly perturbed by the presence of surface than the motion normal to the surface.

5.4.3 About normalization

In above, we have considered and compared the diagonal density of states for both the perpendicular and parallel polarizations in the bulk Debye mode, the surface Debye model and the lattice dynamics calculation. In the bulk Debye model, all atoms in the substrate are equivalent. The diagonal density of states satisfies the sum rule and is normalized. However, in the surface Debye model, all weight functions depend on the phonon frequency and atom positions. Since we replace the surface Brillouin zone by a disc with radius κ_D and simply choose the cutoff frequencies in terms of the surface dispersion relation $\omega_D^{(\sigma)} = c_{min}^{(\sigma)}\kappa_D$, as a result, the weight functions for the surface atoms for all branches are larger than those for atoms much deeper inside the solid for $l_s = 0.5$. There are not enough contributions of oscillating branches to compensate the decay of the Rayleigh mode and generalized Rayleigh mode. The diagonal density of states are no longer correctly normalized for all substrate atoms in this model. For the surface atoms, the normalization depends on the choice of l_s. For the atoms deep inside the solid, the diagonal density of states is nearly normalized. Some of the generalized density of states representing the correlations of different atoms are normalized to a small number instead of exactly zero given in Eq. (5.38). These discrepancies in normalization is not important in the

long wavelength region where $\omega \ll \omega_D{}^{(\sigma)}$, but it is important in the high frequency region where $\omega \sim \omega_D{}^{(\sigma)}$. This normalization will strongly affect our calculation on the line width of the adatom at a surface.

Since the generalized density of states strongly depends on the vertical position of the atoms in the substrate, there is no simple way to normalize all generalized densities of states in the surface Debye model. Following the approximation of the generalized density of states in the bulk Debye model, Kreuzer and Gortel[10] introduced the average surface density of states in the surface Debye model for vibrations parallel and perpendicular to the surface, respectively. In either direction, they averaged the weight functions for all branches and assumed all branches are cutoff at the same frequency so that normalization is satisfied. The new cutoff frequencies are close to the Rayleigh mode cutoff frequency. For $\infty < z < 0$, both average densities of states and cutoff frequencies for the vibrations parallel and perpendicular to the surface depend on ω through the product ωz. Although the averaged density of states can be perfectly normalized in this way, the phonon dynamics in the high frequency region are eliminated. In our calculation, the higher frequency phonon modes play an important role. We should not normalize the generalized density of states in this way.

To keep the basic properties of the surface Debye model in the semi-infinite elastic continuum approach, we normalize the generalized density of states at the surface in an "ad hoc" way by scaling the weight function. Since the generalized density of states for the atoms deep inside the solid are not too much off normalization, we will not consider the "ad hoc" scaling for them. More details on this will be shown in Chapter 6.

Chapter 6. A detailed study of vibrational decay by two phonon emission processes

6.1 Introduction

When a gas molecule is adsorbed at a solid surface, the molecule moves laterally as well as perpendicularly. The number of normal modes depends on the symmetry of the adsorption system. For an adatom adsorbed at a solid surface, there are only three localized normal modes which depend on the symmetry of the adsorption site. Fig. (6.1) shows the motion of an adatom adsorbed at a bridge site of a solid surface.

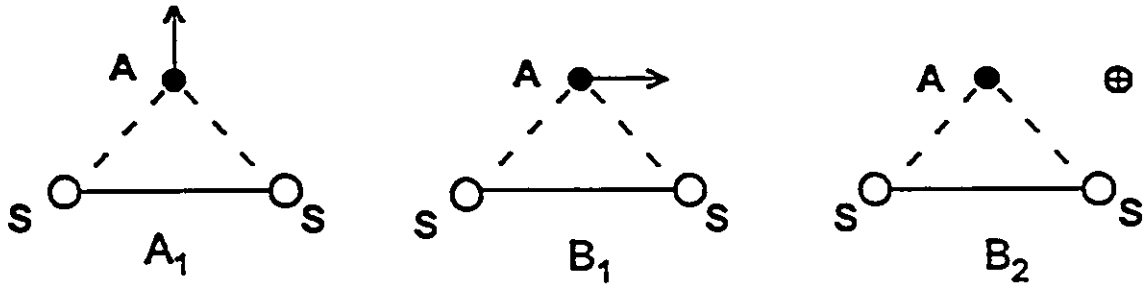

Figure 6.1: Motion of an adatom at a bridge site.

At a bridge site, an adatom is bounded to two surface atoms. The vibration A_1 is an adatom-surface bond stretching mode. The lateral mode B_1 represents a vibration along the bridge, while B_2 denotes the motion perpendicular to the SAS plane. A description of the three modes A_1, B_1 and B_2 in terms of the bond stretching and angle bending depends crucially on the SAS angle. Such a description is closely related to the vibrational frequencies associated with the modes. The expected frequencies of these three modes are a sensitive measure of the SAS bond angle. We

will see more details in Section 2. Only the A_1 mode is active in the infrared.

A molecule adsorbed at a solid surface would have more normal modes. When we study the adsorbate-surface vibration or "T mode", we ignore the internal motion of the molecule itself and treat it as an adatom.

In Chapters 2, 3 and 4, in terms of the one dimensional model, we have shown that the phonon-induced vibrational line shape due to the anharmonicity of the adsorption potential is negligible for an adatom at an ontop site, but not at a bridge site. In order to understand the roles of the geometry of an adsorption system, we study the vibrational lineshape of the "T mode" for an adatom at a bridge site in more details in a three dimensional model in this chapter. Both the anharmonic couplings with the surface atoms and among the substrate atoms themselves will be included. Both the lateral and vertical couplings play roles in the line shape calculation.

Near the surface, the phonon behavior is much different from the bulk case due to the existence of the boundary. There are different approaches to describe the substrate with the consideration of the boundary. We will use the semi-infinite elastic continuum approximation introduced in the last chapter, which enables us to include surface phonon modes absent in the bulk Debye model, in a simple way.

Above all, we can see that it is essential to study an adsorption system in a three dimensional model to have a better understanding of the vibrational line shape of the adatom.

To avoid duplication and complexity, we do not reconsider all the dephasing and decay processes which we have discussed in the one dimensional model, but look into the details of the two phonon emission process. For the typical system CO/Pt(111), the frequency of the "T mode" lies between the maximum substrate

phonon frequency ω_{max} and $2\omega_{max}$. We have shown that the two phonon emission process gives the lowest order contribution to the vibrational line width in the perturbation theory. The vibrational mode localized on the adatom may decay via the energy-conserving two phonon emission processes. Moreover, the line width calculation in the one dimensional model also has shown that the two phonon emission process dominates the "T mode" line width.

In Section 2, the full hamiltonian of an adsorption system in the three dimensional model is constructed and the solution of the harmonic hamiltonian is given. New reduction factors are found in Section 3. The general discussion about the line shape for an adatom at a bridge site is given in Section 4. The vertex function for the two phonon emission process is derived in Section 5. The self energy for the two phonon emission process will be discussed, and its contribution to the vibrational line width is calculated in Section 6. Finally, the theory is applied to the O/Cu(110) adsorption system, in which the adatom-surface stretching frequency lies between the maximum substrate phonon frequency ω_{max} and $2\omega_{max}$, and for which the two phonon emission process may be important. H. Dürr and A. P. Baddorf[61] studied this system in EELS experiments. We will compare our numerical results with their experimental data.

6.2 Hamiltonian in a three dimensional model and its harmonic solution for an adatom at a bridge site

In this section, we construct our model for an adatom at a bridge site, and develop a theoretical description of the hamiltonian of the adsorption system which is the basis of the lineshape calculation.

6.2.1 Model structure of an adatom at a bridge site and its hamiltonian

Similar to Chapter 4, we consider an adsorbed atom at a bridge site. The adatom only interacts with the nearest surface atoms it is bound to, and the substrate atoms interact with their nearest neighbors. All these nearest neighbor interactions are described in terms of pair-wise central-force model here[56]. The basic geometry

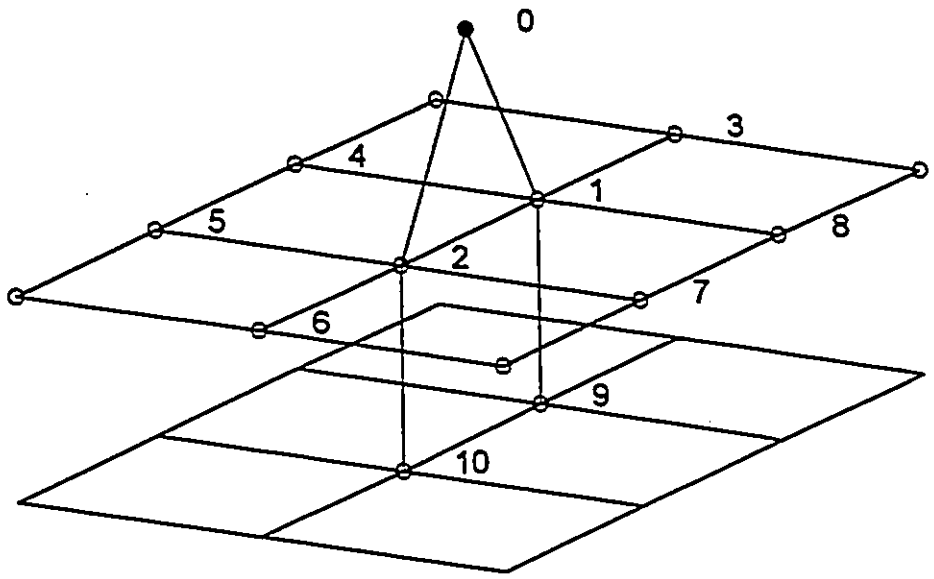

Figure 6.2: Model structure of the adatom at a bridge site of a simple cubic (100) surface.

is illustrated in Fig. (6.2), where we show the adatom sitting at a bridge site on a (100) surface of a simple cubic lattice. The adatom vibrates against the surface with a displacement $\vec{a_0} = (x, y, z)$ from its equilibrium position, while the surface bridge

atoms and their nearest neighbors have displacements $\vec{a}_i$ from their equilibrium positions. They are composed of a cluster ($i = 0, \cdots, 10$), in which each atom has an equilibrium position $\vec{R}_i$ ($i = 0, \cdots, 10$). The separation between two atoms i and j can be written as

$$(\vec{a}_i - \vec{a}_j) + (\vec{R}_i - \vec{R}_j) = \vec{a}_{ij} + \vec{R}_{ij}. \tag{6.1}$$

We assume that the adatom interacts with the two bridge atoms with identical potentials $V(\vec{a}_0 - \vec{a}_i) = V(\vec{a}_{0i})(i = 1, 2)$, and the substrate atoms interact with their nearest neighbors with identical potentials $\phi(\vec{a}_i - \vec{a}_j) = \phi(\vec{a}_{ij})$ where i = bridge atoms, and j = nearest neighbors of the bridge atom i. Hence, we can write these interactions in a unified form

$$h(\vec{a}_{ij}) = \begin{cases} V(\vec{a}_{ij}), & \text{i=0, j=1,2;} \\ \phi(\vec{a}_{ij}), & \text{i=1,2, j=n.n of i.} \end{cases} \tag{6.2}$$

Expanding these interactions in Taylor expansion gives

$$h(\vec{a}_{ij}) = \sum_n \frac{1}{n!} [(\vec{a}_i - \vec{a}_j) \cdot \nabla]^n \, h(\vec{a}_{ij}) \mid_{\vec{a}_{ij}=0}, \tag{6.3}$$

The derivative $h_{ij}^{(n)}$ of the interaction potential $h(\vec{a}_{ij})$ with respect to the separation between atoms i and j is a function of $\vec{R}_{ij} = \hat{n}_{ij} R_{ij}$, where $\hat{n}_{ij}$ a unit vector. We can assume that the first derivative of the pair potential $h'_{ij} = 0$, a condition required if the atoms in the cluster vibrate with respect to their equilibrium positions. Then the total potential energy is

$$\begin{aligned} E_p &= \sum_{i,j pairs} h_{ij} + \frac{1}{2} h''_{ij} (\vec{a}_{ij} \cdot \hat{n}_{ij})^2 \\ &+ \frac{1}{2} h''_{ij} \left[(\vec{a}_{ij} \cdot \hat{n}_{ij}) \frac{a_{ij}^2 - (\vec{a}_{ij} \cdot \hat{n}_{ij})^2}{R_{ij}} + \frac{1}{4} \frac{a_{ij}^2 - (\vec{a}_{ij} \cdot \hat{n}_{ij})^2}{R_{ij}} \frac{a_{ij}^2 - 5(\vec{a}_{ij} \cdot \hat{n}_{ij})^2}{R_{ij}} \right] \end{aligned}$$

$$+ \frac{1}{6}h'''_{ij}\left[(\vec{a}_{ij}\cdot\hat{n}_{ij})^3 + \frac{3}{2}(\vec{a}_{ij}\cdot\hat{n}_{ij})^2\frac{a_{ij}^2-(\vec{a}_{ij}\cdot\hat{n}_{ij})^2}{R_{ij}}\right]$$
$$+ \frac{1}{24}h^{(4)}_{ij}(\vec{a}_{ij}\cdot\hat{n}_{ij})^4+\ldots, \tag{6.4}$$

where h''_{ij}, h'''_{ij} and $h^{(4)}_{ij}$ are the second, third and forth derivatives of the pair potential $h(\vec{a}_{ij})$, respectively. With this potential energy, we can write out the hamiltonian of the adsorption system as

$$H = H_{harm} + H_{anh}, \tag{6.5}$$

where the harmonic hamiltonian

$$\begin{aligned} H_{harm} &= \left[T_{\vec{a}_0} + \frac{1}{2}\sum_{i=1,2}h''_{0i}(\vec{a}_0\cdot\hat{n}_{0i})^2\right] + \left[\frac{1}{2}\sum_{i=1,2}h''_{0i}(\vec{a}_i\cdot\hat{n}_{0i})^2 + H_s^{harm}\right] \\ &\quad - \left[\sum_{i=1,2}h''_{0i}[(\vec{a}_0\cdot\hat{n}_{0i})(\vec{a}_i\cdot\hat{n}_{0i})\right] \\ &= H_{0ad} + H_{0s} + H_{0ad-s}. \end{aligned} \tag{6.6}$$

In this harmonic hamiltonian, H_{0ad} represents the free hamiltonian of an adatom, while H_{0s} represents the free hamiltonian of the substrate. H_{0ad-s} describes the bilinear coupling between them which reduces to $-V''z(a_{1z}+a_{2z})\cos^2\theta$ if we only keep the z component. Note that this is different from the one dimensional model in Chapter 4 since we take the central force model of the pair interaction between atoms.

The anharmonic hamiltonian with only the lower order in $\vec{a}_{ij}$ is

$$\begin{aligned} H_{anh} &= \sum_{(i,j)\ pairs}\left[\frac{1}{2}h''_{ij}(\vec{a}_{ij}\cdot\hat{n}_{ij})\frac{a_{ij}^2-(\vec{a}_{ij}\cdot\hat{n}_{ij})^2}{R_{ij}} + \frac{1}{6}h'''_{ij}(\vec{a}_{ij}\cdot\hat{n}_{ij})^3\right] \\ &\quad + \frac{1}{24}h^{(4)}_{ij}(\vec{a}_{ij}\cdot\hat{n}_{ij})^4+\ldots, \end{aligned} \tag{6.7}$$

For an adatom at a bridge site, $R_{01} = R_{02} = R_0$ because of the symmetry. If we only

consider the nearest neighbor interactions in the substrate, all the nearest neighbor separation $R_{ij} = a$, where (i, j) are substrate atoms and a is the lattice constant. Based on Eq. (6.2), the n^{th} derivative of potential $h(\vec{a}_{ij})$ at equilibrium is

$$h_{ij}^{(n)} = \begin{cases} V^{(n)}(R_0), & \text{i=0, j=1,2;} \\ \phi^{(n)}(a), & \text{i=1,2, j=n.n of i.} \end{cases} \tag{6.8}$$

If we define

$$h_2(R_{ij}) = \frac{h''_{ij}}{2R_{ij}}, \tag{6.9}$$

$$h_3(R_{ij}) = \frac{h'''_{ij}}{6} - \frac{h''_{ij}}{2R_{ij}}, \tag{6.10}$$

the anharmonic hamiltonian given by Eq. (6.7) can be simplified as

$$\begin{aligned} H_{anh} = & \sum_{ij} \left[h_2(R_{ij})(\vec{a}_{ij} \cdot \hat{n}_{ij}) a_{ij}^2 + h_3(R_{ij})(\vec{a}_{ij} \cdot \hat{n}_{ij})^3 \right] \\ & + \frac{1}{24} h_{ij}^{(4)} (\vec{a}_{ij} \cdot \hat{n}_{ij})^4 + \ldots . \end{aligned} \tag{6.11}$$

We will treat this anharmonic hamiltonian as a perturbation in the finite temperature field theory introduced in Section (2.4).

6.2.2 Free fields

Before we get into the equation of motion for the harmonic hamiltonian of the adsorption system, let us look at the free fields for the adatom and substrate in the three dimensional model.

As illustrated in Fig. (6.2), let θ be the angle made by $\vec{R}_{01}$ and the vertical. The free hamiltonian of the adatom can be simplified as

$$H_{0ad} = T_{\vec{a}_0} + (V'' \sin^2\theta)x^2 + (V'' \cos^2\theta)z^2. \tag{6.12}$$

This free hamiltonian shows that the adatom vibrates in the x and z directions independently as a harmonic oscillator with frequencies

$$\omega_{x_0} = \sqrt{2V'' \sin^2\theta/m},$$
$$\omega_{z_0} = \sqrt{2V'' \cos^2\theta/m}, \tag{6.13}$$

respectively. In this simple model, when the angle θ is 45°, the local modes in the x and z directions have the same frequency; while when the angle $\theta < 45°$, the local mode in the z direction is at a higher frequency having the more bond-stretching character. The local vibration of the adatom with the vibrational coordinate z and frequency ω_{z_0} is perpendicular to the surface. In the y direction, the adatom is free to move due to the adoption of a central force model of the pair interactions between the atoms. In the real system, the vibrational frequency in the y direction is usually much smaller than the vibrational frequencies in the other two directions. If it is too small, it will not provide efficient decay channel for the perpendicular localized phonon mode. On the other hand, since the dephasing process by this lower frequency mode was already considered by other people such as D. C. Langreth[17], we will concentrate on the dynamical processes induced by the delocalized phonon modes of the substrate and do not intend to include the effect of this lower frequency mode on the vibration line shape in our model.

Based on this harmonic hamiltonian, we have the free displacement fields of the normal modes in the x and z directions as follows:

$$x^0(t) = \sqrt{\frac{\hbar}{2m\omega_{x_0}}}\left[b_x e^{-i\omega_{x_0}t} + b_x^\dagger e^{i\omega_{x_0}t}\right], \tag{6.14}$$

$$z^0(t) = \sqrt{\frac{\hbar}{2m\omega_{z_0}}}\left[b_z e^{-i\omega_{z_0}t} + b_z^\dagger e^{i\omega_{z_0}t}\right]. \tag{6.15}$$

They are the displacements of the two independent oscillators at a static surface

for an adatom at a bridge site. For an adatom at an on top site, $x^0(t)$ disappears and there is only one free field for the adatom just like what we had in the one dimensional model.

In the harmonic approximation, the hamiltonian of the substrate phonons in the three dimensional model is

$$H_{0s} = H_s^{harm} + \frac{1}{2}V'' \sum_{i=1,2} (\vec{a}_i \cdot \hat{n}_{0i})^2. \tag{6.16}$$

The first term describes a perfect harmonic hamiltonian for the substrate. The second term is ignored as that in Chapter 3 and Chapter 4. However, we will treat the substrate as a semi-infinite elastic continuum here based on the discussion in Chapter 5, where the displacement of an atom in the substrate can be expanded in terms of the phonon normal modes given in Eq. (5.34). In Chapter 2, 3, 4, we treated the substrate as an infinite elastic continuum, and described the displacement of a substrate atom in a bulk Debye model.

According to the definition in Eq. (5.36), the components of the generalized density of states depend on the positions of the atoms in the substrate and the choice of the substrate model. In considering the phonon-induced vibrational line shape of an adatom, our results partly depend on the choice of the substrate model in calculating the generalized density of states. In the previous calculations, we ignored lateral motion and used the bulk Debye model to describe the phonon motion in the direction perpendicular to the surface. In this chapter, we will calculate the generalized density of states with the normal modes solution of H_{0s} in the semi-infinite elastic continuum model, i.e., the displacements of the substrate atoms are described by Eq. (5.34).

6.2.3 Vibrational coordinates for the adatom and bridge atoms at the surface

Now let us come to the bilinear couplings between the adatom and the substrate which can be specifically written as

$$\begin{aligned} H_{0ad-s} &= -h''_{01}\left[\sin^2\theta\; x(a_{1x}+a_{2x})+\cos^2\theta\; z(a_{1z}+a_{2z})\right] \\ &\quad -h''_{01}\left[\sin\theta\;\cos\theta\; x(a_{2z}-a_{1z})+\sin\theta\;\cos\theta\; z(a_{2x}-a_{1x})\right]. \quad (6.17) \end{aligned}$$

Compared to the one dimensional model, there are the perpendicular and lateral couplings as well as the cross terms between them in these bilinear interactions. The first term describes the bilinear couplings of in-phase motion of the two bridge atoms at the surface, while the second term describes the out-of-phase motion. The coupling constants depend on the angle θ. Similar to ω_{z_0} given in Eq. (6.13), we further define $\omega_{xz}{}^2 = 2h''(R)\sin\;\theta\;\cos\;\theta/m$. Along with the definition of ω_{z_0} and ω_{x_0}, we can write the bilinear coupling as

$$\begin{aligned} H_{0ad-s} &= -\frac{1}{2}m\omega_{x_0}{}^2x(a_{1x}+a_{2x})-\frac{1}{2}m\omega_{z_0}{}^2z(a_{1z}+a_{2z}) \\ &\quad -\frac{1}{2}m\omega_{xz}{}^2\left[x(a_{2z}-a_{1z})+z(a_{2x}-a_{1x})\right], \quad (6.18) \end{aligned}$$

In this adsorption situation, when $\theta < 45°$, we have $\omega_{z_0} > \omega_{xz} > \omega_{x_0}$, otherwise, $\omega_{z_0} < \omega_{xz} < \omega_{x_0}$. In the extreme case, $R \gg a$, i.e., $\theta \approx 0$, the bilinear coupling reduce to $\frac{1}{2}m\omega_{z_0}{}^2z(a_{1z}+a_{2z})$. In this case, the adatom seems to sit at an ontop site with the two surface atoms underneath. If these two atoms move in-phase with the average displacement $a_z = \frac{1}{2}(a_{1z}+a_{2z})$, and ignoring their out-of-phase motion, the model reduces to the case of an adatom at an ontop site. In the opposite extreme case, when the adatom is very close to the surface, $R \approx a/2$, i.e., $\theta \approx 90°$, and the bilinear couplings reduce to $\frac{1}{2}m\omega_{x_0}{}^2x(a_{1x}+a_{2x})$. There are no bilinear couplings

present in the z direction, in this case, and there is no localized phonon mode vibrating perpendicular to the surface which is IR active. We will consider physical system with $0 < \theta < 90°$.

When the adatom is placed on a solid surface, each normal mode may involve both the motion of the adatom and the motion of the substrate atoms. Similarly to that in one dimensional model, the displacement of a surface atom $\vec{a}_i(t)$ is expanded in the same form as $\vec{a}_i^0(t)$, i.e.

$$\vec{a}_i(t) = \sum_J \vec{a}^{(J)}(\vec{R}_i)\sqrt{c_\sigma}d_J(t), \tag{6.19}$$

where $\vec{a}^{(J)}(\vec{R}_i)$ are the phonon eigenfunctions given in Chapter 5, and $d_J(t)$ is the amplitude of the J^{th} phonon mode when the bilinear terms are included in the harmonic hamiltonian. We are specifically interested in the relationship between the displacement fields $z(t)$, $x(t)$ and $d_J(t)$ since they determine the quantities $\vec{a}_{ij}$ which enters the anharmonic hamiltonian. The time dependencies of $x(t), z(t)$ and $d_J(t)$ are governed by the harmonic hamiltonian H_{harm} and the free fields $z^0(t)$, $x^0(t)$ and $d_J^0(t)$, which independently follow the hamiltonians of H_{0ad} and H_{0s}, respectively. Based on H_{harm}, the equations of motion now become

$$(-\frac{\partial^2}{\partial t^2} - {\omega_{z_0}}^2)z(t) = -\frac{1}{2}{\omega_{z_0}}^2[a_{1z}(t) + a_{2z}(t)] - \frac{1}{2}{\omega_{xz}}^2[a_{2z}(t) - a_{1z}(t)], \tag{6.20}$$

$$(-\frac{\partial^2}{\partial t^2} - {\omega_{x_0}}^2)x(t) = -\frac{1}{2}{\omega_{x_0}}^2[a_{1x}(t) + a_{2x}(t)] - \frac{1}{2}{\omega_{xz}}^2[a_{2x}(t) - a_{1x}(t)], \tag{6.21}$$

$$\begin{aligned}(-\frac{\partial^2}{\partial t^2} - {\omega_J}^2)d_J(t) = &-\frac{m}{2\rho_0\sqrt{c_\sigma}}x\left[{\omega_{x_0}}^2(a_{1x}^{(J)*} + a_{2x}^{(J)*}) + {\omega_{xz}}^2(a_{2z}^{(J)*} - a_{1z}^{(J)*})\right] \\ &-\frac{m}{2\rho_0\sqrt{c_\sigma}}z\left[{\omega_{x_0}}^2(a_{1x}^{(J)*} + a_{2x}^{(J)*}) + {\omega_{xz}}^2(a_{2x}^{(J)*} - a_{1x}^{(J)*})\right],\end{aligned} \tag{6.22}$$

where $\vec{a}^{(J)*}$ is the complex conjugate of $\vec{a}^{(J)}$. We only consider the case where the

local mode frequencies ω_{x_0} and ω_{z_0} are outside of the continuum phonon band, i.e., $\omega_{x_0}, \omega_{z_0} > \omega_{max}$. Green's function solutions of the equations of motion give the expansions of the vibrational coordinates in analogy with the one dimensional cases studied in Chapter 3 and Chapter 4.

In the weak coupling limit, the solutions to these equations of motion read

$$\begin{aligned} x(t) &= x^0(t) + \sum_J \frac{\frac{1}{2}{\omega_{x_0}}^2}{{\omega_{x_0}}^2 - {\omega_J}^2}\left[a_{1x}^{(J)} + a_{2x}^{(J)}\right]\sqrt{c_\sigma}d_J^0(t) \\ &\quad + \frac{\frac{1}{2}{\omega_{xz}}^2}{{\omega_{x_0}}^2 - {\omega_J}^2}\left[a_{2z}^{(J)} - a_{1z}^{(J)}\right]\sqrt{c_\sigma}d_J^0(t) \end{aligned} \tag{6.23}$$

$$\begin{aligned} z(t) &= z^0(t) + \sum_J \frac{\frac{1}{2}{\omega_{z_0}}^2}{{\omega_{z_0}}^2 - {\omega_J}^2}\left[a_{1z}^{(J)} + a_{2z}^{(J)}\right]\sqrt{c_\sigma}d_J^0(t) \\ &\quad + \frac{\frac{1}{2}{\omega_{xz}}^2}{{\omega_{z_0}}^2 - {\omega_J}^2}\left[a_{2x}^{(J)} - a_{1x}^{(J)}\right]\sqrt{c_\sigma}d_J^0(t) \end{aligned} \tag{6.24}$$

$$\begin{aligned} d_J(t) &= d_J^0(t) \\ &\quad -\frac{m}{2\rho_0\sqrt{c_\sigma}}\left[\frac{{\omega_{x_0}}^2}{{\omega_{x_0}}^2 - {\omega_J}^2}(a_{1x}^{(J)*} + a_{2x}^{(J)*}) + \frac{{\omega_{xz}}^2}{{\omega_{x_0}}^2 - {\omega_J}^2}(a_{2z}^{(J)*} - a_{1z}^{(J)*})\right]x^0(t) \\ &\quad -\frac{m}{2\rho_0\sqrt{c_\sigma}}\left[\frac{{\omega_{z_0}}^2}{{\omega_{z_0}}^2 - {\omega_J}^2}(a_{1z}^{(J)*} + a_{2z}^{(J)*}) + \frac{{\omega_{xz}}^2}{{\omega_{z_0}}^2 - {\omega_J}^2}(a_{2x}^{(J)*} - a_{1x}^{(J)*})\right]z^0(t). \end{aligned} \tag{6.25}$$

Substituting d_J into Eq. (6.19) gives the displacements of the two bridge atoms ($i = 1, 2$) at the surface in the harmonic approximation as

$$a_{i\alpha}(t) = F_{i\alpha}x^0(t) + G_{i\alpha}z^0(t) + \sum_J a_{i\alpha}^{(J)}d_J^0(t), \tag{6.26}$$

where the prefactors $F_{i\alpha}$ and $G_{i\alpha}$ in front of the normal mode coordinates $x^0(t)$ and $z^0(t)$ are defined as follow:

$$F_{i\alpha} = \sum_J -\frac{m}{2\rho_0}a_{i\alpha}^{(J)}\left[\frac{{\omega_{x_0}}^2}{{\omega_{x_0}}^2 - {\omega_J}^2}(a_{1x}^{(J)*} + a_{2x}^{(J)*}) + \frac{{\omega_{xz}}^2}{{\omega_{x_0}}^2 - {\omega_J}^2}(a_{2z}^{(J)*} - a_{1z}^{(J)*})\right], \tag{6.27}$$

$$G_{i\alpha} = \sum_J -\frac{m}{2\rho_0}a_{i\alpha}^{(J)}\left[\frac{{\omega_{z_0}}^2}{{\omega_{z_0}}^2 - {\omega_J}^2}(a_{1z}^{(J)*} + a_{2z}^{(J)*}) + \frac{{\omega_{xz}}^2}{{\omega_{z_0}}^2 - {\omega_J}^2}(a_{2x}^{(J)*} - a_{1x}^{(J)*})\right]. \tag{6.28}$$

They depend on the lateral and perpendicular amplitudes of the phonon modes. In the weak coupling limit, $m/M \ll 1$, $F_{i\alpha}$ and $G_{i\alpha}$ are small.

The solutions of the harmonic hamiltonian given in Eqs. (6.23), (6.24) and (6.25) are similar to those in Chapter 3 and Chapter 4, except that the lateral motions of both the adatom and substrate atoms are included here.

To understand the motions of the adatom and bridge atoms at the surface in the harmonic approximation, we now look at two extreme cases. First, ignoring the localized mode of the adatom, the displacement of the adatom is induced by the motions of the two bridge atoms. The adatom tends to follow the in-phase motion of the delocalized phonon modes of the two bridge atoms. On the other hand, the out-of-phase motion of the delocalized phonon modes of the two bridge atoms in the x direction will result in the adatom moving in the z direction, and vise versa; see Fig. (6.3a). Second, if we instead look at the effect of the localized mode on the bridge atoms, we find that the motion of the adatom in the localized mode will induce out-of-phase motion of the two bridge atoms, in response to the motion of the adatom. See Fig. (6.3b) which shows the motion of the normal mode of the

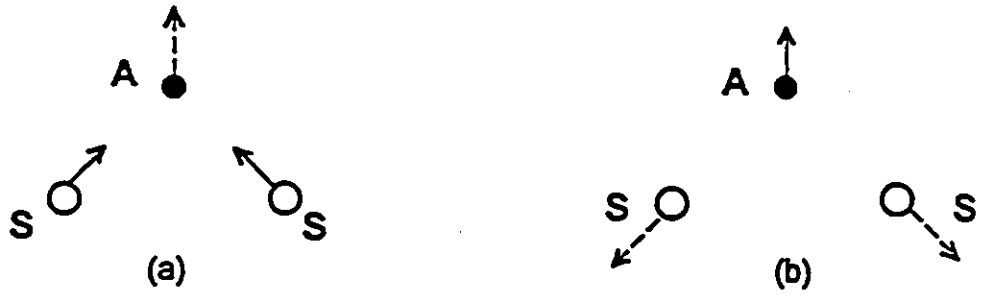

Figure 6.3: Normal modes of an adatom and bridge atoms.

adatom and its effect on the two bridge atoms.

Following the same approximation in Chapter 3 and Chapter 4, the spread of the localized vibrational modes go as far as the first layer surface atoms $i = 1, 2$

only. The substrate atoms other than the nearest neighbors of the adatom are not affected by the adatom. Their displacements are denoted by $\vec{a}_j(t) = \vec{a}_j^0(t)$. Similar to the one dimensional model, since the bridge atoms are affected by local modes, the anharmonic coupling between the bridge atoms and their nearest neighbors will affect the line shape of local mode. The quantities entering the anharmonic coupling is the displacement difference between pairs i and j. For the atom pairs (0,1) and (0,2) in Fig. (6.2), the amplitudes of the adatom due to the J^{th} delocalized phonon mode always come with prefactors, $\frac{\frac{1}{2}\omega_{x_0}{}^2}{\omega_{x_0}{}^2-\omega_J{}^2}$, $\frac{\frac{1}{2}\omega_{x_0}{}^2}{\omega_{x_0}{}^2-\omega_J{}^2}$, $\frac{\frac{1}{2}\omega_{xz}{}^2}{\omega_{x_0}{}^2-\omega_J{}^2}$ or $\frac{\frac{1}{2}\omega_{xz}{}^2}{\omega_{x_0}{}^2-\omega_J{}^2}$. The first two prefactors will induce a reduction factor similar to that in the one dimensional model for the in-phase motion of the bridge atoms, while the last two prefactors will induce similar reduction factors for the out-of-phase motion of the bridge atoms, when we calculate the distances between atoms 0 and 1, or 0 and 2, that is $\vec{a}_{01}$ and $\vec{a}_{02}$, as shown in the next section. In our calculation, we will include both effects of in-phase and out-of-phase phonon motions on the vibrational line shape.

Purely for numerical reasons to simplify our calculation, we can rewrite the displacements of all atoms in the cluster systematically in matrix form. If we define each vector as a row matrix $\vec{a}_i = [a_{ix}\ a_{iy}\ a_{iz}]$, then the displacements of 11 atoms in the cluster become a 11×3 matrix as follows

$$\begin{pmatrix} x & y & z \\ a_{1x} & a_{1y} & a_{1z} \\ a_{2x} & a_{2y} & a_{2z} \\ a_{3x} & a_{3y} & a_{3z} \\ a_{4x} & a_{4y} & a_{4z} \\ a_{5x} & a_{5y} & a_{5z} \\ a_{6x} & a_{6y} & a_{6z} \\ a_{7x} & a_{7y} & a_{7z} \\ a_{8x} & a_{8y} & a_{8z} \\ a_{9x} & a_{9y} & a_{9z} \\ a_{10x} & a_{10y} & a_{10z} \end{pmatrix} = \begin{pmatrix} F_{0x} & F_{0y} & F_{0z} \\ F_{1x} & F_{1y} & F_{1z} \\ F_{2x} & F_{2y} & F_{2z} \\ F_{3x} & F_{3y} & F_{3z} \\ F_{4x} & F_{4y} & F_{4z} \\ F_{5x} & F_{5y} & F_{5z} \\ F_{6x} & F_{6y} & F_{6z} \\ F_{7x} & F_{7y} & F_{7z} \\ F_{8x} & F_{8y} & F_{8z} \\ F_{9x} & F_{9y} & F_{9z} \\ F_{10x} & F_{10y} & F_{10z} \end{pmatrix} x^0(t) + \begin{pmatrix} G_{0x} & G_{0y} & G_{0z} \\ G_{1x} & G_{1y} & G_{1z} \\ G_{2x} & G_{2y} & G_{2z} \\ G_{3x} & G_{3y} & G_{3z} \\ G_{4x} & G_{4y} & G_{4z} \\ G_{5x} & G_{5y} & G_{5z} \\ G_{6x} & G_{6y} & G_{6z} \\ G_{7x} & G_{7y} & G_{7z} \\ G_{8x} & G_{8y} & G_{8z} \\ G_{9x} & G_{9y} & G_{9z} \\ G_{10x} & G_{10y} & G_{10z} \end{pmatrix} z^0(t) + \sum_J \begin{pmatrix} a_{0x}^{(J)} & a_{0y}^{(J)} & a_{0z}^{(J)} \\ a_{1x}^{(J)} & a_{1y}^{(J)} & a_{1z}^{(J)} \\ a_{2x}^{(J)} & a_{2y}^{(J)} & a_{2z}^{(J)} \\ a_{3x}^{(J)} & a_{3y}^{(J)} & a_{3z}^{(J)} \\ a_{4x}^{(J)} & a_{4y}^{(J)} & a_{4z}^{(J)} \\ a_{5x}^{(J)} & a_{5y}^{(J)} & a_{5z}^{(J)} \\ a_{6x}^{(J)} & a_{6y}^{(J)} & a_{6z}^{(J)} \\ a_{7x}^{(J)} & a_{7y}^{(J)} & a_{7z}^{(J)} \\ a_{8x}^{(J)} & a_{8y}^{(J)} & a_{8z}^{(J)} \\ a_{9x}^{(J)} & a_{9y}^{(J)} & a_{9z}^{(J)} \\ a_{10x}^{(J)} & a_{10y}^{(J)} & a_{10z}^{(J)} \end{pmatrix} \sqrt{c_\sigma} d^0(t) \tag{6.29}$$

Comparing Eqs. (6.23), (6.24) and (6.26) with the matrix expression gives

$$F_{0x} = 1,\ F_{0y} = 0,\ F_{0z} = 0, \tag{6.30}$$

$$G_{0x} = 0,\ G_{0y} = 0,\ G_{0z} = 1, \tag{6.31}$$

$$\begin{aligned} a_{0x}^{(J)} &= \frac{\frac{1}{2}{\omega_{x_0}}^2}{{\omega_{x_0}}^2 - {\omega_J}^2}\left[a_x^{(J)}(R_1) + a_x^{(J)}(R_2)\right] + \frac{\frac{1}{2}{\omega_{xz}}^2}{{\omega_{x_0}}^2 - {\omega_J}^2}\left[a_z^{(J)}(R_2) - a_z^{(J)}(R_1)\right], \\ a_{0y}^{(J)} &= 0, \\ a_{0z}^{(J)} &= \frac{\frac{1}{2}{\omega_{z_0}}^2}{{\omega_{z_0}}^2 - {\omega_J}^2}\left[a_z^{(J)}(R_1) + a_z^{(J)}(R_2)\right] + \frac{\frac{1}{2}{\omega_{xz}}^2}{{\omega_{z_0}}^2 - {\omega_J}^2}\left[a_x^{(J)}(R_2) - a_x^{(J)}(R_1)\right], \end{aligned} \tag{6.32}$$

and

$$\vec{F}_i = 0,\ \vec{G}_i = 0 \ for\ i = 3, \cdots, 10. \tag{6.33}$$

6.3 Reduction factors in the adsorption potential

In the central force model, the adsorption potentials depend on the components of the atomic displacements of the adatom and surface atoms both parallel and perpendicular to the adsorption bond directions. From the solution of the harmonic hamiltonian, we find these parallel components of the atomic displacement differences between the adatom and bridge atoms are

$$\begin{aligned} \vec{a}_{01} \cdot \hat{n}_{01} &= z^0(g_x \sin\theta + g_z \cos\theta) \\ &\quad + \sum_J \left[-\sin\theta \frac{{\omega_J}^2}{{\omega_{x_0}}^2 - {\omega_J}^2} a_{+x}^{(J)} + \cos\theta \frac{{\omega_J}^2}{{\omega_{x_0}}^2 - {\omega_J}^2} a_{+z}^{(J)} \right. \\ &\quad \left. - \sin\theta \frac{{\omega_J}^2}{{\omega_{x_0}}^2 - {\omega_J}^2} a_{-x}^{(J)} + \cos\theta \frac{{\omega_J}^2}{{\omega_{x_0}}^2 - {\omega_J}^2} a_{-z}^{(J)} \right], \\ \vec{a}_{02} \cdot \hat{n}_{02} &= z^0(g_x \sin\theta + g_z \cos\theta) \end{aligned} \tag{6.34}$$

$$+\sum_J \left[\sin\theta \frac{{\omega_J}^2}{{\omega_{x_0}}^2-{\omega_J}^2} a_{+x}^{(J)} + \cos\theta \frac{{\omega_J}^2}{{\omega_{x_0}}^2-{\omega_J}^2} a_{+z}^{(J)} \right.$$
$$\left. -\sin\theta \frac{{\omega_J}^2}{{\omega_{x_0}}^2-{\omega_J}^2} a_{-x}^{(J)} - \cos\theta \frac{{\omega_J}^2}{{\omega_{x_0}}^2-{\omega_J}^2} a_{-z}^{(J)} \right], \qquad (6.35)$$

where $g_x = G_{1x} = -G_{2x}, g_z = 1 - G_{1z} = 1 - G_{2z}$, $\vec{G}_1$ and $\vec{G}_2$ describe the bridge atom motion induced by the local mode vibration, and $\vec{a}_+^{(J)} = \frac{1}{2}(\vec{a}_1^{(J)} + \vec{a}_2^{(J)})$ and $\vec{a}_-^{(J)} = \frac{1}{2}(\vec{a}_1^{(J)} - \vec{a}_2^{(J)})$ describe the in-phase and out-of-phase motion of the two bridge atoms. In low frequency region, the reduction factors $\frac{{\omega_J}^2}{{\omega_{x_0}}^2-{\omega_J}^2}$ and $\frac{{\omega_J}^2}{{\omega_{x_0}}^2-{\omega_J}^2}$ are very small and will reduce the substrate phonon amplitude for both in-phase and out-of-phase motions of the two bridge atoms at the surface.

In the anharmonic hamiltonian given by Eq. (6.7), some terms depend purely on these parallel components of the atomic displacement differences of the adsorption bonds, of the form $(\vec{a}_{0i} \cdot \hat{n}_{0i})^n$. In considering the phonon-induced vibrational line shape, these anharmonic terms only give small contributions due to the presence of the reduction factors $\frac{{\omega_J}^2}{{\omega_{x_0}}^2-{\omega_J}^2}$ and $\frac{{\omega_J}^2}{{\omega_{x_0}}^2-{\omega_J}^2}$. We will show some numeric illustrations of this in Section 6.5.

6.4 Vibrational line shift and line width for an adatom at a bridge site in the three dimensional model

Based on the anharmonic hamiltonian for an adatom at a bridge site in the three dimensional model given in Eq. (6.7), we now discuss some aspects of the line shift and line width of the localized vibration of the adatom in this adsorption situation.

6.4.1 Line shift contributed by the self interaction terms

Instead of considering all the line shift contributions due to the local mode self interactions and the interactions with the substrate phonons, here we only consider the line shift contributed by the local mode self interaction terms which is proportional to z^{0n} to compare with the similar calculation of H. Dürr and A. P. Baddorf in a one dimensional model. This will provide us some information about the improvement of the three dimensional model compared to the one dimensional model. Note that in the three dimensional model, the term proportional to z^{03} contains the second and third derivatives of the adsorption potential. Similarly, the term proportional to z^{04} contains the second, third and forth derivatives of the adsorption potential due to the adoption of the central force model for pair-wise interactions between the atoms. As a result, the line shift due to the self interaction of the perpendicular local mode alone is given by

$$\begin{aligned}\Delta\omega &= \frac{7\hbar\omega_{z_0}{}^2}{16V_0}(1-G_{1z})^4\left[1-\frac{15}{7}(1-G_{1z})^2-\frac{18}{7}\frac{\alpha^{-1}}{R_0}\tan^2\theta\right.\\ &\left.+\frac{30}{7}\frac{\alpha^{-1}}{R_0}\tan^2\theta(1-G_{1z})^2-\frac{15}{7}\left(\frac{\alpha^{-1}}{R_0}\right)^2\tan^4\theta(1-G_{1z})^2\right](2n_{\omega_{z_0}}+1),\end{aligned} \tag{6.36}$$

where we have taken the adsorption potential of the Morse form with depth V_0 and width α^{-1}. R_0 is the separation of the adatom and the bridge atoms at surface, and G_{1z} is the coefficient of the local mode component in the displacement of the bridge atoms. The first two terms in the square bracket gives the same result as that in the one dimensional model. The rest are due to the adoption of the pair-wise central force model. Some parts of them will cancel out. The net deviation from the one dimensional model will be small. We will show some numerical results later.

From Eq. (6.36), we can see that the line shift due to the local mode self interaction strongly depends on the local mode frequency and the depth of the potential well.

When the adatom is assumed to be adsorbed at a static surface, $G_{1z} = 0$, which was considered by H. Dürr and A. P. Baddorf for the O/Cu(110) adsorption system.

6.4.2 Line width contribution in the lowest order

As we mentioned in Section 6.1, the anharmonic damping via the two phonon emission process of the localized vibrational mode are expected to give a significant contribution to the vibrational line width. We therefore exclude the line width contributions from the other sources such as dephasing. In the one dimensional model, for O/Cu(110), we have shown that the latter contribution is much smaller. Moreover, the line width of the local mode due to decay is directly related to the life time of the mode, so in this chapter, we will concentrate on the decay processes of the local mode.

A local mode may decay through three processes. The first is the process in which the local mode of the adatom with frequency ω_{z_0} decays into a pair of substrate phonons with frequencies ω_J and $\omega_{J'}$. The energy conservation requires that $\omega_{z_0} = \omega_J + \omega_{J'}$, with $0 \leq \omega_J, \omega_{J'} \leq \omega_{max}$ and $\omega_{max} < \omega_{z_0} < 2\omega_{max}$. A description of such a decay process may be obtained by retaining terms proportional to $d^0_J(t)d^0_{J'}(t)z^0(t)$ in the anharmonic hamiltonian given by Eq. (6.7). We will study in details of this decay channel in the next section. For an adatom adsorbed at a bridge site which we consider, there is a local mode along the bridge and parallel to the surface. In our model, its frequency is determined by Eq. (6.13). The presence of this local mode makes two other decay channels possible in some instances. If $\omega_{z_0} > \omega_{x_0}$, the perpendicular local mode may decay into a parallel polarized local

mode and a substrate phonon, with $\omega_{z_0} = \omega_{x_0} + \omega_J$ required by energy conservation. A description of this second decay process may be found in the terms proportional to $d_J^0(t)x^0(t)z^0(t)$. Similarly, if $\omega_{z_0} < \omega_{x_0}$, the perpendicular localized phonon mode of the adatom can absorb a delocalized phonon of the substrate, exciting to a parallel localized mode of the adatom, with $\omega_{z_0} = \omega_{x_0} - \omega_J$ required by energy conservation. A description of this third process is also contained in the terms proportional to $d_J^0(t)x^0(t)z^0(t)$. Note that in the second and third processes, $0 < \omega_J < \omega_{max}$.

When $0 < |\omega_{z_0} - \omega_{x_0}| < \omega_{max}$, the second or third process may contribute significantly to the vibrational line width of the local mode. On the other hand, when $|\omega_{z_0} - \omega_{x_0}| \sim 0$, the second or third process is not important since the generalized density of phonon states with frequency $\omega_k \sim 0$ is very small. In this case, the anharmonic damping is dominated by the two phonon emission process.

The damping mechanisms of the parallel localized mode of an adatom is analogous to those of its perpendicular localized mode. We do not consider them here. In this chapter, we only concentrate on the first decay channel described above.

6.5 Vertex functions for two phonon emission processes

To avoid unnecessary duplication and numeric complexity, as we mentioned, we now concentrate on the vibrational decay by the two phonon emission process. We start with the lowest order anharmonic coupling terms given in Eq. (6.11). The vertex function for the two phonon emission process is the coupling constant in the anharmonic hamiltonian for terms proportional to $d_J^0(t)d_{J'}^0(t)z^0(t)$. In this section, we calculate the vertex function based on the lowest order anharmonic coupling terms.

In the last section, we have shown the free vibrational coordinates x^0 and z^0 of the

localized modes are coupled by the anharmonicity of the substrate and adsorption bond to the phonon modes. The couplings depend on the displacements of each pair of atoms (i,j), with $(i = 0,1,2;\ j = n.n.\ \text{of}\ i)$ in each anharmonic bond and are determined by the bond structure of the adsorption system.

For the (100) surface of the simple cubic lattice we initially start with, the bond structure determines that there are 11 pairs in question. To simplify the calculation, the displacement difference of each pair can be expressed by

$$\begin{pmatrix} a_{(0,1)x} & a_{(0,1)y} & a_{(0,1)z} \\ a_{(0,2)x} & a_{(0,2)y} & a_{(0,2)z} \\ a_{(1,2)x} & a_{(1,2)y} & a_{(1,2)z} \\ a_{(1,3)x} & a_{(1,3)y} & a_{(1,3)z} \\ a_{(1,4)x} & a_{(1,4)y} & a_{(1,4)z} \\ a_{(1,8)x} & a_{(1,8)y} & a_{(1,8)z} \\ a_{(1,9)x} & a_{(1,9)y} & a_{(1,9)z} \\ a_{(2,5)x} & a_{(2,5)y} & a_{(2,5)z} \\ a_{(2,6)x} & a_{(2,6)y} & a_{(2,6)z} \\ a_{(2,7)x} & a_{(2,7)y} & a_{(2,7)z} \\ a_{(2,10)x} & a_{(2,10)y} & a_{(2,10)z} \end{pmatrix} = \begin{pmatrix} \lambda_{1,0} & \lambda_{1,1} & \cdots & \lambda_{1,10} \\ \lambda_{2,0} & \lambda_{2,1} & \cdots & \lambda_{2,10} \\ \vdots & \vdots & \ddots & \vdots \\ \lambda_{11,0} & \lambda_{11,1} & \cdots & \lambda_{11,10} \end{pmatrix} \begin{pmatrix} x & y & z \\ a_{1x} & a_{1y} & a_{1z} \\ a_{2x} & a_{2y} & a_{2z} \\ a_{3x} & a_{3y} & a_{3z} \\ a_{4x} & a_{4y} & a_{4z} \\ a_{5x} & a_{5y} & a_{5z} \\ a_{6x} & a_{6y} & a_{6z} \\ a_{7x} & a_{7y} & a_{7z} \\ a_{8x} & a_{8y} & a_{8z} \\ a_{9x} & a_{9y} & a_{9z} \\ a_{10x} & a_{10y} & a_{10z} \end{pmatrix} \tag{6.37}$$

or, in a compressed notation, as

$$[\vec{u}_l] = [\lambda_{lm}]\,[\vec{a}_m] \tag{6.38}$$

where $\vec{u}_l = \vec{a}_{ij}$, $\{l\}$ denotes the bonds $\{ij\}$ with $(i = 0, 1, 2;\ j = n.n.\ \text{of}\ i)$, and the matrix $[\lambda_{lm}]$ is determined by the cluster structure. Similarly, the unit vectors also can be expressed in matrix form

$$[\hat{n}_l] = \frac{[\lambda_{lm}]\left[\vec{R}_m\right]}{|\,[\lambda_{lm}]\left[\vec{R}_m\right]\,|}, \tag{6.39}$$

where $\vec{R}_m$ denctes the position of the atom at site m. Now the coupling terms in Eq. (6.11) can be written in terms of $\vec{u}_l, \hat{n}_l$ as

$$h_2^l(\vec{u}_l \cdot \hat{n}_l)u_l^2 = h_2^l[\lambda_{lm}\vec{a}_m \cdot \hat{n}_l][\lambda_{lm}\vec{a}_m] \cdot [\vec{a}_n\lambda_{nl}^*], \tag{6.40}$$

$$h_3^l(\vec{u}_l \cdot \hat{n}_l)^3 = h_3^l[\lambda_{lm}\vec{a}_m \cdot \hat{n}_l]^3. \tag{6.41}$$

We consider the decay of the perpendicular local mode with the vibrational coordinate z. Substituting $\vec{a}_m$ given in Eq. (6.29) into Eq. (6.40) and Eq. (6.41), and expanding them in terms of the normal mode coordinates $x^0(t), z^0(t)$ and $d_J^0(t)$ will give all possible decay channels in the lowest order. For the two phonon emission process, we keep the terms proportional to $d_J^0(t)d_{J'}^0(t)z^0(t)$. The anharmonic hamiltonian representing the two phonon emission process therefore can be written as

$$H_{anh} = \sum_{J,J',l} E_{J,J'}^l d_J^0(t)d_{J'}^0(t)z^0(t), \tag{6.42}$$

where the vertex function is

$$E_{J,J'}^l = \sum_{\alpha,\beta,m,n} \lambda_{lm}a_{m\alpha}^{(J)}H_l^{\alpha\beta}a_{n\beta}^{(J')}\lambda_{nl}^* c_\sigma, \tag{6.43}$$

with

$$H_l^{\alpha\beta} = h_2^l\left[(\vec{g}_l \cdot \hat{n}_l)\delta_{\alpha\beta} + n_{l\alpha}g_{l\beta} + n_{l\beta}g_{l\alpha}\right] + 3h_3^l(\vec{g}_l \cdot \hat{n}_l)n_{l\alpha}n_{l\beta}, \tag{6.44}$$

and

$$\vec{g}_l = \lambda_{lm}\vec{G}_m. \tag{6.45}$$

Here α or β denote the x, y and z components of the vectors $\vec{a}_m^{(J)}$ and $\hat{n}_m$. For each bond l, the vertex function $E^l_{J,J'}$ is contributed by all the components of the delocalized phonon amplitudes $a_m^{(J)}$ and $a_n^{(J')}$ of all atoms in the cluster. This means that both the perpendicular and lateral motions of the substrate atoms in the cluster contribute to the two phonon emission process. $H_l^{\alpha\beta}$ stands as the coupling constant of bond l with one substrate atom moving in the direction α at frequency ω_J and the other substrate atom moving in the direction β at frequency $\omega_{J'}$. It depends on the strength of the couplings and the structure of the surface. The polarizations of the delocalized phonons are included in the index J.

6.6 Self energy and line width

With the anharmonic hamiltonian between the perpendicular local mode and the substrate phonon modes given by Eq. (6.42), the lowest order terms of the self energy are shown diagrammatically in Fig. (6.4). This self energy represents the total

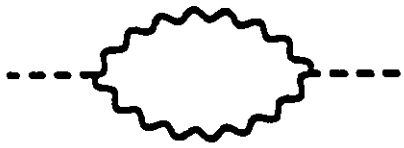

Figure 6.4: Self energy of two phonon emission processes.

contribution from both the anharmonicities of the adsorption potential and the solid. The effect of each bond is reflected by the coupling constant $H_l^{\alpha\beta}$ and the phonon amplitudes. This self energy diagram has two vertices, and therefore can receive

contributions from the anharmonicities of an individual bond or two different bonds. In the weak coupling limit, since the perpendicular local mode components $|\vec{G}_1| < 1$ and $|\vec{G}_2| < 1$ are much less than $G_{0z} = 1$, the line width contributions of the bond $l = (0,1)$ and $l = (0,2)$ are expected to be dominate ones if the coupling constant ϕ_n is less than V_n. The contributions from two different bonds may be negative due to the signs of the coupling constants. This causes some cancellations. The wavy lines now represent the phonon propagators $< Ta_i^{\alpha}(t)a_j^{\alpha'}(0) >$, which is made up of a weighted combination of the free phonon propagators $< Td_j^0(t)d_{-j}^0(0) >$. The weight is determined by the amplitudes of the delocalized phonon motions, or the generalized density of states defined in Chapter 5. The dashed lines represent the local mode propagator $< Tz^0(t)z^0(0) >$. Here we still use thermo-field dynamics introduced in Chapter 2 to calculate the free phonon propagator and local mode propagator. As we derived in Chapter 2, the line width is given by the imaginary part of the self energy, the contributions of the two phonon emission process in the three dimensional model read

$$\begin{aligned}\Gamma &= \frac{\hbar}{2m\omega_{z_0}} U_B(\omega_{z_0}) Im\Sigma(\omega_{z_0}) U_B(\omega_{z_0}) \\ &= \frac{\hbar}{2m\omega_{z_0}} \sum_{\substack{i,\alpha\beta \\ j,\alpha'\beta}} H_i^{\alpha\beta} H_j^{\alpha'\beta'} \sum_{\substack{l,m \\ l',m'}} \lambda_{il}\lambda_{jm}\lambda_{il'}\lambda_{jm'} \\ &\quad \int d\omega d\omega' \rho_{lm}^{\alpha\alpha'}(\omega)\rho_{l'm'}^{\beta\beta'}(\omega') F(\omega,\omega'), \end{aligned} \tag{6.46}$$

where i or j now denotes bonds, $\{\alpha\beta\}$ or $\{\alpha'\beta'\}$ indicate the components of the phonon displacements, $\rho_{lm}^{\alpha\alpha'}(\omega)$ is the generalized density of states and $F(\omega,\omega')$ is defined as

$$F(\omega,\omega') = \frac{2\pi}{\hbar^2}\frac{\hbar}{2\rho\omega}\frac{\hbar}{2\rho\omega'}\left[n_\omega + n'_\omega + 1\right]\delta(\omega_{z_0} - \omega - \omega'). \tag{6.47}$$

This function depends on the occupation number of the phonons $n_\omega = \frac{1}{e^{\hbar\omega/k_BT}-1}$. The function $\delta(\omega_{z_0}-\omega-\omega')$ insures the energy conservation and reduces the double frequency integral to a single one.

In principle, our theory is applicable to any surface structure. As an example, in Fig. (6.2) and Eq. (6.29), we have employed (100) surface of a simple cubic lattice to illustrate our theory, which is applied to O/Cu(110) in an "ad hoc" way. The theory will be improved by considering the fcc structure of the O/Cu(110) system. In the weak coupling limit, the calculation for a system with an fcc lattice substrate structure can be approximated in terms of the simple cubic lattice. The determination of the interatomic potential derivatives ϕ_2 and ϕ_3 from the bulk properties depends on the specific lattice structure. The bulk modulus B determines the harmonic coefficient $\phi_2 = aBr_0$, where the factor a is related to the structure of the crystal, for an fcc lattice, $a = 3\sqrt{2}/4$, and r_0 is the distance between nearest neighbors. The cubic anharmonic coefficient of the solid ϕ_3 is estimated from the linear thermal expansion coefficient ϵ of the substrate by the relation $\phi_3 = -4(\epsilon/k_B)r_0(\phi_2)^2$[92].

6.7 Applications

Since there are some experimental results available for the O/Cu(110) adsorption system, now, we apply our theory to calculate the line shift and line width of an oxygen vibration against this surface.

Bulk copper has a face centered cubic lattice structure. There are two bridge structures at the (110) surface of an fcc lattice: a long bridge with a separation of the lattice constant a and a short bridge with a separation of the nearest neighbor distance $r_0 = a/\sqrt{2}$. On the Cu(110) surface, a (2×1) structure has been observed after the adsorption of a half a monolayer of oxygen. An early low-energy ion-scattering

experiment[93] suggested a missing-row model of the reconstructed surface, where every second of the Cu rows in the [001] direction were missing. Adsorbed oxygen atoms occupy the long bridge sites as shown in Fig. (6.5). In the top layer, the copper and oxygen atoms form a chain at the ideal spacing as the copper bulk structure. Since the oxygen and copper atoms in the chain have almost the same vertical positions, we expect the vibrations in the chain will weakly couple to the vertical local mode of the adatom. As the first step, we leave out the anharmonic interaction of the copper atoms in the chains, and will include them later. Consequently, the adsorbed oxygen atoms sit at the short bridge sites of the second layer Cu atoms. The input and derived parameters are listed in Table (6.1).

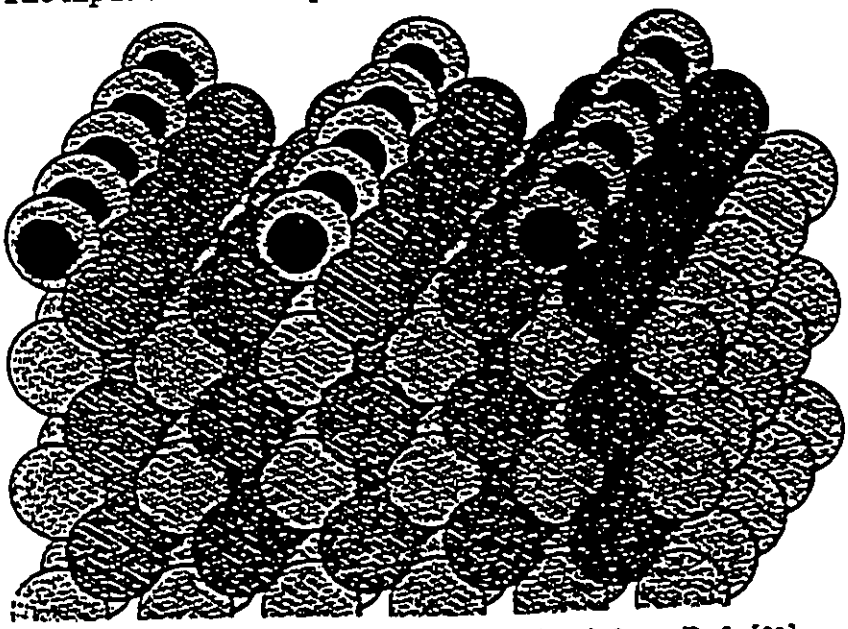

Figure 6.5: Surface structure of O/Cu(110) from Ref. [61].

The adsorption potential of the O/Cu(110) system is not well known[14]. In order to explain the linear increase of the line shift with temperature theoretically, H. Dürr and A. P. Baddorf assumed that the oxygen is bound to the Cu(110) surface with a Morse form potential and the line shift is contributed by the local mode self

Table 6.1: Input and derived parameters for O/Cu(110) at a bridge site

substrate atom mass M_s (amu)	63.5
mass of adatom O (amu)	16.0
well depth $2V_0$ (eV)	4.0
well width α^{-1} (Å)	0.68
local mode frequency ω_{z_0} (cm^{-1})	389
Debye frequency of substrate ω_D (cm^{-1})	219
angle θ	44.3°
bulk modulus (N/m^2)	1.37×10^{11}
thermal expansion coefficient (K^{-1})	1.67×10^{-5}
lattice constant a (Å)	3.61
ratio l_s	0.7

interaction alone. By fitting this line shift with their experimental result, they assumed that the oxygen is simply attached to the surface by one adsorption bond, and estimated the depth of adsorption potential well is about 2.0 eV. However, they misweighted the discrete peaks due to the self interaction terms of the local mode. In correction, we would estimate the depth of the potential well to be about 4.0 eV. Other study shows the total binding energy of the oxygen bonded to four nearest neighbors of the copper atoms is about 10.5 eV[84]. If the adsorption energy is equally divided among the four bonds, the depth of each adsorption potential well is about 2.6 eV. Practically, as a model study, we will vary the depth of each potential well V_0 and see how it affects the vibrational line shape contribution. By assuming that the adsorption potential has a Morse form, the width of potential well α^{-1} is fixed by relation $m\omega_{z_0}{}^2 = 4V_0\alpha^2\cos^2\theta$ which is different from that in a one dimensional model in Chapter 4 due to the use of the central force pair potential.

The angle θ between the adsorption bond and the vertical will determine the relation between the frequencies of the lateral and perpendicular localized modes of the adatom; see Eq. (6.13). In Table 6.1, this angle is taken from the geometric

structure of the (2×1)O-Cu(110) system[94] which is 44.3° < 45° so that $\omega_{x_0} < \omega_{z_0}$. On the other hand, since this angle determines the relation between ω_{x_0} and ω_{z_0}, we will also take it as 55° so that $\omega_{z_0} < \omega_{x_0}$, to study the influence of the adatom's relative position on the surface when it sits at a bridge site.

From the discussion in Chapter 5, we know that the sound wave velocity ratio l_s of the transverse and longitudinal waves combined with the bulk Debye frequency determines the cutoff frequencies for the different branches in the semi-infinite elastic continuum model. For an fcc metal solid, Maradudin showed this ratio is about 0.7[92]. On the other hand, we also choose this ratio to be 0.5 from the peak position of the generalized density of states spectrum similar to the lattice dynamics calculation[95, 86].

6.7.1 Line shift due to the self interactions of the perpendicular local mode

In Chapter 4, we assumed that the oxygen atom is attached to the two bridge atoms at the surface via two adsorption bonds. The adsorption potentials only depended on the vertical displacements of the adatom and the two bridge atoms. The line shift contributed by the self interaction terms of the perpendicular local mode of the adatom is the same as H. Dürr and A. P. Baddorf's result (but corrected by a factor 2) if we assume that the Cu surface is static. For $2V_0$=4.0 eV, we find that the line shift will shift by -3.8 cm^{-1} at T=700 K which agrees with the experimental result. Of course, we do not expect the self interaction alone to explain the experimental result on the vibrational line shift of the O/Cu(110) adsorption system. In the three dimensional model, the line shift contributed by the self interaction we discussed in Section 6.4. is different from that in the one dimensional model, and only shifts by

-2.6 cm^{-1} at T=700 K for $2V_0 = 4.0$ eV if we also assume that the oxygen adatom sits at a static surface.

In comparing with the one dimensional model including the motion of the two bridge atoms for $2V_0 = 10.0$ eV in Chapter 4, the line shift contribution by the local mode self interaction alone is -3.5 cm^{-1} at T=700 K which agrees with the experimental measurement. However, we expect the interaction of the local mode with the substrate phonons or the other local modes also contribute to the line shift. Since we have shown the route of calculating the line shift in the three dimensional model, we will not go into more details here.

6.7.2 Line width of the perpendicular local mode

For the model O/Cu(110) adsorption system, since the angle θ is so close to 45° that $|\omega_{z_0} - \omega_{x_0}| \sim 0$, the decay channels via one substrate phonon and one lateral local mode have very small rate constants. We therefore ignore them here and concentrate on the contribution of the emission of two substrate phonons.

First, as a model study, we approximate copper substrate as a simple cubic lattice. All bond lengths of substrate are equal to the lattice constant, which is taken to be equal to the nearest neighbor distance of the fcc copper lattice. Second, we adopt the reconstructed fcc structure of O/Cu(110)[94].

Simple cubic lattice model

A simple cubic lattice is the simplest lattice structure of a solid. In our model theory, we use the (100) surface of a simple cubic lattice as an example, applied to the O/Cu(110) adsorption system. The separations of the long bridge and short bridge are approximated by the nearest neighbor distance r_0 of the copper atoms

Table 6.2: Line width contributions for fixed θ at 44.3°, $2V_0$ at 4.0 eV and two choices of l_s

	$l_s = 0.5$				$l_s = 0.7$			
T (K)	Γ_{vv}	$\Gamma_{\phi\phi}$	$\Gamma_{v\phi}$	Γ	Γ_{vv}	$\Gamma_{\phi\phi}$	$\Gamma_{v\phi}$	Γ
200	2.6	1.4	-2.3	1.7	3.0	1.5	-1.8	2.7
400	4.9	2.6	-4.2	3.3	5.5	2.7	-3.2	5.0
600	7.2	3.8	-6.2	4.8	8.1	4.0	-4.7	7.4

in the substrate. In this approach, we ignore the effect of the copper atoms in the copper-oxygen chain since their effect on line width is considered small and will include them later when we consider the reconstructed structure of O/Cu(110). Here, we assume that the oxygen atom sits at the bridge site of the two copper atoms in the second layer. Besides the parameters listed in Table 6.1, as model study, we will calculate line width with more sets of V_0, θ and l_s. Through this study, we expect to understand the influences of the different aspects of the adsorption system on the vibrational line width of the adatom via the two phonon emission process.

A. Dependence on l_s

Fixing θ at 44.3° and V_0 at 4.0 eV, the line width contributions, from the anharmonicities of the adsorption bond and substrate, due to the two phonon emission process are listed in Table (6.2) for $l_s = 0.5$ and 0.7, respectively. As l_s increases, the maximum phonon frequency decreases since we kept the bulk Debye frequency fixed. Consequently, the integral range over phonon frequency in the line width formula decreases. On the other hand, near the surface region, the weight function of the Rayleigh mode increases so that the perpendicular component of the generalized density of states will be incorrectly normalized to a larger number, but the normalization of the parallel component of the generalized density of states stays about the

Table 6.3: Line width contributions for fixed θ at 44.3° and l_s at 0.7.

	V_0=2eV				V_0=4eV				V_0=10eV			
T (K)	Γ_{vv}	$\Gamma_{\phi\phi}$	$\Gamma_{v\phi}$	Γ	Γ_{vv}	$\Gamma_{\phi\phi}$	$\Gamma_{v\phi}$	Γ	Γ_{vv}	$\Gamma_{\phi\phi}$	$\Gamma_{v\phi}$	Γ
200	2.8	1.5	-1.7	2.6	3.0	1.5	-1.8	2.7	3.4	1.5	-1.8	3.1
400	5.0	2.7	-3.1	4.6	5.5	2.7	-3.2	5.0	6.1	2.7	-3.2	5.6
600	7.3	4.0	-4.6	6.7	8.1	4.0	-4.7	7.4	9.0	4.0	-4.7	8.3

same. In consequence, the coupling strength given by Eq. (6.44) decreases in magnitude. However, the line width contributions from the anharmonicity of substrate and from the adsorption bonds alone increase due to the increased perpendicular component of the generalized density of states. The line width contributed by the "cross interaction" $V\phi$, between the two anharmonicities decreases because it depends mainly on the lateral motion of the two bridge atoms. This contribution is negative due to the orientation of the anharmonic adsorption bond and the motion of atoms in the cluster, and is mostly contributed by the "cross interaction" between the two adsorption bonds and substrate bond connecting the two bridge atoms. The total width becomes larger. See Appendix F for the contributions from each bond and from the "cross interactions".

B. Dependence on V_0

Fixing θ at 44.3° and l_s at 0.7, we now vary binding energy $2V_0$ from 2.0 eV to 10.0 eV. This variation will not affect the line width contribution of the substrate bonds at all, and only slightly affects the line width contribution of the adsorption bond. Numerically, when we increases $2V_0$ from 2.0 eV to 4.0 eV, the line width due to the two phonon process increases a few percent; see Table 6.3. Note that in this calculation, we have kept ω_{z_0} fixed so that when V_0 increases, α decreases. The second derivative of the Morse potential will not change, but the third derivative will vary with V_0 and α. However, this change will not significantly affect the line

Table 6.4: Line width contributions for fixed l_s at 0.7, $2V_0$ at 4.0 eV and two choices of angle θ

	$\theta = 55°$				$\theta = 44.3°$			
T (K)	Γ_{VV}	$\Gamma_{\phi\phi}$	$\Gamma_{V\phi}$	Γ	Γ_{VV}	$\Gamma_{\phi\phi}$	$\Gamma_{V\phi}$	Γ
200	9.6	2.5	- 5.5	6.6	3.0	1.5	-1.8	2.7
400	17.4	4.5	-10.0	11.9	5.5	2.7	-3.2	5.0
600	25.6	6.6	-14.6	17.6	8.1	4.0	-4.7	7.4

width contributions of the two phonon emission process due to the reduction factors $\frac{\omega_j^2}{\omega_{z_0}^2-\omega_j^2}$ and $\frac{\omega_j^2}{\omega_{z_0}^2-\omega_j^2}$ in the anharmonic term $h_3(\vec{a}_{0i}\cdot\vec{n}_{0i})^3$ as we have discussed in Sec. 6.3.

C. Dependence on θ

Fixing $l_s = 0.7$ and $2\ V_0 = 4.0$ eV, we now change the angle θ to 55°, but still keep ω_{z_0} fixed. Then ω_{z_0} becomes much larger than that for $\theta = 44.3°$. The line width contributions from the anharmonicities of the adsorption bond and the substrate due to the two phonon emission process are listed in Table (6.4) for $\theta = 55°$ and $\theta = 44.3°$, respectively. As θ increases to 55°, the lateral coupling component of the adsorption bonds becomes much stronger due to the changing of ω_{z_0} and θ, but its perpendicular component becomes smaller. The line width contribution of the adsorption bond is much larger than that for $\theta = 44.3°$ since the contribution of the "cross interaction" V_1V_2 of the two adsorption bonds changes sign due to the strengthening of the coupling of the lateral polarizations. The line width contribution of the substrate bonds increases due to the stronger effect of the adatom on the two bridge atoms at the surface. As a result, the total contribution increases a lot. See Appendix F for the contributions from each bond and from the "cross interactions". This calculation has shown the strong dependence of our model to the geometry of the adsorption system.

Table 6.5: Line width contributions from different branches for l_s at 0.7, $2V_0$ at 4.0 eV and angle $\theta = 44.3°$

$\Gamma_{\sigma_1\sigma_2}$	SH	+	-	GR	R
SH	0.0	0.11	0.10	0.0	0.0
+	0.11	0.35	0.08	0.10	0.52
-	0.10	0.08	0.09	0.03	0.23
GR	0.0	0.10	0.03	0.0	0.0
R	0.0	0.52	0.23	0.0	0.0

D. The role of the Rayleigh branch

In the above, all the line widths we calculate are the total contributions of all phonon branches. In order to understand the role of the phonon modes induced by the surface, we have studied the line width contributions of the different branches. For the two phonon emission process, each phonon may be from a different phonon branch. For the O/Cu(110) system we consider, it is impossible to emit two Rayleigh phonons, two generalized Rayleigh phonons or two SH phonons, due to the requirement of energy conservation. In Table 6.5 we list all the line width contributions from different pairs of branches for $l_s = 0.7$, $\theta = 44.3°$ and $V_0 = 4$ eV at T=200 K. From this calculation, we find that the Rayleigh mode gives a dominant contribution to the line width. Although Γ_{++} is significant, we think that it is overestimated due to the model, seen by comparing the spectrum of the generalized density of states at the surface with that in lattice dynamics calculations. Nevertheless, this calculation has delivered a important message: the surface phonon modes are important when we study surface phenomena. Some of the above phonon processes are cut off for some of the choices of the cutoff phonon frequencies.

E. Normalization

So far, we have approximated the Cu(110) surface as a simple cubic (100) surface. The generalized density of states at the surface is unnormalized in the semi-infinite

elastic continuum model as we discussed in the last chapter. The (110) surface unit cell of an fcc lattice is also different from that of the (100) surface in a simple cubic lattice structure. We modify the above model by choosing the true area of the (110) surface unit cell. The cutoff frequency for each phonon branch will be smaller since the two dimensional wave vector cutoff becomes smaller due to the enlargement of the surface unit cell. Furthermore, we scale the generalized density of states to give correct number of modes per unit volume in an "ad hoc" way. For $l_s = 0.7$, we will no longer have the two phonon emission process involving one surface Rayleigh phonon mode which we believe is important. Instead, we choose $l_s = 0.5$ by comparing the cutoff frequencies in the phonon band structure in the lattice dynamics calculation[95], for the calculation here and later for the fcc structure. Fig. (6.6)

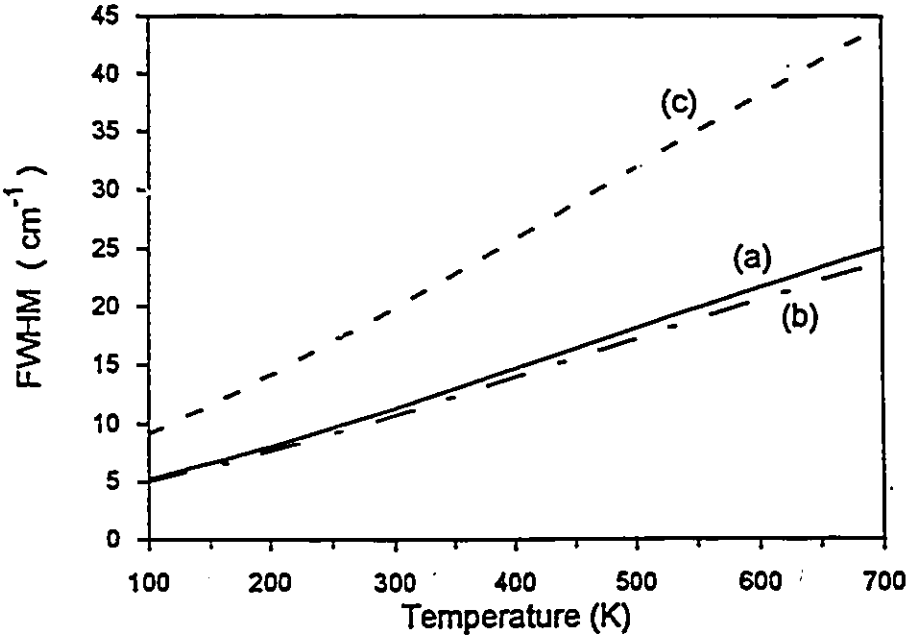

Figure 6.6: Temperature dependent line width contributed by the two phonon emission process. The Cu substrate is treated as simple cubic lattice in (a); fcc lattice after ignoring the first layer Cu atoms in (b); and full fcc structure in (c).

shows the FWHM changing with temperature in three approximations. In the high

temperature region, the FWHM almost linearly increases with temperature. The total increase of FWHM in this approximation is about 20 $cm^{-1}$when the temperature increases from 100 K to 700 K. See line (a) in Fig. (6.6). In H. Dürr and A. P. Baddorf's experiment, this increase is about 34 cm^{-1}. This consistency tells us that two phonon emission processes are important and give a dominant contribution to the vibrational line width.

In the simple cubic approach above, we did not consider the Cu(110) surface reconstruction after absorbing oxygen atoms. Next, we will calculate the vibrational line width in terms of the reconstructed structure of the O/Cu(110) adsorption system.

Results for fcc(110) surface structure

When an oxygen is adsorbed on the Cu(110) surface, the adsorption of the oxygen atom causes Cu(110) surface reconstruction. H. Dürr *et al* studied the actual surface geometry of the (2×1)O-Cu(110) system[94]. In the missing-row type reconstruction, the layer distance between the first and second layers is modified to 1.51 Å compared to the bulk value 1.28 Å, and the second layer atoms show a row-pairing like shift 0.12 Å in [110] direction towards the missing first-layer rows. Oxygen atoms are adsorbed in the long bridge sites of every other [001] copper row below the first copper layer by 0.08 Å. In the ideal bulk structure, the separation of the long bridge and short bridge are the lattice constant a and the nearest neighbor distance r_0, respectively. Since the oxygen atoms sit at about same vertical positions as the first layer copper atoms, the perpendicular local component of the first layer copper atoms is smaller than that of the second layer copper atoms nearest to the adatom. As a first approach, we ignore the effect of copper atoms in the chain on

the vibrational line width of the oxygen mode, and assume that the oxygen atoms sit on the short bridges of the second layer copper atoms. In the second layer down from the surface, there are six atoms nearest to the two bridge atoms. In the third layer down from the surface, there are two atoms nearest to the two bridge atoms. The atoms in the cluster we consider here are numbered by 1 to 10 in Fig. (6.7). Using the same method as we discussed above to normalize the generalized density

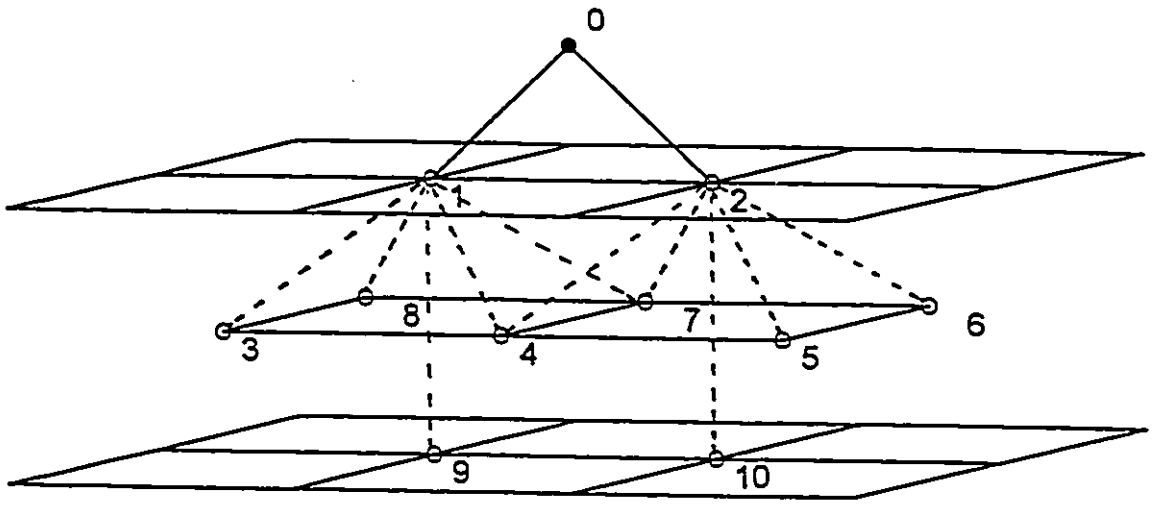

Figure 6.7: Fcc (110) surface structure for an adatom at a bridge site.

of phonon states, we calculated the FWHM for the same temperature range in this approximation for $\theta = 44.3°, l_s = 0.5$ and $2V_0 = 4.0$ eV. The result is shown by line (b) in Fig. (6.6). The total increase is about 18.3 cm^{-1} over this temperature range.

This increase is coincidentally very close to the result in the simple cubic lattice approach and is in the same order of magnitude as the experimental result. However, the reconstructed structure makes the line width contributions due to the anharmonicity of the substrate phonons comparable with that due to the anharmonicity of the adsorption potential. In both cases, the contributions from the "cross interaction" between two anharmonicities always causes some cancellation which brings down the contributions due to each anharmonicity alone.

Finally, in order to learn the effect of the Cu atoms in the oxygen-copper chain in the first layer, we now include the two adsorption bonds in the chain into our calculation. We then have a local mode in the direction along the chain or the y direction with the frequency ω_{y_0}. The phonon amplitude $a_{0y}^{(J)}$ in Eq. (6.32) is given by

$$a_{0y}^{(J)} = \frac{\frac{1}{2}{\omega_{y_0}}^2}{{\omega_{y_0}}^2 - {\omega_J}^2} \left[a_y^{(J)}(R_1) + a_y^{(J)}(R_2) \right] . \tag{6.48}$$

The prefactor $\frac{\frac{1}{2}{\omega_{y_0}}^2}{{\omega_{y_0}}^2-{\omega_J}^2}$ will induce a reduction factor for the in-phase motion of the two surface atoms in the chain when we calculate the bond distances. This reduction factor reduces the phonon-induced line width contribution from these two bonds.

In the cluster we consider now, there are 12 substrate atoms and 15 bonds contributing to the vibrational line width of the two phonon emission process. Note that the layer distance between the first and second layers is larger than the ideal layer spacing for bulk Cu due to the surface reconstruction. The generalized density of states of the second layer atoms are also not correctly normalized due to the rapid decay with z of the Rayleigh mode and the depletion of the generalized Rayleigh mode. In this case, we need to normalize the local density of states for both the first and second layer atoms as described in Section 6.7.2E. In doing this, some of

the off diagonal generalized density of states involving the second layer atoms are incorrectly normalized.

The line (c) in Fig. (6.6) shows the FWHM changing with temperature after we include the effect of the two Cu atoms in the first layer. When the temperature changes from 100 to 700 K, the FWHM increases about 34 cm^{-1} which agrees remarkably well with the experiment result. However, our calculation may not be so accurate compared to the experimental result due to the slight distortion of some off-diagonal generalized density of states and the simplicity of the phonon model. This does not allow us to exclude the line width contributions from other sources completely. We will explore them in the near future.

6.8 Summary

A three dimensional model has been used to calculate and compare the anharmonic coupling effects of the adsorption potential and substrate on the line width of the localized perpendicular vibration of an adatom at a bridge site in terms of two phonon emission processes. The theory includes the anharmonicity in the oxygen-copper and copper-copper bonds for the O/Cu(110) adsorption system. The calculation shows that two phonon emission is an important relaxation process and can not be ignored for an adatom adsorbed at a bridge site. Since we exclude the line width contributions from dephasing processes, our result is a partial contribution to the total vibrational line width. However, our calculations have shown good agreement with the experimental data on the vibrational line width for the O/Cu(110) adsorption system. As a trivial extension of the one dimensional model, we also calculated the line shift due to the perpendicular local mode self interaction. This shift is sensitive to the depth of potential well and the substrate phonon dynamics.

The theory presented in this chapter can be easily extended to include the line widths contributed by dephasing processes and to calculate the line shift contributions due to substrate phonons for the adsorbate mode, and to apply to other adsorption systems with different adsorption geometry.

Chapter 7. Conclusions and outlook

In summary, we have endeavored to present a theory to calculate the homogeneous vibrational line shape of the adsorbate mode in an adsorption system due to different relaxation mechanisms in a unified treatment. We have considered both a diatomic molecule and a dissociated atom adsorbed at solid surfaces. Although we have also studied the dephasing process of the high frequency internal vibrational mode of a diatomic admolecule by a low frequency mode, and the line shift contributed by the low frequency local mode self interaction, our main attention was devoted to the delocalized phonon induced vibrational line shape of an adsorbed atom at a surface. The phonon induced vibrational line shape of the low frequency local mode is shown to be crucially dependent on the interaction of the adsorbed atom or molecule with the solid, and on the anharmonicity of the solid.

We started with a simple one dimensional model and pair wise interaction approximation between atoms. By comparing the different treatments of the bilinear coupling between the adsorbate and substrate, we have found this bilinear coupling plays an important role in the adsorption system. For an admolecule at an ontop site, a reduction factor is induced in some of the anharmonic terms in the adsorption potential, by the nonperturbative treatment of the bilinear term. This reduction factor almost eliminates the delocalized phonon contributions to the vibrational line shape of both the low frequency local mode and the high frequency internal stretching mode of an admolecule, from the anharmonicity of the adsorption potential.

We have shown there is no such reduction factor present in the case where an admolecule is adsorbed at a bridge site for the out of phase motion of two bridge atoms at a surface in the one dimensional model. On the other hand, a nonperturbative treatment of the bilinear term revealed additional delocalized phonon contributions to the vibrational line shape from the anharmonicity of the substrate.

Based on a one dimensional model, we first calculated all possible line shift contributions to the high frequency internal mode of an admolecule and to the low frequency adsorbate-surface stretching mode, in lower order perturbation theory. Then we calculated the vibrational line width contributions to the internal mode, mediated by elastic phonon scattering, the exchange mechanism and a cross-interaction between them, for an admolecule at an ontop site. We also calculate the line width contributions to the adsorbate-surface stretching mode, mediated by phonon emission and elastic phonon scattering for an admolecule at an ontop and at a bridge site. The approximation of pair-wise interactions between atoms has prevented us from including other exchange mechanisms for dephasing of the low frequency local mode via interaction with librational or bending modes.

The theory in the one dimensional model has been applied extensively to the CO/Pt(111) adsorption system since CO occupies both ontop and bridge sites in this system and there are some experimental results available to compare with, and also applied to O/Cu(110) in discussion of the low frequency mode of an adatom absorbed at a bridge site. For an adatom at a bridge site, our practical calculation has shown the same trends as the experimental measurements and are accurate only to order of magnitude, as we expected, because of assumptions and simplifications employed for the adsorbate-surface interaction. In the one dimensional model, we employed a bulk Debye model to describe the substrate phonon dynamics, which is

a very crude model since we ignored the presence of the surface, at which surface phonon modes may be important in some cases.

Later, we have improved on the one dimensional model by extending to a three dimensional picture and treating the substrate as a semi-infinite elastic continuum. The adatom and substrate atoms are allowed to move in all directions. The interactions between atoms are described in terms of a central force model. Surface phonon modes are included in a semi-infinite elastic continuum model. These improvements have increased considerably the complexity of the calculation of the line shape contributed by substrate phonons. Our calculations have shown that the lateral motions of substrate phonons can give important contributions to the vibrational line width. New reduction factors are found in the three dimensional model which reduce the line width contributions from some anharmonic terms in the adsorption potential. Furthermore, the improved theory have provided a possibility to compare line width contributions from different processes in a systematic way, and study the line width dependence on adsorption geometry and on the anharmonicities of the adsorption potential and substrate bonds. This theory can be easily generalized to describe other adsorption systems such as an adatom at three fold or four fold hollow sites.

We have specifically calculated the line width contributed by two phonon emission processes in detail, which is the lowest order vibrational energy decay process when the frequency of the adsorbate mode lies between $\omega_{max} < \omega < 2\omega_{max}$. The new reduction factors make this contribution insensitive to the depth of the potential well when the adsorption potential is approximated by Morse potential with the local mode frequency held constant. Since we adopt a central force pair potential to describe the interaction between atoms, the second derivative of the potential also contributes to the two phonon emission process, and proved to be the main

contribution to the vibrational line width from the anharmonicity of the adsorption potential. This contribution is absent in the one dimensional model. Besides, we have also calculated the vibrational line shift contributed by the local mode self interaction, which is a minor development on the self interaction term treatment of Chapter 4. However, the line shift and line width may also receive additional contributions from other sources such as dephasing processes. Therefore, only qualitative agreement between our theory and experiment results can be expected.

The improved theory has been applied to the O/Cu(110) adsorption system. The line shift due to the local mode self interaction is a little less than that in the one dimensional model in Chapter 4 and close to experimental result. In the calculation of the line width contributed by the two phonon emission processes, we approximated the Cu substrate as a simple cubic lattice and also considered its true reconstructed surface structure in considering the anharmonic bond structure at the surface. However, even when we consider the reconstructed O/Cu(110) surface, we still treat the substrate phonons as those of semi-infinite elastic continuum. This simple treatment revealed the importance of surface phonons but neglected the detailed description of the phonons of the fcc lattice structure. The calculated line width for this process is a few times larger than that in the one dimensional model, and is much closer to the experimental measurements.

Note that even our improved theory describes only a *single* adsorbed atom. We have neglected the interactions between an adatom and neighbouring adsorbed atoms which could have an important effect on the vibrational line shape in some cases[49]. Also note that we neglected the internal degrees of freedom of the admolecule and treat it as an adatom. The interactions between atoms have been approximated in a central force model. In doing this, we have neglected some

possible low frequency lateral modes which might be important in some dephasing processes such as the exchange relaxation mechanism. For some adsorption systems, the decay of the vibrational local mode via emitting one delocalized and exciting a lateral local mode, and higher order terms, may give significant contributions to the line width and need to be included[78, 56].

In order to have a more complete picture of vibrational line shapes, further improvements need to be considered, such as

1. a detailed study of the phonon spectrum at the surface with or without an adatom. These spectrums should be correctly normalized;

2. the influence of dipole-dipole coupling;

3. the influence of other modes besides what we have included in the model, such as frustrated rotational mode.

In experiment, the observed line shape is due to many complex sources. In order to fully explain the observed vibrational line shape, we need to consider all possible line shape contributions. Besides the temperature dependent vibrational line shape we have considered here, electron-hole pair creation is another important relaxation channel. Inhomogeneous line broadening due to surface heterogeneity and adsorbate ordering may also play important roles in determining the vibrational line shape. They may explain the temperature independent part of the experimentally observed vibrational line shape.

Vibrational relaxation of adsorbed atoms and molecules has been of considerable intrinsic interest in recent years, and is also important for understanding the mechanisms of rate processes on solid surfaces such as diffusion and desorption. Experimental data on vibrational relaxation of adsorbed particles are mainly based on

the analysis of vibrational line widths and vibrational lifetimes. However, for low frequency adsorbate-surface stretching modes, many experimental techniques have difficulty giving accurate line widths. The agreement of our theoretical calculations with experiment has shown that our theory provides a way to predict vibrational line widths.

References

[1] Y. J. Chabal, Surf. Sci. Rep. **8** (1988) 211.

[2] R. Ryberg, *Molecular Surface Interactions*, (Editor: K. P. Lawley), Jone Wiley & Sons Ltd., 1989.

[3] J. W. Gadzuk and A. C. Luntz, Surf. Sci. **144** (1984) 429.

[4] Z. W. Gortel, H. J. Kreuzer, P. Piercy, and R. Teshima, Phys. Rev. B **36** (1987) 3059.

[5] D. C. Langreth, Phys. Rev. Lett. **54** (1985) 126.

[6] R. G. Tobin and P. L. Richards, Surf. Sci. **179** (1987) 387.

[7] P. Avouris and B. N. J. Persson, J. Phys. Chem. **88** (1984) 837.

[8] A. G. Eguiluz, Phys. Rev. Lett. **51** (1983) 1907.

[9] A. Liebsch, Phys. Rev. Lett. **54** (1985) 67.

[10] H. J. Kreuzer, Z. W. Gortel, *Physisorption Kenetics*, Springer-Verlag, Berlin, 1986.

[11] C. Noda, H. H. Richardson and G. E. Ewing, J. Chem. Phys. **92** (1990) 2099.

[12] P. Piercy, *Advances in Multi-Photon Processes and Spectroscopy*, (Editor: S. H. Lin), World Scientific Publishing Co. 1987.

[13] D. B. Jack, private communication. 1991.

[14] A. Zangwill, *Physics at surfaces*, Cambridge University Press 1988.

[15] G. Ertl, M. Neumann, and K. M. Streit, Surf. Sci. **64** (1977) 393.

[16] H. H. Richardson, C. Baumann and G. E. Ewing, Surf. Sci. **185** (1987) 15.

[17] D. C. Langreth and M. Persson, Phys. Rev. B **43** (1991) 1353.

[18] N. V. Richardson and N. Sheppard, *Vibrational Spectroscopy of Molecules on Surfaces*, (Editor: J. T. Yates and T. E. Madey), Plenum, New York, 1987

[19] J. A. Leiro and M. Persson, Surf. Sci. **207** (1989) 473.

[20] J. Pritchard, *Vibrational Spectroscopy of Adsorbates*, (Editor: R. F. Willis), Springer-Verlag, Berlin, 1980.

[21] J. C. Ariyasu, D. L. Mills, K. G. Lloyd, and J. C. Hemminger, Phys. Rev. B **28** (1983) 6123.

[22] R. Ryberg, Phys. Rev. B **32** (1985) 2671.

[23] B. N. J. Persson and R. Ryberg, Phys. Rev. B **32** (1985) 3586.

[24] B. N. J. Persson and R. Ryberg, Phys. Rev. Lett. **54** (1985) 2119.

[25] B. N. J. Persson, F. M. Hoffman and R. Ryberg, Phys. Rev. B **34** (1986) 2266.

[26] R. M. Shelby and C. B. Harris, J. Chem. Phys. **70** (1979) 34.

[27] M. Hutchinson and T. F. George, Chem. Phys. Lett. **124** (1986) 211.

[28] D. Hsu and J. L. Skinner, J. Chem. Phys. **81** (1984) 1604.

[29] J. L. Skinner and D. Hsu, Chem. Phys. **128** (1988) 35.

[30] B. Fain and Z. W. Gortel, Physica B **159** (1989) 361.

[31] R. A. Shigeishi and D. A. King, Surface Sci. **58** (1976) 379.

[32] A. M. Bradshaw and F. M. Hoffmann, Surface Sci. **72** (1978) 513.

[33] W. Erley, H. Eagner and H. Ibach, Surf. Sci. **80** (1979) 612.

[34] R. M. Hammaker, S. A. Francis, and R. P. Eischens, Spectrochim. Acta.**21** (1965) 1295.

[35] H. Steininger, S. Lehwald, and H. Ibach, Surf. Sci. **123** (1982) 264.

[36] M. Trenary et al, Surf. Sci. **147** (1984) 269.

[37] E. Schweizer, B. N. J. Persson, M. Tušhaus, D. Hoge, and A. M. Bradshaw, Surf. Sci. **213** (1989) 49.

[38] B. N. J. Persson, Chem. Phys. Lett. **149** (1988) 278.

[39] A. M. Lahee, J. P. Toennies and C. Wöll, Surf. Sci. **177** (1986) 371.

[40] N. V. Richardson and A. M. Bradshaw, Surf. Sci. **88** (1979) 255.

[41] J. Heidberg, K. W. Stahmer, H. Stein, H. Weiss, and M. Folman, Z. Phys. Chem. Neue Folge **155** (1987) 233.

[42] Zhen Ye, Renfang Tu, and P. Piercy, Phys. Rev. B **47** (1993) 13674.

[43] G. D. Mahan and A. A. Lucas, J. Chem. Phys. **68** (1978) 1344.

[44] M. Scheffler, Surface Sci. **81** (1979) 562.

[45] B. N. J. Persson and R. Ryberg, Phys. Rev. B **24** (1981) 6954.

[46] B. N. J. Persson, Surf. Sci. **116** (1982) 585.

[47] B. N. J. Persson, and A. Liebsch, Surf. Sci. **110** (1981) 356.

[48] R. S. Sorbello, Phys. Rev. B **32** (1985) 6294.

[49] B. N. J. Persson, J. El. Spectro. Relat. Phen. **54/55** (1990) 81.

[50] R. Disselkamp, H. C. Chang and G. E. Ewing, Surf. Sci. **240** (1990) 193.

[51] S. Chiang, R. G. Tobin, and P. L. Rechard, J. El. Spectro. Relat. Phen. **29** (1983) 113.

[52] S. Chiang, R. G. Tobin, P. L. Rechard, and P. A. Thiel, Phys. Rev. Lett. **52** (1984) 648.

[53] B. N. J. Persson and R. Ryberg, Phys. Rev. B **40** (1989) 10273.

[54] B. N. J. Persson, J. Phys. C **17** (1984) 4741.

[55] Z. Y. Zhang and D. C. Langreth, Phys. Rev. Lett. **59** (1987) 2211.

[56] J. C. Ariyasu, D. L. Mills, K. G. Lloyd, and J. C. Hemminger, Phys. Rev. B **30** (1984) 507.

[57] A. I. Volokitin, O. M. Braun, and V. M. Yakolev, Surf. Sci. **172** (1986) 31.

[58] S.van Smaalen and T. F. George, J. Chem. Phys. **87** (1987) 7307.

[59] Zhen Ye and P. Piercy, Phys. Rev. B **47** (1993) 9797.

[60] Y. J. Chabal, Phys. Rev. Lett. **55** (1985) 845.

REFERENCES

[61] H. Dürr and A. P. Baddorf, Surf. Sci. (to be published).

[62] J. David Jackson, it Classsical Electrodynamics John Wiley & Sons Ltd., 1925.

[63] A. L. Fetter and J. D. Walecka, *Quantum theory of Many-Particle Systems*, McGrew-Hill, New York, 1971.

[64] G. D. Mahan, *Many-Particle Physics*, Plenum Press, New York 1981.

[65] H. Umezawa, H. Matsumoto and H. Tachiki, *Thermo Field Dynamics and Condensed States*, North-Holland, Amsterdam, 1982.

[66] H. Matsumoto et al., Fortschr. Phys. **25** (1977) 273.

[67] Zhen Ye, Phys. Rev. B **46** (1992) 2628.

[68] K. Clusius, J. Goldmann and A. Perlick, Z. Naturforschg. **4a** (1949) 424.

[69] R. Gevirzman, Y. Kozirovski and M. Folman, Trans. Faraday Soc. **65** (1969) 2206.

[70] A. Ben Ephraim, M. Folman, J. Heidberg, and N. Moiseyev, J. Chem. Phys. **89** (1988) 3840.

[71] R. Ryberg, Phys. Rev. B **40** (1989) 8567.

[72] S. Marks, P. A. Cornelius, and C. B. Harris, J. Chem. Phys. **73** (1980) 3069.

[73] B. N. J. Persson and A. I. Volokitin, Chem. Phys. Lett. **184** (1991) 301.

[74] D. Lurie, *Particles and Fields*, Interscience Publisher 1968.

[75] A. A. Maradudin and A. E. Fein, Phys. Rev. **128** (1962) 2589.

[76] R. A. Cowley, Adv. Phys. **12** (1963) 421.

[77] A. A. Maradudin, P. A. Flinn, and R. A. Coldwell-Horsfall, Ann. Phys. **15** (1961) 360.

[78] Z. Y. Zhang, Phys. Lett. A **143** (1990) 413.

[79] B. E. Hayden and A. M. Bradshaw, Surf. Sci. **125** (1982) 787.

[80] I. J. Malik and M. Trenary, Surf. Sci. **214** (1989) L237.

[81] C. Kittel, *Introduction to Solid States Physics*, Jone Wiley and Sons, New York 1976.

[82] J. E. Black, F. C. Shanes, and R. F. Wallis, Surf. Sci. **133** (1983) 199.

[83] V. Bortolani, A. Franchini, G. Santoro, J. P. Toennies, Ch. Wöll, and G. Zhang, Phys. Rev. B **40** (1989) 3524.

[84] K. W. Jacobsen and J. K. Norskov, Phys. Rev. Lett. **65** (1990) 1788

[85] J. E. Black, B. Laks, and D. L. Mills Phys. Rev. B **22** (1980) 1818.

[86] J. E. Black, Surf. Sci. **105** (1981) 59.

[87] J. E. Black, D. A. Campbell and R. F. Willis, Surf. Sci. **105** (1981) 629.

[88] H. Ezawa, Ann. Phys. **67** (1971) 438.

[89] E. Goldys, Z. W. Gortel, and H. J. Kreuzer, Surf. Sci. **116** (1982) 33

[90] J. E. Black, Surf. Sci. **116** (1982) 240.

[91] Neil W. Ashcroft and N. David Mermin, *Solid State Physics*, Saunders College Publishing, 1976.

[92] A. A. Maradudin and P. A. Flinn, Phys. Rev. **129** (1963) 2529.

[93] R. P. N. Bronckers and A. G. J. Wit, Surf. Sci. **112** (1981) 133.

[94] H. Dürr, Th. Fauster, and R. Schneider, Surf. Sci. **244** (1991) 237.

[95] W. Kress F. W. de Wette, *Surface Phonon*, Springer-Verlag New York, 1991.

Appendix A. The center of mass variables for diatomic molecule

Fig. (2.1a) showed the diatomic admolecule configuration. Here we introduce the center of mass variables for this adsorption system. Define the total mass m, the reduced mass μ, the center of mass position and interatomic distance of admolecule as follow

$$\begin{aligned} m &= m_1 + m_2, \\ \frac{1}{\mu} &= \frac{1}{m_1} + \frac{1}{m_2}, \\ z' &= \frac{1}{m}(m_1 z_1 + m_2 z_2) \\ \xi &= z_2 - z_1, \end{aligned} \tag{A.1}$$

so that the positions of two atoms composing admolecule are given by

$$\begin{aligned} z_1 &= z' - \frac{\mu}{m_1}\xi, \\ z_2 &= z' + \frac{\mu}{m_2}\xi. \end{aligned} \tag{A.2}$$

Further more, if the z_0 is the mean spacing between static surface and the center of mass of an admolecule, ξ_0 is the mean interatomic spacing, the deviations from these equilibrium positions

$$\begin{aligned} \zeta &= \xi - \xi_0, \\ z &= z' - z_0, \end{aligned} \tag{A.3}$$

are small. Therefore the static hamiltonian of admolecule

$$H_{st}(z) = -\frac{\hbar^2}{2m_1}\frac{\partial^2}{\partial {z_1}^2} - \frac{\hbar^2}{2m_2}\frac{\partial^2}{\partial {z_2}^2} + V'(z_1) + U'(z_2 - z_1), \tag{A.4}$$

can be written as,

$$H_{st}(z) = -\frac{\hbar^2}{2m}\frac{\partial^2}{\partial z^2} - \frac{\hbar^2}{2\mu}\frac{\partial^2}{\partial \zeta^2} + V'\left(z - \frac{\mu}{m_1}\zeta\right) + U'(\zeta). \tag{A.5}$$

Appendix B. Bare boson propagator

The bare boson propagator is defined as

$$iD_0^{\alpha\beta}(t) = \langle 0(\beta)|Tz^{\alpha}(t)z^{\beta}(0))|0(\beta)\rangle, \tag{B.1}$$

where $z(t)$ is a Heisenberg operator and describes the displacement field of a harmonic oscillator. Using the Bogoliubov transformation given by Eq. (2.48) in terms of transformation matrix $U_B = \begin{pmatrix} c_B & d_B \\ d_B & c_B \end{pmatrix}$, the bare boson propagator can be written as

$$\begin{aligned} iD_0^{\alpha\beta}(t) &= U_B^{\alpha a}\langle 0(\beta)|Tz^{a}(t,\beta)z^{b}(0,\beta))|0(\beta)\rangle U_B^{b\beta} \\ &= U_B^{\alpha a} id_0^{ab}(t,\beta) U_B^{b\beta}, \end{aligned} \tag{B.2}$$

where the thermal propagator

$$\begin{aligned} id_0^{ab}(t,\beta) &= \langle 0(\beta)|Tz^{a}(t,\beta)z^{b}(0,\beta)|0(\beta)\rangle \\ &= \theta(t)\langle 0(\beta)|Tz^{a}(t,\beta)z^{b}(0,\beta)|0(\beta)\rangle \\ &\quad +\theta(-t)\langle 0(\beta)|Tz^{b}(0,\beta)z^{a}(t,\beta)|0(\beta)\rangle, \end{aligned} \tag{B.3}$$

where $\theta(t)$ is step function and can be given by

$$\theta(t) = \lim_{\delta\to 0}\frac{i}{2\pi}\int_{-\infty}^{\infty} d\omega \frac{1}{\omega + i\delta} e^{-i\omega t} \tag{B.4}$$

or

$$\int_{-\infty}^{\infty} dt e^{i\omega t}\theta(t) = \frac{i}{\omega + i\delta}. \tag{B.5}$$

The displacement field z of a harmonic oscillator is the linear combination of boson creation and annihilation operator as follow

$$z = \frac{\hbar}{2m\omega_0}(b + b^\dagger) \tag{B.6}$$

Using the properties of a thermal operator in TFD, we obtain

$$id_0^{ab}(t,\beta) = \begin{pmatrix} \theta(t)e^{-i\omega_0 t} + \theta(-t)e^{i\omega_0 t} & 0 \\ 0 & \theta(t)e^{i\omega_0 t} + \theta(-t)e^{-i\omega_0 t} \end{pmatrix}. \tag{B.7}$$

Fourier transform of thermal Green's function gives

$$d_0^{ab}(\omega,\beta) = \frac{\hbar}{2m\omega_0}\left(\frac{\tau}{\omega - \omega_0 + i\delta\tau} - \frac{\tau}{\omega + \omega_0 - i\delta\tau}\right), \tag{B.8}$$

where $\tau = \begin{pmatrix} 1 & 0 \\ 0 & -1 \end{pmatrix}$. Therefore, the Fourier transform of bare boson propagator is given in terms of $d_0^{ab}(\omega,\beta)$ in Eq. (B. 8) by

$$D_0^{\alpha\beta}(\omega) = U_B^{\alpha a} d_0^{ab}(\omega,\beta) U_B^{b\beta}. \tag{B.9}$$

Appendix C. The spectral representation of Green's function

In Thermo Field Dynamics, the time ordered Green's function for boson is defined by

$$\begin{aligned} iD^{\alpha\beta}(t) &= \langle 0(\beta)|Tz^{\alpha}(t)z^{\beta}(0))|0(\beta)\rangle \\ &= \theta(t)\langle 0(\beta)|Tz^{\alpha}(t)z^{\beta}(0)|0(\beta)\rangle + \theta(-t)\langle 0(\beta)|Tz^{\beta}(0)z^{\alpha}(t)|0(\beta)\rangle. \end{aligned} \tag{C.1}$$

The Fourier transform of the time ordered Green's function can be given by

$$D^{\alpha\beta}(\omega) = \frac{1}{2\pi}\int d\omega' \left[\frac{C_1^{\alpha\beta}(\omega')}{\omega-\omega'+i\delta} - \frac{C_2^{\alpha\beta}(\omega')}{\omega-\omega'-i\delta}\right] \tag{C.2}$$

where function $C_1^{\alpha\beta}(\omega'), C_2^{\alpha\beta}(\omega')$ are Fourier transforms of correlation functions

$$C_1(t) = \langle 0(\beta)|z^{\alpha}(t)z^{\beta}(0)|0(\beta)\rangle, \tag{C.3}$$

and

$$C_2(t) = \langle 0(\beta)|z^{\beta}(0)z^{\alpha}(t)|0(\beta)\rangle. \tag{C.4}$$

Now let's calculate these correlation functions by inserting the complete set

$$\sum_{n,m}|n,\tilde{m}\rangle\langle\tilde{m},n|, \tag{C.5}$$

between the two operator $z^{\alpha}(t), z^{\beta}(0)$, we have

$$C_1(t) = \sum_{n,m}\langle 0(\beta)|z^{\alpha}(t)|n,\tilde{m}\rangle\langle\tilde{m},n|z^{\beta}(0)|0(\beta)\rangle \tag{C.6}$$

$$
\begin{aligned}
&= \sum_{n,m} e^{-i(E_n-E_m)t/\hbar}\langle 0(\beta)|z^{\alpha}(0)|n,\tilde{m}\rangle\langle\tilde{m},n|z^{\beta}(0)|0(\beta)\rangle \\
&= \sum_{n,m} e^{-i(E_n-E_m)t/\hbar}\langle 0(\beta)|z(0)|n,\tilde{m}\rangle\langle\tilde{m},n|z(0)|0(\beta)\rangle \\
&\quad \begin{pmatrix} 1 & e^{\beta(E_n-E_m)/2} \\ e^{\beta(E_n-E_m)/2} & e^{\beta(E_n-E_m)} \end{pmatrix} \qquad \text{(C.7)}
\end{aligned}
$$

The Fourier transform of this correlation function is therefore given by

$$C_1(\omega) = C(\omega)\begin{pmatrix} 1 & e^{-\beta\omega/2} \\ e^{-\beta\omega/2} & e^{-\beta\omega} \end{pmatrix}, \qquad \text{(C.8)}$$

with

$$C(\omega) = \sum_{n,m} 2\pi\delta\left[\omega - (E_n - E_m)/\hbar\right]\langle 0(\beta)|z(0)|n,\tilde{m}\rangle\langle\tilde{m},n|z(0)|0(\beta)\rangle. \qquad \text{(C.9)}$$

Similarly, the Fourier transform of the correlation function $C_2(t)$ is given by

$$C_2(\omega) = C(\omega)\begin{pmatrix} e^{-\beta\omega} & e^{-\beta\omega/2} \\ e^{-\beta\omega/2} & 1 \end{pmatrix} \qquad \text{(C.10)}$$

Introduce the transformation matrix

$$U_B = \begin{pmatrix} c_B & d_B \\ d_B & c_B \end{pmatrix}, \qquad \text{(C.11)}$$

with

$$c_B = (1+n)^{1/2}, d_B = n^{1/2}, n = \frac{1}{e^{\beta\omega}-1}. \qquad \text{(C.12)}$$

By substituting Eq. (C.8) and Eq. (C.10) into Eq. (C.2) and making use of Bogoliubov transformation matrix $U_B = \begin{pmatrix} c_B & d_B \\ d_B & c_B \end{pmatrix}$, we obtain the spectral representation of the time ordered Green's function

$$
\begin{aligned}
D^{\alpha\beta}(\omega) &= \frac{1}{2\pi}\int d\omega'(1-e^{-\beta\omega'})C(\omega')U_B\frac{\tau}{\omega-\omega'+i\delta\tau}U_B \\
&= \int d\omega'\sigma_c(\omega')U_B\frac{\tau}{\omega-\omega'+i\delta\tau}U_B, \qquad \text{(C.13)}
\end{aligned}
$$

where the spectral function is

$$\sigma_c(\omega) = \frac{1}{2\pi}(1 - e^{-\beta\omega'})C(\omega'),$$

and

$$\tau = \begin{pmatrix} 1 & 0 \\ 0 & -1 \end{pmatrix}. \tag{C.14}$$

Appendix D. Feynman diagram rules in ω-space

The Feynmann diagram rules in ω-space for the evaluation of time ordered Green's function in Eq. (2.71), based on the expansion of S matrix given in Eq. (2.72) are,

1. Draw all distinct connected diagrams for unlabeled vertices, included the internal and external lines. The external lines are due to single $z(t), z(0)$ in the Green's function, while the internal lines are due to interaction hamiltonian with form $a^l z^m$. The vertex functions are from both expansion of interaction hamiltonian and S matrix coefficient.

2. Calculate the permutation factors when any of $l, m > 1$.

3. Each phonon line is assigned to the propagator which is Fourier transform of Green's function $\langle 0(\beta)|Ta^\alpha(t)a^\beta(0)|0(\beta)\rangle$. Similarly, each adsorbate line is assigned to the propagator which is Fourier transform of Green's function $\langle 0(\beta)|Tz^\alpha(t)z^\beta(0)|0(\beta)\rangle$.

4. Label each vertex with $i = 1, 2, \cdots, n$ and each propagator with $k = 1, 2, \cdots, N$. Note $N > n+1$. The internal lines are labeled by frequency ω_i, while external line are labeled by frequency ω only.

5. Each vertex with form $a^l z^m$ contributes a vertex function

$$\frac{1}{i\hbar l!m!}(-1)^l V_{l+m}\varepsilon^\alpha \ with\ l+m>2, \tag{D.1}$$

where $\varepsilon^\alpha = \begin{cases} 1 & \alpha = 1 \\ -1 & \alpha = 2. \end{cases}$

6. Sum over $\alpha_i = 1, 2$ at each vertex to include "tilde" fields.

7. At each vertex, energy conservation gives n relations between frequencies of propagators so that there are only $N - n - 1$ independent frequencies. Each independent frequency contributes a factor $1/2\pi$.

8. Integrating over all independent frequencies and summing over all diagrams gives the Fourier transform of time ordered Green's function.

Example: Evaluation of the two phonon emission process.

1. Feyman diagram

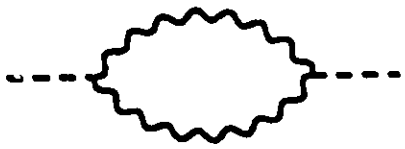

2. Permutation factor=2.

3. One phonon line is assigned to the propagator $iB_0^{\alpha\beta}(\omega_1)$, the other phonon line is assigned to the propagator $iB_0^{\alpha\beta}(\omega_2)$. The left adsorbate line is assigned to the propagator $iC_0^{1\alpha}(\omega)$, the right adsorbate line is assigned to the propagator $iC_0^{\beta 1}(\omega)$.

4. Label each vertex with $i = 1, 2$ and each propagator with $k = 1, 2, 3, 4$.

5. The vertex functions are $\frac{1}{2i\hbar}V_3\epsilon^{\alpha}$ and $\frac{1}{2i\hbar}V_3\epsilon^{\beta}$.

7. At each vertex, energy conservation gives two relations between the frequencies of the propagators so there is only one independent frequency. This independent frequency contributes a factor $1/2\pi$.

8. Integrating over the independent frequency and summing over $\alpha_i = 1, 2$ at each vertex gives the value of two phonon emission process.

$$iC_0^{1\alpha}(\omega)(-i\Pi^{\alpha\beta}(\omega)iC_0^{\beta 1}(\omega) = 2\left(\frac{V_3}{2i\hbar}\right)\varepsilon^{\alpha}\left(\frac{V_3}{2i\hbar}\right)\varepsilon^{\beta}$$
$$\times\left(\frac{i}{2\pi}\right)\int d\omega_1 iC_0^{1\alpha}(\omega)iB_0^{\alpha\beta}(\omega_1)iB_0^{\alpha\beta}(\omega-\omega_1)iC_0^{\beta 1}(\omega). \qquad \text{(D.2)}$$

Appendix E. Solution of Dyson's equation

Dyson's Equation Eq. (2.64) is

$$D^{\alpha\beta}(\omega) = D_0^{\alpha\beta}(\omega) + D_0^{\alpha a}(\omega)\Sigma^{ab}(\omega)D^{b\beta}(\omega). \tag{E.1}$$

From the spectral representation of the Green's function Eq. (C.13), we easily find the full Green's function has the following form

$$\begin{aligned} D^{\alpha\beta}(\omega) &= ReD^{\alpha\beta}(\omega) + iImD^{\alpha\beta}(\omega) \\ &= ReD(\omega)\tau - i\pi\sigma_c U_B U_B. \end{aligned} \tag{E.2}$$

On the other hand, the bare boson Green's function as calculated in Appendix B has the following form

$$\begin{aligned} D_0^{\alpha\beta}(\omega) &= ReD_0^{\alpha\beta}(\omega) + iImD_0^{\alpha\beta}(\omega) \\ &= \frac{\hbar}{\omega_0}\frac{\tau}{\omega^2-\omega_0^2} - i\pi\frac{\hbar}{2m\omega_0}[\delta(\omega+\omega_0)+\delta(\omega-\omega_0)]U_B U_B. \end{aligned} \tag{E.3}$$

If the self energy due to the anharmonic interaction has non zero imaginary part, we can ignore the imaginary part of bare Green's function. Substituting the Eq. (E.2), Eq. (E.3) into Dyson's equation Eq. (E.1), we find that the self energy is required to have the form

$$\begin{aligned} \Sigma^{\alpha\beta}(\omega) &= Re\Sigma^{\alpha\beta}(\omega) + iIm\Sigma^{\alpha\beta}(\omega) \\ &= Re\Sigma(\omega)\tau - i\sigma(\omega)U_B^{-1}U_B^{-1}. \end{aligned} \tag{E.4}$$

With Eq. (E.4) in addition to Eq. (E.2), Eq. (E.3), the solution of Dyson's equation is given by

$$D(\omega) = \frac{A\tau + i\sigma(\omega)U_B U_B}{A^2 + \sigma^2}, \tag{E.5}$$

where

$$A = \frac{m}{\hbar}(\omega^2 - \omega_0^2) - Re\Sigma. \tag{E.6}$$

At resonance, the energy pole is determined by

$$A^2 + \sigma^2 = 0. \tag{E.7}$$

This gives the line shift and line width

$$\begin{aligned} \Delta\omega &= \frac{\hbar}{2m\omega_0} Re\Sigma, \\ \Gamma &= \frac{\hbar}{2m\omega_0}\sigma \\ &= -\frac{\hbar}{2m\omega_0} U_B Im\Sigma U_B. \end{aligned} \tag{E.8}$$

Appendix F. Line width contributions from different pairs of bonds

In the following tables, each linewidth is in units of cm^{-1}.

Table F.1: For $\theta = 44.3°, 2V_0 = 4.0$ eV, and $l_s = 0.5$ at T=200 K.

	$x-a_1$	$x-a_2$	a_1-a_2	a_1-a_3	a_1-a_4	a_1-a_8	a_1-a_9	a_2-a_5	a_2-a_6	a_2-a_7	a_2-a_{10}
$x-a_1$	1.90	-.58	-.46	.01	.00	.00	-.04	.00	-.10	.00	.02
$x-a_2$	-.58	1.90	-.46	-.10	.00	.00	.02	.00	.01	.00	-.04
a_1-a_2	-.46	-.46	.74	.02	.00	.00	.01	.00	.02	.00	.01
a_1-a_3	.01	-.10	.02	.19	.00	.00	.00	.00	.02	.00	.00
a_1-a_4	.00	.00	.00	.00	.01	.00	.00	.00	.00	.00	.00
a_1-a_8	.00	.00	.00	.00	.00	.01	.00	.00	.00	.00	.00
a_1-a_9	-.04	.02	.01	.00	.00	.00	.05	.00	.00	.00	.01
a_2-a_5	.00	.00	.00	.00	.00	.00	.00	.01	.00	.00	.00
a_2-a_6	-.10	.01	.02	.02	.00	.00	.00	.00	.19	.00	.00
a_2-a_7	.00	.00	.00	.00	.00	.00	.00	.00	.00	.01	.00
a_2-a_{10}	.02	-.04	.01	.00	.00	.00	.01	.00	.00	.00	.05

Table F.2: For $\theta = 44.3°, 2V_0 = 4.0$ eV, and $l_s = 0.7$ at T=200 K.

	$x-a_1$	$x-a_2$	a_1-a_2	a_1-a_3	a_1-a_4	a_1-a_8	a_1-a_9	a_2-a_5	a_2-a_6	a_2-a_7	a_2-a_{10}
$x-a_1$	2.21	-.69	-.64	.13	.00	.00	-.08	.01	.01	.01	.14
$x-a_2$	-.69	2.21	-.64	.01	.01	.01	.14	.00	.13	.00	-.08
a_1-a_2	-.64	-.64	.94	-.11	.00	.00	.02	.00	-.11	.00	.02
a_1-a_3	.13	.01	-.11	.24	.00	.00	.00	.00	.00	.00	.00
a_1-a_4	.00	.01	.00	.00	.01	.00	.00	.00	.00	.00	.00
a_1-a_8	.00	.01	.00	.00	.00	.01	.00	.00	.00	.00	.00
a_1-a_9	-.08	.14	.02	.00	.00	.00	.21	.00	.00	.00	.02
a_2-a_5	.01	.00	.00	.00	.00	.00	.00	.01	.00	.00	.00
a_2-a_6	.01	.13	-.11	.00	.00	.00	.00	.00	.24	.00	.00
a_2-a_7	.01	.00	.00	.00	.00	.00	.00	.00	.00	.01	.00
a_2-a_{10}	.14	-.08	.02	.00	.00	.00	.02	.00	.00	.00	.21

Table F.3: For $\theta = 55°, 2V_0 = 4.0$ eV, and $l_s = 0.7$ at T=200 K.

	$x-a_1$	$x-a_2$	a_1-a_2	a_1-a_3	a_1-a_4	a_1-a_8	a_1-a_9	a_2-a_5	a_2-a_6	a_2-a_7	a_2-a_{10}
$x-a_1$	4.02	.80	-1.92	.35	.00	.00	-.06	.01	.11	.01	.12
$x-a_2$	.80	4.02	-1.92	.11	.01	.01	.12	.00	.35	.00	-.06
a_1-a_2	-1.92	-1.92	1.83	-.23	.00	.00	.03	.00	-.23	.00	.03
a_1-a_3	.35	.11	-.23	.46	.00	.00	.00	.00	.00	.00	.01
a_1-a_4	.00	.01	.00	.00	.01	.00	.00	.00	.00	.00	.00
a_1-a_8	.00	.01	.00	.00	.00	.01	.00	.00	.00	.00	.00
a_1-a_9	-.06	.12	.03	.00	.00	.00	.24	.00	.01	.00	.02
a_2-a_5	.01	.00	.00	.00	.00	.00	.00	.01	.00	.00	.00
a_2-a_6	.11	.35	-.23	.00	.00	.00	.01	.00	.46	.00	.00
a_2-a_7	.01	.00	.00	.00	.00	.00	.00	.00	.00	.01	.00
a_2-a_{10}	.12	-.06	.03	.01	.00	.00	.02	.00	.00	.00	.24